

Phospholipid- and gold-induced gelation of Thai silk fibroin
and its applications for cell and drug delivery



A Dissertation Submitted in Partial Fulfillment of the Requirements
for the Degree of Doctor of Philosophy in Biomedical Engineering
Common Course
FACULTY OF ENGINEERING
Chulalongkorn University
Academic Year 2019
Copyright of Chulalongkorn University

การเกิดเจลของไฟโบรอินใหม่ไทยที่เหนียวนำด้วยฟอสโฟลิพิดและทอง
และการประยุกต์ใช้ในการนำส่งเซลล์และยา



วิทยานิพนธ์นี้เป็นส่วนหนึ่งของการศึกษาตามหลักสูตรปริญญาวิทยาศาสตรดุษฎีบัณฑิต
สาขาวิชาวิศวกรรมชีวเวช ไม่สังกัดภาควิชา/เทียบเท่า
คณะวิศวกรรมศาสตร์ จุฬาลงกรณ์มหาวิทยาลัย
ปีการศึกษา 2562
ลิขสิทธิ์ของจุฬาลงกรณ์มหาวิทยาลัย

Thesis Title	Phospholipid- and gold-induced gelation of Thai silk fibroin and its applications for cell and drug delivery
By	Mr. Chavee Laomeephol
Field of Study	Biomedical Engineering
Thesis Advisor	Professor Siriporn Damrongsakkul, Ph.D.
Thesis Co Advisor	Supansa Yodmuang, Ph.D.

Accepted by the FACULTY OF ENGINEERING, Chulalongkorn University in
Partial Fulfillment of the Requirement for the Doctor of Philosophy

..... Dean of the FACULTY OF
ENGINEERING
(Professor SUPOT TEACHAVORASINSKUN, Ph.D.)

DISSERTATION COMMITTEE

..... Chairman
(Assistant Professor Juthamas Ratanavaraporn, Ph.D.)
..... Thesis Advisor
(Professor Siriporn Damrongsakkul, Ph.D.)
..... Thesis Co-Advisor
(Supansa Yodmuang, Ph.D.)
..... Examiner
(Assistant Professor Sorada Kanokpanont, Ph.D.)
..... Examiner
(Assistant Professor Jittima Luckanagul, Ph.D.)
..... External Examiner
(Assistant Professor Piyanuch Thitiwuthikiat, Ph.D.)

จุฬาลงกรณ์มหาวิทยาลัย
CHULALONGKORN UNIVERSITY

ชาวี เหล่ามีผล : การเกิดเจลของไฟโบรอินไหมไทยที่เหนียวนำด้วยฟอสโฟลิพิดและทอง และการประยุกต์ใช้ในการนำส่งเซลล์และยา. (Phospholipid- and gold-induced gelation of Thai silk fibroin and its applications for cell and drug delivery) อ.ที่ปรึกษาหลัก : ศ. ดร.ศิริพร ดำรงค์ศักดิ์กุล, อ.ที่ปรึกษาร่วม : อ. ดร.สุพรรณษา ยอดเมื่อง

ในปัจจุบัน มีการนำการเกิดเจลชนิดอินซิทูมาใช้ ซึ่งกระบวนการดังกล่าวเป็นกระบวนการเกิดเจลในระยะเวลาอันสั้นภายใต้สภาวะไม่รุนแรง เหมาะสมต่อการบรรจุเซลล์สิ่งมีชีวิต หรือสารออกฤทธิ์ในโครงสร้างไฮโดรเจลสามมิติ นอกจากนี้ การเกิดเจลชนิดอินซิทูอาจใช้เพื่อเตรียมไฮโดรเจลให้มีรูปร่างตามความต้องการ และความสะดวกของผู้ใช้งาน ไฮโดรเจลชนิดอินซิทูของโปรตีนไฟโบรอินไหมจากรังหนอนไหมบ้านสายพันธุ์ *Bombyx mori* ได้นำมาศึกษาในงานวิจัยนี้ เนื่องจากคุณลักษณะการจัดเรียงโมเลกุลของตนเอง และมีหมู่ฟังก์ชันที่คัดแปรได้ในโมเลกุลไฟโบรอินไหม อย่างไรก็ตาม สารละลายโปรตีนไฟโบรอินไหมสามารถเกิดเจลได้ แต่กระบวนการดังกล่าวใช้เวลานานหลายวัน หรือสัปดาห์ ซึ่งไม่เหมาะสมต่อการนำมาใช้เป็นไฮโดรเจลชนิดอินซิทู ในการนี้ จึงนำฟอสโฟลิพิด dimyristoyl glycerophosphoglycerol หรือ DMPG และเกลือของทองคำ มาใช้เป็นตัวกระตุ้นเพื่อเร่งกระบวนการเกิดเจลของสารละลายโปรตีนไฟโบรอินไหม

การเกิดเจลของสารละลายโปรตีนไฟโบรอินไหมที่กระตุ้นด้วย DMPG เกิดขึ้นในระยะเวลา 10 ถึง 40 นาที ขึ้นกับความเข้มข้นของ DMPG โดยแรงยึดเหนี่ยวทางไฟฟ้าสถิต และอันตรกิริยาระหว่างหมู่ที่ไม่ชอบน้ำส่งผลต่อการเปลี่ยนแปลงโครงสร้างทุติยภูมิของโปรตีนไฟโบรอินไหม ไฮโดรเจลนี้ได้ถูกนำไปใช้เพื่อกักเก็บ และเพาะเลี้ยงเซลล์ไฟโบรบลาสต์ชนิด L929 และ NIH/3T3 และพบว่าเซลล์มีการเจริญเติบโตเป็นปกติ แสดงให้เห็นว่าไฮโดรเจลไฟโบรอินไหมที่กระตุ้นด้วย DMPG มีความเข้ากันได้ทางชีวภาพต่อเซลล์เพาะเลี้ยง ต่อมา ไฮโดรเจลที่เตรียมจากฟอสโฟลิพิด DMPG ได้ถูกนำมาใช้ในการกักเก็บยาต้านมะเร็งเคอร์คูมิน โดยไฮโดรเจลดังกล่าวสามารถเพิ่มปริมาณเคอร์คูมินที่บรรจุได้ และยึดความคงตัวของเคอร์คูมิน รวมทั้งกระตุ้นการเกิดเจลของสารละลายโปรตีนไฟโบรอินไหม เคอร์คูมินที่ปลดปล่อยจากไฮโดรเจลมีฤทธิ์ยับยั้งเซลล์มะเร็ง และเซลล์ที่เพาะเลี้ยงบนพื้นผิวไฮโดรเจลมีอัตราการรอดชีวิตต่ำ อาจเนื่องมาจากการยึดเกาะของเซลล์บนพื้นผิวโปรตีนไฟโบรอินไหมต่ำ และความเป็นพิษต่อเซลล์ของเคอร์คูมิน นอกจากนี้ เกลือของทองคำสามารถกระตุ้นการเกิดเจลของสารละลายโปรตีนไฟโบรอินไหม และไฟโบรอินไหมที่คัดแปรด้วยหมู่ไทออล โดยเกลือของทองคำกระตุ้นการสร้างพันธะระหว่างหมู่แขนงข้างของกรดอะมิโนไทโรซีนในโปรตีนไฟโบรอินไหม ขณะที่ไฟโบรอินไหมที่คัดแปรด้วยหมู่ไทออล เกลือของทองคำจะกระตุ้นการสร้างพันธะไดซัลไฟด์ และระหว่างหมู่ซัลเฟอร์กับทองคำ การทดสอบทางชีวภาพของไฮโดรเจลที่เตรียมได้แสดงถึงความเข้ากันได้ต่อเซลล์ไฟโบรบลาสต์ชนิด L929

โดยสรุป การกระตุ้นการเกิดเจลของสารละลายโปรตีนไฟโบรอินไหมทำได้โดยการเติมฟอสโฟลิพิด DMPG หรือเกลือของทองคำ ซึ่งสารแต่ละชนิดนั้นกระตุ้นการเกิดเจลด้วยกลไกแตกต่างกัน ไฮโดรเจลที่เตรียมได้มีความเข้ากันได้ทางชีวภาพในการทดสอบระดับห้องปฏิบัติการ แสดงให้เห็นถึงศักยภาพของชีววัสดุที่พัฒนาขึ้นในการประยุกต์ใช้ทางชีวเวช

จุฬาลงกรณ์มหาวิทยาลัย
CHULALONGKORN UNIVERSITY

สาขาวิชา วิศวกรรมชีวเวช
ปีการศึกษา 2562

ลายมือชื่อนิติดี
ลายมือชื่อ อ.ที่ปรึกษาหลัก
ลายมือชื่อ อ.ที่ปรึกษาร่วม

5871407621 : MAJOR BIOMEDICAL ENGINEERING

KEYWORD: Silk fibroin, Hydrogel, Cytocompatibility, Phospholipid, Gold, Curcumin, Cell encapsulation, Drug delivery

Chavee Laomeephol : Phospholipid- and gold-induced gelation of Thai silk fibroin and its applications for cell and drug delivery. Advisor: Prof. Siriporn Damrongsakkul, Ph.D. Co-advisor: Supansa Yodmuang, Ph.D.

Recently, an *in situ* gelation, which is a rapid sol-to-gel transition under mild conditions, has been employed, allowing an entrapment of cells or substances in 3D structures as well as tailorable geometries and point-of-care uses. Silk fibroin (SF), a natural polymer from *Bombyx mori* silkworm cocoons, was chosen in this study as a substrate for the *in situ* hydrogel fabrication, due to self-assembly characteristic and a presence of modifiable functional groups. However, regenerated SF solution poses a slow gelation (several days or weeks) which is impractical for an *in situ* application. Therefore, a phospholipid, dimyristoyl glycerophosphoglycerol (DMPG), and a gold salt (Au^{3+}) were introduced as chemical inducers to accelerate the gelation process of SF.

SF hydrogels induced by DMPG can be obtained within 10-40 min depending on the concentration of DMPG. Electrostatic and hydrophobic interactions were proposed as driving forces for inducing SF structural transition. Encapsulated L929 and NIH/3T3 fibroblasts in the hydrogel displayed a normal proliferation, confirming the cytocompatibility of DMPG-induced SF hydrogel. Subsequently, DMPG-based liposomes were prepared and loaded with an anticancer drug, curcumin. The liposomes can enhance loading amount and extend curcumin stability as well as induce the rapid gelation of SF. Curcumin released from liposome-SF hydrogels can inhibit the growth of cancer cells. When using the hydrogel as a substrate for cell culture, low cell survival was observed, possibly due to the combination of low cell attachment on SF and cytotoxicity of curcumin. Moreover, an addition of a gold salt (Au^{3+}) in regenerated and thiolated SF solutions can accelerate the sol-to-gel transition. Dityrosine formation was proposed as an underlying mechanism of gelation for regenerated SF, while the formation of disulfide and Au-S bonds was proposed for thiolated SF. The obtained hydrogels exhibited good cytocompatibility with L929 fibroblasts.

In summary, the rapid gelation of SF can be achieved by the addition of DMPG or Au^{3+} salt. Different gelation mechanisms were proposed, and the obtained hydrogels showed the *in vitro* cytocompatibility, indicating the potential uses as a biomaterial for different biomedical applications.

จุฬาลงกรณ์มหาวิทยาลัย
CHULALONGKORN UNIVERSITY

Field of Study: Biomedical Engineering
Academic Year: 2019

Student's Signature
Advisor's Signature
Co-advisor's Signature

ACKNOWLEDGEMENTS

Firstly, I would like to acknowledge PhD grants supported by “The 100th Anniversary Chulalongkorn University Fund for Doctoral Scholarship” and “The 90th Anniversary Chulalongkorn University Fund (Ratchadaphiseksomphot Endowment Fund)”, Chulalongkorn University. The collaborative research and exchange program with 3B’s research group, University of Minho, Portugal were funded by “Erasmus+ program – International credit mobility” and “REMIX project – HORIZON 2020 Marie Skłodowska-Curie actions (G.A.778078)” by European Union. The fellowship at the National Institute for Materials Science (NIMS), Japan was awarded by “Chulalongkorn University – NIMS Cooperative Graduate School Program”. Financial supports for the research activities provided by 3B’s research group, NIMS, and Biomaterial Engineering for Medical and Health Research Unit are acknowledged.

With my utmost respect, I would like to thank my advisor, Prof. Siriporn Damrongsakkul, who has perpetually provided physical, mental, academic, and financial supports for my entire PhD study. Under her supervision, I have learned and improved my skills in various aspects which are necessary for my future. I would also thank to my co-advisor, Dr. Supansa Yodmuang, for her support in my thesis work, especially in biological studies. Her help in cell culture training gave me a lot of confidence to begin the cell culture works which I used to be inconfident to do so.

I would like to express my gratitude to Asst. Prof. Sorada Kanokpanont, Asst. Prof. Juthamas Ratanavaraporn, Dr. Peerapat Thongnuek, and all other professors, lecturers, or teachers at Chulalongkorn University, who provide me instructions, comments, and suggestions to improve my knowledge and skills, and always support me to accomplish the thesis work. Prof. Nuno M. Neves, Dr. Helena Ferreira, Prof. Rui L. Reis, and all other members of 3B’s research group, Portugal are also acknowledged for their support and the kindness housing me while I was there. Additionally, I would like to thank Prof. Hisatoshi Kobayashi-sensei, Masami Usui-san, Takako Honda-san, and Shinya Hattori-san for their cordiality and kind hospitality when I was an exchanged student at NIMS, Japan.

From my sincerest gratitude, I do not even have the words to thank my dad, my mom, and my sister for their supports to my PhD study, for their understanding of the PhD life, and for patience of the 5-year PhD study. I would give all the credit of my degree to my family. Without them, I probably never make my dream to carry on the PhD study. Furthermore, I would like to thank all my friends at the lab, my old friends from the secondary school, from the bachelor’s

degree, and from Bumrungrad international hospital who always physically and mentally supported and encouraged me. It was very nice to have a lot of good friends surrounding who always supported me even everything was going down.

Finally, and utmost importantly, I would thank myself for keeping up the passion to pursue my dream of the PhD, from the beginning to the end. Thank myself to be patient, be optimistic, be a hard-worker, and not be so dramatic for the entire PhD life.

Chavee Laomeephol



TABLE OF CONTENTS

	Page
.....	iii
ABSTRACT (THAI)	iii
.....	iv
ABSTRACT (ENGLISH).....	iv
ACKNOWLEDGEMENTS	v
TABLE OF CONTENTS.....	vii
LIST OF TABLES	xvi
LIST OF FIGURES	xvii
Chapter 1 Introduction.....	1
1. Background and significance of the research problem.....	1
2. Objectives of the research.....	3
3. Scope of the research.....	3
4. Expected benefits	4
Chapter 2 Literature Reviews.....	5
1. Biomaterials	5
1.1. Biomaterials for tissue engineering	5
1.2. Biomaterials for drug delivery	6
1.3. Biodegradable polymers as biomaterials	6
1.3.1. Proteins or natural-origin polypeptides	6
a. Collagen and gelatin	6
b. Fibrin and fibrinogen	7
c. Elastin	7
d. Silk.....	7
1.3.2. Polysaccharides	8
a. Alginate.....	8

b.	Chitosan	8
c.	Hyaluronan.....	8
d.	Chondroitin sulfate	9
1.3.3.	Synthetic polymers	9
a.	Poly(glycolic acid), poly(lactic acid) and their co- polymers.....	9
b.	Poly(caprolactone).....	10
c.	Poly(dioxanone)	10
d.	Poly(propylene fumarate)	10
2.	Hydrogels.....	10
2.1.	Required properties of hydrogels for biomedical uses	11
2.1.1.	Water absorption and mass transportation.....	11
2.1.2.	Mechanical stability.....	11
2.1.3.	Biodegradability	12
2.1.4.	Biocompatibility and bioactivity.....	13
2.2.	Hydrogel formation.....	13
2.2.1.	Covalent crosslink	13
2.2.2.	Ionic gelation.....	14
2.2.3.	Thermo-gelation	14
2.2.4.	Self-assembly	15
3.	Silk biomaterials.....	15
3.1.	Historical aspects of silk biomaterials used as medical devices	15
3.2.	Classification of silk fibroin by the origin	15
3.2.1.	Silkworm silks.....	15
a.	Non-mulberry or wild silkworm silks	16
b.	Mulberry or domestic silkworm silks.....	16
3.2.2.	Spider silks.....	17
3.3.	Properties of silk fibroin	18
3.3.1.	Physicochemical properties	18

a.	Primary structure	18
b.	Secondary structure	22
c.	Mechanical properties.....	23
d.	Thermal properties.....	24
3.3.2.	Biological properties	24
a.	Biodegradability	24
b.	Biological responses	24
3.4.	Silk fibroin gelation	27
3.4.1.	Conditions affecting the gelation of silk fibroin solution.....	38
a.	SF concentration and temperature.....	38
b.	pH	38
c.	Ionic strength.....	39
3.4.2.	In situ silk fibroin gelation systems.....	39
a.	Physical methods	39
1)	Sonication.....	39
2)	Vortex	40
3)	Electrical fields.....	41
4)	Hydrophilic silk fibroin extraction	42
5)	Soft freezing	43
b.	Chemical additives	44
1)	Alcohols	44
2)	Surfactants.....	45
3)	Salts.....	50
4)	Tannic acid	52
c.	Enzymatic crosslink.....	53
1)	Horseradish peroxidase	53
2)	Tyrosinase	55
d.	Blends and composites	56
1)	Ploxamer/silk fibroin	56

2)	Polyethylene oxide or polyethylene glycol/silk fibroin.....	56
3)	Cellulose/silk fibroin.....	58
4)	Short peptides/silk fibroin.....	59
5)	Non-mulberry silk fibroin/mulberry silk fibroin.....	60
e.	Photo-crosslinking.....	61
f.	Functionalization of silk fibroin.....	63
4.	Phospholipids and Liposomes.....	64
4.1.	Phospholipid characteristics.....	64
4.1.1.	Structure and classification of phospholipids.....	65
4.1.2.	Self-assembly in aqueous medium.....	66
4.1.3.	Physiological properties.....	66
4.2.	Phospholipid-protein interactions.....	67
4.3.	Liposomes.....	67
4.3.1.	Liposome classification.....	67
4.3.2.	Preparation of liposomes.....	68
4.4.	Biomedical applications of phospholipids and liposomes.....	68
4.4.1.	Bioactive agent delivery.....	68
4.4.2.	Tissue engineering applications.....	68
5.	Gold.....	69
5.1.	Current therapeutic approaches of gold.....	69
5.2.	Characteristics of gold nanoparticles.....	70
5.3.	Gold nanoparticle synthesis.....	70
5.3.1.	Physical methods.....	70
5.3.2.	Chemical methods.....	70
5.3.3.	Biological methods.....	70
5.4.	Biomedical applications.....	71
5.4.1.	Applications based on radiative properties.....	71
5.4.2.	Applications based on non-radiative properties.....	71

5.4.3. Scaffolds containing golds.....	72
Chapter 3 Materials and Methods	73
1. Material.....	73
2. Experimental design	74
3. Method.....	76
3.1. Silk fibroin (SF) solution preparation.....	76
3.2. Phospholipid-induced silk fibroin hydrogels for cell carrier application	76
3.2.1. Gelation time and mechanisms of gelation.....	76
a. Gelation time determination of DMPG-SF mixtures	76
b. FTIR measurement and secondary structure quantification.....	77
c. Fluorescence spectroscopy for the study of protein-lipid interactions.....	78
3.2.2. Physico-chemical characterizations of DMPG-SF hydrogels.....	79
a. SEM analysis of freeze-dried hydrogels.....	79
b. Viscoelastic properties of DMPG-SF hydrogels.....	79
c. Determination of <i>in vitro</i> biodegradability	79
3.2.3. Biological evaluation of DMPG-SF hydrogels.....	79
a. Cell cultures	79
b. Indirect cytotoxicity test of DMPG-SF hydrogels	80
c. Preparation of cell-encapsulated DMPG-SF hydrogels.	80
d. Viability of encapsulated cells using live/dead staining	80
e. Cell morphology detection using immunohistochemistry	81
f. Cell viability and proliferation using cell metabolic activity assay	81
3.3. Liposome-induced silk fibroin hydrogels for drug delivery system.....	81
3.3.1. Preparation and characterization of curcumin-containing liposomes	81
a. Preparation of curcumin-containing liposomes	81
b. Yield determination and curcumin content analysis	82

c.	Size analysis of liposomes	82
d.	Transmission electron microscope (TEM) imaging of liposomes	83
e.	Analysis of active curcuminoids by liquid chromatography/mass spectrometry (LC/MS).....	83
3.3.2.	Determination of gelation and properties of liposome-SF hydrogels.....	84
a.	Gelation time determination of liposome-SF mixtures .	84
b.	Micromorphology determination and elemental analysis of freeze-dried liposome-SF hydrogels	84
c.	TEM observation of liposome-SF hydrogels.....	84
d.	Curcumin release from liposome-SF hydrogels.....	85
e.	Mechanical test of liposome-SF hydrogels.....	85
3.3.3.	Cytocompatibility and anti-proliferative of cancer cells of liposome-SF hydrogels	85
a.	Cell culture tests with liposome-SF hydrogels.....	85
b.	Cell viability assay	86
c.	Cell apoptosis staining and cell imaging	86
3.4.	Gold-induced silk fibroin hydrogels and the cytocompatibility of hydrogels	86
3.4.1.	Preparation of thiolated SF solution and the gelation of SF and tSF with Au ³⁺	86
a.	Preparation of thiolated SF (tSF) and quantification of sulfhydryl group	86
b.	Gelation of SF and tSF with Au ³⁺	87
3.4.2.	Investigation of mechanism of Au-SF and Au-tSF gelation.....	87
a.	Determination of secondary structures of freeze-dried Au-SF and Au-tSF hydrogels.....	87
b.	Formation of dityrosine, Au-S bonds and Au nanoparticles	87
c.	X-ray photoelectron spectroscopy (XPS) for determining chemical states of Au and S	88

3.4.3. Physico-chemical characterizations of Au-SF and Au-tSF hydrogels.....	88
a. SEM analysis of freeze-dried Au-SF and Au-tSF hydrogels.....	88
b. Viscoelastic properties of Au-SF and Au-tSF mixtures	88
3.4.4. In vitro cell culture experiments of Au-SF and Au-tSF hydrogels	88
a. Cytocompatibility tests of Au-SF and Au-tSF hydrogels	88
b. Caspase-3 activation for cell apoptosis determination ..	89
3.5. Statistical analysis.....	89
Chapter 4 Results and Discussion	90
1. Phospholipid-induced silk fibroin hydrogels for cell carrier application	90
1.1. Gelation time of DMPG-SF mixtures.....	90
1.2. Gelation mechanisms of DMPG-induced SF hydrogels.....	91
1.2.1. SF conformational transition during the gelation induced by DMPG	91
1.2.2. Microenvironment changes of SF	92
1.3. Properties of DMPG-SF hydrogels.....	94
1.3.1. Micromorphology of lyophilized DMPG-SF hydrogels	94
1.3.2. Viscoelastic properties of DMPG-SF.....	95
1.3.3. Degradation profile of the DMPG-SF hydrogels	96
1.4. Cytocompatibility evaluations of DMPG-SF hydrogels.....	97
1.4.1. Proliferation profile of the cell lines.....	97
1.4.2. Indirect cytotoxicity test of the DMPG-SF hydrogels.....	98
1.4.3. Viability and morphology of cells encapsulated in DMPG-SF hydrogels.....	99
1.4.4. Proliferation of encapsulated cells	100
2. Liposome-induced silk fibroin hydrogels for drug delivery system	106
2.1. Characterizations of curcumin-loaded DMPG-based liposomes	106
2.1.1. Yield, size, and curcumin content analysis.....	106

2.1.2.	TEM images of the liposomes	107
2.1.3.	Content and stability of active curcuminoids.....	108
2.2.	Gelation time of liposome-SF mixtures.....	109
2.3.	Physical properties of liposome-loaded SF hydrogels.....	110
2.3.1.	Microstructures and element compositions of freeze-dried hydrogels.....	110
2.3.2.	Curcumin release from the hydrogels.....	112
2.3.3.	Compressive mechanical properties of liposome-SF hydrogels	113
2.4.	Biological properties of curcumin-loaded liposome-SF hydrogels.....	114
2.4.1.	Viability and proliferation of L929 and MDA-MB-231	114
2.4.2.	Cell apoptosis staining and cell imaging	116
3.	Gold-induced silk fibroin hydrogels and the cytocompatibility of hydrogels	121
3.1.	Amount of sulfhydryl group of thiolated SF.....	121
3.2.	Gelation and kinetic structural transition of Au-SF and Au-tSF.....	122
3.2.1.	Gelation of Au-SF and Au-tSF	122
3.2.2.	Conformational changes of SF and tSF mediated by Au ³⁺	122
3.3.	Gelation mechanisms of Au-mediated SF and tSF hydrogels.....	125
3.3.1.	Dityrosine and Au-S bond formation and a presence of AuNPs	125
3.3.2.	XPS analysis for the chemical states of Au and S.....	126
3.4.	Physical properties of Au-SF and Au-tSF hydrogels.....	129
3.4.1.	Microstructural features of freeze-dried Au-SF and Au-tSF hydrogels.....	129
3.4.2.	Viscoelastic properties of Au-SF and Au-tSF.....	130
3.5.	Cytocompatibility and bioactivities of Au-SF and Au-tSF hydrogels...	130
3.5.1.	Viability and proliferation of L929 and MCF-7 cultured on Au-SF and Au-tSF hydrogels.....	130
3.5.2.	Cellular apoptosis by an activation of caspase-3	131
	Chapter 5 Conclusion	133
	REFERENCES.....	136
	VITA.....	149



จุฬาลงกรณ์มหาวิทยาลัย
CHULALONGKORN UNIVERSITY

LIST OF TABLES

	Page
Table 1 Amino acid profile of SF derived from various sources (values reported as % w/w).....	20
Table 2 Mechanical properties of natural and synthetic fibers	23
Table 3 In vivo tests of SF materials	26
Table 4 Gelation time of SF solution affected by physical interventions or chemical additives, and the mechanical properties, in vitro/in vivo experiment of the obtained hydrogels.....	28
Table 5 Commonly used glycerophospholipids classified by the head group [18]....	65
Table 6 Liposome formulation.....	82
Table 7 Attachment and proliferation profile of the cell lines used in the biological experiments	98
Table 8 Population doubling time (day) of encapsulated cells in DMPG-SF hydrogels, compared to 2D culture on tissue culture plate (TCP).	103
Table 9 Proliferation of the encapsulated cells in SF hydrogels induced by various methods and with different SF concentration	104
Table 10 Yield, encapsulation efficiency (EE) and loading capacity (LD) percentage of curcumin in the liposomes, and size and polydispersity index (PDI) of the liposomes	106
Table 11 Gelation time (average \pm s.d.) of the 10 mg/ml liposomes and 3% SF mixtures. Asterisk (*) indicates no gelation within 6 h.....	110
Table 12 The relative amount percentage of different chemical state analyzed from XPS spectra in Au4f _{7/2} and S2p _{3/2} regions of the freeze-fried 1 mM Au-3% SF and 1 mM Au-3% tSF hydrogels	127

LIST OF FIGURES

	Page
Figure 1 (A) Larvae of <i>Bombyx mori</i> silkworms, (B) Thai silkworm cocoons, (C) traditional method to extract silk fibers in textile manufacturing using warm soap water, and (D) non-mulberry silkworm cocoons (Photo in figure A was taken from Yokohama silk museum, Yokohama, Japan, and figure B, C, and D were taken from Queen Sirikit sericulture center, Saraburi, Thailand)	16
Figure 2 <i>Bombyx mori</i> silk cocoons from different strains, namely Chinese, Japanese, Thai hybrid, and Thai domestic strains (Photos of silk cocoons were taken from available strains in Biomaterial Engineering for Medical and Health Research Unit, Faculty of Engineering, Chulalongkorn University, Thailand).....	17
Figure 3 Amino acid sequence of heavy chain of <i>Bombyx mori</i> silk fibroin. The crystalline domains are shown as GX1-12, separated by amorphous linkers. Lowercase letters indicate the sequences of hexapeptide as following; s = GAGAGS, y = GAGAGY, a = GAGAGA, μ = GAGYGA (adapted from [52]).....	19
Figure 4 Structural organization of beta sheet in fibroin (A) The alignment of beta sheet crystallites and amorphous regions (B) Inter-stacking or intermolecular assembly by the formation of van der Waals forces between side chains of glycine and alanine (C) Intramolecular assembly by the hydrogen bonding between NH and O of peptide backbones (adapted from [11])	22
Figure 5 Schematic illustration describing the SF chain interactions at a different pH condition	39
Figure 6 Chemical structure of alcohols used in the study of SF gelation	45
Figure 7 Chemical structure of sodium dodecyl sulfate	46
Figure 8 Chemical structure of sodium N-lauroyl sarcosinate.....	47
Figure 9 Chemical structure of sodium oleate	47
Figure 10 Chemical structure of SOS, SDS and STS.....	48
Figure 11 Chemical structure of a non-ionic surfactant, Triton X-100, an anionic surfactant, SDBS, and cationic surfactants, OTAB, DETAB, DTAB, CTAB and STAB	49
Figure 12 Chemical structure of (1) lactonic and (2) acidic sophorolipids	50

Figure 13 SF gelation mechanisms mediated by NaNO ₃ : (a) the generation of HNO ₃ (b) the formation of tyrosine and nitrate radicals (c) the formation of nitrotyrosine (d) the formation of dityrosine (adapted from [104])	51
Figure 14 (a) Fenton reaction, and (b) with a presence of ascorbic acid.....	52
Figure 15 Chemical structure of tannic acid	53
Figure 16 HRP catalytic reaction. With a presence of H ₂ O ₂ , HRP was oxidized, resulting in an activated state with a power reducing property. The electrons from activated HRP were transferred to phenolic oxidizing agent, leading to a formation of tyrosyl radicals. The tyrosyl radicals can react with each other to form dityrosine. (adapted from [45]).....	54
Figure 17 Reaction scheme of tyrosinase reacting with the tyrosine residues of SF. Tyrosine was oxidized by the enzyme to form dihydroxyphenyl, before spontaneously form o-quinone. The o-quinone further undergo non-enzymatic reactions, including Michael addition reaction with primary amine and the coupling reaction to form dityrosine. (Adapted from [135])	56
Figure 18 General formula of poloxamer 407 composed of ethylene oxide and propylene oxide monomers.....	56
Figure 19 Chemical structure of PEO or PEG	57
Figure 20 Chemical structure of HPC and HPMC	59
Figure 21 Chemical structure of NapFF and NapFFRGD	60
Figure 22 Reaction mechanism of Ru (II)-mediated dityrosine formation. Ru (II) transforms to Ru (III) upon the light activation. Ru (III) then reduces tyrosine to form tyrosyl radical, which can react with another tyrosine to form dityrosine crosslink. (Adapted from [123]).....	62
Figure 23 Chemical structure of 1,2-dimyristoyl-sn-glycero-3-phosphocholine (DMPC), a glycerophospholipid. The composition of two fatty acid chains, glycerol backbone, and the polar phosphate headgroup (choline) is displayed.	65
Figure 24 Experimental framework. The SF gelation system and their applications were divided into 3 groups, namely phospholipid-SF hydrogels for cell carrier application, liposome-SF hydrogels for drug delivery, and cytocompatible gold-SF hydrogels with anti-proliferation of cancer cells.....	75
Figure 25 Chemical structures of DMPG and DMPC	77
Figure 26 Peak assignment in amide I region corresponding to the secondary structures of SF.....	78

Figure 27 Chemical structures of curcumin, demethoxycurcumin and bisdemethoxycurcumin.....	84
Figure 28 Thiolation reaction of proteins using 2-iminothiolane to attach a sulfanyl butanimidine group to a primary amine.....	87
Figure 29 The gelation time of 3% SF with different concentrations of DMPG (A), different DMPG:DMPC molar ratios (B), and with a presence of Ca ²⁺ (0.1, 0.5 and 1 mM) in DMPG-SF mixtures (C). The gelation was observed by the spectroscopic method at 37°C. All experiments were done in quadruplicate. * indicates the statistical difference at $p \leq 0.05$	91
Figure 30 FTIR spectra of (A) 5, (B) 10, and (C) 15 mM DMPG-3% SF collected every 10 min for 90 min. (D-F) Secondary structures quantification by FSD and curve-fitting of FTIR spectra in amide I region (1,575-1,725 cm ⁻¹). Dash line indicates the gelation time.	92
Figure 31 (A) Fluorescence emission spectra after exciting the 5 mM DMPG-3% SF at 290 nm. The spectra were collected from 300-450 nm every 5 min. An inset displays an emission intensity at 320 nm over an experimental time. (B) Stern-Volmer plot of the acrylamide quenching experiment of SF solution, SF hydrogel and DMPG-SF hydrogels. An inset table shows the Stern-Volmer constant (k_{sv}).	93
Figure 32 The proposed mechanisms of DMPG-induced SF hydrogelation. The negative-charged DMPG interacts with SF chains, leading to the chain extension or unfolding through the electrostatic repulsion. The hydrophobic interaction between DMPG and the hydrophobic regions of SF results in a chain rearrangement and the formation of beta sheet structure.	94
Figure 33 SEM micrographs of freeze-dried (A) regenerated SF hydrogel and the 3% SF hydrogels induced by (B) 5 mM, (C) 10 mM, and (D) 15 mM DMPG. Scale bar = 100 μ m. (E) Pore diameter of SF and DMPG-SF hydrogels.	95
Figure 34 Viscoelastic properties of DMPG-SF hydrogels. (A) Complex modulus (G^*) of the hydrogels from time sweep experiment. (B) Elastic (G') and viscous (G'') moduli of the hydrogels over the frequency ranging from 0.1-100 Hz with a fixed 0.5% strain. (C) G' and G'' of the hydrogels over the strain ranging from 0.1-100% with a constant 1 Hz frequency. (D) The ratio of G'/G'' over 0,1-100% strain. The dash line indicates $G'/G'' = 1$	96
Figure 35 Degradation profile of SF and DMPG-SF hydrogels in the control media (HEPES buffer) and in the proteolytic media (1 unit/ml protease XIV in HEPES buffer). The symbol (*) indicates the significant difference at p -value ≤ 0.05	97

Figure 36 Proliferation profiles of (A) L929, (B) NIH/3T3, (C) SaOS-2 and (D) CaSki. The cells were cultured on tissue culture plate and the cell number was assessed by MTT cell metabolic activity assay.....	98
Figure 37 (Upper) Cell morphology after 24-h exposed to the extracts from the test materials (5, 10 and 15 mM DMPG-SF hydrogels), blank (serum-free DMEM), negative (DMEM/10% FBS) and positive (DMEM + zinc acetate) controls. (Lower) Cell viability percentage after exposed to the extracted media. The dash line indicates 70% viability, the cut-point for determining cytotoxicity of the materials according to the ISO standard.	99
Figure 38 Live/dead staining of encapsulated L929 cells in 10 mM DMPG-3% SF hydrogels at day 1 (A), 3 (B), 7 (C), 14 (D) and 21 (E). Green and red dots indicate live and dead cells, respectively. Scale bar = 100 μ m. (F) Morphology of encapsulated L929 at day 21. Blue and green stains represent nucleus and cytoskeleton, respectively. Scale bar = 50 μ m.	100
Figure 39 Proliferation profile of encapsulated (A) L929, (B) NIH/3T3, (C) SaOS-2 and (D) CaSki in the 5, 10, and 15 mM DMPG-3% SF hydrogels. The asterisk (*) represents the statistical difference at p-value \leq 0.05.....	103
Figure 40 Box plot of the size and size distribution of the liposomes comparing between after-prepared liposomes (black box) and the liposomes stored at 4°C for 2 weeks (red box)	107
Figure 41 TEM images of the liposome (A) A1, (B) B1, (C) C1 and (D) D1 (scale bar = 50 nm).....	108
Figure 42 (A) PDA and (B) MS spectra of standard cur. Curcuminoid contents of freshly prepared (clear column) and 2-week old (patterned column) liposomes presenting as (C) actual content and (D) the amount normalized by curcumin amount determined by colorimetric assay.....	109
Figure 43 SEM images and elemental analysis of sonicated SF hydrogel and Curcumin-SF hydrogel, and liposome-SF hydrogels (scale bar = 300 μ m).....	111
Figure 44 TEM images of liposome-3% SF hydrogels; (A) A1-SF, (B) B1-SF, (C) C1-SF and (D) D1-SF (scale bar = 100 μ m).....	112
Figure 45 Release of curcumin from sonicated Curcumin-SF hydrogels and liposome-induced SF hydrogels presented as (A) cumulative release amount of curcumin and (B) cumulative percentage release of cur	113
Figure 46 Stress-strain plots of the sonicated 3% SF and cur-3% SF hydrogels, and liposome-3% SF hydrogels. The hydrated samples were tested by the unconfined compression at room temperature.	113

Figure 47 Compressive mechanical properties of the sonicated SF and Curcumin-SF hydrogels, and liposome-SF hydrogels; (A) elastic modulus, (B) yield stress and (C) yield strain.....	114
Figure 48 The metabolic activity of (A) L929 and (B) MDA-MB-231 assessed by WST-1 assay in the indirect contact experiment. Cells were plated on the TCP and exposed to the release curcumin from the hydrogels. The alphabets indicate the statistic difference at p-value ≤ 0.05 comparing within the same time-point.....	114
Figure 49 Cell metabolic activity of (A) L929 and (B) MDA-MB-231 cultured on the hydrogels assessed by WST-1 assay. The number of cells evaluated by DNA quantification of (C) L929 and (D) MDA-MB-231, and (E&F) the metabolic activity normalized by the number of cells, reported only the results of cells cultured on TCP and SF hydrogels.....	115
Figure 50 Bright field and fluorescence images of stained L929 and MDA-MB-231 cultured on SF hydrogel for 1 and 3 days. Annexin V and 7-AAD staining is presented by green and red fluorescence, respectively. Scale bar = 50 μm	117
Figure 51 Bright field and fluorescence images of (A) L929 and (B) MDA-MB-231 of the indirect contact experiment after exposing for 1 day. The staining by annexin V (green) and 7-AAD (red) was performed (scale bar = 50 μm). Single staining by annexin V indicates the early apoptosis, while dual staining indicates the late apoptosis or cell necrosis.	118
Figure 52 Morphology of L929 cultured on tissue culture plate (TCP) and the hydrogels for 1, 3, 5 and 7 days (scale bar = 50 μm)	119
Figure 53 Morphology of MDA-MB-231 cultured on TCP and the hydrogels for 1, 3, 5 and 7 days (scale bar = 50 μm)	120
Figure 54 The amount of available sulfhydryl group assessed by Ellman reagent assay of regenerated SF and tSF solution after reacting with different 2-IT concentrations	121
Figure 55 Appearances of regenerated 3% SF (left vial) and 3% tSF (right vial) solution (no Au^{3+}), and Au-SF and Au-tSF mixtures with different Au^{3+} concentrations	122
Figure 56 Beta sheet content of freeze-dried (A) SF and (B) tSF hydrogels with different Au^{3+} concentrations determined from FTIR spectra in amide I region using FSD and curve-fitting techniques.....	123
Figure 57 Analysis of secondary structures of the freeze-dried hydrogels, including regenerated 3% SF and tSF hydrogels, and 0.5, 1, and 5 mM Au-SF and Au-tSF	

hydrogels using FSD and curve-fitting techniques of FTIR spectra in amide I region	124
Figure 58 (A) Fluorescence measurement (ex 320 nm/em 410 nm) of SF and tSF with different Au^{3+} concentrations, indication the formation of dityrosine (B) Amount of the available SH group of tSF mixed with various Au^{3+} concentrations. UV-vis absorbance spectra of (C) Au-SF and (D) Au-tSF mixtures, presenting the surface plasmon resonance band of AuNPs.	126
Figure 59 XPS spectra in Au4f region of (A) 1 mM Au-3% SF and (B) 1 mM Au-3% tSF, and (C) in S2p region of Au-tSF.....	127
Figure 60 The proposed mechanisms of Au^{3+} -mediated SF and tSF hydrogels. For Au-SF (upper), Au^{3+} was reduced to Au^+ by the amine groups. The proton-coupled transfer reaction was then occurred by an electron donation of tyrosine residues, resulting in a generation of protons and the formation of dityrosine. Au^+ was reduced to Au^0 and formed the AuNPs. An increase of protons led to a lower local pH, enhancing the SF chain aggregation and hydrogel formation. For tSF (lower), the reduction of Au^{3+} to Au^+ occurred. The Au^+ formed Au-S bonds without further reduction. The generation of protons from S-S and Au-S bond formation resulted in a beta sheet formation of tSF.	129
Figure 61 SEM images of the freeze-dried (A&B) 1 mM Au-3% SF and (C&D) 1 mM Au-3% tSF hydrogels	129
Figure 62 The complex (G^*), elastic (G') and viscous (G'') moduli of the regenerated and the mixtures with different concentrations of Au^{3+} , (A&B) SF and (C&D) tSF, collected over a range of frequency between 0.01-100 Hz with a fixed 0.1% strain	130
Figure 63 Metabolic activities of (A) L929 and (B) MCF-7 cultured on SF and tSF hydrogels with different Au^{3+} concentration. The cells cultured on TCP were regarded as controls.	131
Figure 64 The activation of caspase-3, a cell apoptosis marker, of MCF-7 cultured for 72 h on the samples (TCP, regenerated SF and tSF hydrogels, and 1 mM Au-3% SF (1SF) and 1 mM Au-3% tSF (1tSF)).....	132

Chapter 1

Introduction

1. Background and significance of the research problem

Structural or functional loss of an organ or tissue is a major unsolvable issue in human health care. So far, the treatment strategies are transplantation, surgical reconstruction, or using mechanical devices such as hemodialyzers. These therapeutic options are costly, ineffective, and unsustainable. Tissue engineering, firstly termed by Langer and Vacanti in 1993, has been introduced as the combination knowledge and technologies of engineering and health sciences toward the development of substitutes that restore, maintain, or improve tissue structures or functions [1]. Three core components in the tissue engineering field, known as the tissue engineering triad, are (1) isolated cells to facilitate tissue formation, (2) tissue-inducing substances to direct cell decision in growth or development, and (3) scaffolds to provide supporting substrates and mimic cellular microenvironments [1, 2].

Hydrogels are the three-dimensional polymeric matrices containing high content of water and a porous structure, which allow the exchange of gas, nutrients, biological substances, and waste with their surrounding environment. These systems resemble the characteristics of native extracellular matrix, making them suitable platforms as tissue-engineered constructs [3]. Additionally, drugs or bioactive molecules can be entrapped in the hydrogels, enabling the target delivery or controllable release kinetics. Hence, hydrogels are suitable biomaterial formats for broad applications in biomedical fields [4].

Several biomaterials from different origins (natural, synthetic or hybrid polymers) have been used to prepare different hydrogels depending on desired applications. The biocompatibility and biodegradability of natural polymers have attracted great attention for being used as biomaterials for scaffold preparation [5]. Among other natural polymers, silk fibroin (SF) gains lots of interest in biomaterial field from its large amount availability in nature, versatility in preparation, biocompatibility, excellent mechanical properties, and tunable degradability [6-8]. Intriguingly, the gelation of SF can be triggered via physical or chemical methods, with a controllable gelation time and defined properties of final hydrogels. Hence, SF hydrogels can be obtained *in situ* under mild, aqueous-based and cell-friendly conditions, enabling an application as engineered construct for homogeneous encapsulation of isolated cells [5, 9].

SF is a naturally derived biomaterial found in various arthropods, including larvae of Lepidoptera and spiders. Especially, SF from mulberry *Bombyx mori* silkworm cocoons occupies a prominent position, due to their historic production and uses as textile materials and surgical sutures [10]. The polypeptides of SF are composed of three domains, heavy chains, light chains,

and P25 glycoproteins with molecular weight of approximately 350, 25, and 30 kDa, respectively. Heavy and light chains are chemically linked by disulfide bridge, while P25 is physically associated as a complex with other domains [11]. Interestingly, the peptide of heavy chain consists of repetitive glycine-alanine sequences, leading to the formation of the thermodynamically stable structure through hydrophobic interactions and hydrogen bonding [11, 12]. To date, aqueous SF solution can be easily obtained by dissolving SF fibers in chaotropic agents [13-15], which disrupt hydrogen bonds and interfere hydrophobic interactions, to obtain random coil-dominated SF solution. However, the SF solution gradually undergoes structural transitions from unordered structure to beta sheet conformer within several days or weeks, leading to gel formation [16]. Several methods have been introduced to accelerate the gelation process of SF. Physical methods, such as a pH perturbation [16, 17] or the introduction of physical stimuli can induce SF structural transitions, leading to subsequent gelation. Similarly, many chemical additives, e.g. surfactants, polymers, or enzymes, are effective in accelerating the SF gel formation by intriguing self-assembly or covalent crosslinking.

Although physical strategies allow a controllable gelation time and good biocompatibility without the presence of other chemicals, the requirement of equipment (e.g. probe sonicator or vortex mixer) may be inconvenient for some clinical requests. Chemical additives, therefore, have become interesting alternatives since the SF gelation occurs by simple mixing SF solution with chemical inducers. Additionally, hydrogel formation can be optimized to take place within desired time. In this work, the rapid gelation of SF was achieved by an addition of a phospholipid or a crosslinking by a gold salt. The gelation mechanisms and the biocompatibility of the obtained hydrogels were proven.

Phospholipids are biological substances which function as the components of physiological membrane to preserve cell integrity and as surfactants to maintain homeostasis [18, 19]. Anionic phospholipids are found to bind with cellular proteins and transform the protein conformation which lead to different protein activities [20]. Various *in vitro* studies reveal the role of an anionic phospholipid, phosphatidylglycerol (PG), in inducing conformational transitions of several water-soluble. The electrostatic and/or hydrophobic interactions between lipid-proteins complexes are proposed as major driving forces in inducing the changes of protein conformers [21, 22].

In this work, the effects of a PG on the gelation of SF and the mechanisms were extensively investigated. A PG with 14-carbon atoms, 1,2-dimyristoyl-*sn*-glycero-3-phospho-(1'-*rac*-glycerol) sodium salt (DMPG), was selected. The properties of obtained hydrogels, including micromorphology, mechanical properties, degradability, were thoroughly examined. In addition, the cytocompatibility testing was conducted using different cell lines by cell encapsulation to evaluate the potential of the hydrogels as cell-laden constructs.

Metal-induced SF gelation was reported using a transitional metal salt, Fe^{2+} , which induces the formation of dityrosine linkage [23]. Gold (Au) salt

(the most stable form is Au^{3+} or Au(III)) is commonly used as a substrate for the production of gold nanoparticles. The reduction of Au^{3+} to Au^0 and subsequent nanoparticle formation can be caused by various functional groups such as amine, hydroxy, and phenoxy, which are typically found in several biological molecules [24].

Thiol is another reactive group with various functional groups including Au. Thiol-functionalized polymers were reported to form the hydrogel network with a presence of Au^{3+} . A reduction of Au^{3+} to Au^+ together with the generation of Au-S and S-S bonds were proposed [25, 26]. In this work, thiol-functionalized SF was synthesized by a chemical reaction. The gelation of regenerated SF solution with Au^{3+} was investigated, comparing to the thiolated SF. Gelation mechanisms were explored as well as the cytocompatibility of the developed hydrogels to prove the feasibility in using for biomedical applications.

2. Objectives of the research

- 2.1. To investigate the effects of phospholipid and a gold salt on the gelation mechanisms of silk fibroin and the properties of the obtained hydrogels
- 2.2. To determine a cytocompatibility of phospholipid-induced silk fibroin hydrogels, a gold-mediated regenerated silk fibroin and thiolated silk fibroin hydrogels

3. Scope of the research

The study is divided into three main parts according to the gelation systems as follow.

Part I: Phospholipid-induced silk fibroin hydrogels for cell carrier application

The regenerated SF solution, prepared from cocoons of Thai silkworms Nangnoi Srisaket 1, was mixed with a phospholipid DMPG, and the gelation kinetics were observed. The lipid concentration, lipid component and a perturbation by a divalent cation to the gelation time of SF were investigated. The gelation mechanisms were determined from the transition of protein secondary structures, protein folding and the protein-lipid interaction.

Hydrogel characteristics, including microstructures, viscoelasticity, and biological degradation, were evaluated. The cytocompatibility of the hydrogels was confirmed using an indirect cytotoxicity assay according to ISO 10993-1, before performing cell encapsulations. Four types of cell lines were loaded in the hydrogels and cultured for 21 days. The viability and proliferation of the encapsulated cells were determined.

Part II: Liposome-induced silk fibroin hydrogels for drug delivery system

Continuing from Part I, DMPG-based liposomes were prepared and used as a drug carrier and a gelation enhancer. Curcumin was chosen as a model drug for encapsulation. Liposome geometry and encapsulation efficiency of

curcumin were evaluated with the variations of liposome ratio between DMPG and DMPC, and an addition of cholesterol in the liposome formulations. Subsequently, liposomes were used to induce the gelation of SF. The obtained hydrogels were determined for their micromorphology and mechanical properties.

The bioactivity of curcumin was confirmed by the liquid chromatography/mass spectrometry. The release kinetics of curcumin from the liposome-entrapped hydrogels were determined. Cell culture experiment was performed using L929 mouse fibroblasts and MDA-MB-231 human breast cancer cells. The viability and proliferation as well as apoptotic events of cells after exposed to curcumin release from the hydrogels were evaluated.

Part III: Gold-induced silk fibroin hydrogels and the cytocompatibility of hydrogels

Firstly, SF was functionalized with thiol groups using a chemical reaction, and the obtained biopolymer solution was analyzed for the amount of conjugated thiol. The gelation of regenerated SF solution induced by Au³⁺ was evaluated, comparing to the thiolated SF solution. The formation of dityrosine bonds and the structural transition during the gelation were investigated to reveal the mechanism of gelation. Physical and biological properties of the obtained hydrogels were then investigated. The cytocompatibility test of the hydrogels with L929 and MCF-7 human breast cancer cells was conducted to assure the potential as substrates for biomedical uses.

4. Expected benefits

- The rapid gelation of SF solution is achieved using a phospholipid or a gold salt as chemical inducers, and the mechanisms of gelation are explored.
- The obtained hydrogels are appropriate for further uses as tissue-engineered constructs or drug carriers, being biocompatible and bioactivities.
- The developed hydrogels can be used as cell culture substrates or cell-laden constructs which support cell growth and tissue development

Chapter 2

Literature Reviews

1. Biomaterials

1.1. Biomaterials for tissue engineering

To treat structural or functional loss or failure of tissues or organs, organ transplantation, surgical reconstruction, or using mechanical devices have been generally performed by physicians. However, several limitations are evidenced. For example, the shortage of donor is a major restriction of transplantation. Surgical reconstruction would lead to long-term complications, and mechanical devices cannot completely replace tissue functions or prevent disease progression. In 1993, Langer and Vacanti termed “tissue engineering” [1], which is an interdisciplinary field combining the principles of engineering and life sciences with an intention to restore, maintain, or improve tissue function. Tissue engineering composes of three milestones, including isolated cells, signaling molecules, and scaffolds [2]. A source of cells has been used to facilitate tissue formation and directed to proliferate or differentiate by the presence of defined regulatory signals. Scaffolds provide structural support for tissue growth and development [1, 2]. Tissues in all germ layers (ectoderm, mesoderm, and endoderm) can be engineered. The followings are the tissues to which tissue engineering has been applied; ectodermic layer includes tissues in nervous system, cornea, and skin, mesodermic layer includes cartilage, bone, muscle, blood vessels and related cells, and endodermic layer includes liver, pancreas, and tubular structures [1].

The essential role of biomaterials in tissue engineering is to serve as a structural support for cells and allow them to function appropriately. Polymeric scaffolds provide a very large surface area per unit volume, allowing a delivery of high cell density to the defected tissues. Ideally, cells can be obtained from patients in a small amount, multiplied them *in vitro*, and placed back to the patients with high cell content. By doing this, the limitation of donor shortage is overcome, and the cells can function better due to sufficient cell-cell and cell-material interactions [27].

The additional advantage of polymeric biomaterials is an ability to serve as smart biomaterials which response to external stimuli. Functional groups of the material can be modified to achieve desired physical, chemical, and biological properties. For example, biomaterials with thixotropic and self-healing properties are developed for injectable applications, namely minimally invasive administration to patients. Self-healing and shape memory also prevent materials from mechanical damage while served as load-bearing tissue constructs. The degradability of materials can be tuned to match cellular remodeling processes under physiological conditions. Cell binding affinity to the materials is enhanced by the conjugation of cell adhesion motifs, such as

RGD or IKVAV sequences [3]. Recently, biomaterial sealant or glue which can attach to several biological surfaces are developed by the incorporation of dopamine-based groups [28].

1.2. Biomaterials for drug delivery

Drug delivery systems (DDS) are designed to modulate pharmacokinetics of drugs and reduce undesired effects. Polymeric materials are, therefore, implemented as drug delivery carrier to control drug release profile, confine drug accumulation for local therapeutics, or modulate drug release upon an activation of external stimuli. Active macromolecules, such as therapeutic proteins and oligonucleotides, typically have a very short half-life after administration, because of the first pass metabolism, as well as a difficulty in penetration through physiological barriers. Hence, an encapsulation in well-designed biomaterials can enhance drug stability and prolong drug release until optimum therapeutic effects are obtained.

Another benefit of polymeric biomaterials in DDS is that they can be modified to response specific stimuli and triggered drug release upon an activation. Stimuli can be pH, temperature, magnetic field, ultrasonication, or specific receptors at each target site. Moreover, the degradation of materials can be modulated with enzyme-specific linkage, such as matrix-metalloprotease, which presents numerously at tumor site. Therefore, the carrier can allow site-specific drug release and limit systemic adverse events from entrapped chemotherapeutics [27, 28].

1.3. Biodegradable polymers as biomaterials

Natural polymers, composed of DNA, proteins, and polysaccharides, are widely used as the substrates for biomaterial fabrication [5]. Furthermore, synthetic polymers have been attracted for tissue engineering from their controllable and reproducible chemistry and properties. An overview of biodegradable polymers which are frequently applied as biomaterial bases is given below.

1.3.1. *Proteins or natural-origin polypeptides*

a. Collagen and gelatin

Collagen is a protein which was the first material used in tissue engineering as it is a major component of mammalian extracellular matrices. Collagen-based scaffolds have been applied for several target tissues or organs, including bladder, blood vessel, bone, cartilage, cornea, heart, ligament, pancreas, and skin. However, collagen gels are mechanically weak and easily undergo biological degradation by collagenase. Physical and chemical crosslinks are required to overcome those issues [4]. In addition, different formats can be fabricated depending on target tissues. For example, cylindrical tubes have been developed for blood vessel regeneration [29].

Several collagen-based medical devices have been approved by FDA. Artificial skin grafts were the first engineered products launched for skin

tissue engineering or cosmetic purposes, namely Apligraf[®], Revitix[™], VCTO1[™] and FortaDerm[™] by Organogenesis, USA. Furthermore, collagen-based scaffolds are introduced as bone substitutes. The launched products are exemplified as following; inFUSE[®] (Medtronic Sofamor Danek, USA), Collagraft[®] (Angiotech Pharmaceuticals, Canada), Healos[®] (Depuy Orthopedics, USA), and Biomend[®] (Integra LifeSciences, USA) [30].

Derived from collagen, gelatin is a partially hydrolyzed product of collagen through acidic or basic hydrolysis. According to its thermo-responsive sol-gel mechanism, gelatin provides a wide variety of applications from foods to pharmaceutical and biomedical products. Because the transition temperature of gelatin is around 30°C, crosslinks are required to prevent dissolution at physiological temperature. Several crosslinkers, e.g. glutaraldehyde, carbodiimides, genipin, have been used. Furthermore, methacrylamide-functionalized gelatin was developed since its methacrylate group can be photochemically crosslinked upon UV irradiation [29].

The mostly recognized gelatin-based product is Gelfoam[®], developed by Phizer, USA, as a hemostatic sponge. Gelatin microspheres are launched, e.g. CultiSpher-G[®] (Percell Biolytica, Sweden), to serve as microcarrier cell culture beads [30].

b. Fibrin and fibrinogen

Fibrinogen is a component in blood plasma relating to clotting cascades. During the cascades, fibrinogen is cleaved by thrombin, yielding a fibrin, a protein monomer which can polymerize into blood clots. Due to high cell affinity as well as it autologously obtainable, fibrin and fibrinogen are being used as a biological sealant for surgery wounds. Several fibrin sealants are commercialized, namely Tisseel VH[®] by Baxter, USA, CryoSeal[®] by Thermogenesis, USA, and Vivostat[®] by Vivolution, Denmark [30].

Moreover, fibrin can be applied as a base material for cell carrier from its inherent properties supporting cell adhesion, migration, and proliferation. The materials can be rapidly remodeled and replaced with newly formed tissues. However, fibrin and fibrinogen scaffolds showed fast degradation, which limits the application as shape-retention scaffolds [30].

c. Elastin

Elastin is a protein containing a repetitive sequence of VPGXG, where X is any natural amino acid residue except proline. This characteristic results in outstanding elastic properties which are appropriate for mechanically active tissues, such as tendon, blood vessel, and elastic cartilage. Moreover, elastin can be bulk-produced using the genetic recombination, which the amino acid sequences can be modified for better cell-interactive properties by inserting RGD motif into recombinant elastin [29].

d. Silk

Silk biomaterials, mainly referred to silk fibroin (SF), are obtained from several arthropods, namely silkworms or spiders. In the primary structure of

SF, a high ratio of hydrophobic amino acid residues, such as glycine and alanine, is noticed, and the arrangement of hydrophobic sequences influences its characteristic secondary structure. The strong and stable beta sheet is formed, resulting in an excellent mechanical property and slower degradability, comparing to other natural polymers. Additionally, SF protein can be processed into several formats, e.g. films, nanofibers, scaffolds, gels and powders. SF-based materials have been increasingly explored for the applications in several purposes, such as the tissue engineering of tendon, bone, cartilage or ligament, and drug delivery system [6, 29]. The information related to SF will be extensively discussed in the next sections.

1.3.2. Polysaccharides

a. Alginate

Alginate is the polysaccharide derived from brown algae, consisted of β -D-mannuronic acid and α -L-guluronic acid monomers. Alginate solution rapidly solidified from the addition of multivalent cations, leading to the wide applications for the biomedical-related purposes, especially as microcarriers for cell encapsulation. However, alginate does not support cell adhesion or growth. The strategies to combine alginate with RGD-containing materials or growth factors are applied to facilitate cell-material interactions [29].

Alginate is one of the most biomaterials which are widely studied and applied due to its abundance in nature and the ionic gelation characteristic. Wound dressing products developed from alginate are commercially available, namely Nu-Derm[®] (Johnson & Johnson, USA), Curasorb[®] (Kendall, USA), AlgiSite[®] (Smith & Nephew, USA) and geniaBeads[®] (Genialab, Germany). Apart from the skin applications, alginate beads were launched as cartilage tissue-engineered constructs by Articular Engineering LCC, USA for research purposes [30].

b. Chitosan

Chitosan is a partially deacetylated derivative of chitin which originates from the shell of arthropods. Its pH-dependent gelation, including thermo-responsiveness when in combination with polyol salts, provides wide applications in biomedical field. Bone, cartilage, and skin tissue regeneration are the main targets of using chitosan as a part of scaffolds. Inorganic materials (e.g. calcium phosphates), synthetic polymers (e.g. poly(L-lactic acid), poly(butylene-succinate)), and ceramics (e.g. hydroxyapatite) are incorporated to the chitosan-based scaffolds to improve mechanical properties. The presence of glycosaminoglycans in chitosan hydrogels is used as the main strategy for cartilage regeneration. Collagen and its derivatives thereof are used in combination with chitosan for skin repair [29].

c. Hyaluronan

Hyaluronan, so called hyaluronic acid or HA, is a major component found in extracellular matrices of skin, cartilage, and vitreous humor. HA is a non-sulfated glycosaminoglycan, composed of D-glucuronic acid and D-N-acetylglucosamine which are linked by alternating β -1,4 and β -1,3 glycosidic

bonds. The commercially available HA products are found with different molecular weight and crosslinking degrees, resulting the differences in mechanical properties and biological response. Therefore, the properties of HA can be adjusted upon the purposes to match target tissues. HA with high load-bearing properties are launched for cartilage engineering, e.g. Hyalgan[®], Hyalubrix[®] (Fidia, Italy) and Artz[®] (Seikagaku Corporation, Japan). A viscoelastic HA gel is developed for wound dressing, such as Bionect[®] (CSC Pharmaceutical, USA) and Jossalind[®] (Hexal, Germany) or for intraocular application, namely Healon[®] (Advanced Medical Optics, USA), Opegan R[®] (Seikagaku, Japan), Opelead[®] (Shiseido, Japan), and Orthovisc[®] (Anika, USA) [30]. Scaffolds fabricated from HA or its combination with other polymers were studied and reported in several biomedical applications, such as bone, cartilage, heart, nerve, liver, muscle, skin, and vascular tissue engineering, and gene therapy [29].

d. Chondroitin sulfate

Chondroitin sulfate is a glycosaminoglycan consisted of alternating monomers of N-acetyl-D-galactosamine and D-glucuronic acid. As chondroitin sulfated is water-soluble, the crosslinking processes are required. Carbodiimide protocols, namely EDC/NHS, are popularly used to crosslink chondroitin sulfate with the presence of amine-containing materials, such as collagen, gelatin or 1,12-diaminododecane [29]. The combination of chondroitin sulfate with other polymers, including gelatin or hyaluronan, were reported to be more advantageous in the applications of controlled release system and tissue regeneration, e.g. cartilage, heart, liver, lung, skin, and intervertebral disk.

In addition to commercially available products as nutritional supplements for osteoarthritis, chondroitin was approved as a skin substitute for burn wounds. A well-known product is Integra[®] developed by Integra LifeSciences, USA [30].

1.3.3. Synthetic polymers

a. Poly(glycolic acid), poly(lactic acid) and their co-polymers

Poly(glycolic acid) (PGA) is an aliphatic polyester with high crystallinity, resulting in a high melting point, high tensile modulus, and a resistance to organic solvents. Another polyester is poly(lactic acid) (PLA) with an additional methyl group on its monomer, leading to high hydrophobicity. The crystallinity and hydrophobicity are tunable by the copolymerization of PGA and PLA. By doing this, the morphological features of the copolymers are affected due to the changes of the hydration as well as the degradability by hydrolysis [31, 32].

PGA, PLA, and the copolymers PLGA are non-enzymatic degradable materials, but they undergo simple hydrolysis due to their ester backbone. The degradation products compose of carbon dioxide and water, which are safe metabolites and can be excreted via kidneys [31]. Thus, these materials are approved for human uses, such as medical sutures. Interestingly, PLGA

exhibits a good cell affinity and proliferation, making it suitable for tissue engineering applications [32]. PLGA can be combined with other materials, such as collagen, and fabricated as a scaffold serving as a tissue-engineered construct.

b. Poly(caprolactone)

Poly(caprolactone) (PCL) is a semi-crystalline aliphatic polyester with low melting temperature (55-60°C) and glass transition temperature (-60°C). The good solubility and compatibility with organic solvents of PCL make it feasible to mix with several polymers. PCL can be degraded by microorganisms and hydrolysis under physiological conditions. However, it takes approximately 2-3 years for completing the degradation. Therefore, PCL-based materials are developed for long-term medical devices or drug-delivery vehicles. For example, Capronor[®] is a PCL-based contraceptive device to slowly deliver levonorgestrel. Additionally, PCL can be blended with PLA, PGA or PLGA, or copolymerized with lactic acid to adjust the mechanical properties and accelerate the degradation rate [31, 32].

c. Poly(dioxanone)

Another polyester, poly(dioxanone), was developed for the fabrication of monofilament sutures, instead of multifilament sutures from PLA or PGA. The monofilament sutures outperform the conventional sutures in lowering risk of infection due to the friction at penetrating tissues. Furthermore, poly(dioxanone) was investigated for serving as fixation screws in bone applications. The degradation of this polymer is controlled by non-specific hydrolysis of ester bonds. Its metabolite composes of glycoxylate which is excreted via kidneys or further metabolized to glycine and to carbon dioxide and water as in PGA [32].

d. Poly(propylene fumarate)

A co-polyester, poly(propylene fumarate) (PPF), was developed to serve as a high-strength biomaterial for orthopedic applications. PPF can be hydrolyzed by the ester cleavage and its degradation products are non-toxic fumaric acid and propane diol. An available unsaturated fumarate groups in PPF enable a crosslinkable point with other polymers. For instance, acrylic monomers, e.g. methacrylate or N-vinyl pyrrolidone, can be co-polymerized with PPF, and the mechanical strength of the obtained co-polymers is significantly enhanced [32].

2. Hydrogels

Hydrogels are hydrated and porous 3-dimensional scaffold which mimic extracellular matrix. These organizations mimic cellular microenvironments and provide supports for cellular adhesion and proliferation, differentiation and new tissue formation [3, 4].

The emerging trend of using hydrogels in tissue engineering is cell-laden hydrogels, where living cells can be added in an aqueous-based precursor prior

to gelation under mild and cell-friendly conditions. Cells can be encapsulated and cultured in a 3-dimensional structure which closely resembles natural tissues [4, 5]. The gelation mechanisms include covalent or ionic crosslinking or self-assembly via physical bonds [5]. Besides, hydrogels can be injected through a needle directly into critical defects, resulting in a minimally invasive mode to promote regeneration [3].

Ideally, scaffolds used for tissue engineering, should support cell activities, including attachment, proliferation, and differentiation. They should be biocompatible, inducing no or low immune-related reactions when applied *in vivo*. The biodegradability of materials should match neo-tissue formation rate with non-toxic degradation by-products. Additionally, materials for scaffold fabrication should provide versatile processing options into various formats with tunable structure and morphology [33].

Moreover, hydrogels can be used as barriers to protect the encapsulated cells from host's immune system [4]. They can be applied as space-filling scaffolds to prevent adhesions after surgery, since hydrogels can maintain their volume and structural integrity for the a required time period [3].

Drugs, cell-signaling molecules, and biological factors can be loaded and the release of such loaded entities from hydrogels can be delivered to surrounding cells in a controllable manner [4]. Loaded substances can be released by either diffusion, mechanical stimulation, or hydrogel degradation [3].

2.1. Required properties of hydrogels for biomedical uses

2.1.1. *Water absorption and mass transportation*

Water in the hydrogels can be classified as bound and free water. Bound water represents the water molecules binding to either hydrophilic or hydrophobic groups of polymer chains. The additional water that fills the space between network chains, pores, or voids, is regarded as free or bulk water. Typically, water molecules presenting in the hydrogels determine the mass transportation, by absorption or partition into the hydrogels and the diffusion of the entrapped molecules to the surrounding [34].

The amount of free water relates to the pore characteristics of the hydrogels, including pore size, pore distribution and interconnectivity. These characteristics are influenced by the composition and the crosslinking density [34]. Consequently, the pores filled with water molecules as medium determine the diffusion distance of the molecules according to the size, as defined by Stoke radii [3, 34]. Small molecules display a higher diffusion coefficient than that of macromolecules, such as proteins, growth factors or biological wastes.

2.1.2. *Mechanical stability*

Typically, hydrogels are used to fill the space where natural tissues were occupied. Therefore, the hydrogels should provide a structural integrity to bear load at implanted site as well as a micro-mechanical properties which facilitate

a proper response of biological tissues [3]. The mechanical characteristics of the hydrogels are usually dictated from the inherent properties of the polymers and the crosslinking methods. The surrounding conditions, such as temperature and pH, and the properties of hydrogels from swelling or degradation also influence the mechanical performance of the hydrogels.

One of the main factors attributed to the mechanical properties of hydrogel is the concentration of polymer solution. An increasing of polymer fraction enhances the hydrogel strength significantly due to the denser hydrogel networks. Silk fibroin hydrogels prepared by temperature-, sonication- and vortex-induced gelation displayed a higher compressive modulus as an increasing fibroin content [16, 35, 36]. A crosslinking type and density also attribute to mechanical properties of obtained hydrogels. Alginate ionically crosslinked with a high ion concentration or using higher affinity divalent ions showed a high mechanical strength [3]. For self-assembly polymers, such as silk fibroin, a transition of secondary structure significantly changes the mechanical status of the hydrogels. Take the crosslinked silk fibroin hydrogels by either metals or biological enzymes as examples, the predominated random coil structure existed as prepared before gradual transition to highly stable beta sheet within 7-10 days. The compressive or elastic modulus increased with a higher beta sheet content [23, 37], indicating the relationship between the formation of highly stable structures with the mechanical properties of the hydrogels.

The conditions of the hydrogels, including the hydration state, the storage temperature, the degradation or dissolution of hydrogels, obviously influence the mechanical strength [3]. Hydrogels in dry state usually possess a higher strength than in hydrated state [38]. The mechanical properties of hydrogels composed of thermo-sensitive polymers, such as gelatin, can be changed upon different surrounding temperature [39]. Moreover, the mechanical strength is typically deteriorated with a degradation or dissolution of the hydrogels, due to the loosen or weakening of hydrogel matrix [3].

Recently, hydrogels with thixotropic and self-recovery properties have gain lots attention due to their potential of injectability and 3D printing. The hydrogels show low viscosity when shear stress is applied and regain their initial mechanical strength after stop applying shear. The weak and reversible bonds, namely electrostatic forces, hydrogen bonding, and hydrophobic interaction, play an important role in the shear-thinning and self-healing of the hydrogels [40].

2.1.3. Biodegradability

In tissue engineering, the degradation of hydrogels is required for enabling matrix remodeling which is important for the functions of tissue as well as the tissue ingrowth and new tissue formation. Furthermore, the release of encapsulated substances in hydrogels is dictated by the rate of degradation. Hence, it is worth noting that tuning the degradability of the hydrogels to match their functionality is crucial. Degradation by hydrolysis, enzymatic cleavage, and dissolution are three basic mechanisms for biomaterial

degradation [3]. More importantly, the degradation products of the polymers and any leachable moieties must be non-toxic to confirm the biocompatibility of the hydrogels [41, 42].

2.1.4. *Biocompatibility and bioactivity*

Biocompatibility is a key property of biomaterials. It is defined as the ability of materials in inducing an appropriate host immune response in a specific application. Another term, biotolerability, is also used to refer to a material that resides for a long period with a low immunological response [41].

Generally, biomaterials used for hydrogel fabrication are proven for their non-toxic. However, some materials do not support cell adhesion and functions, such as proliferation, migration, and differentiation, due to the lack of cell adhesion receptors. Furthermore, the hydrophilic nature of the materials hinders the adsorption of ECM proteins, e.g. laminin, fibronectin, and vitronectin, which usually act as linkers for cell adhesion on the substrates. To promote the bioactivities of the hydrogels, several cell-recognized amino acid sequences, e.g. RGD, REDV, YIGSR, IKVAV, are conjugated covalently. Moreover, some growth factors which facilitate specific cellular functions, such as transforming growth factor- β (TGF- β) or bone morphogenic protein-2 (BMP-2), are covalently attached or incorporated to hydrogel polymers [3, 42].

2.2. Hydrogel formation

2.2.1. *Covalent crosslink*

Photo-crosslinking method has been introduced as a cell-friendly hydrogel formation method for more than a decade. With a conjugated photo-sensitive groups, e.g. acrylate or methacrylate, and a presence of photo-initiator, a formation of hydrogel networks from chain polymerization with entrapped water molecules occurs readily upon an irradiation of UV or visible light. This approach is potentially used for drug-releasing hydrogels, especially for delivery of proteins. Furthermore, if the polymerization takes place at physiological tissues, an adherent hydrogel forms, due to the interactions with extracellular proteins. This leads to promising applications as sealants to prevent fibrosis or scar adhesion for wound care or after surgery [43, 44].

Enzymatic crosslinking is another feasible approach for enhancing the gelation. Polymers with a presence of phenol-containing groups, such as tyramine, tyrosine, or L-3,4-dihydroxyphenylalanine (DOPA), can be crosslinked by horseradish peroxidase (HRP) using H_2O_2 or other reactive oxygen generators. Phenol moieties are then conjugated through a carbon-carbon bonding at the ortho position or carbon-oxygen at the phenoxy group. The crosslinking method is performed under mild conditions, which is favorable for cell encapsulation or *in situ* gelation [43, 45].

Transglutaminase can be used to crosslink between amino groups and gamma-glutamyl groups, due to its catalytic process via an acyl transfer

reaction. Therefore, the enzyme is used to crosslink between lysine residues and glutamine. Proteins or polypeptides with a high content of these amino acid residues, such as gelatin and soy protein, can form an *in situ* hydrogel using transglutaminase as a crosslinking enzyme [44].

There are several enzymes reported for their uses in the hydrogel formation. Phosphatase is utilized as a gelation enhancer of phosphate-rice biopolymers. This enzyme catalyzes dephosphorylation reaction, leading to a decreased water solubility. Hence, the hydrophobic interaction is enhanced, and the gelation is accelerated. Tyrosinase is used to oxidize tyrosine residues presenting in proteins or polypeptides to quinone groups, which are reactive groups. The quinone is then react with available amino groups or other tyrosine to form a stable hydrogel network [44].

Instead of using crosslinkers, such as glutaraldehyde, carbodiimide, or genipin, which are toxic to cells and tissues, a click chemical crosslinking can be used. Thiol groups are one of the functional groups chosen for gel forming application because they can undergo Michael addition reaction with various groups. Thiol groups spontaneously form bonds with vinylsulfone or acrylate groups, and they themselves can form disulfide bonds from the oxidation. Since, the bond formation occurs under mild conditions, polymers functionalized with these functional groups are mixed with other polymers with thiol groups to form hydrogel networks. Another chemical crosslinking is hydrazone formation by the Schiff's base formation between aldehyde-functionalized polymers with hydrazide groups [43].

2.2.2. Ionic gelation

Alginate is a well-known biomaterial which readily forms a hydrogel with an addition of divalent or polyvalent cations. The monomers of alginate include β -D-mannuronic acid (M) and α -L-glucuronic acid (G), which G moieties form complexes with cations, leading to a crosslinking. Therefore, the gelation rate and the structural integrity of obtained alginate hydrogels are dictated by the ratio of G presenting in alginate. Additionally, the type and number of cations used for the crosslinking process affect the properties of the obtained hydrogels. Calcium is the most used cation for inducing the gelation of alginate. Different calcium salts result in a different gelation kinetic. Rapid gelation but inhomogeneous and mechanically weak is obtained when CaCl_2 is used, while CaCO_3 and CaSO_4 induce a slower gelation with more homogeneous [42, 43].

Additionally, chitosan hydrogels can be obtained by ionic gelation as well as chemical crosslinking using glutaraldehyde. The gelation of chitosan can be achieved by mixing polycationic chitosan with metallic anions, e.g. Pt (II), or tripolyphosphate [43].

2.2.3. Thermo-gelation

Thermo-sensitive hydrogel is one of the physically crosslinked gelation mediated by the change of temperature. Various natural polymers are reported for their thermo-sensitive phase transition, namely cellulose derivatives,

chitosan, and gelatin. In some synthetic polyesters, namely Pluronic[®], a block copolymer of poly(ethylene oxide) and poly(propylene oxide), PEO-PLGA, PLGA-PEG-PLGA block copolymers, an increasing of the temperature leads to a dehydration of polymer chains. Therefore, the distance between chains is reduced, enhancing hydrophobic interactions and subsequent gel formation. Furthermore, some polymers possess a lower critical solution temperature (LCST), which the gelation occurs at the temperature above LCST. This phenomenon is found in poly(*N*-isopropylacrylamide) (pNiPAAm) and poly(2-hydroxypropyl methacrylamide) [42, 43].

2.2.4. *Self-assembly*

Self-assembly hydrogel system is defined as a gel formation by the innate properties of polymers without a utilization of crosslinking agents or initiators. Typically, hydrogel network formed by self-assembly is resulted from supramolecular interaction rather than covalent bonding, leading to a mechanically weak hydrogel. Self-assembly is commonly found in amphiphile polymers since they possess both hydrophilic and hydrophobic domains. In aqueous medium, polymers readily assemble to the lowest interface energy by exposing the hydrophilic domains to the environment and hiding the hydrophobic parts from water molecules [42].

3. Silk biomaterials

3.1. Historical aspects of silk biomaterials used as medical devices

Silk has been well known as a textile material since 2,700 B.C. in China, before spreading throughout Asia, Europe, and Africa. Silk is a fibrous protein produced by various arthropods, in 113,000 species of insects in lepidoptera and 30,000 species of spiders in araneae [10, 46]. Due to outperformed mechanical properties, high elasticity and wear resistance, comparing to other fibrous proteins [6], such as collagen, silk is not only used for textile manufacturing, but, recently, also implemented as medical devices. The firstly introduced silk-based medical device is suture. Typically, silk proteins used for biomedical purposed are derived from mulberry silkworms, wild silkworms, and spiders. The difference in term of physicochemical properties and applications between the silk obtained from different species are described in the next section.

3.2. Classification of silk fibroin by the origin

3.2.1. *Silkworm silks*

Silkworms can be classified into 2 groups either from their habitat, including domesticated and wild silkworms, or the feeding behavior, namely mulberry and non-mulberry silkworms. Silkworm larvae and cocoons of mulberry and non-mulberry silkworms are presented in **Figure 1**.

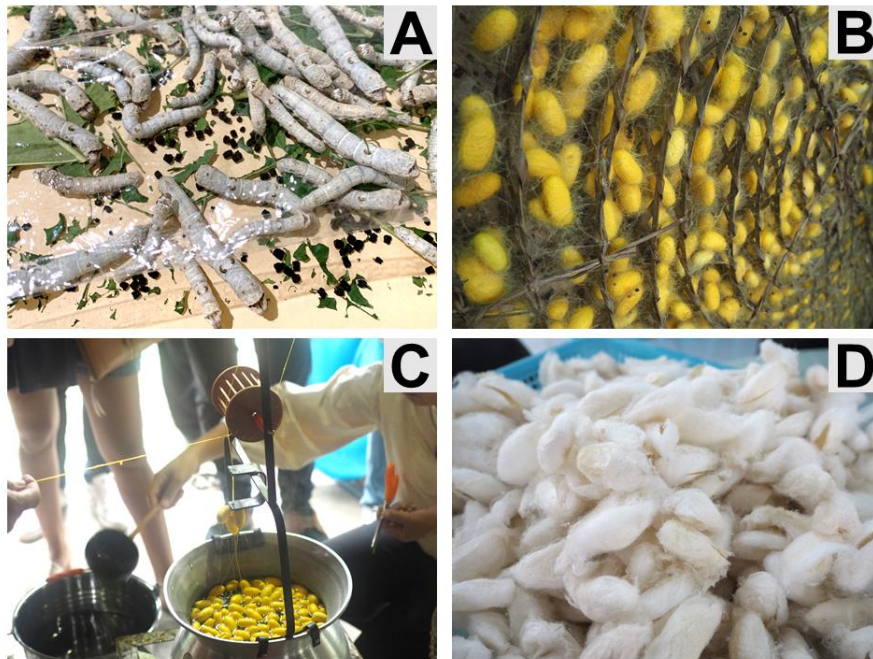


Figure 1 (A) Larvae of *Bombyx mori* silkworms, (B) Thai silkworm cocoons, (C) traditional method to extract silk fibers in textile manufacturing using warm soap water, and (D) non-mulberry silkworm cocoons (Photo in figure A was taken from Yokohama silk museum, Yokohama, Japan, and figure B, C, and D were taken from Queen Sirikit sericulture center, Saraburi, Thailand)

a. Non-mulberry or wild silkworm silks

Silkworms resided in the wild and fed by various plants are recognized as non-mulberry or wild silkworms. In this group, there are several species of silkworms which can be identified into 2 major groups, tasar and eri silkworms. Tasar silkworms include the silkworm in genus *Antheraea*, namely *A. mylitta*, *A. frithi*, *A. pernyi*, *A. proylei* and *A. yamamai*, and the example specie of the eri silkworms is *Samia (Philosamia) ricini* [10].

b. Mulberry or domestic silkworm silks

Mulberry silkworms are classified from their feeding habit limited to plants in genus *Morus*, such as mulberry leaf. These silkworms are Bombycidae species, and all of them are bred domestically since they cannot survive in nature [10]. **Figure 2** showed the cocoons of *Bombyx mori* silkworms obtained from different strains. Different shape, size and color can be noticed. Noticeably, cocoons of Chinese and Japanese are white and larger than those of Thai domestic strains. The characteristic of Thai silk cocoons is yellow color, which results from carotenoids presenting in silk glue. Most of yellow pigments are accumulated in sericin protein. Therefore, the dyes can be bleached during degumming process and the residual can be eliminated with simple washing [47].

In this study, silk fibroin (SF) extracted from *B. mori* silk cocoons was used as a base material for hydrogel fabrication. Physicochemical and

biological characteristics of *B. mori* silks are described in the following sections.

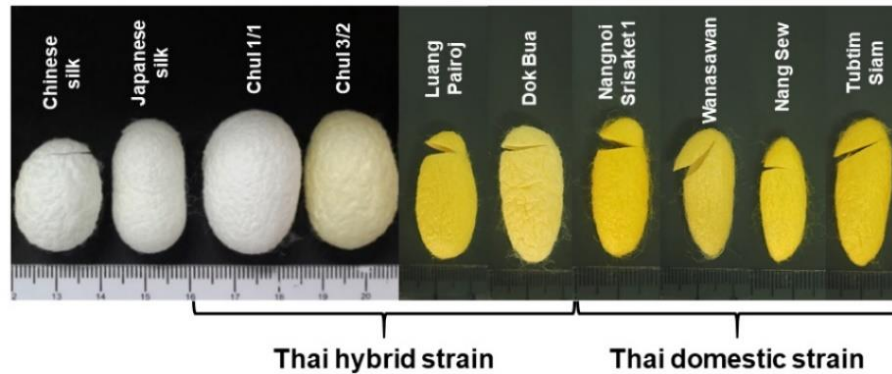


Figure 2 *Bombyx mori* silk cocoons from different strains, namely Chinese, Japanese, Thai hybrid, and Thai domestic strains (Photos of silk cocoons were taken from available strains in Biomaterial Engineering for Medical and Health Research Unit, Faculty of Engineering, Chulalongkorn University, Thailand)

3.2.2. Spider silks

Spider silks are known for their excellent mechanical properties. However, due to difficulty in large-scale productions, the textile manufacturing of spider silks is impossible. Recently, the outstanding characteristics of spider silks have intrigued biomedical researchers to implement them as medical devices.

Spiders can be categorized into 2 groups, web-builders and hunters. Only the silks from the former group are being studied. The web-building spiders produce different types of silk fibers for various purposes, such as habitation, prey capturing, hunter alarming and reproduction. Each type of silk displays different properties, since they are produced from different silk glands, resulting in different primary structures [48]. In *Aranea* spiders, there are at least 7 silk glands, and each gland functions differently for specific silk fiber production. Major ampullate is responsible for major structural fibers, including orb frame, radii, and dragline silk fibers, which possess high mechanical strength comparing to other natural fibers. Minor ampullate produces supportive fibers to support the whole orb web structure. High elastic fibers for prey capturing are made from flagelliform gland. Cylindrical and aciniform silk glands produce cocoon silks for protecting eggs during reproduction, and aggregate and piriform glands are responsible for glue-like silk and attachment silk fiber, respectively, for the attachment to different surfaces [49].

Spider silks used in recent research are mainly derived from two species of the web-building spiders, including *Nephila* and *Araneus*. *Nephila clavipes*, commonly found in USA, is known as golden orb-web spiders, golden orb-weavers, giant wood spiders or banana spiders. While *Araneus* spiders, e.g. *Araneus diadematus*, are habituated in Europe and known as European garden

spiders, diadem spiders, orangies, cross spiders, crowned orb weavers or pumpkin spiders [48, 49].

Different from silkworm silks, which can be manufactured in a large scale, the sericulture of spider silk is more difficult due to less production in nature. Furthermore, farming system is not suitable for spiders because of their aggressive and habitat possessive natures [49]. Therefore, biotechnology has been applied using recombinant protein techniques in different organisms, namely bacteria, yeasts, insects, plants, culture cells and vertebrates, to produce spider silks in a large amount [49, 50]. Recently, several spider silk-based materials are commercialized, mainly for biomedical purposes, such as sutures, microfibers and medical coating. AMSilk company from Germany, Spider Technologies from Japan, and Araknitek Holdings from USA are leading companies in spider silks technology and large-scale production [51].

3.3. Properties of silk fibroin

Silk fibroin (SF) refers to fibrous proteins presenting in silk fibers. In some arthropods, such as silkworms, SF is secreted from silk gland together with silk sericin which acts as a binder. In *B. mori* silk cocoons, two types of proteins are presented, including 72-81% fibroin and 19-28% sericin. Sericin is an amorphous protein containing a high ratio of hydrophilic amino acid residues, resulting in its water-soluble. While the primary structure of fibroin constitutes of high content of hydrophobic amino acids. Therefore, fibroin and sericin can be separated using an alkaline treatment with heat. Insoluble SF fiber is obtained and sericin is dissolved in aqueous phase [10, 15].

In this work, SF from the *B. mori* silk cocoon is used as the based material. Hence, the reviews on physicochemical and biological activities of this material are focused. SF from others are also reviewed in brief to compare with those of *B. mori* SF.

3.3.1. Physicochemical properties

a. Primary structure

B. mori SF is a heterodimeric protein composed of heavy chain, light chain and P25 with the molecular weight of 325-395, 25-26 and 30 kDa, respectively. Heavy chain is linked with light chain through disulfide linkage to form a dimer, and six dimers are associated with P25 in a molar ratio of 6:1 [10]. **Table 1** shows amino acid content analyzed from SF of silkworms and spiders. In all SF, a high content of hydrophobic amino acid is noticed.

Alanine, glycine, and serine constitute up to 70-80% of total amino acid in SF. The amount of each amino acid is comparable for the *B. mori* obtained from different strains. In heavy chain of SF, the repetitive sequences of hexapeptides, GAGAGS and GAGAGY, are the major components and regarded as crystalline moieties. Moreover, the determination of responsible encoding gene for heavy chain indicates that 12 crystalline segments are interspersed by amorphous regions, which are mainly made of bulky aromatic

Table 1 Amino acid profile of SF derived from various sources (values reported as %w/w)

Amino acid	<i>B. mori</i>				<i>A. pernyi</i> [55]	<i>N. clavipes</i> [56]	<i>A. diadematus</i> [57]
	Lucas et al ¹ [55]	Thai strain [58]	Japanese strain [58]	Chinese strain [58]			
Hydrophobic amino acids (non-polar side chains)							
Glycine (G)	43.7	38.32	33.00	35.76	26.50	37.10	41.30
Alanine (A)	28.8	34.29	31.26	29.39	44.10	21.10	18.30
Proline (P)	0.3	0.42	0.64	0.64	0.30	4.30	9.55
Valine (V)	2.2	1.15	1.67	1.53	0.70	1.80	0.90
Leucine (L)	0.5	0.27	0.38	0.43	0.80	3.80	1.76
Isoleucine (I)	0.7	0.20	0.31	0.32	n/a ²	0.90	0.53
Methionine (M)	n/a ²	0.08	0.13	0.10	n/a ²	0.40	n/a ²
Hydrophobic amino acids (aromatic side chains)							
Tyrosine (Y)	5.1	5.75	7.66	7.16	4.90	0.40	0.03
Phenylalanine (F)	0.6	0.98	1.69	1.39	0.60	0.70	3.50
Tryptophan (W)	0.3	0.21	0.33	0.45	1.10	2.90	4.38
Total	82.2	81.67	77.07	77.17	79.00	73.40	80.25

Amino acid	<i>B. mori</i>				<i>A. pernyi</i> [55]	<i>N. clavipes</i> [56]	<i>A. diadematus</i> [57]
	Lucas <i>et al</i> ¹ [55]	Thai strain [58]	Japanese strain [58]	Chinese strain [58]			
<i>Hydrophobic amino acids (non-polar side chains)</i>							
Aspartic acid (D)	1.3	1.63	2.08	2.18	4.70	2.50	1.08
Glutamic acid (E)	1.0	1.15	1.52	1.51	0.80	9.20	11.86
<i>Hydrophilic amino acids (basic side chains)</i>							
Arginine (R)	1.8	0.30	0.31	0.44	2.60	7.60	0.49
Lysine (K)	0.6	0.20	0.26	0.30	0.10	0.50	0.28
Histidine (H)	0.5	0.83	0.81	1.02	0.80	0.50	0.68
<i>Hydrophilic amino acids (polar side chains)</i>							
Serine (S)	11.9	13.42	16.87	16.30	11.80	4.50	4.74
Threonine (T)	0.9	0.80	1.08	1.08	0.10	1.70	0.46
Cysteine (C)	n/a ²	n/a ²	n/a ²	n/a ²	0.10	0.10	0.16
Total	18.0	18.33	22.93	22.83	21.00	26.60	19.75

Note: ¹The strain of *B. mori* is not specified, ²lower than the sensitivity limit of the measurement

b. Secondary structure

The secondary structures of SF can be investigated by various techniques, including X-ray diffraction (XRD), nuclear magnetic resonance (NMR) spectroscopy, Fourier-transformed infrared (FTIR) spectroscopy, and Raman spectroscopy, together with protein simulation modeling. It was suggested that anti-parallel beta sheet is mainly formed, but not limit to, within the crystalline domains in the solid-state SF. In turn, random coil structure is preferably elicited in soluble silk, indicating an important role of structural transition to the states of SF.

The structural organization of SF was clearly described and depicted by Murphy *et al* [11] (**Figure 4**). The peptide modeling revealed that the repetitive GX (where X can be alanine, serine or tyrosine) in crystalline domains forms hydrogen bonding between NH and O of peptide bonds (**Figure 4C**). By doing this, the side chains of alanine and glycine point outward, allowing the inter-sheet stacking by van der Waals forces (**Figure 4B**). These interactions between side chains of glycine and alanine are identified as hydrophobic interactions. Taking together, the formation of secondary structures of SF arises from the intramolecular assembly via hydrogen bonding and the inter-sheet stacking through hydrophobic interaction [11].

Due to the amorphous characteristic of linkers, composed of bulky hydrophilic amino acids, long-range hydrogen bond forming generally occur without the formation of ordered structures. These hydrogen bonds form with surrounded free water, increasing the elasticity and plasticity of macroscale mechanical properties of SF. In addition, the presence of proline in linkers dictates the anti-stacking parallel beta strands, which are the major characteristic of SF [11].

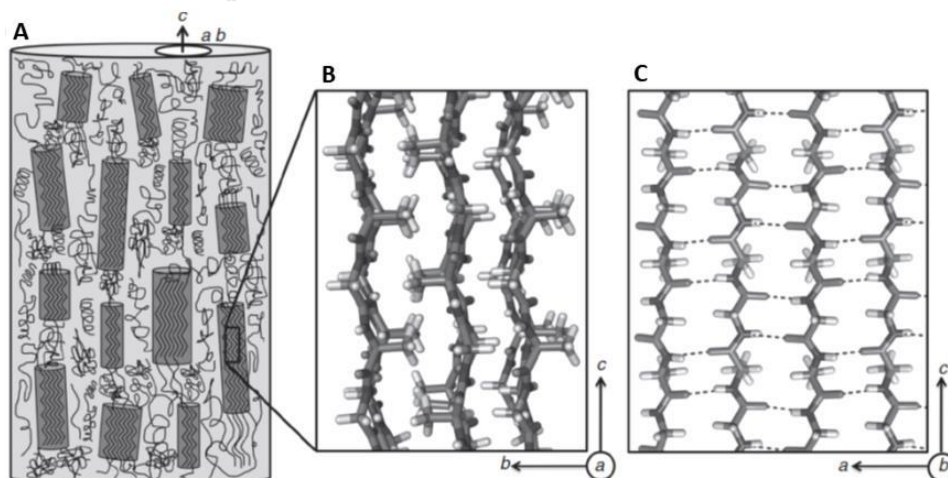


Figure 4 Structural organization of beta sheet in fibroin (A) The alignment of beta sheet crystallites and amorphous regions (B) Inter-stacking or intermolecular assembly by the formation of van der Waals forces between side chains of glycine and

alanine (C) Intramolecular assembly by the hydrogen bonding between NH and O of peptide backbones (adapted from [11])

c. Mechanical properties

Table 2 shows the mechanical properties of *B. mori* silk fibers with other natural and synthetic fibers. Silkworm and spider silk fibers display an excellent mechanical strength outperforming natural collagen and synthetic polylactic acid fibers. However, the mechanical integrity of fibers is still weaker than Kevlar, which is the strongest fiber.

The high mechanical performance of SF fiber results from predominant beta sheet structure. As discussed previously, the secondary structure of SF composes of beta sheet embed in amorphous matrix, and hydrophobic interaction, van der waals force and hydrogen bond contributed to its structural stability. When a mechanical load is applied to the SF, weak forces exhibited in amorphous matrix are firstly deformed, before transferring to beta sheet crystals until fracture [59].

Several structural aspects of SF relate to the mechanical properties. For example, the formation of high intra-molecular beta sheet yields the superb mechanical strength than the inter-molecular beta sheet crystals. In spider silks, a huge content of intra-molecular beta sheet exists in their structure, resulting in a higher strength comparing to those of silkworm silk fibers. Furthermore, the size of beta sheet crystallites and their orientation affect the mechanical properties of SF fibers [59].

Since SF is obtained from natural sources, the quality of silk fibers is varied depending on farming conditions, namely foods, rearing and spinning conditions, and health of silkworms or spiders. Additionally, the mechanical properties of silk materials fabricated from regenerated SF solution can be modified by several factors, including the geometry of the materials, the chemical functionalization or crosslinking, the concentration of SF and processing temperature [59]. It was found that degumming conditions, e.g. temperature and degumming time, significantly affects the molecular weight distribution of obtained SF due to hydrolysis, which links to the deteriorated mechanical properties of the SF materials [15]. Therefore, it is crucial to strictly control the degumming conditions to reduce variation between production batches.

Table 2 Mechanical properties of natural and synthetic fibers

Types of fiber	Ultimate tensile strength (UTS: MPa)	Modulus (GPa)	%Elongation	Ref.
<i>B. mori</i>	400-570	5.13-8.61	23.2-26.8	[53]
<i>A. pernyi</i>	340-430	4.72-4.76	26.7-29.6	
<i>N. clavipes</i>	875-972	10.9-12.7	16.7-18.1	[60]

<i>A. diadematus</i>	1,190	31	2.8	
Collagen	0.9-7.4	0.0018-0.046	24-68	[6]
Polylactic acid	28.50	1.2-3.0	2-6	
Kevlar	3,600	130	2.7	

d. Thermal properties

Differential scanning calorimetry (DSC) and thermal gravimetric analysis (TGA) have been used to study the thermal properties of either raw silk fibers or processed SF. Degradation temperature (T_d) of silkworm SF is reported with a higher value than that of spider SF. The T_d of *B. mori* SF and *A. pernyi* SF are 335 and 380°C, respectively [53]. While those of spider silks, *N. clavipes* and *A. diadematus* SF, are approximately 230°C [60, 61].

3.3.2. Biological properties

a. Biodegradability

The concept of biomaterials used in organisms is that the materials should be disappeared after their functions is completely fulfilled, with non-toxic by-products. SF can undergo degradation by various catalytic hydrolyzers, including acids, alkalines, salts, and proteolytic enzymes. Acid and alkaline hydrolysis are general degradation process found in various proteins. Furthermore, inorganic salt solutions, e.g. CaCl_2 , $\text{Ca}(\text{NO}_3)_2$, LiSCN , can catalyze the degradation of SF [62].

The effects of various proteolytic enzymes, including α -chymotrypsin, collagenase 1A, and protease XIV, on the degradation of porous SF sheets were investigated. The weight loss after incubation with α -chymotrypsin was on par of phosphate buffer saline [63]. It can be discussed that the accessible of α -chymotrypsin is limited [62]. Collagenase 1A and protease XIV were found to be more aggressive to SF degradation. Since collagenases are the specific enzymes to GX domains, which are highly populated in both crystalline and amorphous regions. While proteases are specific to peptide bonds, resulting in a non-specific cleavage without regarding of amino acid sequences. Thus, it can be concluded that SF materials would be susceptible for physiological degradation [63].

The degradation rate can be controlled by the modifications of either chemical structure, micro-, or macrostructure. For example, different degumming protocols can affect the molecular weight of SF, which subsequently influences viscosity, diffusivity, and degradation behavior [15, 62]. The secondary structure of processed SF materials also dictates degradation behavior, which the materials with high β -sheet content undergo slower degradation than those with random coil predominance [62]. This indicates the potentials of SF materials to be fabricated to products with tunable rate of degradation.

b. Biological responses

The biological responses, including the immunological reactions of host against foreign materials, relate to not only the physicochemical properties of materials but also the degradation products. SF is cleaved into small pieces of peptides or amino acids, which are physiologically absorbed, metabolized, and subsequently excreted [62, 63]. The inflammatory responses to porous SF films were performed *in vitro* and *in vivo*, compared to collagen and polylactic acid. The *in vitro* results indicated the comparable responses, as the expression of interleukin-1 β , cyclooxygenase-2 and PGE2, of SF films to collagen. Interestingly, the inflammatory reactions in mice to SF films were lower than those observed in collagen films [64]. The macrophage responses to SF, both raw fibers and regenerated products, were evaluated. After 7 days of exposure, the release of tumor necrosis factor, which is an indicator of macrophage activation, was comparable to collagen, indicating the low immunogenicity of SF materials [65]. Also, Thai SF, derived from Thai strain of *Bombyx mori*, exhibited no to slight irritant when subcutaneously implanted as scaffolds to Wistar rats for 4 weeks according ISO 10993-6. The immune responses were comparable to the control sample (Gelfoam[®]), indicating the biocompatibility of SF materials [66].

Wang *et al* [33] stated the properties of scaffolds for cell-based tissue engineering including the bioactivities to support cell activities, low immunogenicity, biodegradability, mechanical stability and versatility in material fabrication. SF reaches almost all requirements except the low cell affinity to SF substrates. Compared to treated polystyrene, collagen or non-mulberry SF, the attachment of L929 mouse fibroblasts on mulberry SF surface was lower, and the cultured cells presented round morphology with less cytoskeleton prominence. The cell proliferation was delayed and lower cell number was achieved [67, 68]. Additionally, when epithelial type cell line and primary cell were cultured on untreated mulberry SF, the low cell affinity to the SF film was noticed [69]. The cultured cells preferably formed clusters to enhance cell-cell interactions rather than cell-matrix interaction. Hydrophobicity and the absence of cell adhesion motifs in SF were proposed as the factors for low cell binding affinity and cell activities [67-69]. However, the number of viable cells cultured on SF was determined using flow cytometry and the results were comparable to those of cell culture-treated polystyrene [68]. This elucidated that cells cultured on SF substrates displayed low attachment and delayed growth but remained viable, confirming the biocompatibility of SF material.

In vivo biocompatibility, biodegradability and bioactivity of SF biomaterial were evaluated to elucidate its potential as an implantable device. **Table 3** summarizes the animal trail data focusing on the biocompatibility tests of implanted SF. It can be concluded that SF induced no or low host immune responses. The implanted SF starts to degrade at around 8-12 weeks, which are longer than those of other biomaterials. New forming tissue regeneration and vascular infiltration are noticed.

Table 3 In vivo tests of SF materials

Test material	Objective	Animal	Site	Duration	Outcome	Ref.
SF film	Host immune responses, comparing to collagen, PLA, and RGD modified SF	Rats	IM	6 weeks	Lower immune responses for SF and RGD-modified SF films than those of collagen and PLA	[64]
Water vapor annealed SF film	Host immune responses	Mice	SC	4 weeks	Low immune responses and macrophage activation. No degradation in 4 weeks	[70]
Electrospun SF scaffold	Biodegradability	Mice	SC, IM	8 weeks	Implanted scaffold started to degrade within 5 weeks and completed in 8 weeks. Normal immune responses were noticed.	[71]
Salt-leached SF 3D scaffold	Biodegradability and immune responses	Rats	SC	12 weeks	Samples remained at the implanted site after 12 weeks. Low immune responses in all groups.	[66]
Lyophilized SF 3D scaffold with different crystallinity	Host immune responses and angiogenesis	Rats	SC	4 weeks	Formation of blood vessels was enhanced in samples with lower crystallinity as well as cell infiltration and tissue regeneration	[72]
Somicated SF hydrogel	Biodegradability tracking with ultrasound imaging	Rats	IM	15 weeks	Ultrasound imaging can be used to track <i>in situ</i> biodegradability and new blood vessel formation. No degradation observed in the first 8 weeks, but fast degradation and tissue formation began after 15-18 weeks	[73]
Non-woven SF mat	Host immune responses and angiogenesis	Mice	SC	3 months	No adverse immune responses. Blood vessel formation surrounding the samples in 1 month. Newly formed connective tissues and aligned collagen in 3 months.	[74]

Abbreviations: IM (intramuscular); SC (subcutaneous)

3.4. Silk fibroin gelation

As previously stated, SF protein derived from silkworm cocoons contains a high content of beta sheet structure due to molecular interactions between repetitive crystalline regions. The dissolution of SF fibers can be achieved using several chaotropic agents, namely LiBr [13], LiSCN [15], or an ethanolic solution of CaCl_2 [14]. The hydrogen bonds, which contribute to the beta sheet formation, are disrupted, and the SF solution with high random coil content can be obtained.

However, due to the high thermodynamic stability of beta sheet structure, the SF solution gradually turns to soft-solid state in a period of time, depending on storage conditions. The sol-to-gel transition of SF intrigue several researchers to study the conditions or apply any intervention than can accelerate the process, to use as a facile method for the fabrication of the SF hydrogel. Herein, the conditions affect the gel formation of SF solution as well as the physical or chemical interventions used to induce the SF network crosslinking are reviewed. **Table 4** summarizes the gelation of SF under different condition or induced by physical or chemical interventions. The mechanical properties and the brief details of *in vitro* and *in vivo* biocompatibility tests are displayed.

Table 4 Gelation time of SF solution affected by physical interventions or chemical additives, and the mechanical properties, in vitro/in vivo experiment of the obtained hydrogels

Method	Condition	SF concentration	Gelation time	Mechanical properties	In vitro	In vivo	Ref.
Temperature	RT, 37, 60°C pH 6.5-6.8	2-20%	4-65 days	E' 0.2-6 MPa	n/a	n/a	[16]
	RT, 37°C	0.6-7.2%	5-15 days	n/a	n/a	n/a	[12]
Ionic strength	5-30 mM Ca ²⁺ RT, 37, 60°C pH 5.6-5.9	2-16%	4-50 days	n/a	n/a	n/a	[16]
	RT, 37, 60°C pH 5-8	4%	1-50 days	n/a	n/a	n/a	[16]
pH	RT, pH 2-10	1.8, 3.6%	1-37 days	n/a	n/a	n/a	[12]
	RT, pH 3-4	3%	<2 days	n/a	n/a	n/a	[17]
	20-70°C pH 6.5-6.8	0.05-1%	200-1,000 min	n/a	n/a	n/a	[75]
Sonication	20% amp, 5-30 sec	1-20%	5 min-100 h	E' 369-1,712 kPa	hMSC, 3D 5x10 ⁵ cell/ml, 21 days	n/a	[35]
	50% amp, 15 sec	1%	~1 h	G' 1.366-2.902 kPa	hNSC, 3D 4x10 ⁶ cell/ml, 7 days	n/a	[76]

Method	Condition	SF concentration	Gelation time	Mechanical properties	<i>In vitro</i>	<i>In vivo</i>	Ref.
	30% amp, 30 sec on-off, 3-6 cycles	2-5%	n/a	G' 0.17-5.46 kPa	Mouse MSC, 3D 4x10 ⁶ cell/ml, 14 days	Mice, Brain tissues	[77]
Sonication (cont.)	25% amp, 30 sec	5%	1-6 h	n/a	n/a	Rabbit, Maxillary sinus bone, 12 weeks	[78]
	20% amp, 15-20 sec	2%	15-30 min	G' 3-8 kPa	hMSC, 3D, 1.2x10 ⁵ -2x10 ⁶ cell/ml, 8 weeks	n/a	[79, 80]
Vortex	25°C, 3,200 rpm, 7-11 min	5.2%	35-100 min	G' 0.1-70 kPa	n/a	n/a	[36]
	37°C, 3,200 rpm, 7 min	1.2%	~2 h	n/a	n/a	Diabetic mice, fat pads, 42 days	[81]
Electric field	25 VDC, 3 min	8%	Seconds	G' 1 kPa	n/a	n/a	[82]
	25 VDC, 5-120 sec	5, 10%	Seconds	Adhesive strength 0.37±0.09 MPa	n/a	n/a	[83]

Method	Condition	SF concentration	Gelation time	Mechanical properties	<i>In vitro</i>	<i>In vivo</i>	Ref.
Electric field (cont.)	25 VDC, 1.5 h	3%	Seconds	Shear bond strength 2-3 MPa Tensile bond strength 1.25-1.75 MPa	MC3T3-E1, 7 days	n/a	[84]
	25-50°C	0.25-0.75%	2-9 h	G' 0.1-1.1 kPa	n/a	n/a	[85]
Extraction of hydrophilic SF	37°C	0.25-0.75%	280-680 min	G' 1.1 kPa	n/a	n/a	[86]
	37°C	0.2-1%	2-6 h	G' 0.5 kPa	n/a	Tumor-bearing mice, intratumor, 60 days	[87]
Soft-freezing	-7°C, 24 h and thaw	1-2%	6-12 h	n/a	n/a	n/a	[88]
Alcohols	30% Glycerol RT	2%	2 days	n/a	MG63, 2D 5x10 ³ cell/sample, 72 h	n/a	[89]
	7% Ethanol 24 h & 25-125 mM NaCl	0.14%	10 min	G' 1.1-3.7 kPa	L929, 3D 1x10 ⁶ cell/ml, 7 days	n/a	[90]
	10-80% Ethanol	1.3-5.7%	4 sec-24 h	G' 0.02-0.15 MPa	hMSC, 2D 8x10 ³ cell/sample, 48 h	n/a	[91]

Method	Condition	SF concentration	Gelation time	Mechanical properties	<i>In vitro</i>	<i>In vivo</i>	Ref.
Alcohols (cont.)	10% Methanol, 25°C	5%	9.1 h	G' 105 kPa E' 210.2±8.8 kPa	L929, 2D 1x10 ⁴ cell/cm ² 7 days	n/a	[92, 93]
	10% Ethanol, 25°C		8.7 h	G' 115 kPa			
	10% n-Propanol, 25°C		8.2 h	G' 140 kPa E' 300.3±2.0 kPa			
	10% n-Butanol, 25°C		39.6 min	G' 165 kPa E' 355.9±6.3 kPa			
	10% 1,3-Propanediol, 25°C		n/a	G' 144 kPa			
	10% Glycerol, 25°C		73.5 h	G' 147 kPa E' 217.7±3.0 kPa			
	8-12 mM SDS, 37°C		4%	15-18 min			
0.25-0.75% SDS, 37°C	1.5%	18-168 min	G' 1-2 kPa	n/a	n/a	[95]	
Surfactants	4.5-6.5 mM SDS, 37°C	4% (+1.5% agarose)	5-50 min	E' 18.6 kPa	MC3T3-E1, 2D 1x10 ⁵ cell/sample 10 days	n/a	[96]
	0.03-0.45% SOS	2%	113-144 h	n/a	n/a	n/a	[97]
	0.03-0.45% STS		20-30 min				
	0.2-1.2% SNS, 37°C	1-3.5%	40-100 min	n/a	L929, 2D 1x10 ⁴ cell/sample 7 days	n/a	[98]

Method	Condition	SF concentration	Gelation time	Mechanical properties	<i>In vitro</i>	<i>In vivo</i>	Ref.			
Surfactants (cont.)	0.2-1% SO, 37°C	2-5%	81-1,289 min	G' 1.6-34.0 kPa	NIH/3T3 Indirect assay	n/a	[99]			
	50-100 mM Triton X-100, 37°C	2.5%	12-15 h	n/a	n/a	n/a	[100]			
	5-100 mM SDBS, 37°C		1-50 h							
	5-20 mM OTAB, 37°C		55-60 h							
	10-60 mM DETAB, 37°C	5%	Immediately-2 days	Immediately-2 days	G' 100-200 Pa	n/a	n/a	[101]		
	10-60 mM DTAB, 37°C								Immediately-1 h	G' 500-1,000 Pa
	10-6- mM CTAB, 37°C								Immediately-1.5 h	G' 2-6 kPa
	10-20 mM STAB, 37°C								Immediately-2 h	G' 75-350 Pa
	1-5% Sophorolipids, 37°C, pH 7.4	3%	140-189 min		E' 9 kPa G' 1 kPa	L929, 2D 1x10 ³ cell/sample 7 days	n/a	[38]		
	3% Sophorolipids, 25°C, pH 7.3	3%	0.8-10 h		G' 1-10 kPa	n/a	n/a	[102]		
3% Sophorolipids, 25°C, pH 6-8	3%	2.3-10 h		G' 0.5-2 kPa	n/a	n/a	[103]			
0.1-3.5% LiNO ₃ , NaNO ₃ , KNO ₃	4.5%	1-14 min		n/a	n/a	n/a	[104]			

Method	Condition	SF concentration	Gelation time	Mechanical properties	<i>In vitro</i>	<i>In vivo</i>	Ref.
Salts (cont.)	1.28 mM Fe ²⁺ , 32.5 mM H ₂ O ₂ , 0.4 mM ascorbic acid, 37°C	2.1%	2 min	G' 0.1 kPa E' (day 1) 0.17-0.38 kPa E' (day 7) 1.15-2.29 kPa	L929, 2D 8x10 ³ cell/cm ² 7 days	n/a	[23]
Tannic acid	0.1-0.7%, pH 7.4 37°C	1%	10.5-25.5 h	G' 152-2,236 Pa	NIH/3T3, 2D 1x10 ⁴ cell/sample 5 days	Mice with infection full thickness wound, 14 days	[105]
HRP	10 u/ml HRP, 1.65 mM H ₂ O ₂ 37°C	2-6%	<1 h	G' 3-10 kPa	hMSC, 2D&3D 2.1x10 ⁴ cell/cm ² 7 days 0.5-1x10 ⁴ cell/ml 29 days	Mice, SC implant, 4 weeks	[106]
	0.13-0.52% HRP, 0.8-1.45% H ₂ O ₂ 37°C	16%	5-36 min	G' 0.2-5 kPa	ATDC5, 3D 1x10 ⁶ cell/ml 10 days HeLa, 3D 1x10 ⁶ cell/ml 14 days	Mice, SC implant, 2 weeks	[37]
	10 u/ml HRP, 1.65 mM H ₂ O ₂	8% (+4-16% PVA)	5-10 min	E' 0.692-3.012 kPa	L929 Indirect assay	n/a	[107]

Method	Condition	SF concentration	Gelation time	Mechanical properties	<i>In vitro</i>	<i>In vivo</i>	Ref.
HRP (cont.)	10 u/ml HRP, 0.01-0.05% H ₂ O ₂	3, 5%	Immediately -6 min	G' 0.1-2 kPa E' 1-100 kPa	hMSC, 2D&3D 4x10 ³ cell/cm ² 7 days 2x10 ⁵ cell/ml 28 days	Mice, SC implant, 3 days	[108]
	10 u/ml HRP, 0.1 mM riboflavin 300 W/m ² light	1-3%	30 min	n/a	L929, 2D 1.6x10 ³ cell/sample 7 days	n/a	[109]
Tyrosinase	500 u. 37°C	8% (+15% gelatin)	15-30 min	G' 166-530 kPa	hMSC, 3D 2-5x10 ⁶ cell/ml 21 days	n/a	[39]
Poloxamer 407	10-15%, 35°C pH 7	1.43-2.98%	5-210 min	n/a	n/a	n/a	[110]
PEG	900 kDa, 5-30% RT, 37, 60°C pH 6.1-6.4	4%	10-30 days	n/a	n/a	n/a	[16]
	300, 400 Da, 37.5-42.5%, 37°C	3.75-15%	7-360 min	G' 20-70 kPa	hMSC, 2D 300 cell/sample 10 days	Rats, SC implant, 20 days	[111]
	1.5 kDa, 10-20% 37°C	10-20%	2-115 min	n/a	Platelets, 3 h	Rabbits, Hemostatic patch for liver wound	[112]

Method	Condition	SF concentration	Gelation time	Mechanical properties	In vitro	In vivo	Ref.
PEG (cont.)	20 kDa, 8-56%	8% (dopamine conjugated)	10-116 min	Adhesive strength 48.33-217.25 kPa	n/a	n/a	[113]
	100 kDa, 3-7%, 37°C	3-7%	48-120 min	G' 1-2 kPa	L929, 3D 3x10 ⁵ cell/ml <1 day	n/a	[114]
HPC	3%, 37°C	7%	75-88 min	G' 10-100 kPa	HepG2, 2D 2x10 ⁴ cell/cm ² 12 days	Tumor-bearing mice, intratumor, 30 days	[115]
	1%, 70°C	9%	<2 h	E' 1.45 MPa	L929, Indirect assay	n/a	[116]
Short peptides, NapFF & NapFF-RGD	0.2-0.4%, 37°C	0.1-2%	97 sec-1.5 h	G' 659-18,560 Pa	HUVEC, 2D 8x10 ³ cell/sample 5 days	Mice, SC implant, 21 days	[117]
	1%, 37°C	2%	20 min	G' 6.679 kPa	Mouse MSC, 3D 1x10 ⁶ cell/ml 14 days	Mice, Bone calvarial defect, 21 days	[118]
Non-mulberry SF	<i>A. pernyi</i> SF 1.25-3.75% 37°C	1.75-3.75%	33 min-1 day	n/a	n/a	n/a	[119]
	<i>A. assama</i> SF 1.5%, 37°C	1.5%	20 min	G' 336.42 Pa E' 2.960 MPa	HDF, 3D 1x10 ⁸ cell/ml 14 days	Rats, 3 rd -degree burn wound, 21 days	[120]

Method	Condition	SF concentration	Gelation time	Mechanical properties	In vitro	In vivo	Ref.
Non-mulberry SF (cont.)	<i>A. assamensis</i> SF 1-2.5%	0.5-2%	8-40 min	G' 1-8 kPa E' 4.1-259.94 kPa	NP cells, 2D 2x10 ⁴ cell/sample 7 days	n/a	[121]
	<i>A. assama</i> SF 0.67-2%	0.67-8%	11-30 min	n/a	RIN-5, 2D&3D 1x10 ⁴ cell/sample 9 days, 1x10 ⁸ cell/ml, 14 days Islets, 3D 1x10 ³ islet/ml, 14 days Porcine endothelial cells, 2D 5x10 ⁴ cell/sample, 7 days	Mice, SC implant, 10 days	[122]
Photo-crosslinking	0.16-10 mM Ru(II) 20-100 mM APS 250 W light, 120 sec	30%	Immediately	G' 81-4,000 MPa	ATDC5, 2D 1.2x10 ⁵ cell/sample 7 days	n/a	[123]
	5 mM Ru(II) 5 mM SPS 250 mW/cm ² light, 3 min	2% (±0.5% gelatin)	5 sec	E' 18-24 kPa	Human articular chondrocytes, 3D 15x10 ⁶ cell/ml 5 weeks	n/a	[124]
	1 mM LAP, 5 mW/cm ² 365-nm UV light	10-20% (methacrylated SF)	<5 min	G' 0.35-80 kPa	n/a	n/a	[125]

Method	Condition	SF concentration	Gelation time	Mechanical properties	<i>In vitro</i>	<i>In vivo</i>	Ref.
Photo-crosslinking (cont.)	0.05-0.4% LAP, 30 mW/cm ² 365-nm UV light	10-30% (glycidyl methacrylated SF)	41-137.5 sec	G' 642 Pa-25.6 kPa E' 17.7-125.8 kPa	NIH/3T3, 3D 1x10 ⁶ cell/ml 14 days Chondrocytes, 3D 1x10 ⁷ cell/ml 4 weeks	n/a	[126]
	0.6% LAP, 30 mW/cm ² 365-nm UV light	30% (glycidyl methacrylated SF)	3-5 sec	n/a	NIH/3T3, 3D 1x10 ⁶ cell/ml 14 days Chondrocytes, 3D 1x10 ⁷ cell/ml 4 weeks	Mice, SC implant, 8 weeks Rabbits, Trachea partial defect model, 6 weeks	[127]
	30 W 405-nm UV light	5% (thiolated SF) (+5% PEG-DA)	30 sec-3 min	E' 3.81 kPa	HEK293, Indirect assay	Mice, SC implant, 3 days	[128]
	2% bisphosphonate hyaluronan binder ±acrylation ±UV light	4% (CaP-coated SF microfibers)	<10 min	G' 250 Pa-2.5 kPa	hMSC, 2D 2x10 ³ cell/sample 7-14 days	Mice, Bone calvarial defect, 8 weeks	[129]

Abbreviations: RT (room temperature); E' (compression modulus); G' (storage or elastic modulus); n/a (data not available); hMSC (human mesenchymal stem cell); hNSC (human neural stem cell); 2D (2-dimensional culture); 3D (3-dimensional culture); HRP (horseradish peroxidase); SC (subcutaneous); PEG (polyethylene glycol); PVA (polyvinyl alcohol); HPC (hydroxypropyl cellulose); HPMP (hydroxypropylmethyl cellulose)

3.4.1. Conditions affecting the gelation of silk fibroin solution

a. SF concentration and temperature

The gelation of SF solution relates to the formation of beta sheet, which is resulted from the molecular interactions through hydrophobic interactions and hydrogen bonds. It was found that the sol-to-gel transition of SF was accelerated with an increasing of SF concentration and incubation temperature. An increasing of the SF concentration reduced distances between SF chains, increasing the chance of inter- or intra-molecular interactions [12, 16]. However, at low concentration (<1%), the gelation time weakly depends on SF concentration [12, 75]. In addition, higher temperature can increase chain mobility, resulting in higher chain interactions [16]. Due to the high content of hydrophobic moieties presenting in SF molecules, water could be a poor solvent for SF. Increasing of the temperature can induce phase separation, resulting in the dehydration of SF chains. The local concentration of SF increases and the molecular interactions are enhanced, resulting in gel formation [12].

b. pH

The isoelectric point (pI) of SF protein is reported at around 4 [17, 75]. Therefore, the gel formation is enhanced when the pH of the SF solution shifts toward its pI, as reported by Ayub *et al* [17], Kim *et al* [16] and Matsumoto *et al* [12]. The relationship between the gel formation and the structural transition was noticed. The SF solution contains a high content of random coil, and the transition to the predominated beta sheet structure occurs at gel state. At pI, the carboxyl groups of SF are protonated and become uncharged, increasing their possibility to form hydrophobic interactions. At neutral pH (pH 6-9), both carboxyl and amino groups are charged, resulting in a low chance of molecular interactions. Thus, the gelation time is extended. Noticeably, the pKa of carboxyl and amino groups of SF molecules are reported at around 4.5 and 10. At the pH more than 10, the amino groups are deprotonated and the carboxyl groups become charged, the gelation should be accelerated, but the findings were opposite. The gelation time of SF at basic conditions was longer, indicating more contribution of the carboxyl groups in the structural transition of SF [12, 17]. To simplify the phenomenon, the scheme of pH-dependent SF chain interactions is depicted in **Figure 5**.

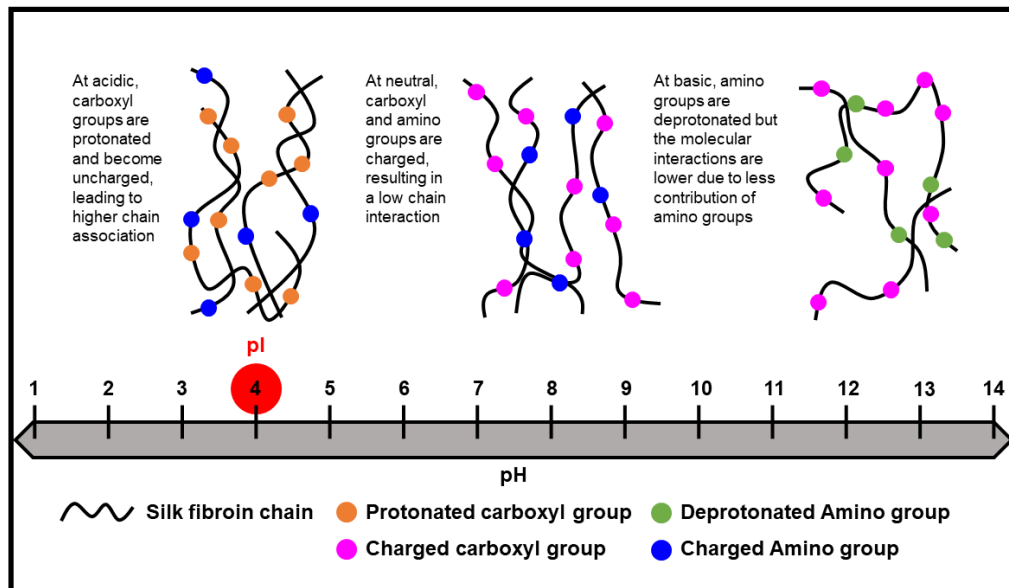


Figure 5 Schematic illustration describing the SF chain interactions at a different pH condition

c. Ionic strength

Divalent Ca^{2+} and monovalent K^+ were added to the SF solution to mimic the conditions presenting in silk glands of *B. mori* silkworms before injecting through the spinneret. An addition of Ca^{2+} resulted in a shorter gelation time, but no relationship between the concentration of Ca^{2+} and the gelation time was noticed. The presence of K^+ did not affect the SF gel formation. Therefore, the divalent cation was proposed to react with the negatively charged amino acids in the SF chains, inducing chain aggregation and rapid gel transition [16].

3.4.2. In situ silk fibroin gelation systems

a. Physical methods

1) Sonication

The rapid gelation of SF induced by the ultrasonication was firstly introduced by Wang *et al* [35] as an approach to accelerate the SF gelation without using chemical additives. The gelation time was tunable from about 5 min to 100 h depending on the energy output, sonication time and the concentration of SF solution. An abrupt increase of the beta sheet conformation after sonication linked to the gel formation. The mechanical vibration resulted in an increase of local temperature as well as a perturbation to the hydrophobic hydration of SF chains, leading to accelerated chain aggregation and beta sheet formation.

The mechanical properties of the SF hydrogels depended on the SF concentration. The compressive modulus of the sonicated 4% and 12% SF hydrogels were 369 and 1,712 kPa, respectively [35]. Furthermore, the

chemical functionalization of SF could influence the modulus of the obtained hydrogels. From the report of Sun *et al* [76], the storage modulus of 1% SF hydrogels, using modified SF with IKVAV peptides crosslinked by carbodiimides, was $2,902 \pm 96$ Pa, compared to $1,366 \pm 37$ Pa of the regenerated SF hydrogels.

The cytocompatibility of sonicated SF hydrogels and their potential for cell encapsulation were evaluated. Human mesenchymal stem cells (hMSCs) were loaded in 4%, 8% and 12% SF hydrogels and cultured for 21 days. Altered cell morphology and a degree of cell death can be noticed with the high SF concentration of 8% and 12%, due to limited mass transportation. The results were in accordance with Osama *et al* [77], which the mouse MSCs were encapsulated in 2%, 3% and 4% SF hydrogels. Encapsulated cell in 2% SF hydrogels proliferated at a significant rate, while those in the hydrogels with higher SF concentration showed low or steady growth rate.

Additionally, sonication-induced SF gelation can be employed for the biological studies relating to the SF material properties and the cell regulation without perturbations of chemicals. For example, the charges of the SF hydrogels were varied by blending regenerated SF with either SF ionomers (SF functionalized with poly-glutamic acid) or tropoelastin, a signaling protein presenting in ECM, and SF gelation was induced by sonication [79, 80]. The positive charges of SF materials were more pronounced with a higher added content of these proteins. The influences of the charges to the differentiation potentials of encapsulated MSCs were determined. The SF and blended SF hydrogels were reported to support long term culture. Furthermore, the hydrogels with more negative charges supported the MSC differentiations towards osteogenic or chondrogenic lineage. However, some properties of the hydrogels rather than the net charges were affected by the addition of tropoelastin of SF ionomers, such as hydrophilicity and mechanical properties [79]. It was worth noting that the complexity of biomaterial properties should be concerned and well optimized for the expected outcomes.

The sonicated SF hydrogels were assessed for *in vivo* applications. The hydrogels were injected to an ischemic cavity in rat brain. The good space conformity was noticed as well as a low host rejection and adverse responses after implanting for 14 days [77]. Furthermore, the hydrogels can be implanted in bone defects and delivered the bioactive factors, VEGF and BMP-2 [78]. In addition to the cytocompatibility of SF, the sonicated SF hydrogels can be administered to irregular-shape defects and enable the controlled release of loaded substances.

2) Vortex

High shear force was applied to accelerate the SF gelation using a high-speed vortex at 3,200 rpm [36]. The gelation of 5.2% SF solution can be obtained within 35, 50 and 100 min after vortex for 11, 9 and 7 min, respectively. The gelation induction by shear force was typically used with the amphiphilic polymers or polymers in poor solvent. Due to the primary structure of SF containing the segments of hydrophobic regions interspersed

with hydrophilic likers, water could be regarded as a poor solvent for SF. Hence, vortex of SF solution could increase the fluctuation of local concentration, resulting in the assembly of SF chains. Furthermore, the shear force could cause the extension of SF chains which facilitated the hydrophobic interaction.

The vortex-induced SF hydrogels were used to encapsulate autologous islets and deliver in diabetic mice [81]. With a co-culture with mouse MSCs, the cell-loaded SF hydrogels showed the potential in controlling blood glucose and enhancing euglycemia, compared to blank SF gel or cell therapy. The 3D encapsulation in SF hydrogels as well as the implantation of foreign materials which induce host immune responses favored blood vessel formation. Together with an inherent property of MSCs, angiogenesis in the implants was benefit for the functions of islet grafts.

3) Electrical fields

Applying the electrical current to SF solution resulted in a rapid formation of SF gels. According to Liesk *et al* [82], the accumulation of SF gels occurred at the anode immediately after exposed to 25 V of direct current. The obtained SF hydrogels were highly viscous and very tacky. Interestingly, the gels can return to solution state after switching the applied current, and the gels were formed at the newly created positive electrode. However, several reversible cycles as well as a long exposure time to the applied current could result in irreversible gel formation.

The electrically induced SF hydrogels showed high elastic and adhesive properties [82]. Strain-to-failure was up to 2,500% and the work of adhesion on stainless steel surface, acrylic and wood were 1-1.5 mJ in the hydrated state.

FTIR analysis revealed a significant decrease of random coil and an abundant formation of helical structures, and the SEM images of the freeze-dried hydrogels exhibited spherical and micellar structures [82, 130]. The authors proposed that the generation of proton at the anode led to a decrease local pH towards the pI of SF, resulting in the assemble of nanoparticles. The nanoparticles were then aggregated due to charge balance at the positive electrode. The intermolecular self-assembly, such as beta sheet, could not form within the relatively short time in the electric field. Lu *et al* [130] confirmed the role of the nanoparticle formation to the aggregation of SF electrogels using the metastable nanoparticle SF solution (by incubating fresh SF solution at 60°C for 2 h). The authors reported that the SF electrogel cannot be obtained when using the fresh SF solution with a concentration lower than 7%, unless preconditioned by stored at 4°C for 2 weeks. However, the preformed SF nanoparticle solution can form the hydrogels with ease even at the low concentration as 1%. Furthermore, the reversibility of the SF gels was resulted from the generation of negative charge after the reversal of the electrode. Therefore, the charged nanoparticles repulsed each other and dispersed into solution.

Apart from the pre-conditioning of SF solution by aging at 4°C for 2 weeks or 60°C for 8 h, the pH adjustment to pH 4, which was close to the reported pI of SF, was utilized before applying the electrical field [131]. The compression modulus of the dry hydrogel was significantly high, compared to those of spontaneously formed and acidified SF hydrogels. The role of alpha helix formation and different microstructures were proposed for such distinct mechanical properties.

The electrogelation system was utilized for SF coating of metals, namely titanium [83] and zirconia [84]. The thickness of SF coating was thicker and more uniform than dip coating in SF solution. The coating process was more controllable and reproducible. However, the adhesive strength of the SF coating was relatively low comparing to other techniques using co-deposition or chemical bonding [83]. This provided an uncomplicated technique and did not require harsh or expensive processing conditions. Furthermore, SF is biocompatible, biodegradable and supports *in vivo* tissue integration. The SF electrogel was tested for its cytocompatibility against rat epithelial cells [131] and MC3T3-E1 osteoblasts [84], which the cells were able to survive and grow on the SF surfaces.

4) Hydrophilic silk fibroin extraction

Regenerated SF film was prepared and immersed in water for 1 h, and the lexivium was collected and regarded as hydrophilic SF (HSF). The gelation occurred within 2-9 h at 25-50°C [85, 86] even at low concentration of 0.25%. At this concentration, regenerated SF solution took several weeks or month to form gel. Interestingly, the HSF hydrogels possessed a shear-thinning property and were able to form gel within 30 s after stop shear application. The reversible sol-gel transition can be performed for several cycles. The appearance changes and different mechanical properties between each state were noticed. The initial HSF solution was clear and transparent before becoming opaque after gelation. The shear-thinning solution was also opaque and exhibited higher storage modulus than that of the initial HSF solution. FTIR, Raman and XRD analysis revealed the dominant random coil and amorphous structures of the initial HSF solution, while the beta sheet conformer and the silk II crystal structure were presented in the HSF hydrogel and the shear-thinning solution. Hence, the formation of beta sheet could not be only driving force for gel formation, but other weak and reversible interactions, such as loosely connected hydrogen bonds, also played a role in the gelation [85].

The gelation of HSF was investigated at different temperature. At extremely low (4°C) and high (75-100°C) temperature, the gelation time was very long. It can be confirmed that the formation of beta sheet played a crucial role in gel formation, since the aggregation of beta sheet was more difficult at low temperature. Furthermore, even there was a high content of beta sheet in the HSF solution treated at the temperature higher than 75°C, the gelation time was drastically extended. Presumably, the hydrogen bonding cannot occur at high temperature. The hypothesis was confirmed by an addition of urea, a

quencher of hydrogen bonding, which the gel formation kinetics were deteriorated upon the content of added urea.

Microstructure analysis of HSF revealed the micellar morphology with the diameter between 20-200 nm, similar to the microstructures of regenerated SF solution. However, amino acid analysis showed a higher ratio of hydrophilic amino acid residues presenting in HSF than those of SF. Also, the higher surface tension energy of HSF solution, indicating the higher hydrophilicity, was noticed. The authors proposed that since SF is hydrophobic block copolymer, the SF chains readily assemble to micellar structures in aqueous medium, exposing the hydrophilic parts to the surroundings and turning the hydrophobic blocks inside. A higher hydrophilicity of HSF could lead to an effortless chain unfolding or extension, which links to hydrogen bonding and beta sheet aggregation [85].

The hydrophilic SF gelation system was applied for the delivery of chemotherapeutic, doxorubicin, and a near-infrared (NIR) absorbing dye, Cy7, for the treatment of solid tumor *in vivo*. The release of doxorubicin from HSF hydrogel was sensitive to external stimuli. For example, a reduction of pH and a generation of reactive oxygen species accelerated the drug release due to the perturbation of beta sheet structure. A cleavage of disulfide bonds presenting in HSF by external glutathione resulted in an increasing release rate. An increase of local temperature, from an activation of NIR, enhanced the drug release due to the chain relaxation. Furthermore, encapsulation of Cy7 in the hydrogel preserved the radiation stability, comparing to the administration of Cy7 solution. The combination doxorubicin/Cy7 HSF hydrogel was administered to tumor-bearing mice with NIR therapy, and a rapid ablation of tumors within 12 days was presented [87].

5) Soft freezing

The gelation of SF solution obtained after soft-freezing at -7°C for 24 h and thawing at room temperature, so called FT-SF solution, occurred within 6-12 h depending on the initial concentrations (1-2%) [88]. At a temperature close to the freezing point of SF solution, the formation of ice crystals could expel SF molecules, leading to a concentrated SF solution. The soft freezing allowed the slow mobility of SF chains to form the metastable structures, such as alpha helix and beta turn. FTIR and XRD results confirmed the formation of alpha-helical conformer and the silk I structure, respectively [88, 132]. However, the low temperature prevented the transformation from the intermediate helix to a higher stable beta sheet structure. Therefore, the thawed solution maintained its solution state while keeping at 4°C for 2 weeks. When incubating at 37°C , the sol-to-gel transition occurred. Because SF molecules could rearrange and form the high content of beta sheet which linked to gel formation.

Due to the formation of alpha helix structures after mild freezing, this strategy was applied to prepare the scaffold for an application requiring high elasticity, such as nerve conduits [132]. The SF solution was firstly frozen at -80°C , transferred to $-3\sim-5^{\circ}\text{C}$ for 3 days, and thawed, and the water-insoluble

nerve conduit was obtained. The elongation at break of the scaffold was enhanced, comparing to the ethanol-induced SF scaffold.

b. Chemical additives

1) Alcohols

An addition of alcohols was found for accelerating the gelation kinetic of SF. Motta *et al* [89] reported a non-porous SF hydrogel prepared by an addition of 30% glycerol. The gelation occurred within 2 days, relating to a decrease of random coil and an increase of beta sheet content. The cytocompatibility of the glycerol-SF hydrogel was confirmed by culturing with MG63 osteoblast-like cells.

The enhancement of SF gelation was further assessed using different types of alcohols with different carbon length and the number of hydroxyl group reported in the recent work of Kaewprasisit *et al* [92]. The structures of alcohols used in the study are shown in **Figure 6**. A longer carbon chain length resulted in an accelerated sol-to-gel transition which linked to a higher beta sheet content. With a fixed chain length, a greater number of hydroxyl group led to a longer gelation time. A reduction of the polarity of solvent caused by low polar alcohols resulted in a greater opportunity of the hydrophobic interaction of SF chains. Conversely, a higher number of hydroxyl group, relating to the higher solvent polarity, could hinder the hydrophobic interaction and delay the SF gelation kinetics.

Even the gelation of alcohol-enhanced SF related to a beta sheet formation, the content of this structure was not as high as that of the regenerated SF hydrogel. The content of random coil and beta turn conformers of the alcoholic hydrogels was higher. The authors reported that the alcohol-SF hydrogels showed the high flexibility with an enhanced strain at break, compared to the regenerated SF hydrogel. Furthermore, an attachment and proliferation of L929 cultured on the samples were promoted [93].

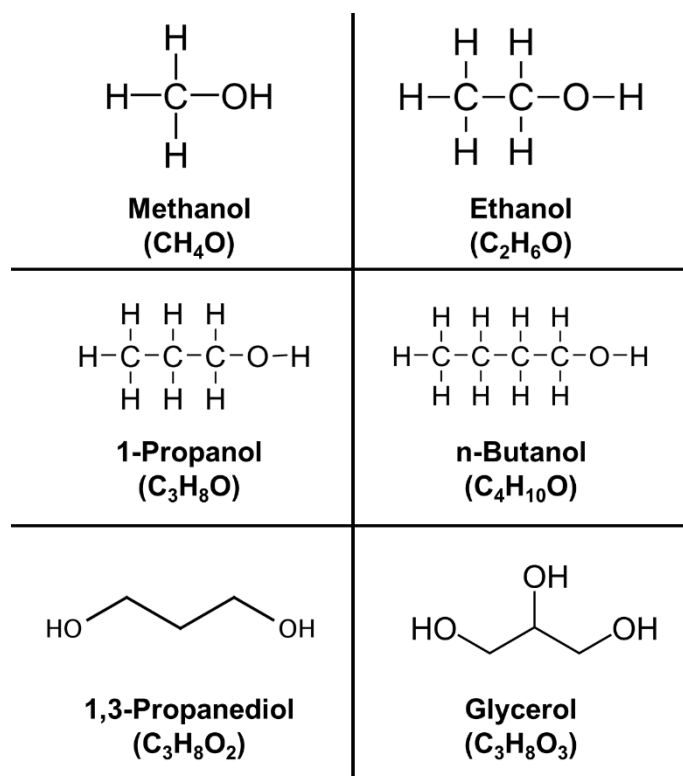


Figure 6 Chemical structure of alcohols used in the study of SF gelation

In addition to the alcohol-triggered SF gel formation, ethanol was used to induce the formation of SF nanofibrils [90]. The SF nanofibril solution can be stored at room temperature for 6 months. The gelation occurred after the addition of NaCl solution. The authors proposed that an increasing of ionic properties of solvents led to the balance of surface charges. Therefore, the repulsion between the nanofibrils was decreased and subsequently entangled to the hydrogel network. The mechanical properties of the hydrogels were tunable by the amount of NaCl added, and the self-healing properties can be noticed. The hydrogels were further used as encapsulated carrier for L929. The results showed that the SF nanofibril-based hydrogels were cytocompatible, showing the potential as the cell-load bioink for 3D printer.

2) Surfactants

The roles of surfactants in changing the secondary structures of proteins are well known [133]. Due to the relationship between SF structural transition and the gel formation, various surfactants were introduced for accelerating the SF self-assembly through the enhancement of conformational changes. Sodium dodecyl sulfate (SDS; **Figure 7**), a negative surfactant, was firstly reported as the gelling agent for SF [94]. The gelation time of SF can be shortened to 15-18 min with a presence of 8-12 mM, and the gel formation kinetics were in accordance with the structural transition from random coil to beta sheet.

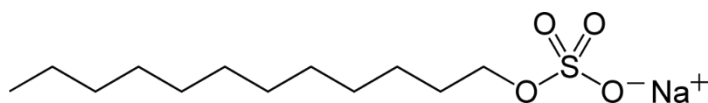


Figure 7 Chemical structure of sodium dodecyl sulfate

Hydrophobic and electrostatic interactions were proposed as main drive forces for SDS-induced SF gelation system. The adsorption of SDS on the SF chains, between the alkyl chain of SDS and the hydrophobic regions of SF or by the negative-charged head groups of SDS, led to the unfolding of SF chains. The size of SDS-SF micellar clusters was increased upon the gelation kinetics, resulting in a lower surface charge as described by Henry equation. The electrical repulsion, therefore, was overwhelmed by the attractive force between the mixed micelles. A higher opportunity of beta sheet formation was achieved due to a greater number of fibroin chain association.

The mechanisms of SDS-SF gelation were confirmed by Hirlekar et al [95] using small-angle neutron scattering (SANS) and nuclear magnetic resonance (NMR) techniques. The SF chains were unfolded, and the surfactant micelles were bound, forming the SDS-SF clusters. Tyrosine and valine residues presenting in the repeated motifs, GAGYGAG and GAGVGAG, possessed the high affinity to SDS binding and acted as the initial site for SF conformational transition. Furthermore, the higher SDS concentration led to a longer gelation time. Wu *et al* [94] mentioned that the higher negative charge could prevent chain association. The hypothesis was confirmed by SANS [95] and the binding model between SDS and SF was proposed. At an appropriate SDS concentration, the SDS micelles bound on the SF chain and reduced the distance between the chains, which facilitated the chain interactions. The higher SDS resulted in the larger micelles. The number of micelles per cluster was decreased, and the possibility of chain interaction was reduced accordingly.

The SDS-induced SF hydrogel was used as a substrate for cell culture [96]. SF solution was blended with agarose before inducing the gelation by SDS to enhance the mechanical stability. However, due to the cell toxicity of SDS, the hydrogels were lyophilized and soaked in water prior to the biological tests. The results showed that the presence of agarose did not only enhance the mechanical properties but the thermal stability against steam sterilization was also improved. The scaffolds supported cell proliferation and differentiation to the mature bone.

Later, a cytocompatible surfactant, sodium N-lauroyl sarcosinate (SNS), was introduced as an SF gelation inducer [98]. As the structure shown in **Figure 8**, SNS is a negatively charged amino acid-based surfactant synthesized from lauric acid and creatine, and its uses for cosmetics have been well reported. The gelation of SNS-induced SF was accelerated, and the gelation kinetics related to the SF conformational changes as found in SDS-SF gelation. The hydrogels supported cell survival and growth without removing

step of SNS, but the number of viable cells were far lower than those of the regenerated SF hydrogel.

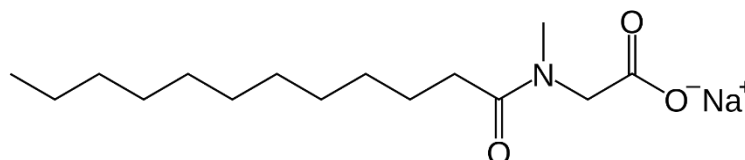


Figure 8 Chemical structure of sodium *N*-lauroyl sarcosinate

Additionally, an unsaturated, long chain fatty acid salt, sodium oleate (SO; **Figure 9**), was evaluated as a SF gelation enhancer [99]. The concentration of SF and the ratio between SF and SO affected the gel formation time, the viscoelastic properties, and the microstructures. With a fixed SF/SO content ratio, the gelation time decreased with an increase of SF concentration. The higher SF/SO ratio with a fixed SF content linked to a longer gelation. Similarly, the storage modulus was increased with a greater SF content and slightly decreased with a higher SF/SO ratio. Also, the ratio between SF and SO affected the pore size of the lyophilized samples, which the hydrogels with a smaller pore size were obtained at the lower SO content. The cytotoxicity of the SO-induced SF hydrogels was assessed using an indirect LDH cytotoxicity assay, and the results showed the slight cytotoxicity which the authors confirmed the possibility for biological-related applications.



Figure 9 Chemical structure of sodium oleate

Apart from the role of negatively-charged head group on the SF gelation, the effects of different chain lengths were evaluated [97]. Sodium oleyl sulfate (SOS) and sodium tetradecyl sulfate (STS), anionic surfactants with 8 and 14 carbon, respectively, were used to compare with SDS (12 carbon chain length), and their respective chemical structures were presented in **Figure 10**. The gelation time of STS-SF and SDS-SF were 20-30 min and 14-24 min, and the optimal concentration of the surfactants were 0.09% and 0.15%, respectively. The longer gelation was noticed for SOS-SF, of which the hydrogels were obtained in 113-144 h. The findings could indicate the role of carbon chain length in the gelation kinetics of SF which related to the hydrophobic interaction of the peptide chains.

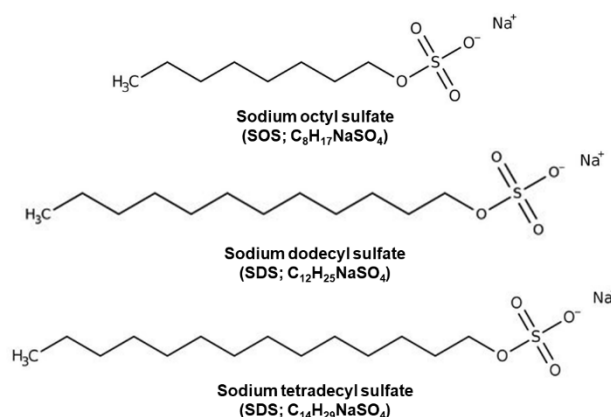


Figure 10 Chemical structure of SOS, SDS and STS

Besides the role of negatively charged surfactants in inducing SF gelation, the effects of non-ionic and cationic surfactants were also evaluated [100, 101]. The chemical structures of the surfactants were illustrated in **Figure 11**. Triton X-100, a non-ionic surfactant, can accelerate the SF gelation to 12-15 h. Because Triton X-100 cannot form the micellar structure in aqueous medium, the dehydration or salting-out effect was proposed as the main mechanism for the SF gelation rather than the formation of mixed micellar structures as described for the anionic surfactants. Dehydration of SF chains could reduce the distance between the molecules and, therefore, enhance the hydrophobic interaction.

Another anionic surfactant, sodium dodecyl benzene sulfonate (SDBS), was found to induce rapid SF gelation within 1 h when 100 mM was used. The proposed mechanisms similar to those of SDS and SNS were described, including the electrostatic forces of polar head group and the hydrophobic interaction between hydrophobic regions of SF and the alkyl chain of the surfactant [100].

For cationic surfactants, the immediate gelation of SF solution, resulting in the aggregate formation and phase separation, occurred. However, the surfactants with shorter alkyl chain, such as octyl trimethyl ammonium bromide (OTAB) and decyl trimethyl ammonium bromide (DETAB), were able to induce the homogeneous SF gel formation and the gelation time was tunable by varying the concentration. Strong electrostatic effect between the cationic polar head and the negative SF molecules was proposed. However, the charge effect was not supposed to be only interaction for the SF gel formation since other cations without the hydrophobic part cannot induce such rapid gelation. The hydrophobic interaction was also proposed. The results were confirmed by the FTIR and XRD which indicated predominated random coil and amorphous structure in the cationic surfactant-induced SF hydrogels.

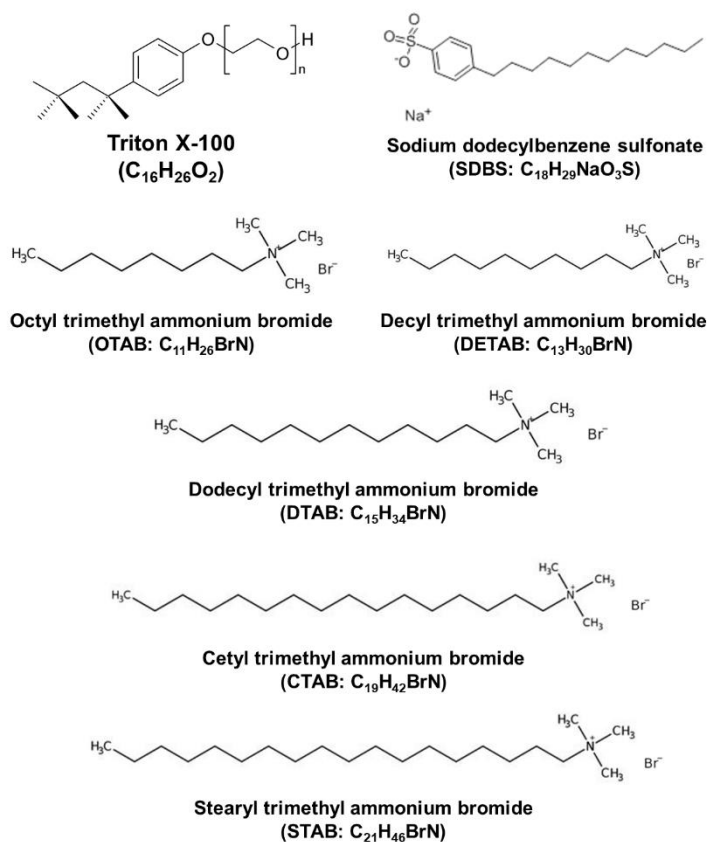


Figure 11 Chemical structure of a non-ionic surfactant, Triton X-100, an anionic surfactant, SDBS, and cationic surfactants, OTAB, DETAB, DTAB, CTAB and STAB

To enhance the viability of cells cultured with surfactant-induced SF hydrogels, a biocompatible surfactant, sophorolipid (SL), was found to accelerate the SF gelation within 140-189 min, and higher SL content linked to a greater cell proliferation [38]. Typically, there are two forms of SL, including lactonic SL and acidic SL (as shown in **Figure 12**). It was found that the different form of SL resulted in the different SF gelation kinetic. By using only acidic SL, the gelation was delayed, while pure lactonic SL significantly accelerated the SF gelation, comparing to the mixed SL [102]. NMR and SANS analysis revealed that the lactonic SL can be adsorbed on the hydrophobic pockets of SF, forming micellar-like structures. Subsequently, the hydrophobic interactions are enhanced, facilitating the beta sheet formation. While the acidic SL preferably forms micelles in aqueous medium. At a slower rate, the free acidic SL diffuses from the micelles and interact with SF chain. The diffusion of free acidic SL could be the rate-limiting step which delays the structural transition of SF. In the mixed SL system, lactonic and acidic SLs readily form the mixed micelles. The presence of acidic SL enhances the aqueous solubility of the lactonic SL. When mixing with SF solution, lactonic SL escapes from the mixed micelles and bind to SF molecules as well as the role of the charged acidic SL in unfolding SF chains [38, 102].

Furthermore, due to the presence of carboxylic group of acidic SLs, pH of the medium can influence the degree of ionization. At a low pH (pH 6), the SF gelation was slow, and the gelation time was faster when the pH of medium was increased towards pH 10 [103]. It was proposed that the larger negative charge of the SL micelles at pH 8 could enhance the electrostatic repulsion between SF chains. The chain extension, therefore, facilitates the formation of beta sheet from hydrogen bonding and hydrophobic interaction.

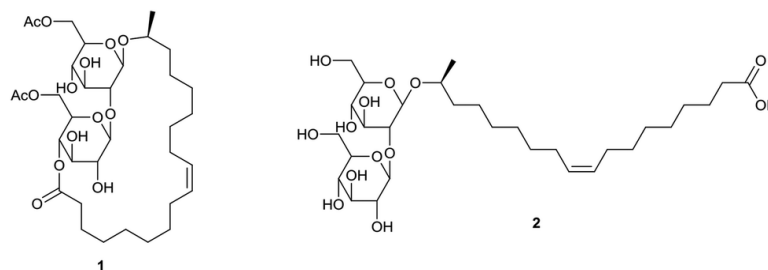


Figure 12 Chemical structure of (1) lactonic and (2) acidic sophorolipids

3) Salts

Even the addition of salts, such as Ca^{2+} , can influence the gelation of SF, the gelation time was still within several days [16]. As the proposed mechanisms of gelation of the anionic surfactants described previously, the gelation process of SF requires the electrostatic and hydrophobic interactions. Thus, the amphipathic molecules containing the polar head and the hydrophobic tail are mostly effective in accelerating the gelation kinetics of SF. However, some salts have been reported as a crosslinker of SF, resulting in a rapid hydrogel formation. The mechanism was mainly the generation of new bonds rather than an enhancement of the SF self-assembly.

Im *et al* [104] reported that nitrate salts, namely lithium nitrate (LiNO_3), sodium nitrate (NaNO_3), and potassium nitrate (KNO_3), can accelerate the gelation of SF solution within 14 min. However, SF was needed to be dissolved in formic acid, making the solution ineligible for biological uses. The proton generated by acid reacts with NO_3^- to form HNO_3 . Tyrosine residue presenting in SF molecule acts as a nucleophile, and take an electron from NO_3^- , resulting in the formation of tyrosine radical and NO_2^\bullet . The nitrate radicals subsequently attack the tyrosine radicals to form nitrotyrosines. Furthermore, two tyrosine radicals can crosslink with each other to form dityrosine. The mechanisms of SF gelation mediated by nitrate salts are depicted in **Figure 13**.

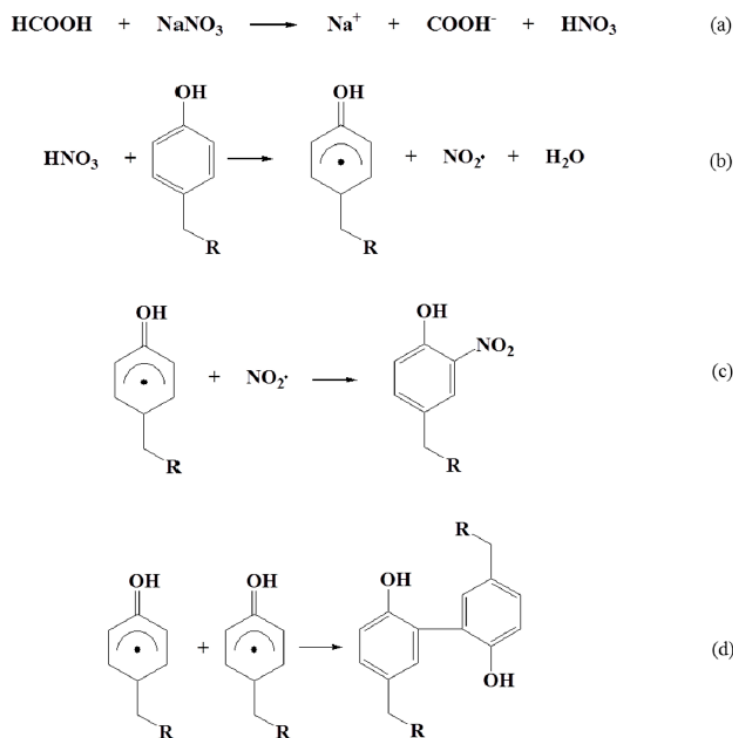


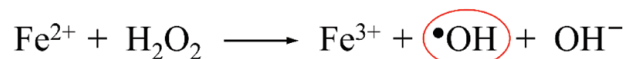
Figure 13 SF gelation mechanisms mediated by NaNO_3 : (a) the generation of HNO_3 (b) the formation of tyrosine and nitrate radicals (c) the formation of nitrotyrosine (d) the formation of dityrosine (adapted from [104])

The formation of dityrosine can be initiated by radicals generated from the chemical state change of transition metals. For example, the Fenton reaction (**Figure 14a**), which hydroxyl radicals are generated by the oxidation of Fe^{2+} to Fe^{3+} , was reported to crosslink tyrosine in SF molecules, leading to a rapid hydrogel formation [23]. Tyrosine residues are oxidized by hydroxyl radicals and cross-linked between two tyrosyl radicals to form dityrosine. Furthermore, Fe^{3+} was proposed to electrostatically bind to tyrosine, glutamate, and aspartate residues. The formation of beta sheet of SF was, therefore, accelerated due to a less chain extension. A presence of ascorbic acid leads to the reduction of Fe^{3+} to Fe^{2+} , shifting the Fenton reaction towards the products and increasing hydroxyl radicals (**Figure 14b**). The number of tyrosine was increased with a higher content of ascorbic acid. However, the high concentration of ascorbic acid linked to a lower pH of the mixed solution, which might be reduced closer to pI of SF, making the SF chains spontaneously self-assemble.

Due to the generation of dityrosine, the predominated secondary structure of the SF hydrogel was random coil. However, the beta sheet content was gradually increased after incubating the cross-linked hydrogel several days. The structural transition of dityrosine-crosslinked SF hydrogels upon incubation was previously reported [37]. The increase of beta sheet content linked to a stiffer hydrogel determined from higher compressive modulus. The gradual conformational transition could result from spontaneous self-assembly

to a more stable beta sheet conformer or the adsorption of Fe^{3+} to tyrosine, glutamate, and aspartate residues. The binding of Fe^{3+} to SF chains could facilitate the formation of beta sheet structures, triggering the rapid SF gelation [23].

(a) Fenton reaction



(b) Fenton reaction with ascorbic acid

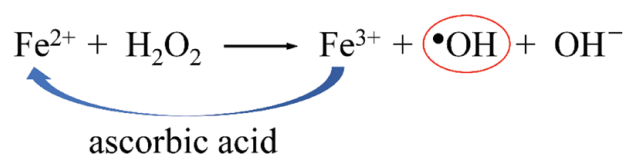


Figure 14 (a) Fenton reaction, and (b) with a presence of ascorbic acid

4) Tannic acid

Tannic acid, a natural-derived polyphenol, was introduced as a gelation enhancer of SF proteins. Apart from using as a gel inducer, the SF hydrogels with various functions, including high adhesiveness, shear-thinning, self-healing, antioxidation and antibacterial, can be obtained [105]. The gelation mechanisms of SF mediated by tannic acid was proposed as the induction of conformational transition to beta sheet and hydrogen-bonding interactions. Because of the presence of weak and reversible interactions between SF and tannic acid, the obtained hydrogels showed self-healing and shear-thinning properties, which are applicable as a bioink for 3D printer.

The developed hydrogels possessed a high adhesiveness, due to the presence of catechol groups in tannic acid, which is favorable for wound healing applications. Furthermore, the biological activities of tannic acid, namely antioxidant and antibacterial properties, were presented in the tannic acid-SF hydrogels. Viability and growth of gram-negative and gram-positive bacteria were inhibited.

The hydrogels were tested *in vitro* and *in vivo* to confirm the applicability for wound healing and skin infection treatment. NIH/3T3 fibroblasts cultured on the hydrogels exhibited normal proliferation without any adverse effects. When applying the tannic acid-SF hydrogels on the full thickness skin wound with bacterial infection in mice, comparable wound closure and disinfection to Tegaderm within 14 days were noticed. The hydrogels also supported wound healing and tissue regeneration better than the SF hydrogels without tannic acid.

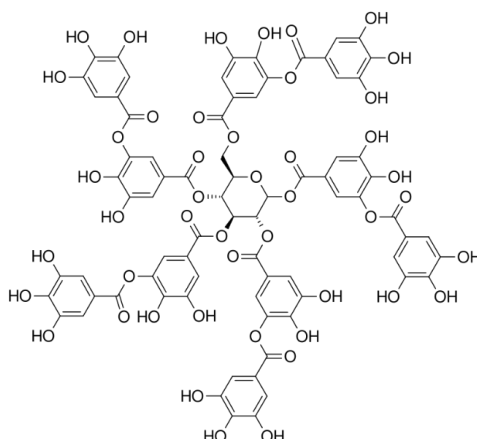


Figure 15 Chemical structure of tannic acid

c. Enzymatic crosslink

1) Horseradish peroxidase

Horseradish peroxidase (HRP) is a catalytic enzyme for the formation of dityrosine through oxidation of tyrosine, yielding the generation of tyrosyl radicals and subsequent dityrosine crosslinking [45]. The schematic reaction mechanisms are illustrated in **Figure 16**. HRP has been applied for the hydrogel formulation which can be fabricated *in situ*. This strategy is applied to several biopolymers, namely hyaluronic acid, gelatin, alginate and chitosan [45, 106]. Due to a substantial amount of tyrosine in SF (approximately 5.1-7.6%) [55, 58], the HRP-catalyzed SF gelation can be performed. The gelation of SF occurred within less than 1 h [106] and the gelation time was tunable by varying the content of HRP and H_2O_2 [37]. The formation of dityrosine was confirmed by fluorometry and random coil structure was predominated in the hydrogels, indicating that the gelation was irrelevant to the beta sheet formation [106]. However, upon an incubation *in vitro* or subcutaneous implantation in mice for 10 days, a beta sheet content increased, relating to a transition from transparent to opaque hydrogels [37].

Instead of using H_2O_2 as a reactive oxygen for the activation of HRP, riboflavin was introduced as an alternative [109]. Upon a light activation, riboflavin induces the generation of a singlet oxygen, which can produce a peroxide. The generation of peroxide further oxidize the HRP enzyme and initiate the crosslink process. Hence, the photocurable SF hydrogel could be implemented with the presence of HRP and riboflavin, initiating the gelation with a simple light activation.

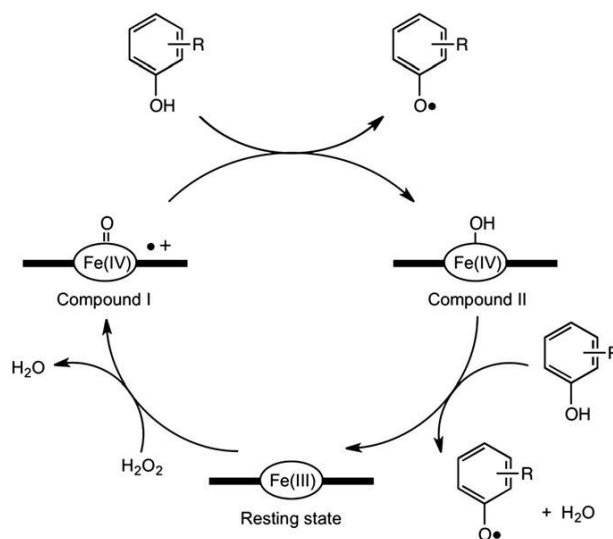


Figure 16 HRP catalytic reaction. With a presence of H_2O_2 , HRP was oxidized, resulting in an activated state with a power reducing property. The electrons from activated HRP were transferred to phenolic oxidizing agent, leading to a formation of tyrosyl radicals. The tyrosyl radicals can react with each other to form dityrosine. (adapted from [45])

The HRP-catalyzed SF hydrogels showed the stimuli responsiveness to the changes of ionic strength and pH. An immersion of the hydrogels in PBS resulted in condense and stiffer hydrogels, but the hydrogel dimension and the mechanical stiffness were reversible when immersed in water [37, 106]. Acidic conditions affected the shrinkage of the hydrogels which can be reversed after an immersion in the basic medium [37].

Because the formation of HRP-mediated SF hydrogels underwent in mild conditions, the hydrogels can be used to encapsulate viable cells in 3D environment. Human MSCs were laden in the hydrogels and their viability was observed after cultured for 29 days. However, due to the inherent property of SF, cells retained round-shaped morphology with few spreading, indication a low interactions with the matrix [106]. Similar results were observed for encapsulated ATDC-5 and HeLa. The number of viable cells and the proliferation rate decreased after 10 days, which related to the structural transition to beta sheet conformers [37]. The authors stated that the conformational transition to beta sheet induced the apoptosis of the encapsulated cells. For the tumor growth, the predominated beta sheet SF hydrogels could prevent tumor formation as well as the invasion of endothelial cells, which is necessary for tumor angiogenesis.

Apart from the in situ gelation mediated by HRP/ H_2O_2 , this strategy was also used for the preparation of hydrogels. For example, the composite hydrogels composed of SF and polyvinyl alcohol (PVA) were crosslinked by HRP/ H_2O_2 [107]. The hydrogels were used for the encapsulation of lipophilic drug, using the emulsifying property of PVA, which enhanced the loading

amount in aqueous medium and controlled the release from the hydrogels. However, PVA was blended with SF with a weak interaction between the polymer chains, resulting in a fast degradation and low mechanical stability. Another example of the preformed scaffold fabricated by HRP enzymatic crosslink was reported in the work of Ribeiro *et al* [134]. The bilayer scaffold was designed to mimic cartilage and subchondral tissues, using HRP-mediated SF scaffold and tri-calcium phosphate loaded HRP-SF scaffold, respectively. The scaffolds were undergone *in vitro* experiment by co-culturing of human osteoblasts and human articular chondrocytes. The bilayer scaffolds showed a higher expression of both osteoblast and chondrocyte activities, determining from the generation of ECM proteins and glycosaminoglycans, the mineralization and the expression of relevant genes.

To enhance the gelation kinetics and the mechanical properties of the HRP-mediated SF hydrogels, the tyramine-functionalized SF was introduced to provide more accessible phenolic hydroxide groups as the crosslinking points [108]. Furthermore, tyramine-functionalized gelatin was prepared to enhance the bioactivity of the hydrogels. It can be noticed that the conjugation of tyramine to either SF or gelatin improved the gelation kinetics and increased the storage modulus, due to an increasing of crosslinking points.

2) Tyrosinase

Tyrosinase is another enzyme used for crosslinking phenolic groups. Therefore, it has been implemented for the proteins with tyrosine residues. Later, Kang *et al* [135] reported the crosslinking reaction of SF mediated by tyrosinase and illustrated the reaction mechanisms as shown in **Figure 17**. Firstly, tyrosine residue in SF is oxidized to form dihydroxyphenyl, which subsequently forms *o*-quinone. This reactive group can undergo non-enzymatic reactions, including the addition between two *o*-quinone residues, to form dityrosine, or between *o*-quinone and primary amine groups.

Later, this strategy was implemented to SF-gelatin blends serving as cell-encapsulated bioinks for 3D printing applications [39]. The tyrosinase-crosslinked SF-gelatin hydrogels outperformed sonicated hydrogels in several aspects. Firstly, due to the chemical crosslink between SF and gelatin, gelatin was retained in the hydrogels, maintaining the shape, and preserving the mechanical stability for a long period. While gelatin presented in the sonicated hydrogels was physically bound, resulting in a gradual release to surrounding environment. The release of gelatin affected the physicochemical properties of the hydrogels and deteriorated the bioactivities of gelatin in supporting cell attachment and proliferation. Furthermore, the secondary structures of the hydrogel matrices influenced cell viability. Cells encapsulated in the enzymatic-crosslinked hydrogels with the predominated random coil structure were more viable than those of the sonicated SF-gelatin hydrogels with high beta sheet content. These results were in an agreement with the report from Yan *et al*, stating that the transition to beta sheet resulted in a low proliferation rate of the encapsulated cells as well as inhibited the penetration of other cells into the hydrogels [37].

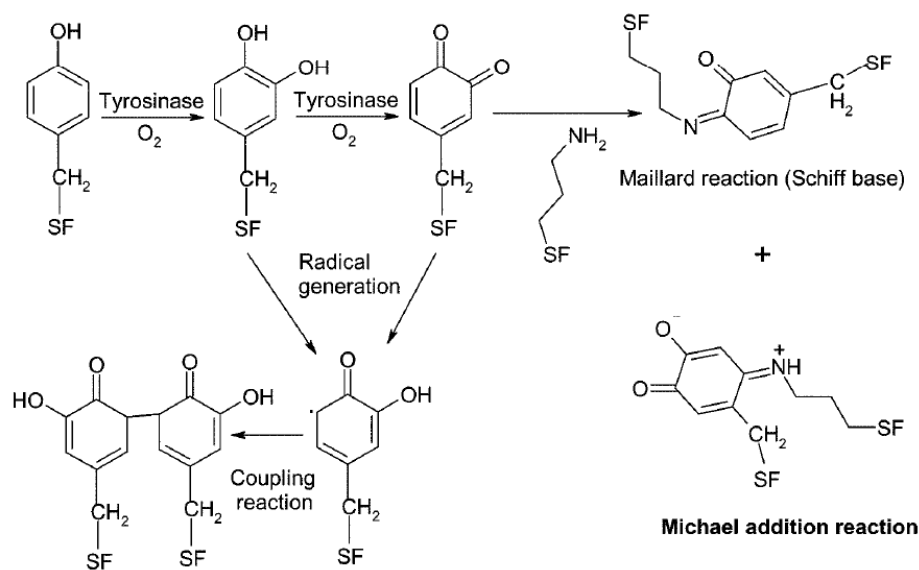


Figure 17 Reaction scheme of tyrosinase reacting with the tyrosine residues of SF. Tyrosine was oxidized by the enzyme to form dihydroxyphenyl, before spontaneously form o-quinone. The o-quinone further undergo non-enzymatic reactions, including Michael addition reaction with primary amine and the coupling reaction to form dityrosine. (Adapted from [135])

d. Blends and composites

1) Poloxamer/silk fibroin

Poloxamer 407, a triblock copolymer which is popularly used as a non-ionic surfactant, was blended with SF solution, and the gelation of SF was accelerated [110]. Molecular weight of poloxamer 407 used was 12,500 g/mol and the amount of monomers was 97 and 69 for ethylene oxide and propylene oxide, respectively (*a* and *b* in **Figure 18**). The SF hydrogels can be achieved in 5-210 min depending on the concentrations of SF and poloxamer. The structural transition of SF from random coil to beta sheet was evidenced after the gelation was induced by poloxamer. The dehydration of SF chains due to the water absorption of poloxamer was proposed as a driving force for enhancing SF chain interactions. Furthermore, x-ray diffraction (XRD) and differential scanning calorimetry (DSC) confirmed an interaction between SF and poloxamer, presumably hydrophobic interaction and hydrogen bonding.

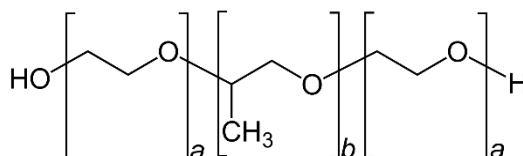


Figure 18 General formula of poloxamer 407 composed of ethylene oxide and propylene oxide monomers

2) Polyethylene oxide or polyethylene glycol/silk fibroin

Polyethylene oxide (PEO) or polyethylene glycol (PEG) is a bioether widely used for several applications, and FDA-approved for biomedical uses. The structure of PEG is depicted in **Figure 19**. The gelation of SF induced by PEG was firstly reported by Kim *et al* [16]. In this report, PEG with molecular weight of 900 kDa was used, and the gelation occurred in 10-30 days upon a content of added PEG. The structural transition of SF from predominated random coil in solution state to beta sheet structure in a freeze-dried hydrogel was noticed. The authors proposed that PEG caused water movement from the SF molecules, resulting in a higher chain interactions and subsequent beta sheet formation.

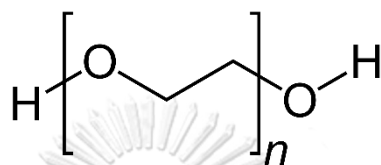


Figure 19 Chemical structure of PEO or PEG

Subsequently, low molecular weight PEG, 300 and 400 Da, was able to accelerate the SF gelation tunable by the concentration of SF or PEG and the molecular weight of PEG, as reported by Wang *et al* [111]. A higher concentration of SF or PEG resulted in a lower gelation time, and the PEG with the molecular weight of 400 Da caused a faster SF gelation than 300-Da PEG. Furthermore, the mechanical properties were influenced by the SF concentration and the molecular weight of PEG. The gelation of PEG-induced SF linked to a transition from amorphous random coil to highly stable beta sheet, and the gelation mechanisms were described as previously. As the substrates for the cell culture, PEG-SF hydrogels did not well support cell attachment and proliferation in an initial period, due to a high osmotic pressure caused by PEG and the burst release of PEG into culture medium. However, cultured cells began to attach, spread, and proliferate after 5 days of culture. Subcutaneous implantation of the hydrogels in rats showed no significant adverse host response and maintained their shape in 10 days, before noticeably degraded into small pieces in 17-20 days.

Another interesting approach of the PEG-SF hydrogels was introduced by Wei *et al* [112]. Instead of blending PEG and SF and allowing the complete gelation, the PEG-SF was readily frozen after mixing and then lyophilized. Then, the obtained lyophilized sponge was reconstituted with water and allowed to turn gel for using as hemostatic materials. The gelation time of reconstituted PEG-SF mixtures ranged from 2 to 115 min depending on the solid content of PEG-SF. The major secondary structure of lyophilized PEG-SF sponge was random coil while that of the PEG-SF gel forming after reconstitution was beta sheet. Hemostatic properties of the PEG-SF hydrogel were determined *in vitro* and *in vivo*. Using a liver wound model in rabbits, PEG-SF sponge showed superior hemostasis properties, including hemostatic time and the adhesion to wound surface, compared to those of pure SF or gelatin sponge. Moreover, PEG-SF sponge promoted platelet aggregation by

stimulating a conversion from fibrinogen to fibrin and the adhesion of platelets. The authors proposed that the fibrous-like microstructures of SF sponge could resemble ECM environment, which favored platelet adhesion.

The adhesiveness of SF materials can be improved by the functionalization of catechol-presenting moieties, such as dopamine, to the SF molecules. Dopamine-conjugated SF was prepared using the EDC/NHS chemical reaction, and the gelation of the obtained SF was induced by PEG (20 kDa) [113]. Theoretically, the catechol presenting in the dopamine undergo an oxidation to form *o*-quinone, which can spontaneously form the covalent bond with primary amine. Since the presence of primary amine groups in several biological surfaces, the adhesion is enhanced. The developed PEG-induced dopamine-conjugated SF hydrogels was found to efficiently adhere to several surfaces, including a porcine skin, and can be injected through a spinneret without shape failure. The results presented a potential application as a sealant or biological adhesive.

3) Cellulose/silk fibroin

Hydroxypropylcellulose (HPC: structure as shown in **Figure 20**) was blended with SF solution and a rapid gel formation was achieved [114]. The gelation time was tunable by varying the ratio between SF and HPC. An increasing of beta sheet structure was noticed which linked to the gelation of the blends. HPC-induced phase separation was proposed as a main gelation mechanism. As the intermolecular hydrophobic interactions are enhanced at 37°C, the HPC molecules spontaneously assemble, triggering the phase separation from SF. Therefore, the local concentration of SF increases, enhancing the chain interaction and beta sheet formation.

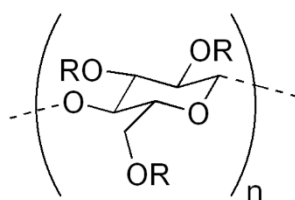
Shear-thinning and self-healing properties were noticed for the HPC-SF blended hydrogel. After the application of 3,000% strain, the hydrogel recovered within 5 min with the elastic modulus approximately 80% of the initial value. The structural changes and the mechanisms affected the thixotropic properties of the hydrogels were further evaluated [115]. After applying shear force to the hydrogels, phase inversion occurred. SF which was originally formed as the continuous phase became dispersed phase after the injection, and HPC converted to the continuous phase. It can be proposed that a large strain applied to the HPC-SF hydrogels induced the deformation between beta sheet domains, disrupted weak interactions between them, resulting in the slippage of beta sheet, before the reconstruction of weak crosslinks after resting.

The thixotropic HPC-SF hydrogels showed the feasibility to serve as an injectable hydrogel or a bioink for 3D printer. L929 was encapsulated in the hydrogels and injected through a needle. Most of the cells survived after the injection, confirming the application as an injectable cell carrier [114]. Furthermore, the hydrogels can be used as drug delivery polymers for local administration. For example, anticancer drugs, doxorubicin, and curcumin, were loaded in the hydrogels and intratumor-injected in tumor-bearing mice.

The drug-loaded hydrogels effectively inhibited tumor growth, reduced the tumor progression and prevented tumor relapse [115].

Hydroxypropylmethylcellulose (HPMC: structure is shown in **Figure 20**), another cellulose with substituted methoxy groups, was introduced as a gelation inducer of SF with substantially enhanced mechanical properties of the hydrogels [116]. The compressive modulus of the HPMC-SF hydrogels was higher than that of HPC-SF and methoxypropylcellulose (MPC)-SF hydrogels. The coordination roles of methoxy groups and hydroxypropyl groups in the hydrophobic interaction and hydrogen bonding were proposed for the enhancement of the mechanical stiffness as well as the SF gel formation. However, due to the high lower critical solution temperature (LCST) of HPMC, which is 62°C, the gel formation of the HPMC-SF mixture was needed to conduct at 70°C. At this temperature, cell encapsulation in the hydrogels was impossible. Therefore, this hydrogel system was solely applied as a preformed bioink for 3D printing because of its thixotropic property which facilitates the injection through a needle.

For example, Zhong *et al* [136] prepared and printed the 1% HPMC-27% SF hydrogels and printed. High SF concentration was used to improve shape integrity and minimize structural shrinkage after printing. Furthermore, HPMC-SF hydrogel with 30% solid weight was proven for the appropriate thixotropic and self-standing properties for 3D printing applications [137]. Cytocompatibility of the printed scaffolds was evaluated and the results showed no significant cytotoxicity. However, the cultured cells, including human bronchial epithelial cell line, BEAS-2B, and hMSC, exhibited a low attachment and delayed proliferation, which the authors proposed that the smooth microtopography of the hydrogels could not well support cell adhesion [136, 137].



Hydroxypropylcellulose (HPC):
R = H or CH₂CH(OH)CH₃

Hydroxypropylmethylcellulose (HPMC):
R = H or CH₃ or CH₂CH(OH)CH₃

Figure 20 Chemical structure of HPC and HPMC

4) Short peptides/silk fibroin

Naphthalene-diphenylalanine (NapFF: **Figure 21**), a synthetic peptide, showed a property in enhancing the SF gelation and the complete gel formation can be achieved in 97 sec to 1.5 h with the concentration of SF as

low as 0.1% [117]. Physical interactions, including hydrophobic interactions and hydrogen bonding, between SF and NapFF were proposed and linked to the SF beta sheet formation, resulting in hydrogel formation. Shear-thinning and recovery properties were observed. However, when using the NapFF-SF hydrogels as substrates for cell culture, cells showed low affinity as well as delayed attachment and proliferation. Therefore, RGD, a cell adhesion motif, was conjugated to NapFF, yielding NapFFRGD (**Figure 21**). The binding affinity of the cells to the hydrogels and the proliferation rate were substantially enhanced.

Potential applications of the NapFFRGD-SF hydrogel as drug delivery carrier and tissue-engineered injectable scaffold were evaluated. Vascular endothelial growth factor (VEGF) was loaded in the hydrogels and subcutaneously injected in mice. Tissue ingrowth was noticed as well as a formation of new blood capillaries inside the implanted hydrogel. The area of the new capillaries in the VEGF-loaded hydrogel group was significantly higher than that of the mice injected with the blank hydrogel, indicating the feasibility of the NapFFRGD-SF hydrogel for delivery system [117]. Another example was the implementation of the hydrogel as a bone substitute. For *in vitro* investigation, mouse MSCs were cultured under osteogenic conditions, and it was found that culturing on the hydrogel promoted osteogenic differentiation, determining from gene expression, protein production and mineralization. Subsequently, mouse MSCs were encapsulated in the hydrogel and injected to a calvarial defect in mice. After 6-week implantation, the area of new bone formation in the mice implanted with the hydrogels was larger than the control, supporting the application of the hydrogel as an injectable scaffold in tissue engineering [118].

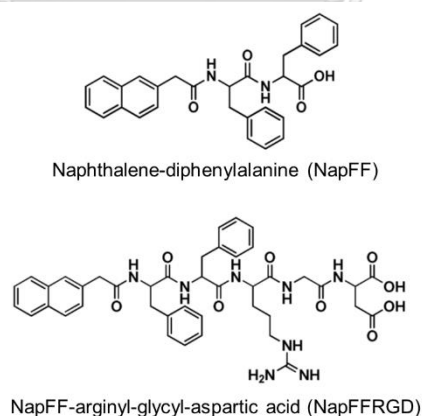


Figure 21 Chemical structure of NapFF and NapFFRGD

5) Non-mulberry silk fibroin/mulberry silk fibroin

SF derived from non-mulberry or wild silkworms, such as *Antheraea pernyi*, *Antheraea assamensis* or *Antheraea assama*, shows a distinct characteristic from *Bombyx mori* silk fibroin. A presence of high ratio of alanine-glycine and poly-alanine sequences in its primary structure results in a more difficult in dissolution and rapid conversion from the solution to gel

state. Furthermore, the dissolution process of non-mulberry silkworm requires harsh conditions, which deteriorate the mechanical stability of the obtained biomaterial [119]. Therefore, non-mulberry SF was blended with mulberry SF to induce the rapid gelation as well as enhance the mechanical properties of the resulted hydrogel. The gelation can be achieved in less than 1 h depending on the ratio of the proteins [119-121]. The hydrophobic interaction between peptide chains was proposed as a driving force for the formation of beta sheet and hydrogel formation.

The mechanical properties of the blended hydrogels were significantly influenced from the ratio between two types of SF. A higher ratio of mulberry SF resulted in higher compression modulus. Even a high ratio of mulberry SF related to an enhanced modulus, the blended hydrogels became more brittle. When performing a cyclic compressive experiment, the hydrogels with high *B. mori* SF ratio showed lower recoverability after several compressive cycles were applied. Furthermore, the pH-responsive mechanical properties were noticed, which the hydrogels immersed in acidic media showed more stiffness and the modulus reduced with a pH shifted towards the alkalinity [121].

In addition to the improvement of the gelation kinetics and the mechanical stiffness, the RGD sequence presenting in non-mulberry SF can improve the cell affinity to the SF hydrogel. By varying the ratio between different types of SF, a higher ratio of the non-mulberry SF linked to a higher proliferation rate and the encapsulated cells were able to function higher bioactivities [121, 122]. Several cells were encapsulated in the blended SF hydrogels, namely porcine nucleus pulposus (NP) cells [121], RIN-5 rat insulinoma cells, mouse islets [122], and a high proliferation rate was observed in the hydrogels with high ratio of non-mulberry SF. The encapsulated islets displayed a greater bioactivity, including the expression of RNA and insulin production, in proportion with the ratio of non-mulberry SF [122]. Furthermore, the hydrogel was implemented as a wound sealant in third-degree burn wounds in mice, and the comparable results for wound closure, blood vessel formation and re-epithelialization to the collagen hydrogels were noticed [120]. The hydrogel was administered subcutaneously in animals and showed no adverse host response, such as severe inflammation, at implanted site [122]. It can be proven that the strategy in inducing SF gelation by blending different SF types could be advantageous for fabricating protein-based biomaterials without using other small molecules or biopolymers. The obtained hydrogels displayed a better mechanical stability than the *B. mori* SF and the improved bioactivity of non-mulberry SF.

e. Photo-crosslinking

Several crosslinking strategies were used to fabricate either pre-formed or *in situ* SF hydrogels. Chemical crosslinkers, namely glutaraldehyde, carbodiimides and genipin, were introduced for forming the hydrogel structure through the generation of covalent bonds. However, the processes are conducted in harsh conditions, which are inappropriate for the applications as *in situ* hydrogels. Subsequently, physiological-friendly enzymatic crosslinkers, such as HRP and tyrosinase, were reported as discussed previously.

Alternatively, photo-crosslinking is introduced as a facial strategy for the rapid gelation of SF and might be used as *in situ* crosslinkers.

Ruthenium catalyst (Ru (II)) was able to crosslink SF molecules through a generation of dityrosine [123, 124]. With a presence of an electron acceptor, ammonium persulfate, and an activation by visible light, the gel formation occurred immediately. Upon the light activation, Ru (II) transforms to Ru (III) which can reduce tyrosine residues presenting in the SF molecules to form tyrosine radicals. The reactive tyrosine automatically tautomerizes with another tyrosine to form dityrosine crosslinks. The schematic reaction is illustrated in **Figure 22**. Therefore, the gelation occurred immediately after light exposure, approximately within 5 sec.

There was no evidence of the structural transition to a highly-ordered beta sheet after crosslinked, indicating that the Ru (II)-mediated photo-crosslinking of the SF was not relevant to the SF self-assembly. Interestingly, the gradual conformational change from random coil to beta sheet was noticed in the case of the HRP-mediated SF hydrogel, which presented the similar dityrosine crosslinking for the SF gelation, after incubation for several days or implanted in mice for 10 days [37]. The formation of beta sheet led to an increase of the mechanical stiffness. However, this phenomenon was not observed in the Ru (II)-mediated photo-crosslinked SF hydrogel. Amount of the beta sheet structure determined after 5-week incubation was not significantly different from that of the as-cast hydrogels [124]. Thus, the compression modulus of the hydrogel was not changed over time.

The photo-crosslinked SF hydrogel using Ru (II) was then implemented as a cell culture substrate for ATDC5 pre-chondrocyte cells. The photo-crosslinked showed a potential as a cell culture material as the cultured cells were able to survive and proliferate [123]. Furthermore, the Ru (II)-mediated SF hydrogel showed an advantageous over the HRP-SF hydrogel for the 3D cell encapsulation. With a high cell density, such as 15×10^6 cells/ml, the gelation of the enzymatically crosslinked SF hydrogel cannot be achieved, but the photo-crosslinked SF hydrogel was able to do so. The authors proposed that, due to the lower molecular weight of Ru (II) (750 Da) than that of HRP (44,000 Da), Ru (II) could be more accessible to propagate the crosslinking reaction, leading to a more homogeneous and complete gel formation [124].

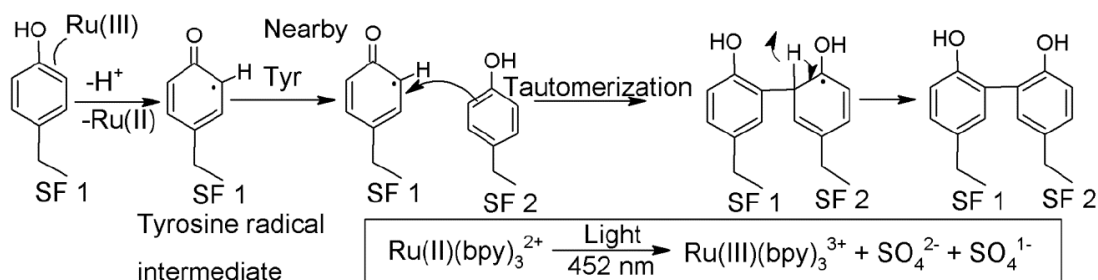


Figure 22 Reaction mechanism of Ru (II)-mediated dityrosine formation. Ru (II) transforms to Ru (III) upon the light activation. Ru (III) then reduces tyrosine to form

*tyrosyl radical, which can react with another tyrosine to form dityrosine crosslink.
(Adapted from [123])*

f. Functionalization of silk fibroin

Due to the presence of several functional groups which are possible for chemical reactions in SF, namely hydroxyl, carboxyl and amine groups, the SF structure can be modified by conjugation or functionalization to obtain the functional material. The modification of SF can be performed to improve the sol-to-gel transition kinetics by introducing stimuli-responsive or auto-crosslinkable groups.

Methacrylate, which is a photocurable group, was conjugated to hydroxyl groups presenting in the SF molecules [125]. Fortunately, a high content of hydroxyl amino acid residues, namely serine, tyrosine, and threonine, is found in the SF with an approximately 14.2 mol%. Therefore, a high degree of methacrylate conjugation of SF can be achieved. With a presence of a photoinitiator, the gelation of methacrylated SF occurred upon an activation by UV light with, and the gel formation did not relate to the conformational change from random coil to beta sheet. The low content of beta sheet resulted in a resilience property of the hydrogel, which was able to withstand the cycle compressive stress and maintain its structural integrity after compression. The shear-thinning and self-recovery of the hydrogel presented a facile material for 3D printing applications.

Kim et al [126] presented the applications of methacrylated SF as the bioink for 3D printer equipped with digital light processor, which is able to project UV light with high resolution and precision. The obtained hydrogel showed a high mechanical stability and an excellent self-recovery, even compressed with 7-kg load. Methacrylated SF solution was printed and exposed to UV light controlled by digital light processor, resulting in a facile printing method for a high resolution and a printability of complex objects.

The photo-crosslinked methacrylated SF hydrogel was loaded with NIH/3T3 cell lines and primary human chondrocytes. For 14-day culture of the NIH/3T3, the cells distributed evenly in the hydrogel matrix and proliferate along the time-course. For the long-time culture of the chondrocytes, the cells were able to survive, proliferate and express the chondrogenic properties, namely an expression of genes relating to chondrogenesis and a production of cartilage ECM proteins [126, 127]. Furthermore, the chondrocyte-loaded hydrogel was implanted subcutaneously in mice. After 8 weeks, the degradation of the implanted hydrogel occurred, and the histological characteristic of cartilage tissue can be observed at the implant site [127].

Due to the elastic and self-healing properties of the photo-crosslinked methacrylated SF hydrogel, the material was applied as the regenerative matrix for a defected tissue with high mechanical stress, such as trachea. Rabbits with trachea defects were treated with the hydrogels, and the outcomes after 6 weeks were evaluated. The regeneration of the defected

tissue can be noticed via a newly formed cartilage-like tissue and blood vessels [127]. The results confirmed the feasibility of the methacrylated SF as a biomaterial for the cell encapsulation carrier as well as the printing process for the fabrication of highly detailed cell-laden scaffolds.

Due to the reactivity of thiol groups in forming covalent bonds with various functional groups spontaneously, several polymers functionalized with thiol were used as base materials for the hydrogel fabrication. For SF, thiol groups were conjugated using reduced glutathione coupled with EDC/NHS chemicals, and the thiolated SF was mixed with PEG diacrylate (PEG-DA) to form the hydrogel. UV light activation was applied to crosslink either between the thiol groups of SF and the acrylate groups of PEG-DA or between PEG-DA itself. The hydrogel with excellent structural integrity was obtained within less than 3 min. Subsequently, the hydrogel was assessed for the biocompatibility both *in vitro* and *in vivo* to ensure its potential as the biomaterial for hydrogel fabrication [128].

Instead of forming the SF hydrogel from the SF solution, Shi et al [129] reported the fabrication of SF-based hydrogel from hydrolyzed SF fibers coated by calcium and phosphate. The gelation was intrigued by the addition of a binder made of functionalized hyaluronan with bisphosphonate groups. Because of the spontaneous binding between bisphosphonates and Ca^{2+} by chelation, the hydrogel was formed immediately after mixing the CaP coated SF microfibers and the bisphosphonated hyaluronan binder. Furthermore, the reversibility of the coordination bond between CaP and bisphosphonates, the resulted hydrogel performed the shear-thinning and self-healing properties after applying the shear strain from 150%. However, the mechanical stability of the crosslinked hydrogel was extremely low (storage modulus ~ 250 Pa), which was difficult to handle. Photo-crosslinking was applied. The hyaluronan binder was conjugated with photocurable acrylamide groups, before the functionalization of bisphosphonates. The binder was mixed with the CaP-SF microfibers and cured by UV light for 10 min. The storage modulus of the hydrogel increased up to 250 kPa, 10-times higher than that of the single crosslinked hydrogel.

Human MSCs were cultured on the dual-crosslinked CaP-SF hydrogel and evaluated their osteogenic differentiation potentials. Seemingly, the coating CaP of SF microfibers deteriorated the osteogenic differentiation, as the expression of related markers was lower than those of the uncoated SF microfiber hydrogel. However, the expression of VEGF was higher, indicating the promotion of angiogenesis. The scaffold was then implanted in the bone cranial defect of mice. After 8 weeks, the signs of bone regeneration were noticed as well as the formation of blood vessels. No accumulation of inflammatory can be detected at the implantation site [129].

4. Phospholipids and Liposomes

4.1. Phospholipid characteristics

4.1.1. Structure and classification of phospholipids

Phospholipids (PLs) are lipids containing phosphorus, a polar and non-polar portion, which can be structurally classified by alcohol linkers. Glycerophospholipids and sphingomyelins are the PLs with glycerol and sphingosine linkers, respectively [18]. Only glycerophospholipids are discussed in the subsequent sections since sphingomyelins are not used in this work. **Figure 23** illustrates the chemical structure of DMPC, which consists of a glycerol backbone linked with phosphate group (PO_4^{2-}) and two 14-carbon fatty acids. In some cases, the phosphate group is linked with another small molecule, resulting in different types of PL which is shown in **Table 5**.

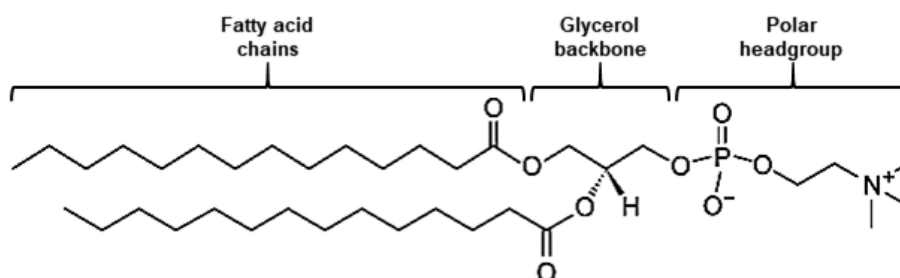
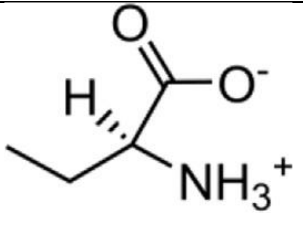
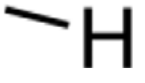
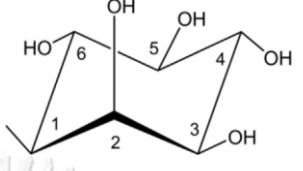
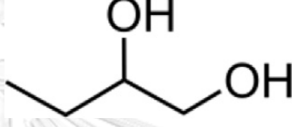
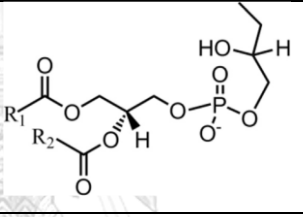


Figure 23 Chemical structure of 1,2-dimyristoyl-*sn*-glycero-3-phosphocholine (DMPC), a glycerophospholipid. The composition of two fatty acid chains, glycerol backbone, and the polar phosphate headgroup (choline) is displayed.

PLs can be identified by the different length of acyl chain. For example, dilauroyl, dimyristoyl, dipamitoyl, distearoyl PC are phosphatidylcholines with acyl chain length of 12, 14, 16, and 18 carbon atoms, respectively. The source of PLs, natural-derived, semi-synthetic, and synthetic, can be used to identify PLs. Generally, egg yolk, animal brain and soybean are the main sources of natural PLs, but the purity of obtained PLs is low and possesses high degree of unsaturation. Semi-synthetic and synthetic PLs are performed to obtain high purity PLs or to modify the chemical properties [18].

Table 5 Commonly used glycerophospholipids classified by the head group [18]

Phospholipids	Phosphate side groups	Net charge at pH 7
Phosphatidylcholine (PC)		0
Phosphatidylethanolamine (PE)		0

Phosphatidylserine (PS)		-1
Phosphatidic acid (PA)		-1
Phosphatidylinositol (PI)		-1
Phosphatidylglycerol (PG)		-1
Cardiolipin (CL)		-2

4.1.2. Self-assembly in aqueous medium

PLs contain both hydrophilic and hydrophobic elements, which are referred as amphiphile. This characteristic allows them to spontaneously form vesicular structures via self-assembly in the presence of water [18, 19]. Since the acyl chains of PL do not preferably interact with hydrophilic environment, the hydrophobic regions interact with each other to hide themselves from water molecules through van der Waals forces. The hydrophilic headgroup points outward to aqueous milieu, forming hydrogen bonding or electrostatic interaction with surrounding water [19]. The obtained organized structures can be varied, e.g. lipid monolayers, lipid bilayers, micelles, liposomes, and tubules, depending on the chemical structures of PLs and the preparation parameters. Liposomal structures have been used in several applications since they offer both hydrophilic and hydrophobic compartments. The internal hydrophilic core with hydrophobic outer layer mimics the structure of cells. Moreover, several bioactive agents, both hydrophiles and lipophiles, can be encapsulated in internal core and lipid bilayers, respectively [18, 19]. The applications of phospholipids in tissue engineering and bioactive agent delivery will be discussed in the next section.

4.1.3. Physiological properties

PLs are biological substances found in several prokaryotic and eukaryotic cells, mainly serving as cellular membrane. Apart from the compositions of cell membrane, PLs act as emulsifiers or surface-active substances. It can be

found in an air-mucous membrane interface in lung or as lipoprotein complexes in blood circulation [18].

Intriguingly, the localization of PLs in cellular membrane is highly specific, where zwitterionic PLs (PC and sphingomyelins) are located externally and anionic PLs (PS, PI, PG, CL) are populated inside the cells. The interfacial interactions between anionic PLs and intracellular proteins are crucial for cellular functions and biological responses. The major role of PLs which causes the different protein function is to induce or enhance the conformational transition of protein [20]. The mechanism of PL-protein interaction will be discussed later.

4.2. Phospholipid-protein interactions

In molecular biology point of view, anionic PLs possess a crucial role in cell regulation by binding with proteins and induce their conformational changes. Electrostatic forces and non-polar interactions, namely hydrophobic interaction, have been proposed as the main driving forces for lipid-protein binding event [20].

The interactions between PLs and proteins are not limited to the biological processes. The *in vitro* studies to investigate protein conformational changes with the presence of PLs have been reported elsewhere. PGs, the anionic PLs, are found to effectively initiate and enhance structural changes of various water-soluble proteins, such as α -lactalbumin [22], β -lactoglobulin [21], physiological proteins, e.g. trypsin inhibitor, myoglobin, ribonuclease, lysozyme, and cytochrome oxidase subunit IV [138, 139], and synthetic oligopeptides [140]. Physical adsorption processes, including electrostatic and/or hydrophobic interactions between proteins and lipids, are being proposed as the main driving forces rather than covalent bonding in inducing protein conformational changes.

4.3. Liposomes

As previously described, the inherent self-assembly of PLs in aqueous medium leads to a formation of liposomes. Liposomes are the spherical structures of PL bilayers filled with water with size ranging from nanometer to micrometer scale. They are known as the oldest carrier system enabling the encapsulation of water-soluble and hydrophobic substances. In addition to the application as delivery systems, liposomes are used as model membrane systems, due to their resemblance of cellular structures, and as templates for nanogel fabrication [19].

4.3.1. Liposome classification

Typically, liposomes are classified into 2 groups based on the number of bilayers of the vesicles, including multi-lamellar vesicles (MLVs) and uni-lamellar vesicles (ULVs). ULVs are the vesicular structure with single PL bilayers surrounded and filled with water, while MLVs represent a vesicle with multiple bilayers separated by water layers. ULVs can be sub-categorized

by size as large ULVs (LUVs) with the size between 100 nm to 1 μ m and small ULVs (SUVs) with the size of 25-50 nm [19, 141].

4.3.2. *Preparation of liposomes*

To prepare liposomes, there are 4 basic steps, including dissolving PLs in organic solvents, evaporating organic solvents to obtain dry lipid film, dispersing in aqueous media, purifying and analyzing of the obtained liposomes [141]. Thin film hydration is the most simple and conventional method of preparation. MLVs are obtained after the addition of water or buffer to the thin lipid film. Sonication is used to apply energy for breaking the MLVs to SUVs. However, due to the heat generated during sonication which might affect loaded substances, membrane extrusion can be used, and the liposomal size is highly controllable by membrane orifice. LUVs can be fabricated from the SUVs using several freeze-thaw cycles. The SUVs spontaneously aggregate and form LUVs after the processes of freezing and thawing [19, 141].

Solvent injection is another approach to fabricate liposome. The PLs are dissolved in organic solvents, such as ether or ethanol, before injecting to a large amount of aqueous media. The SUVs form rapidly with the size as low as 30 nm. This method allows the encapsulation of very sensitive substances, since no chemical or physical treatment presents in the process. However, drawbacks of this method are the very dilute liposomes obtained and the residual amount of organic solvent entrapping in the liposomes.

To attain high encapsulation efficiency, reverse phase evaporation method is preferably used. To do this, the water-in-oil emulsion of PLs dissolved in organic solvents is sonicated. After that, the organic solvent is slowly eliminated using a reduced pressure, and the gel-like intermediate phase, which is characterized as LUVs, is obtained after complete solvent evaporation. This approach is used for loaded macromolecules, such as proteins, with high encapsulation efficiency (~80%) [19, 141].

4.4. Biomedical applications of phospholipids and liposomes

4.4.1. *Bioactive agent delivery*

A versatile structure of liposomes provides an inner hydrophilic core and lipid bilayers, which either hydrophilic, lipophilic, or amphiphilic molecules can be encapsulated and precisely delivered to targets. As carrier, PLs are biocompatible and fully biodegradable. The loaded substances can gradually release along the gradient of concentration or can be controlled to release under specific stimuli, e.g. pH, temperature, ultrasonic waves, magnetic fields, and light [19].

4.4.2. *Tissue engineering applications*

An ultimate approach of tissue engineering and regenerative medicine is to resemble the biological structures and functions, promoting and supporting tissue development. Lipids are known as basic building blocks of organisms and their specific characteristic to assemble in aqueous environment which can

be used as controlled release system. However, without supporting scaffolds, the restoration of tissue cannot be fully completed. The combination of lipid-based vesicles with scaffolds provides the advantageous properties in delivery bioactive agents with mechanical supports. So far, not only the bioactive agents such as growth factors are encapsulated and delivered in a controllable manner, but nucleic acids are also incorporated with the purposes for gene therapies in both genetic abnormalities and non-inherited diseases [19].

In tissue engineering point of view, growth factors are used to control stem cell fate and effectively direct the correct differentiation. The encapsulation of TGF- β 1 in liposomes loaded in scaffolds was successful for cartilage repair in an *in vivo* model. For bone tissue engineering, BMP-2 and dexamethasone were entrapped in liposomes with scaffolds and the effects on stem cell differentiation were clarified. The controlled release of loaded growth factors promotes an osteogenic induction and the complete differentiation can be obtained within 21 days [19, 142].

Apart from using growth factors to induce stem cell differentiation, the current approach is using genetic interventions to control stem cell fate and correct the inherited gene abnormalities. Small interfering RNAs (siRNAs), small hairpin RNAs (shRNAs), or micro RNAs (miRNAs) are the current popular methods in gene therapy. Lipid vesicles can enhance the effective delivery of RNAs to target sites and stabilize their activities along the regeneration process. The genes encoding BMPs and TGF- β were successfully entrapped in liposomes loaded inside scaffolds for bone and cartilage restoration. Also, liposomes loaded with VEGF-encoding DNA were injected into an animal model with stimulated wounds and the results showed an effective healing [19]. These indicate the potential of lipid-scaffold system in the application of tissue engineering.

5. Golds

5.1. Current therapeutic approaches of golds

Gold has been noticed to ward off diseases since pre-historical period, being used as gold flakes suspended in water with no scientific proven for its therapeutic efficacy in the later period. Subsequently, gold compounds have been found to successfully treat some diseases, such as pulmonary tuberculosis. Therefore, the study on therapeutic gold compounds has been increasing. Rheumatoid arthritis is effectively treated by gold thiolates due to the anti-inflammatory and immunomodulating effects of gold salts. From these properties, the studies on immune-related diseases, namely cancer, HIV and AIDS, and asthma, are being conducted. Furthermore, gold salts possess antimicrobial properties using common mechanisms as found in anti-malarial agents. Hence, gold has been researched for its anti-malarial properties [143].

Nanoparticles have gained lots of interest in wide applications due to their huge surface area per volume. The functionalization of the surface can be done to achieve desired properties. Gold nanoparticles (AuNPs) exhibit various

outstanding features, namely x-ray and plasmon absorption, binding affinity to thiols, disulfides and amines, optical and electronic properties. Furthermore, their responsive to plasmon resonance in visible and near infrared region allow AuNPs to be used in medical applications, such as diagnostic and therapeutic devices. Herein, the characteristics, fabrication processes, and biomedical applications of AuNPs are briefly discussed [24].

5.2. Characteristics of gold nanoparticles

AuNPs possess various properties which lead to the wide applications in different fields, namely biomedicines, electronics, optics, imaging and sensors, and catalysis. The important characteristics of AuNPs include the optoelectronic properties, high surface area, and biocompatibility. Regarding the optical properties, the shape and size of AuNPs relate to the different light absorption, yielding the different color appearances based on morphology. Therefore, by the fabrication of controllable size and shape of AuNPs, the optical properties are controllable in the range of visible light or near infrared spectra to achieve specific applications [24].

5.3. Gold nanoparticle synthesis

5.3.1. Physical methods

One of the dominant features of AuNPs is the ease and controllable of fabrication process. The procedures can be performed using physical interventions. Irradiation by γ -ray, microwave or ultraviolet light induces the reduction of Au salts, and the AuNPs are subsequently formed. The size between 5-40 nm is obtained depending on the optimizing parameters. Heating methods, e.g. thermolytic process, laser ablation, and sonochemical method, are regarded as a top-down process for AuNPs preparation [24].

5.3.2. Chemical methods

In chemical methods, Au salts, typically Au^{3+} , are reduced in an aqueous medium by reducing agents. The most popular reducers are citrate and sodium borohydride. Turkevich method, using sodium citrate as a reducer, is a well-known procedure because of its ease of procedure. The obtained AuNPs show narrow size distribution and high stability [24].

5.3.3. Biological methods

Due to the presence of reducing moieties, e.g. amine, thiol, in several biological compounds, they can serve as reducing agents in transforming Au^{3+} to Au^0 and the subsequent formation of AuNPs without producing hazardous reducing agent waste. This method is so-called “green chemistry” production, and the obtained AuNPs are free from toxic substances, allowing practical uses in biological conditions. Plant-based products and microorganisms, namely bacteria, fungi, algae, yeast and viruses, are used [24]. Furthermore, proteins or polypeptides, such as bovine serum albumin [144] and silk fibroin [145], and some monoclonal antibody, such as rituximab and cetuximab [144],

are investigated for their potential in the preparation of AuNPs without leaving harmful toxics.

5.4. Biomedical applications

5.4.1. Applications based on radiative properties

AuNPs exhibit a strong light absorption at around 520-550 nm depending on the morphology. Additionally, the size and shape of AuNPs can be tuned to shift the surface plasmon resonance absorption to the near infrared (NIR) regions (between 650-900 nm). In NIR region, high contrast from tissue, blood, and water can be achieved, enabling the clear imaging of accumulated AuNPs. Hence, AuNPs are applied for biological imaging or sensors due to their radiative properties [146].

In addition to using a dye as a probe for biological imaging, AuNP can be implemented as an optical labelled probe. Furthermore, AuNP labelling outperforms typical dye in term of the intensity and feasibility. For dye labelling, sophisticate imaging systems, such as fluorescence lasers and detectors, or image processing software, are required, while AuNP absorbs simple white light and scatters the light frequencies within its corresponding surface plasmon absorption. Therefore, only simple optical microscope with a dark background is required for AuNP-labelled images. For a specific application, AuNP can be designed with specific antibody to target an interest tissue, enabling high accuracy and precision image detector [146].

The ability of AuNP in surface modification enables its application as optical sensor for ions or molecules, e.g. saccharides, nucleotides, proteins and toxins [24]. The surface of AuNP can be conjugated with recognition molecules corresponding to target analyte. Upon a binding, a plasmon band shift can be noticed. The sensitivity of the analytical assay can be tuned by the geometry of AuNP, including size and shape [146].

A high x-ray absorption coefficient of AuNPs allows their application as an x-ray contrast agent. Combining with the surface properties of AuNPs which enable surface functionalization of specific target, AuNPs can be used for *in vivo* imaging with high precision. Furthermore, the cell internalization of AuNPs extends the half-life in the circulation system, expanding a longer imaging window comparing to conventional methods, such as iodinated contrast agents [24].

5.4.2. Applications based on non-radiative properties

Photodynamic and photothermal therapy are alternative approaches in the treatment of cancers and some skin or infectious diseases. Due to the surface plasmon resonance absorption of AuNPs, the generation of singlet oxygen and reactive species upon light activation can induce the apoptosis or necrosis of overgrowth or malfunction cells. Furthermore, the light absorption within visible or near infrared region of AuNPs results in a heat generation. Heat, therefore, causes the death of malignant cells. AuNPs can be designed in nanoscale size which can penetrate through cell membrane or be internalized

by cells, and surface-functionalized to be specific to a target. Thus, AuNPs act as theranostic medical devices performing both diagnostic of the defects and therapeutic properties [24].

According to the aforementioned properties of AuNPs including their ability to bind various functional groups, AuNPs can be used as nanocarriers in drug delivery systems. Several bioactive molecules, e.g. proteins, peptides, plasmid DNAs, small interference RNAs, and chemotherapeutic agents, are bound to AuNPs and transferred to the target site depending on the modification of AuNPs [24].

5.4.3. Scaffolds containing golds

AuNPs are incorporated to the tissue-engineered scaffold to enhance properties, including electric conductivity, mechanical integrity, and biological activity. They can be either grafted onto the preformed scaffolds or mixed with polymer solution and fabricated to the desired format. Hydrogel is a widely used scaffold in tissue engineering. The fabrication of AuNP-loaded hydrogels can be performed by direct addition of AuNP into the hydrogel or using the reducing properties of polymer substrate for the *in situ* formation of AuNP along with the formation of hydrogel [147].

Since an addition of small particles, such as AuNPs, in polymer matrices can enhance the mechanical performance of the obtained materials, AuNPs are introduced to various biological scaffolds. The mechanical properties of the polymeric hydrogels or electrospun fibers were increased achieving the values mimicking to those of native tissues. Electrostatic interactions between AuNPs and polymer backbones also exert the mechanical strength of the resulting scaffold [147].

Electrically conductive scaffolds are required for the tissue engineering of cardiac muscles and neuronal tissues. However, most biopolymers are electrically inert, while the conductive polymers exhibit low biocompatibility. The hybrid scaffolds embed with AuNPs are the promising materials with tunable physical properties, good biocompatibility, and, more importantly, electrical conductivity [147].

The bioactivities of the scaffolds can be enhanced by incorporating modified AuNPs. Since the reactivity of AuNP with various functional groups, the surface modification is highly feasible. AuNPs can be functionalized with RGD motifs and embedded into the scaffold to promote cell adhesion and proliferation. Other growth factors are also conjugated to achieve such desired properties matching to the target native tissues [147].

Chapter 3

Materials and Methods

1. Material

- 1) Cocoons of Thai domesticated *Bombyx mori* silkworms (Nangnoi Srisaket 1) (Queen Sirikit sericulture center, Srisaket province, Thailand)
- 2) 1,2-dimyristoyl-*sn*-glycero-3-phosphocholine (DMPC; Lipoid GMBH, Germany)
- 3) 1,2-Dimyristoyl-*sn*-glycero-3-phospho-*rac*-(1-glycerol) sodium salt (DMPG; Lipoid GMBH, Germany)
- 4) 2-iminothiolane (2-IT; Acros Organics, USA)
- 5) 3-(4,5-Dimethylthiazol-2-yl)-2,5-Diphenyltetrazolium Bromide (MTT; Thermo Fisher Scientific, USA)
- 6) 4-(2-Hydroxyethyl) piperazine-1-ethanesulfonic acid (HEPES; Sigma-Aldrich, USA)
- 7) 4',6-Diamidino-2-phenylindole (DAPI; Thermo Fisher Scientific, USA)
- 8) 4-Dimethylaminopyridine (DMAP; Sigma-Aldrich, USA)
- 9) 5,5'-dithio-*bis*-(2-nitrobenzoic acid) (DTNB or Ellman reagent; Sigma-Aldrich, USA)
- 10) 7-amino-actinomycin D (7-AAD; Sony Biotechnology, USA)
- 11) Acrylamide (Loba Chemie, India)
- 12) Calcein AM (Thermo Fisher Scientific, USA)
- 13) Calcium chloride (CaCl₂; Sigma-Aldrich, USA)
- 14) Caspase-3 assay kit (Abcam, USA)
- 15) Cholesterol (Wako Chemicals, Japan)
- 16) Curcumin from *Curcuma longa* (Sigma-Aldrich, USA)
- 17) Cysteine (Sigma-Aldrich, USA)
- 18) Dextrose solution for injection, 50% (ANB Laboratories, Thailand)
- 19) Dimethyl sulfoxide (DMSO; Quality Reagent Chemical, New Zealand)
- 20) Dulbecco's modified eagle medium/high glucose (DMEM-HG) with L-glutamine; without sodium pyruvate and sodium bicarbonate (HyClone, USA)
- 21) Ethanol (Wako Chemicals, Japan)
- 22) Ethylenediaminetetraacetic acid (EDTA; Sigma-Aldrich, USA)
- 23) Fetal Bovine Serum (FBS; HyClone, USA)

- 24) Fluorescein annexin V (Sony Biotechnology, USA)
- 25) Fluorescein Phalloidin (Thermo Fisher Scientific, USA)
- 26) Gold (III) chloride trihydrate ($\text{HAuCl}_4 \cdot 3\text{H}_2\text{O}$; Acros Organics, USA)
- 27) Hoechst 33258 (Thermo Fisher Scientific, USA)
- 28) Lithium bromide (LiBr; Sigma-Aldrich, USA)
- 29) MEM non-essential amino acid (100X; Gibco, USA)
- 30) Minimum essential medium eagle - alpha modification (α -MEM) with L-glutamine, ribo- and deoxyribonucleosides, without sodium bicarbonate (HyClone, USA)
- 31) MTS assay kit (Abcam, USA)
- 32) Penicillin-Streptomycin (10,000 U/mL) (Gibco, USA)
- 33) Phosphate buffer saline (PBS; Sigma-Aldrich, USA)
- 34) Phosphotungstic acid (Wako Chemicals, Japan)
- 35) Propidium iodide (PI; Sigma-Aldrich, USA)
- 36) Protease from *Streptomyces griseus*, Type XIV (Sigma-Aldrich, USA)
- 37) Sodium azide (Wako Chemicals, Japan)
- 38) Sodium bicarbonate (NaHCO_3 ; Sigma-Aldrich, USA)
- 39) Sodium carbonate (Na_2CO_3 ; Sigma-Aldrich, USA)
- 40) Sodium chloride (NaCl ; Wako Chemicals, Japan)
- 41) Sodium dodecyl sulfate (SDS; Sigma-Aldrich, USA)
- 42) Sodium phosphate, dibasic (Na_2HPO_4 ; Sigma-Aldrich, USA)
- 43) Sodium phosphate, monobasic (NaH_2PO_4 ; Sigma-Aldrich, USA)
- 44) Sodium pyruvate (100 mM; Gibco, USA)
- 45) Tri-sodium citrate dihydrate (Wako chemicals, Japan)
- 46) Trypsin, 0.25 with EDTA, without calcium, magnesium (HyClone, USA)
- 47) WST-1 cell proliferation assay kit (Takara Bio, Japan)
- 48) Zinc acetate (Loba Chemie, India)

2. Experimental design

The gelation of silk fibroin (SF)-based hydrogel was accelerated by an addition of different chemicals divided into 3 groups, including phospholipid-, liposome-, and gold-induced SF hydrogels. All hydrogel systems were investigated for the gelation time and the mechanisms of gelation. Also, the physico-chemical characterizations of the obtained hydrogels were determined, and their potential for biomedical applications were evaluated

using *in vitro* cell culture experiments. The experimental framework was depicted in **Figure 24**.

Base Material

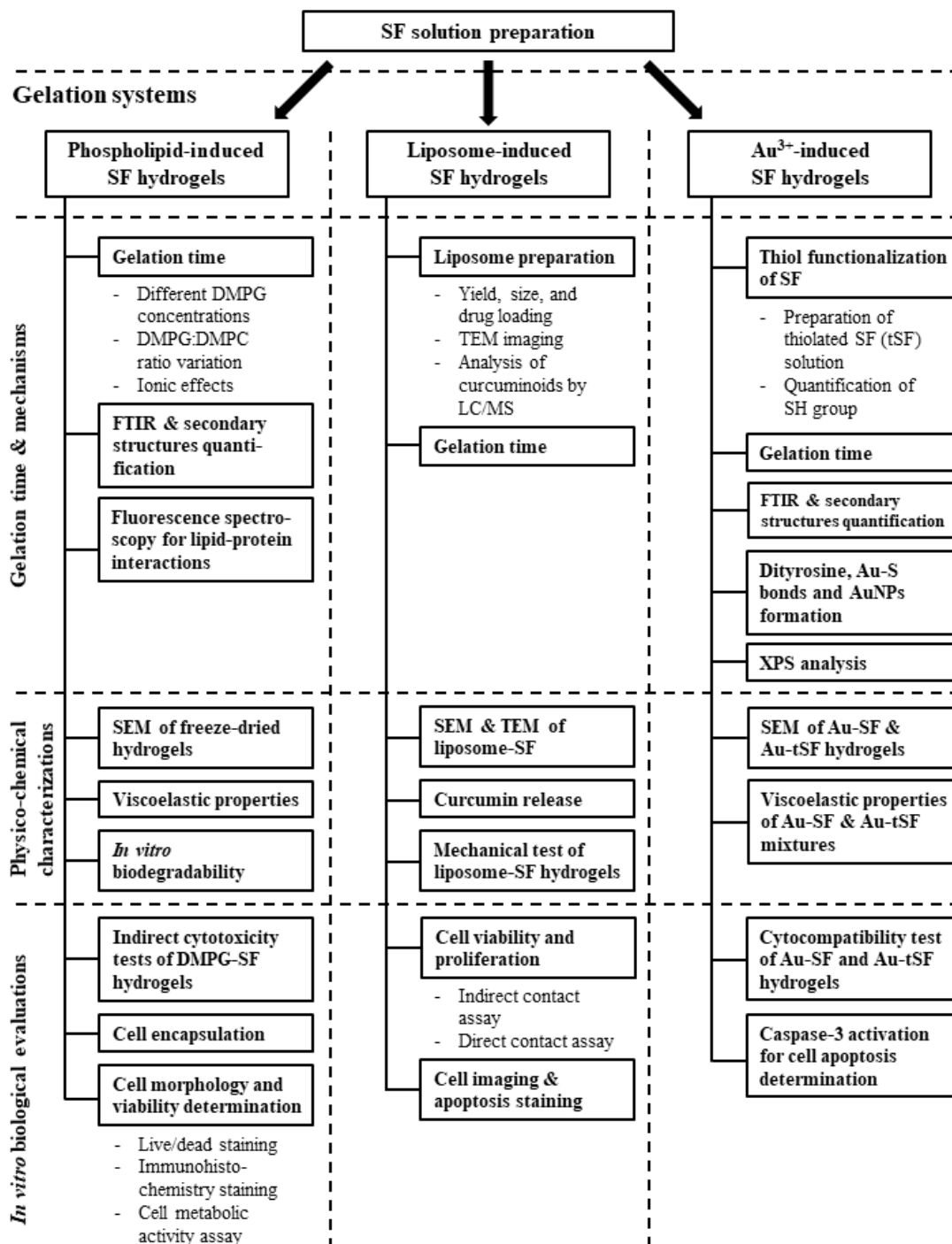


Figure 24 Experimental framework. The SF gelation system and their applications were divided into 3 groups, namely phospholipid-SF hydrogels for cell carrier application, liposome-SF hydrogels for drug delivery, and cytocompatible gold-SF hydrogels with anti-proliferation of cancer cells.

3. Method

3.1. Silk fibroin (SF) solution preparation

Silk fibroin (SF) solution was extracted from Thai domesticated Nangnoi Srisaket 1 *Bombyx mori* silkworm cocoons following an established protocol reported by Kim *et al* [13] with a slight modification. Sericin and other silk glues were firstly removed by boiling the cocoons in 0.02 M Na₂CO₃ for 20 min twice. The obtained fibers were then dissolved in 9.3 M LiBr in a weight-to-volume ratio of 1:4 and incubated at 60°C for 4 h. The obtained amber and viscous solution was subsequently dialyzed against deionized (DI) water using a dialysis membrane with molecular weight cut-off of 12-16 kDa (Sekisui, Japan) to remove the residual LiBr. After that, the solution was centrifuged at 9,000 rpm, 4°C, 20 min to remove debris and stored in a refrigerator until used. The concentration of SF solution was determined from its dry weight.

3.2. Phospholipid-induced silk fibroin hydrogels for cell carrier application

The gelation of SF was accelerated by an addition of a negatively charged phospholipid, DMPG. The gelation time of SF intrigued by different DMPG concentrations was evaluated as well as the effects on the gelation time from the lipid charge and the ionic effect. Mechanisms of gelation were studied by FTIR and protein fluorescence spectroscopy. The features of the obtained hydrogels relating to the cell carrier applications, namely microstructures, viscoelastic properties, and biodegradability, were investigated. Finally, the hydrogel system was used to encapsulate cells, and the viability and proliferation of cells in hydrogels were evaluated to confirm the cytocompatibility as well as the suitability for the practical uses.

3.2.1. Gelation time and mechanisms of gelation

a. Gelation time determination of DMPG-SF mixtures

The gelation of DMPG-SF mixture was determined by varying the DMPG concentration from 5 to 15 mM. Firstly, DMPG was hydrated with DI water and sonicated at 40°C for 1 h, before mixing with 3% SF solution. The pH of mixtures was controlled at pH 7.4 using 10 mM HEPES buffer. The mixtures were transferred to 96-well microplates and their absorbance values at 550 nm were periodically measured by a microplate reader (Synergy HT, BioTek, USA). As reported by Matsumoto *et al* [12], the gelation of SF solution relates to an increase of the opacity due to a formation of the heterogenous microstructure. Therefore, the gelation time can be identified from the changes in optical density. In this study, the gelation time was determined from the time-point where the 550-nm absorbance value reaches a half maximum.

To determine a role of lipid charge to the gelation of SF solution while maintaining a hydrophobicity, DMPC, a zwitterionic phospholipid with 14-carbon chains, was mixed with DMPG at different ratio (DMPG-to-DMPC molar ratio 10:0, 7:3, 5:5, 3:7, 0:10). The DMPG and DMPC structures are

illustrated in **Figure 25**. 10 mM of phospholipids were mixed with 3% SF solution and the gelation was observed as previously described.

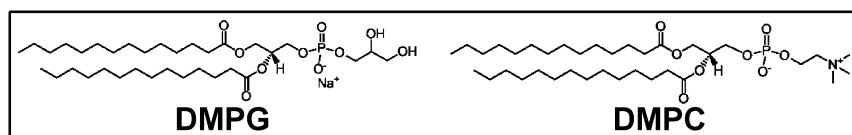


Figure 25 Chemical structures of DMPG and DMPC

The ionic effects on the gelation of DMPG-SF mixtures were investigated by an addition of Ca^{2+} . The calcium ion was chosen since it is commonly found in cell culture media and physiological milieu. Different concentrations of CaCl_2 (0.1, 0.5 and 1 mM) were added to 10 mM DMPG-3% SF mixtures, and the gelation time was determined. The greater concentration of Ca^{2+} than 1 mM can cause white precipitates which could result from the formation of insoluble DMPG- Ca^{2+} complex.

b. FTIR measurement and secondary structure quantification

The transition of SF secondary structures during the gelation was analyzed by Fourier-transform infrared spectrophotometer (FTIR; IRPrestige 21, Shimadzu, Japan), and quantified by Fourier self-deconvolution and curve-fitting techniques. FTIR analysis was performed in an attenuated total reflection (ATR) mode and the DMPG-SF mixtures were loaded onto the measurement cells. FTIR spectrum was collected from 4,000 to 800 cm^{-1} with 2.0 cm^{-1} resolution and 1 cm^{-1} interval.

FSD and curve-fitting processes were conducted according to Hu *et al* [148]. The spectrum located in amide I region (1,575 – 1,725 cm^{-1}) was deconvoluted using Omnic 8.0 software. The Voigt lineshape was applied with a half bandwidth of 10 cm^{-1} and an enhancement factor of 3.0. Then, the deconvoluted spectrum was curve-fitted using Origin 9.0 software. The fitted peaks were assigned as following; beta sheet (1,616 – 1,637 cm^{-1} , 1,696 – 1,703 cm^{-1}), tyrosine residue (1,595 – 1,615 cm^{-1}), random coil (1,638 – 1,655 cm^{-1}), alpha helix (1,656 – 1,662 cm^{-1}) and beta turn (1,663 – 1,696 cm^{-1}) [38, 148]. The area under the defined peaks was used to quantify the secondary structures. An example for peak assignment of deconvoluted FTIR spectrum is shown in **Figure 26**.

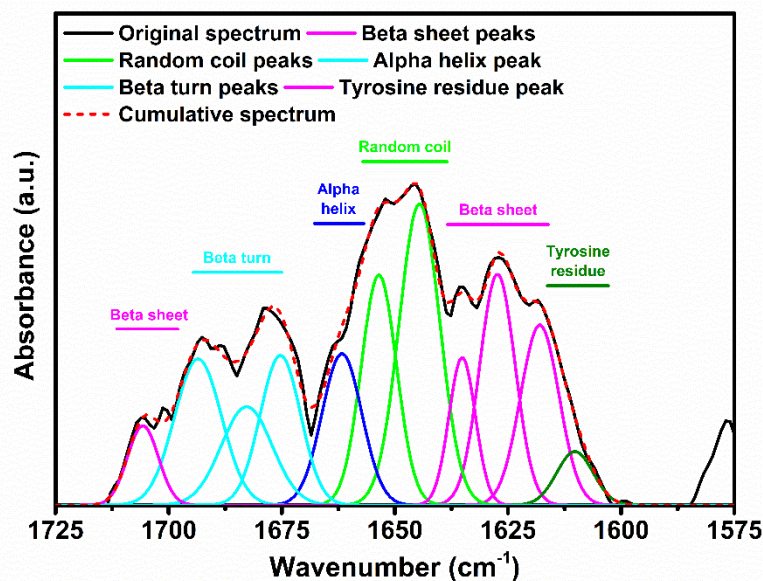


Figure 26 Peak assignment in amide I region corresponding to the secondary structures of SF.

c. Fluorescence spectroscopy for the study of protein-lipid interactions

Due to the fluorescence absorption of tryptophan residues and its hydrophobic characteristic, the fluorescence measurement can be used to trace the localization of tryptophan which can be used to investigate the hydrophobic interaction of protein [149]. Fortunately, about 0.2 – 0.5% of tryptophan is presented and located in the non-crystalline regions of the SF chains [52, 58]. Hence, the fluorescence emission spectra of the mixtures of DMPG and SF between 300 and 450 nm were collected after an excitation of 295-nm ultraviolet light using a spectrofluorometer (Viroskan flash, Thermo Fisher Scientific, USA).

Fluorescence quenching technique was performed to investigate an interaction between proteins and lipids by determining an accessibility of a hydrophilic quencher to tryptophan [21, 149]. In this study, a hydrophilic quencher, acrylamide, was mixed with DMPG-SF mixtures from 0 – 0.4 M before allowing the gelation. For the controls, SF solution was mixed with acrylamide accordingly and incubated at 37°C in a humidified atmosphere. The spontaneous gelation of SF solution without DMPG occurred within approximately 7 days. After that, the fluorescence intensity at 320 nm was collected with a 295-nm excitation. Data analysis was performed using the following equation;

$$\frac{F_0}{F} = 1 + k_{sv}[Q]$$

where F_0 and F are the emission intensities with an absence or a presence of acrylamide at different concentration $[Q]$, respectively. The k_{sv} is a Stern-Volmer constant obtained from the slope of the plot between F_0/F and $[Q]$. A

lower k_{sv} indicates a higher difficulty of the quencher in accessing to tryptophan residues [21, 149].

3.2.2. Physico-chemical characterizations of DMPG-SF hydrogels

a. SEM analysis of freeze-dried hydrogels

After obtaining the 5, 10 and 15 mM DMPG-3% SF hydrogels, the hydrogels were frozen at -80°C overnight and freeze-dried (CryoDos 80, Telstar, Japan). 3% SF hydrogels were prepared as described in the section 3.2.1c and freeze-dried accordingly. The samples were cut, coated with platinum, and their micromorphological features were visualized by a scanning electron microscope (SEM; JSM-6010LV, Jeol, Japan). Pore size was determined by ImageJ software ($n = 5$).

b. Viscoelastic properties of DMPG-SF hydrogels

To determine the mechanical stability of the hydrogels, rheological properties were measured to evaluate the parameters, storage or elastic (G') modulus and loss or viscous (G'') modulus. G' indicates a stored deformation energy of a test material during shear, such as the stiffness of the material. While G'' corresponds a dissipated energy during shear, which relates to the fluid-like characteristic of the material [150].

The viscoelastic properties of DMPG-SF hydrogels were evaluated using a rheometer (Kinexus Pro+, Malvern Instrument, USA). Time-sweep experiment was performed at 0.5% strain and 1 Hz after loading 5, 10 and 15 mM DMPG-3% SF mixtures onto the 1-mm gap parallel plate. The experiment was lasted until the constant moduli were obtained, indicating the complete gel formation. After that, the moduli were collected over a range of frequency from 0.1 to 100 Hz at a fixed 0.5% strain. Strain-sweep experiment was then conducted at 1 Hz and the moduli were measured over a strain ranging from 0.1-100%.

c. Determination of *in vitro* biodegradability

Biodegradation of DMPG-SF hydrogels was performed by immersing the hydrogels in 1 unit/ml protease XIV in 10 mM HEPES buffer (pH 7.4). The protease enzyme was used because of its digestive activity against SF [63]. The media was changed every other day. The hydrogels were weighed at a designated time-point (day 0, 1, 3, 7, 14, 21) ($n=4$).

3.2.3. Biological evaluation of DMPG-SF hydrogels

a. Cell cultures

L929 mouse fibroblasts, NIH/3T3 mouse embryonic fibroblast, SaOS-2 human osteosarcoma, and CaSki human cervical cancer cell line were chosen for cytocompatibility tests of the developed hydrogels, and their viability and proliferation were evaluated while encapsulated. L929, NIH/3T3, SaOS-2 were maintained in DMEM-HG supplemented with 10% FBS and 1% antibiotics. The culture medium for CaSki was α -MEM + 10% FBS + 1% antibiotics. All cells were cultured in a humidified, 5% CO_2 -supplemented air

incubator at 37°C. Media were changed once or twice weekly and subculture was done when the confluency reaches about 80% using trypsin enzymatic detachment protocol.

b. Indirect cytotoxicity test of DMPG-SF hydrogels

A cytotoxicity assessment of the DMPG-SF hydrogels was performed according to an ISO standard [151]. Firstly, SF solution was steam-sterilized at 121°C for 20 min and DMPG solution was irradiated by UV light. The 5, 10 and 15 mM DMPG-3% SF hydrogels were prepared as previously described under aseptic conditions. The samples were cut into a disc shape (10-mm diameter and 5-mm thickness, calculated surface area 3.14 cm²) and immersed in 1 ml FBS-free DMEM for 24 h at 37°C.

An indirect cytotoxicity test was conducted using MTT assay as described in ISO 10993-5:2009 [152]. To do this, 1 x 10⁴ cells/cm² L929 was plated in a 96-well tissue culture plate and cultured for 24 h. After that, the media were removed and replaced with 100 µl extracts with their respective dilutes (12.5, 25 and 50% v/v). FBS-free DMEM, DMEM + 10% FBS, and DMEM containing 20 ppm zinc acetate were used as a blank, negative and positive control, respectively. All cultures were continued for more 24 h.

The alteration of cell morphology was visualized by a phase-contrast microscope (Eclipse Ti-S, Nikon Instruments, Japan). The cell viability was assessed by MTT assay. The cells were firstly washed with PBS, mixed with 50 µl 0.5 mg/ml MTT solution and incubated at 37°C for 30 min. 100 µl DMSO was added to extract blue formazan products. The absorbance at 570 nm was collected and the %viability was calculated according to the equation;

$$\%viability = \frac{100 \times OD_{570e}}{OD_{570b}}$$

where OD_{570e} and OD_{570b} are absorbance values of the sample group and the blank, respectively. According to the ISO standard, the %viability lower than 70% is considered as cytotoxic.

c. Preparation of cell-encapsulated DMPG-SF hydrogels

The cells were encapsulated in 5, 10 and 15 mM DMPG-3% SF hydrogels and their viability and proliferation were assessed at day 0, 1, 3, 7, 14 and 21. Firstly, the UV-irradiated DMPG film was hydrated with 5% dextrose solution. Dextrose was added to maintain the physiological osmolarity of the mixtures [153]. Cell suspension was added to sterile SF solution to make 1 x 10⁶ cells/ml. Two components were mixed, transferred to a silicone mold, and incubated in a CO₂-incubator to complete the gelation. Subsequently, the hydrogels were punched into a disc shape (5-mm diameter and 2-mm thickness) and transferred to a 24-well tissue culture plate. 1 ml of culture media was added and changed every other day.

d. Viability of encapsulated cells using live/dead staining

At the designated time point, the hydrogels were washed with PBS, sliced into a thin piece, and stained with 1 µM calcein AM and 1 µM PI for 15 min.

Calcein AM is used to detect viable cells, generating a green fluorescence emission. While PI is a cell exclusion dye which lead to a red fluorescence stain of dead cells. The fluorescence-labeled cells were visualized by a fluorescence microscope (Eclipse C1, Nikon Instruments, Japan).

e. Cell morphology detection using immunohistochemistry

Hydrogels obtained from each time point were fixed in 10% neutral-buffered formalin for 1 h. To visualize the cell nucleus and cytoskeleton, the samples were stained with DAPI and fluorescein phalloidin, respectively, giving a blue and green fluorescent labelling. The fluorescence-stained cells were observed using the fluorescence microscope as aforementioned.

f. Cell viability and proliferation using cell metabolic activity assay

MTT cell metabolic activity assay was used to evaluate the number of cells viable in the hydrogels. At each time point, the samples were washed with PBS, ground into small pieces, and mixed with 0.5 ml MTT solution. 1 ml of DMSO was then replaced to extract the colored product and the absorbance at 570 nm was measured. The number of cells was calculated using a standard curve. Population doubling time (PDT) was analyzed from the specific growth rate (μ) obtained from the slope of the plot of cell number versus culture time. The calculation was done using the following equation;

$$PDT = \frac{\ln 2}{\mu}$$

3.3. Liposome-induced silk fibroin hydrogels for drug delivery system

From the previous section, DMPG was known to accelerate the gelation of SF. Due to the inherent characteristic of phospholipid in forming liposomes, DMPG-based liposomes were prepared and used as the dual-functional system for intriguing SF gelation and as drug delivery carrier. Curcumin was selected for entrapped in the liposomes and its content and stability were evaluated. The gelation of SF induced by the liposomes was assessed. The obtained hydrogels was characterized for the micromorphology, the mechanical properties and the release of curcumin. In vitro cell culture experiments were conducted to assess the applicability of the hydrogels as the sealant used after the resection of solid tumors.

3.3.1. Preparation and characterization of curcumin-containing liposomes

a. Preparation of curcumin-containing liposomes

DMPG-based liposomes containing curcumin were prepared by simple hydration method followed by bath sonication. The mixture of DMPG, DMPC, cholesterol and curcumin was prepared in a 20-ml round bottom flask and the ratio of each component is shown in **Table 6**. Organic solvents were eliminated by rotary evaporator (N-1100, Eyela, Japan) at 50-mbar pressure and 40°C. Subsequently, the dry lipid film was hydrated with 2 ml water, vortexed, and sonicated at 40°C for 1 h with occasional shaking. The liposomal mixture was then centrifuged at 2,500 rpm, 4°C, 10 min, and

filtered through 0.22- μm filter to remove the untrapped cur. The liposomes were kept in the dark at 4°C and used within 1 week after prepared.

Table 6 Liposome formulation

DMPG:DMPC:Chol:Cur weight ratio	Code	DMPG (mg)	DMPC (mg)	Chol (mg)	Cur (mg)
10:0:0:0.5	A0	50	0	0	2.5
7:3:0:0.5	B0	35	15	0	2.5
5:5:0:0.5	C0	25	25	0	2.5
3:7:0:0.5	D0	15	35	0	2.5
10:0:1:0.5	A1	50	0	5	2.5
7:3:1:0.5	B1	35	15	5	2.5
5:5:1:0.5	C1	25	25	5	2.5
3:7:1:0.5	D1	15	35	5	2.5
10:0:2:0.5	A2	50	0	10	2.5
7:3:2:0.5	B2	35	15	10	2.5
5:5:2:0.5	C2	25	25	10	2.5
3:7:2:0.5	D2	15	35	10	2.5

b. Yield determination and curcumin content analysis

Yield of production was determined from the dry solid weight of liposomes. Curcumin content in liposomes was analyzed by disrupting the liposomes in ethanol at 2.5% v/v, and their absorbance at 415 nm was collected by a microplate reader (MTP-880Lab, Corona Electric, Japan). Loading capacity (LD) and encapsulation efficiency (EE) of curcumin in liposomes were calculated from the following equations;

$$\%LD = \frac{Cur_A}{W_L} \times 100$$

$$\%EE = \frac{Cur_A}{Cur_T} \times 100$$

where W_L is a solid weight of the liposomes, Cur_A and Cur_T are an actual amount of curcumin calculated from the absorbance and a theoretical amount calculated based on the actual liposome weight.

c. Size analysis of liposomes

Diameter of liposome and size distribution (polydispersity index, PDI) were determined by light scatter techniques. A dynamic light scattering photometer (DLS-800HAL, Otsuka Electronics, Japan) equipped with a 488-nm laser was used to assess the size of liposomes.

d. Transmission electron microscope (TEM) imaging of liposomes

Micromorphological feature of liposomes was observed using a TEM (JEM-2100, Jeol, Japan) and the samples were prepared by negative staining. To do this, the liposomes (A1, B1, C1, D1; 0.5 mg/ml) were dropped onto a high resolution carbon film copper grid (HRC-10, Okenshoji, Japan), allowed there for 2 min, and blotted away using a filter paper. A drop of 2% phosphotungstic acid (pH 7) was then dropped on the grid, waited for 2 min, and blotted away. The grip was left to dry until TEM analysis. The TEM visualization was conducted with an acceleration voltage of 200 kV.

e. Analysis of active curcuminoids by liquid chromatography/mass spectrometry (LC/MS)

In commercially available curcumin extracted from turmeric, three bioactive curcuminoids were found, including curcumin, demethoxycurcumin (DMC) and bisdemethoxycurcumin (BDM), which lacks one and two methoxy groups attached to the phenol ring, respectively [154]. Structural difference of these derivatives, as shown in **Figure 27**, results in different chemical properties. Therefore, it is distinguishable by chromatographic separation. LC/MS can be used to detect and quantify the amount of each derivatives. LC/MS Protocol for detecting curcuminoids was followed the report by Ramalingam *et al* [155]. The liposomes were dissolved in ethanol at 2.5% vol and injected to a liquid chromatography system (Prominence LC-20AD, Shimadzu, Japan) equipped with an InertSustain™ reverse phase C18 column (150 x 4.6 mm I.D. 5 µm; GL Sciences, Japan). An isocratic flow of 70% acetonitrile in 0.1% formic acid was used with a fixed flow rate at 400 µl/min. Temperature of the autosampler and column was fixed at 4 and 40°C, respectively. The running time was 10 min, and the spectrum was collected by an equipped photodiode array (PDA; Prominence SPD-M20A, Shimadzu, Japan) detector.

MS/MS system (LXQ, Thermo Scientific, USA) was used to identify curcuminoids. The MS system was set in a negative mode. The electrospray ionization (ESI) parameters were set as following: 25 eV for a capillary voltage and the desolvation temperature was set at 320°C. Multiple reaction monitoring (MRM) mode was used to monitor an ionization transition of analytes (368 > 217 m/z for curcumin, 338 > 217 for DMC, and 308 > 187 for BDM).

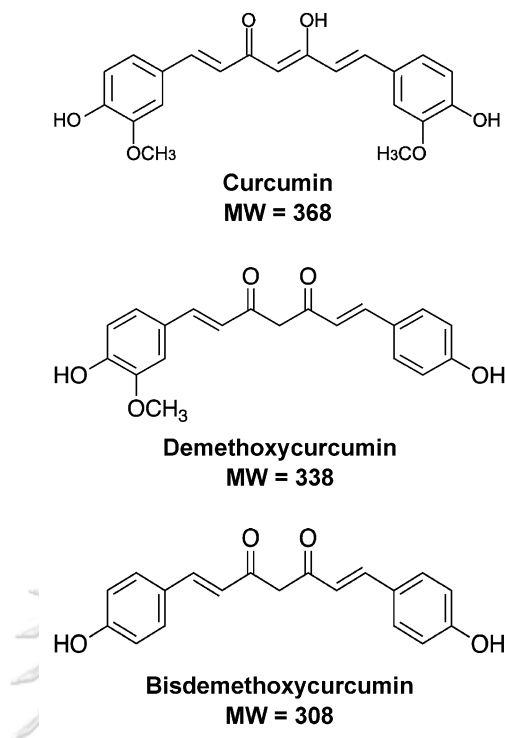


Figure 27 Chemical structures of curcumin, demethoxycurcumin and bisdemethoxycurcumin

3.3.2. Determination of gelation and properties of liposome-SF hydrogels

a. Gelation time determination of liposome-SF mixtures

Liposomes were mixed with SF solution, yielding 10 mg/ml liposomes (equivalent to 15 mM phospholipids) and 3% SF. The mixtures were then gently pipetted to 96-well microplates and the turbidity changes were observed by colorimetry. The absorbance at 540 nm was measured every minute for 6 h by a microplate reader (iMark™, Bio-rad, USA). Gelation time was determined from the kinetic plot of the absorbance values as described previously.

b. Micromorphology determination and elemental analysis of freeze-dried liposome-SF hydrogels

After 24-h incubation at 37°C of sonicated SF, Curcumin-SF, and liposome-SF mixtures, the hydrogels were frozen at -20°C overnight and lyophilized for 48 h using a freeze dryer (AdVantage 2.0, SP scientific, USA). Micromorphological features of the hydrogels were visualized by a SEM (Miniscope TM3000, Hitachi High-Technologies, Japan) without coating and the elemental analysis was conducted by an equipped energy-dispersive x-ray spectroscopy (EDX).

c. TEM observation of liposome-SF hydrogels

The mixtures of 0.075% SF and 0.5 mg/ml liposomes (A1, B1, C1 and D1) were coated on the TEM grid, stained and observed by TEM as aforementioned.

d. Curcumin release from liposome-SF hydrogels

SF solution was steam-sterilized, and liposomes were filtered before making the hydrogels. The hydrogels were cut into a disc shape with 5-mm diameter and 2-mm thickness. Controls, including SF and Curcumin-SF hydrogels, were formed by sonication [35]. 3% SF solutions were sonicated at 50% amplitude for 1 min. Curcumin in DMSO was added to SF solution before sonication. The samples were placed in 1 ml release media, composed of PBS (pH 7.4), 10% FBS and 0.01% sodium azide, and incubated at 37°C. At each time-point, 100 µl supernatant was collected and the absorbance at 415 nm was measured. An equal amount of release media was replaced. The amount of released curcumin was calculated using a standard curve. All procedures were conducted under aseptic conditions to avoid microbial contamination.

e. Mechanical test of liposome-SF hydrogels

The hydrogel samples were prepared as describe in the section 3.3.2d and immersed in PBS until the experiment. Mechanical test was performed in a compression mode using a texture analyzer (TA-XT2i, Hidehiro, Japan) equipped with 5-mm diameter probe and 1 kN load. The preload of 0.005 N was applied and the probe speed was set at 0.1 mm/sec. The measurement was run until reaching 80% strain. Plot between stress (σ ; kPa) and strain (ϵ) was used to analyze compressive modulus (E) of the test materials regarding the following equation;

$$E = \frac{\sigma}{\epsilon}$$

3.3.3. *Cytocompatibility and anti-proliferative of cancer cells of liposome-SF hydrogels*

a. Cell culture tests with liposome-SF hydrogels

L929 was cultured as described in section 3.2.3a. MDA-MB-231 human breast cancer cell line was maintained in DMEM supplemented with 10% FBS, 1% penicillin/streptomycin, non-essential amino acid and 1 mM sodium pyruvate. All cells were incubated at CO₂-incubator at 37°C.

The biological responses of cells to liposome-SF hydrogels were assessed by an indirect and direct contact method. The indirect contact method was performed by plating the cells (10,000 cells/cm²) in a well of 24-well tissue culture plate and cultured for 6 h. After that, the hydrogels, cut in a disc shape as described in the section 3.3.2d, were put in the culture medium. All plates were cultured at 37°C in a humidified 5% CO₂/95% air.

The direct contact assay was conducted by plating the cells onto the samples. Liposome-SF hydrogels and controls, SF and Curcumin-SF

hydrogels, were coated in wells of 48-well plates. L929 and MDA-MB-231 were seeded at 20,000 cells/cm² and cultured as previously described.

b. Cell viability assay

At each time-point, the viability of cells, either cultured on plates or on the samples, was determined by a WST-1 cell metabolic activity assay using a protocol recommended by the manufacturer. To do this, the cells were washed with PBS and incubated with 300 μ l WST-1 solution at 37°C for 2 h in the dark. The absorbance of the supernatant was measured at 450 nm with a reference filter at 570 nm.

Hoechst 33258 DNA quantification assay was performed to determine the number of cells cultured on the samples. Firstly, the cells were disrupted using a SDS lysis buffer (0.02% SDS in saline-sodium citrate (SSC) buffer (0.15 M NaCl and 0.015 M trisodium citrate)) followed by several freeze-thaw cycles [156]. The supernatants were then collected, mixed with Hoechst 33258, and measured their fluorescence intensity with an excitation of 355 nm and emission at 460 nm. The standard curve was used to convert the fluorescence intensity values to the number of cells.

c. Cell apoptosis staining and cell imaging

At each time-point, the cells were imaged by a fluorescence microscope (IX71, Olympus Lifescience, Japan). Apoptosis staining was performed for the cells of the indirect contact experiment cultured for 1 d. Cells were washed with PBS, stained with Fluorescein-annexin V and 7-AAD for 15 min, and observed their fluorescence image by the microscope.

3.4. Gold-induced silk fibroin hydrogels and the cytocompatibility of hydrogels

Gold (III) salt of Au³⁺ was used to induce the rapid gelation of SF. Furthermore, the thiol-functionalized SF (tSF) was prepared and the mechanisms of gelation between Au-SF and Au-tSF were evaluated. The structural transition as well as the formation of chemical bonds within SF or tSF chains induced by Au³⁺ were assessed. The developed hydrogels were analyzed for their physical properties. Finally, the cytocompatibility of the Au-SF and Au-tSF hydrogels as well as the bioactivity against the cancer cells were tested.

3.4.1. Preparation of thiolated SF solution and the gelation of SF and tSF with Au³⁺

a. Preparation of thiolated SF (tSF) and quantification of sulfhydryl group

An introduction of sulfhydryl group to SF was modified from the study of Monteiro *et al* [157]. 2-Iminoethanol (2-IT) was used to introduce SH group by attaching a sulfanyl butanimidine to a primary amine of the protein. The chemical reaction was illustrated in **Figure 28**. For SF, 6% SF solution was firstly dialyzed against 0.1 M sodium phosphate (pH 8). After that 5 – 50 mM

2-IT and DMAP, as a nucleophilic catalyst, was mixed with SF solution and incubated at 37°C for 3 h. 2-IT and DMAP was then removed by dialysis against DI water at 4°C for 24 h and the concentration of the obtained solution, so called thiolated SF or tSF solution, was determined from its dry solid weight.

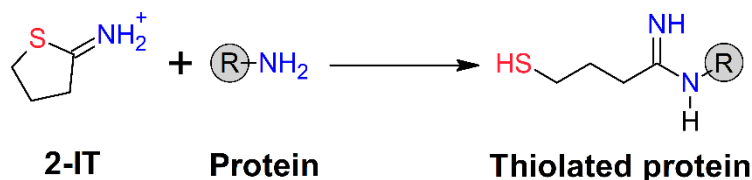


Figure 28 Thiolation reaction of proteins using 2-iminothiolane to attach a sulfanyl butanimidine group to a primary amine

The amount of available sulfhydryl (SH) group was quantified by Ellman reagent assay [158]. The 1% tSF solution was mixed with 0.1 M DTNB or Ellman reagent and 1 mM EDTA. The mixtures were incubated at 37°C in the dark for 3 h, and the absorbance at 412 nm was measured. Cysteine was used to prepare a standard curve.

b. Gelation of SF and tSF with Au^{3+}

The mixtures of SF or tSF solution were mixed with gold (III) chloride trihydrate ($\text{HAuCl}_4 \cdot 3\text{H}_2\text{O}$), yielding 3% SF or tSF and 0.5, 1, 5 mM Au^{3+} . After that, the mixtures were incubated at 37°C and their changes were observed. At designated time-points (day 0, 1, 3, 7, 10 and 14), the samples were collected, frozen at -80°C, and lyophilized for FTIR determination.

3.4.2. Investigation of mechanism of Au-SF and Au-tSF gelation

a. Determination of secondary structures of freeze-dried Au-SF and Au-tSF hydrogels

The freeze-dried samples were ground, mixed with KBr, and prepared as thin discs for FTIR determination. FTIR spectrum between 4,000 to 400 cm^{-1} was collected in an absorbance mode with 2.0 cm^{-1} resolution and 1.0 cm^{-1} interval. The secondary structures were quantified by FSD and curve-fitting as described in the section 3.2.1b.

b. Formation of dityrosine, Au-S bonds and Au nanoparticles

Due to the fluorescence absorption of dissociated phenolic hydroxyl group presenting in tyrosine residues, fluorescence measurement can be used to assess the formation of dityrosine [159]. The mixtures of 0.1 to 5 mM Au^{3+} and 1% SF or 1% tSF were prepared, controlled the pH at 7.4 by 10 mM HEPES, and incubated for 3 h. The fluorescence spectra between 350 and 500 nm of the samples load in a 10-mm quartz cell were collected with an excitation of 320 nm using a fluorescence spectrometer (FP-8500, Jasco, USA).

After the addition of 0.1-5 mM Au³⁺ in 1% tSF solution, the amount of SH group was quantified using the Ellman reagent assay as aforementioned. The experiment for Au-SF mixtures was unable to conduct due to the low presence of SH in SF.

The formation of Au nanoparticles (NPs) was assessed by a surface plasmon spectroscopy [160]. Au-SF and Au-tSF mixtures with different Au³⁺ concentrations were prepared, incubated for 3 h, and collected the absorbance spectra from 300 to 700 nm by a microplate reader (Synergy HT, Bio-Tek, USA)

- c. X-ray photoelectron spectroscopy (XPS) for determining chemical states of Au and S

XPS analysis was performed to determine the chemical state of Au and S presenting in the Au-mediated SF or tSF hydrogels. The lyophilized samples were finely ground and analyzed by an Axis ultra DLD spectrometer (Kratos Analytical, Japan) equipped with a monochromatic Al K α x-ray source. The characteristic spectra of Au4f and S2p located at 81-94 and 159-174 eV, respectively, were collected. The curve-fitting was conducted using Origin Pro 9.0 software. Peaks of Au4f_{7/2} at 84.0, 84.7 and 85.5 eV corresponding to Au⁰, Au⁺ and Au³⁺, and of S2p_{3/2} at 162.2 and 164.2 eV for bound and free S, respectively, were assigned [161, 162].

3.4.3. Physico-chemical characterizations of Au-SF and Au-tSF hydrogels

- a. SEM analysis of freeze-dried Au-SF and Au-tSF hydrogels

The freeze-dried Au-SF and Au-tSF hydrogels were cut and sputter coated with platinum. SEM visualization was performed using a SEM (JSM-IT500HR, Jeol, Japan) at 300X and 15,000X magnifications.

- b. Viscoelastic properties of Au-SF and Au-tSF mixtures

The viscoelastic properties of the regenerated SF, tSF solution, Au-SF and Au-tSF mixtures were determined by a rheometer (Kinexus Pro+, Malvern Instruments, UK). Frequency sweep experiments was performed after loading the samples and equilibrated at 37°C for 10 min. The G', G'' and G* were collected over a frequency ranging from 0.01-100 Hz and the strain was fixed at 0.1%. All experiments were conducted in triplicate.

3.4.4. In vitro cell culture experiments of Au-SF and Au-tSF hydrogels

- a. Cytocompatibility tests of Au-SF and Au-tSF hydrogels

SF and tSF solutions were UV irradiated for 30 min. The steam sterilization cannot be used for tSF solution because the solution turns to gel after heating. Au³⁺ solution was filtered through 0.22- μ m filter. Regenerated SF and tSF hydrogels were formed in a 96-well tissue culture plate by allowing the spontaneous gel formation at 37°C for approximately 7 days. The Au-SF and Au-tSF hydrogels were prepared as previously described.

Before seeding, the hydrogels were washed with PBS once. L929 or MCF-7 human breast cancer cells were plated at 10,000 cells/cm² and cultured in CO₂-cabinet. Culture medium was changed three times a week.

MTS assay was used to assess the metabolic activity of cells cultured on the samples. At day 1, 3, 5 and 7, cells were washed and incubated with MTS reagent for 3 h. The absorbance at 490 nm was collected with a blank correction. All experiments were done in quadruplicate.

b. Caspase-3 activation for cell apoptosis determination

After 3-day culture, the apoptotic events of the cells were assessed from an activation of caspase-3 using the colorimetric caspase-3 assay kit. Cells (n=4) were lysed and the supernatants were mixed with dithiothreitol, labelled with a chromophore substrate DEVD-pNA, and incubated for 2 h. After that the absorbance values at 405 nm were measured, before normalized by the number of cells obtained from Hoechst 33258 DNA quantification assay as described previously.

3.5. Statistical analysis

The analysis of data was conducted using an IBM SPSS Statistics software (version 22). Statistical tests were performed using an analysis of variance (ANOVA) to compare the means and detect the difference within groups. Bonferroni post-hoc tests were used to analyze the difference between each independent variable. The difference was signified at *p-value* < 0.05.

Chapter 4

Results and Discussion

1. Phospholipid-induced silk fibroin hydrogels for cell carrier application

In this work, an acceleration of SF gelation was conducted using the chemical additives. Three strategies were applied, namely DMPG phospholipid, liposomes, and metallic Au salt. In the first part, a negatively charged phospholipid, DMPG, was found to induce the rapid gelation of SF solution. The mechanisms of gelation were investigated as well as the physico-chemical properties of the developed hydrogels. The hydrogel system was then used as cell carrier for the cell encapsulation in 3D microenvironment. Different types of cell lines were chosen for the encapsulation. The viability, proliferation and the morphology of cells while encapsulated were evaluated to determine the applicability of the DMPG-SF hydrogels as the potential matrices for cell carrier applications.

1.1. Gelation time of DMPG-SF mixtures

The gelation of 3% SF solution with 5, 10 and 15 mM DMPG was kinetically observed by the spectroscopic method. With an increase of DMPG from 5 to 15 mM, the gelation time was shorter from 40 min to 10 min (**Figure 29A**).

DMPG was mixed with DMPC at different ratios before mixing with 3% SF in order to investigate the role of lipid charge on the SF gelation. Because phosphatidylglycerol head group of DMPG displays a negative charge in a physiological pH, while phosphatidylcholine head group of DMPC is a zwitterion [18]. The binary phospholipid system was used to vary lipid charge while keeping hydrophobicity constant [21]. From **Figure 29B**, a higher ratio of DMPC to DMPG led to significantly longer gelation time. At 10 mM DMPC and 3:7 DMPC:DMPG, the SF gelation did not occur within 240 min. The results showed that DMPC was not as effective as DMPG in accelerating the gelation of SF. Furthermore, the lipid charges could play a crucial role in the initiation and enhancement of the sol-to-gel process of SF.

Ca^{2+} addition to the DMPG-SF mixtures was conducted to determine the ionic effect on the gelation of DMPG-SF. Ca^{2+} was chosen due to its presence in several physiological milieu and cell culture media. The SF gelation with a small Ca^{2+} amount (0.1 mM) showed no significant difference with no Ca^{2+} samples. While at higher Ca^{2+} , the gelation time was significantly longer (**Figure 29C**). The precipitation of DMPG with Ca^{2+} as well as an ordered molecular packing due to the presence of counterions were plausible for a delayed gelation of SF [163, 164]. As it can be noticed that a higher concentration of DMPG was more tolerate to the perturbation of the Ca^{2+} ion. The interaction between the cation and the phospholipid could be in a stoichiometric fashion.

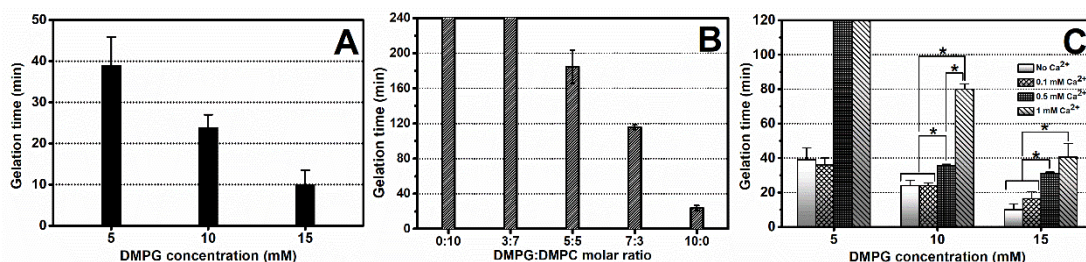


Figure 29 The gelation time of 3% SF with different concentrations of DMPG (A), different DMPG:DMPC molar ratios (B), and with a presence of Ca²⁺ (0.1, 0.5 and 1 mM) in DMPG-SF mixtures (C). The gelation was observed by the spectroscopic method at 37°C. All experiments were done in quadruplicate. * indicates the statistical difference at $p \leq 0.05$.

1.2. Gelation mechanisms of DMPG-induced SF hydrogels

1.2.1. SF conformational transition during the gelation induced by DMPG

FTIR spectra of 5, 10 and 15 mM DMPG-3% SF mixtures were collected every 10 min immediately after mixing, for the period of 90 min and the results were presented in **Figure 30A-C**. It can be noticed the spectral shift towards 1625 cm⁻¹, corresponding to the structural transition from random coil to beta sheet conformer [148]. The secondary structures were quantified from FITR spectra in amide region by FSD and curve fitting techniques. **Figure 30D-F** showed the content of secondary structures upon the gelation. The beta sheet conformer was gradually increased until reaching the gelation point before keeping constant afterwards. Other less ordered structures, such as random coil and alpha helix, were lower over the time. These characteristics indicate the self-assembly of SF, leading to a transition of SF solution to the hydrogel. The results were in accordance with previous reports using amphipathic molecules, e.g. sodium oleate [99], sodium dodecyl sulfate [94], sophorolipids [38], which an initiation of SF self-assembly occurred after the addition of these chemicals. The gelation and structural transition of the regenerated SF solution was discussed in this chapter at section 3.2.1 and 3.2.2. In brief, the regenerated SF solution took around 7 days to turn gel, and the structural analysis showed the increase of beta sheet was in accordance with the gelation.

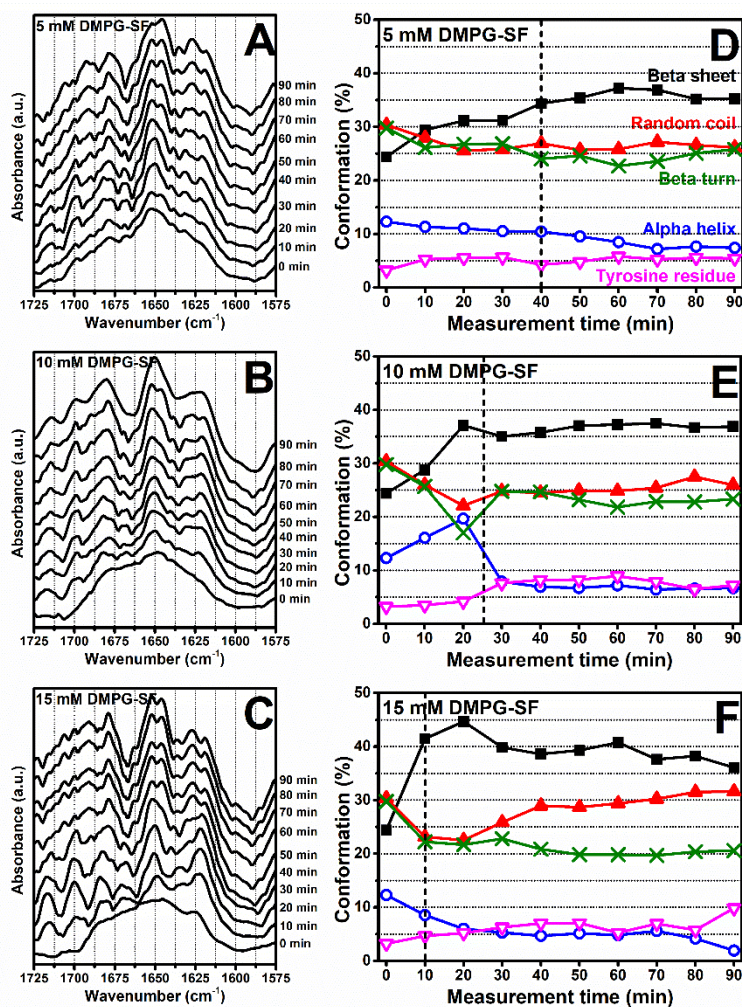


Figure 30 FTIR spectra of (A) 5, (B) 10, and (C) 15 mM DMPG-3% SF collected every 10 min for 90 min. (D-F) Secondary structures quantification by FSD and curve-fitting of FTIR spectra in amide I region (1,575-1,725 cm⁻¹). Dash line indicates the gelation time.

1.2.2. Microenvironment changes of SF

Due to the fluorescence absorption of tryptophan residues, tracing of tryptophan localization by fluorospectrometry is useful to determine the hydrophobic or hydrophilic interactions as well as the folding of proteins [149]. Tryptophan residues are able to emit the fluorescence energy at 320 nm after an intrigue of 290-nm UV light. An intensity of the emission energy relates to a quenching effect by surrounded hydrophilic environment, and an increase of intensity corresponds to a shielding of tryptophan from the quencher. **Figure 31A** showed the fluorescence emission spectra of 5 mM DMPG-SF hydrogels using an excitation at 290 nm. The emission intensity in the first 30 min, corresponding to the gelation time, was gradually increased before becoming plateau. Moreover, the blue shift from 324 nm to 314 nm can

be noticed. Hence, the protection of tryptophan residues from hydrophilic environment was evidenced, relating to the transition of SF solution to gel.

Acrylamide was used as a quencher to determine the interactions between the phospholipid and protein. Stern-Volmer plot in **Figure 31B** indicated that DMPG-SF possessed the lower k_{sv} than those of SF solution and SF hydrogel. The lower k_{sv} related to a higher difficulty of acrylamide in accessing to the tryptophan. Due to the inherent hydrophobicity of tryptophan, the interaction with the hydrophobic regions of DMPG could be occurred, preventing the access of the quencher to the tryptophan.

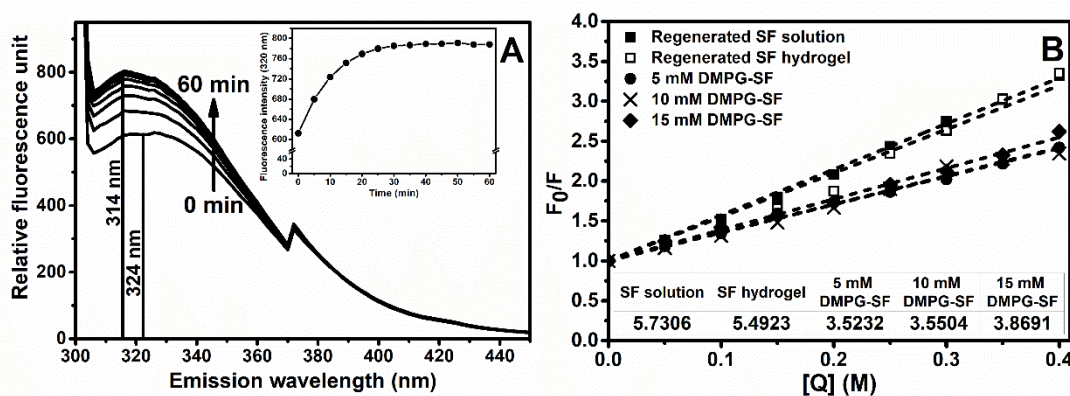


Figure 31 (A) Fluorescence emission spectra after exciting the 5 mM DMPG-3% SF at 290 nm. The spectra were collected from 300-450 nm every 5 min. An inset displays an emission intensity at 320 nm over an experimental time. (B) Stern-Volmer plot of the acrylamide quenching experiment of SF solution, SF hydrogel and DMPG-SF hydrogels. An inset table shows the Stern-Volmer constant (k_{sv}).

Taken all the results together, the mechanisms of SF gelation mediated by DMPG were proposed as illustrated in **Figure 32**. The negative charge of DMPG polar head could result in an electrostatic repulsion with SF chains, since SF also possesses a negative charge at pH 7.4 [94]. These phenomena led to an extension or unfolding of SF chains from their inherent arrangement. The hydrophobic interactions between DMPG and SF were confirmed by the fluorescence spectroscopy. These processes could facilitate the rearrangement of SF chains into a thermodynamically stable beta sheet structure. An increase of DMPG concentration resulted in a higher number of negative charges and hydrophobic contents, leading to a more rapid gelation of SF. These proposed mechanisms were in an agreement with previous studies using the surfactant [94] and lipids [38], which described the main driving forces of SF gelation mediated by the amphipathic molecules were the electrostatic and hydrophobic interactions.

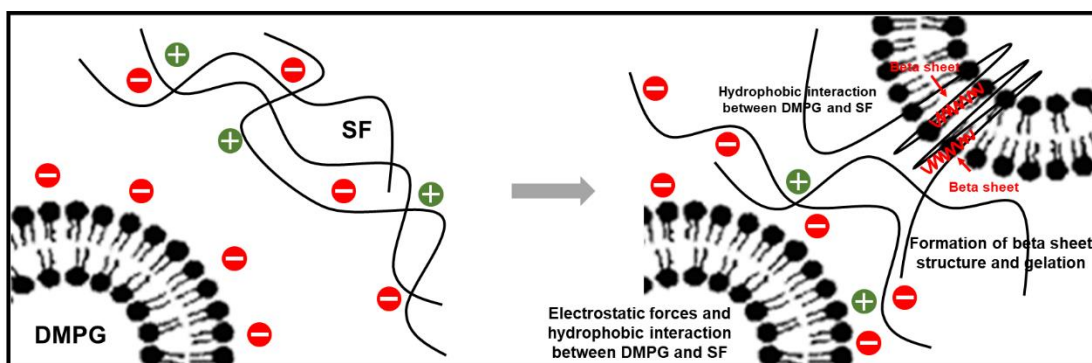


Figure 32 The proposed mechanisms of DMPG-induced SF hydrogelation. The negative-charged DMPG interacts with SF chains, leading to the chain extension or unfolding through the electrostatic repulsion. The hydrophobic interaction between DMPG and the hydrophobic regions of SF results in a chain rearrangement and the formation of beta sheet structure.

1.3. Properties of DMPG-SF hydrogels

1.3.1. Micromorphology of lyophilized DMPG-SF hydrogels

Microstructures of SF hydrogel and DMPG-SF hydrogels were presented in **Figure 33A-D** and the pore size was showed in **Figure 33E**. An interconnected porous architecture was noticed in all samples. No significant difference between the pore size of DMPG-SF hydrogels (52.8 ± 11.3 , 50.4 ± 12.4 and 59.7 ± 14.0 μm for 5, 10 and 15 mM DMPG-3% SF hydrogels, respectively) was noticed. A relatively small pore size was found in the regenerated SF hydrogel of which its pore diameter was 4.89 ± 1.28 μm . Presumably, due to the long gelation time of regenerated SF (approximately 7 days at 37°C), the loss of water occurred, leading to a higher SF concentration. This could result in closer SF chains and reducing pore diameter.

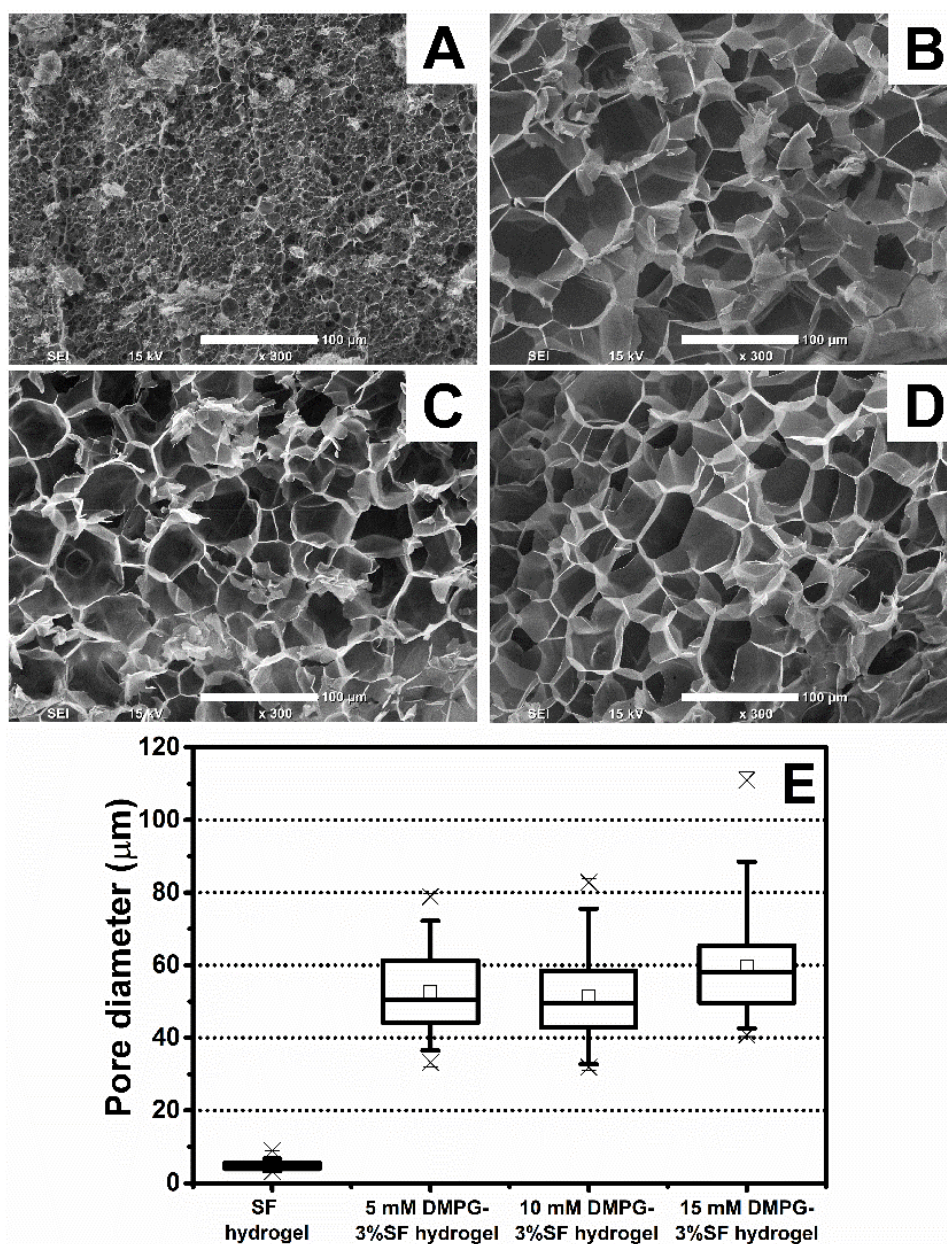


Figure 33 SEM micrographs of freeze-dried (A) regenerated SF hydrogel and the 3% SF hydrogels induced by (B) 5 mM, (C) 10 mM, and (D) 15 mM DMPG. Scale bar = 100 μm. (E) Pore diameter of SF and DMPG-SF hydrogels.

1.3.2. Viscoelastic properties of DMPG-SF

After loading the DMPG-SF mixtures, the time sweep experiment was firstly conducted for 1 h to ensure the complete gel formation which can be noticed from the constant complex modulus (G^*), as exemplified in **Figure 34A**. Subsequently, the oscillatory shear force sweeping over a range of frequency was applied while the elastic (G') and viscous (G'') moduli were collected (**Figure 34B**). The G' modulus of DMPG-SF hydrogels decreased with an increment of DMPG. Between a range of frequency of 1-10 Hz, the

average G' of 5, 10 and 15 mM DMPG-3% SF hydrogels were approximately 50, 35 and 11 kPa, respectively. It was possible that an addition of the small organic molecule (DMPG) interfered the inherent mechanical properties of SF hydrogels. The results were in an agreement with previous study using sophorolipids as the gelator of SF. A higher content of sophorolipids led to a lower compressive modulus of the freeze-dried hydrogels [38].

Regarding the strain sweep experiment, the order of the average G' between 0.1 to approximately 20% strain of DMPG-SF hydrogels were like those of the frequency sweep experiment (Figure 34C). At high shear strain, the G'' modulus was noticeably predominated G' at 41.3%, 32.3% and 20.2% for 5, 10 and 15 mM DMPG-3% SF (Figure 34D). The results confirmed that higher DMPG amount led to lower mechanical stability of the DMPG-SF hydrogels.

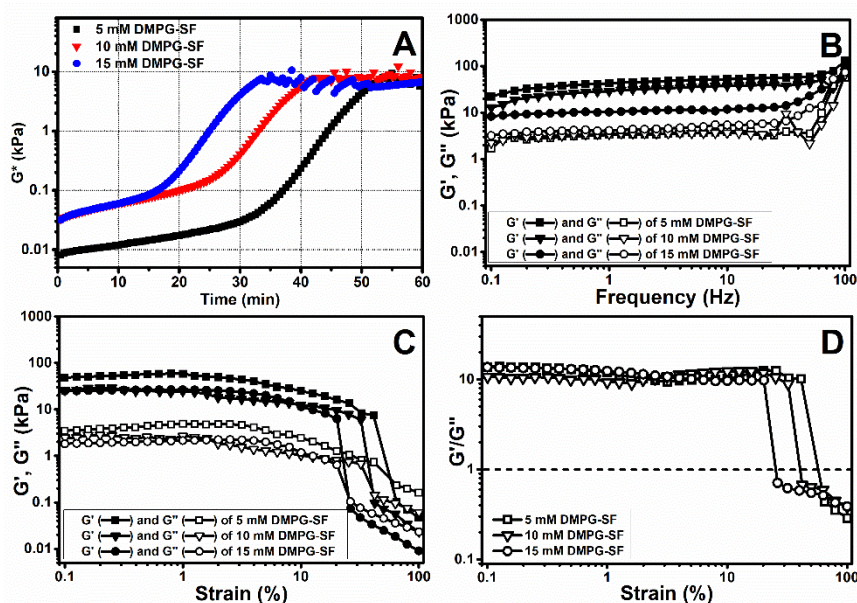


Figure 34 Viscoelastic properties of DMPG-SF hydrogels. (A) Complex modulus (G^*) of the hydrogels from time sweep experiment. (B) Elastic (G') and viscous (G'') moduli of the hydrogels over the frequency ranging from 0.1-100 Hz with a fixed 0.5% strain. (C) G' and G'' of the hydrogels over the strain ranging from 0.1-100% with a constant 1 Hz frequency. (D) The ratio of G'/G'' over 0,1-100% strain. The dash line indicates $G'/G'' = 1$.

1.3.3. Degradation profile of the DMPG-SF hydrogels

The enzymatic degradation of SF and DMPG-SF hydrogels showed approximately 15-30% weight loss over 21 days of incubation (Figure 35). Interestingly, weight reduction of DMPG-SF hydrogels in the first 7 days can be noticed in both control and enzymatic media. While this phenomenon cannot be observed in the regenerated SF hydrogel group. Possibly, the initial weight loss of DMPG-SF hydrogel could result from the release of DMPG from the hydrogels. At day 14 and 21, a significant difference of weight loss percentage between 5 and 15 mM DMPG-3% SF hydrogels, indicated the

relationship between the amount of DMPG and the degradability in such proteolytic condition. It is possible that, with more DMPG, the interaction between DMPG and SF chains increases. DMPG might prevent the protease enzyme to cleave the SF chains, reducing the accessibility of the enzyme to cleavage sites of SF.

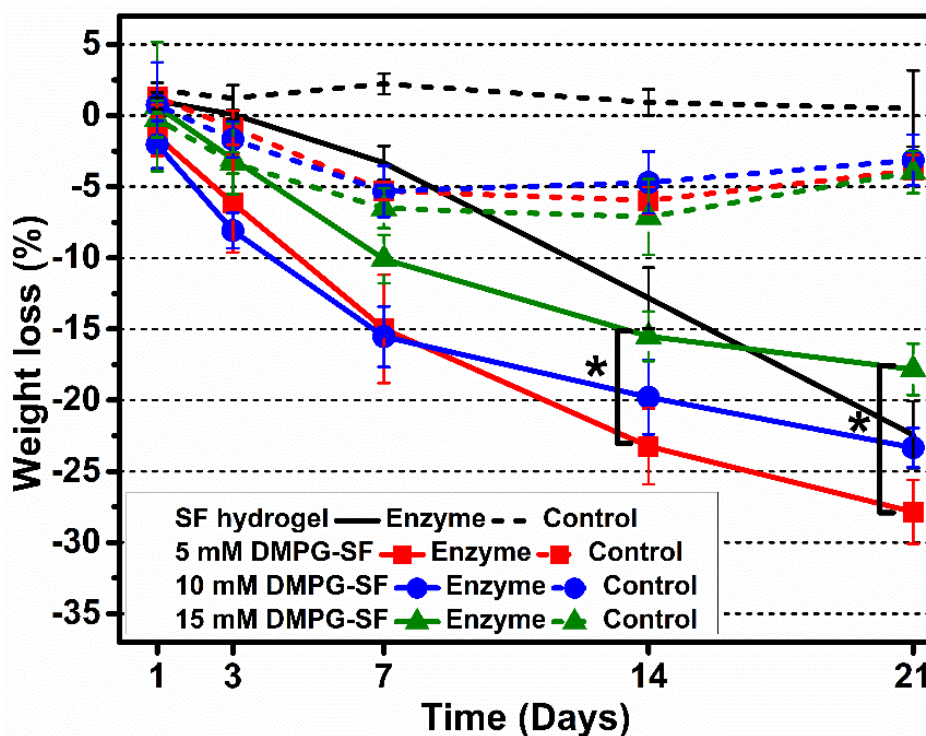


Figure 35 Degradation profile of SF and DMPG-SF hydrogels in the control media (HEPES buffer) and in the proteolytic media (1 unit/ml protease XIV in HEPES buffer). The symbol (*) indicates the significant difference at p -value ≤ 0.05 .

1.4. Cytocompatibility evaluations of DMPG-SF hydrogels

1.4.1. Proliferation profile of the cell lines

Proliferation of the cell lines, including L929, NIH/3T3, SaOS-2 and CaSki, was tested on 2D substrates to ensure normal cell growth by comparing the results with the existing data. The cells were cultured on the tissue culture plate, and the proliferation profile, as shown in **Figure 36**, presented an exponential growth between 6 and 96 h. The specific growth rate (μ) and population doubling time (PDT) were calculated. The results were shown in **Table 7**. The experimental PDT values were slightly different from those reported in the databases. The difference might be a result from different culture conditions, the passage number of cells, and the interpretation of obtained data, but the result could indicate the normal growth behavior of the cell lines

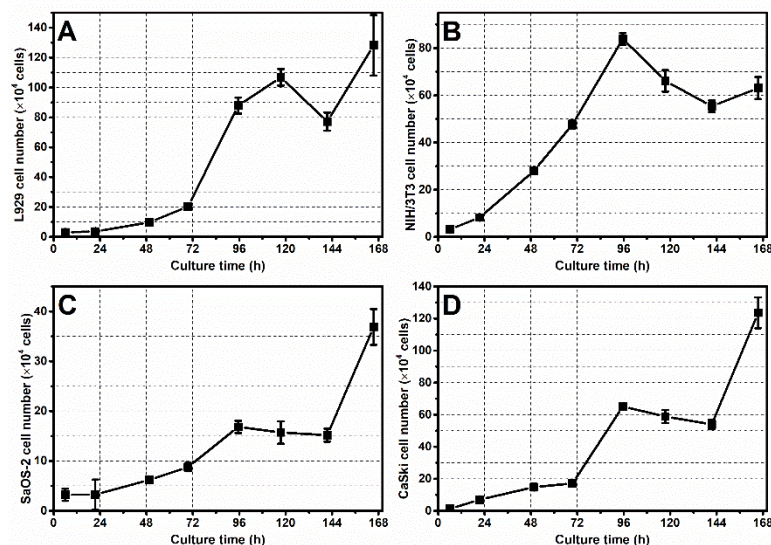


Figure 36 Proliferation profiles of (A) L929, (B) NIH/3T3, (C) SaOS-2 and (D) CaSki. The cells were cultured on tissue culture plate and the cell number was assessed by MTT cell metabolic activity assay.

Table 7 Attachment and proliferation profile of the cell lines used in the biological experiments

Cell lines	6-h cell attachment (%) (average \pm S.D.)	μ (h^{-1})	PDT (h)	Reported PDT (h) [Ref.]
L929	96.5 \pm 10.2	0.0425	16.3	20 – 25 [165]
NIH/3T3	99.0 \pm 13.6	0.0311	22.3	20 [166]
SaOS-2	101.0 \pm 37.7	0.0219	31.7	43 [167]
CaSki	38.6 \pm 13.4	0.0285	24.3	24 [168]

1.4.2. Indirect cytotoxicity test of the DMPG-SF hydrogels

The indirect cytotoxicity test was performed to assess the cytocompatibility of DMPG-SF hydrogels according to the guideline by ISO 10993-1:2009. The extract media of DMPG-SF hydrogels were used to culture L929 for 24 h, and the cell morphology and viability were then observed. From **Figure 37**, the morphology of cells in all test groups (5, 10, and 15 mM DMPG-3% SF hydrogels) was fibroblast-like morphology, similar to those in blank (serum-free media) and negative control (DMEM/10% FBS). Furthermore, the average %viability of L929 exposed to the extracts of DMPG-SF hydrogels were over 70%, indicating no cytotoxic of the test materials according to the ISO standard [152]. Hence, the results confirmed the cytocompatibility of the DMPG-SF hydrogels.

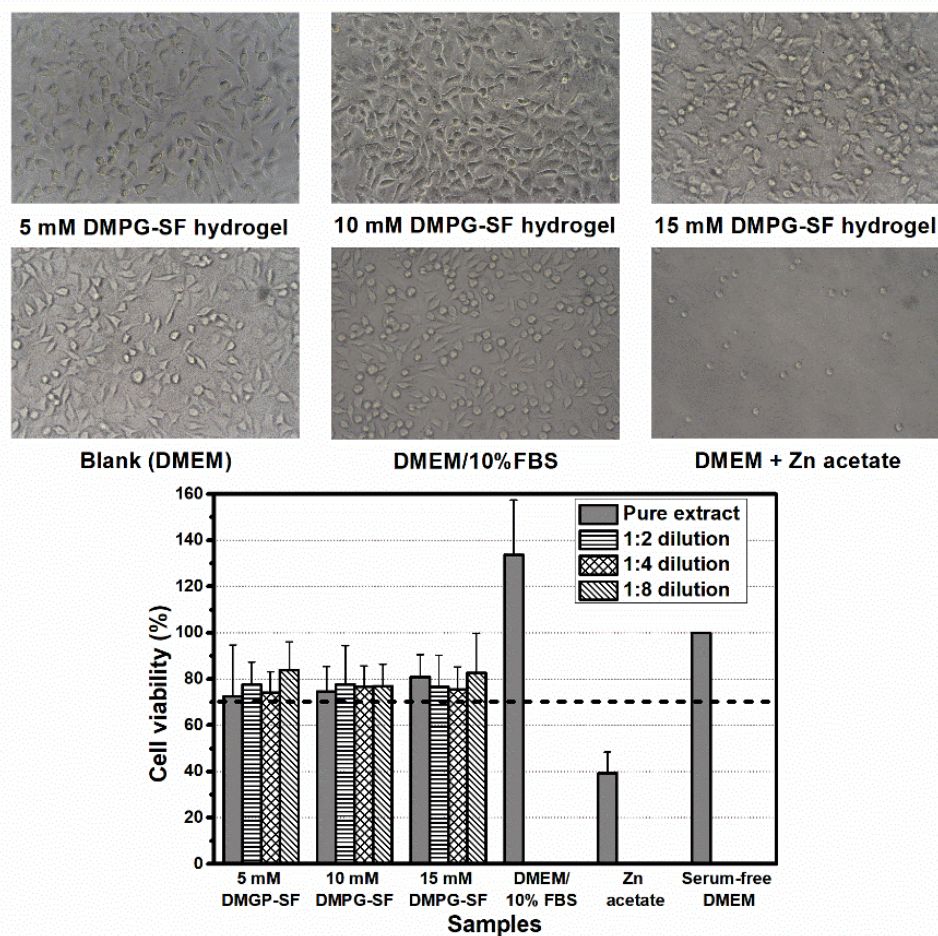


Figure 37 (Upper) Cell morphology after 24-h exposed to the extracts from the test materials (5, 10 and 15 mM DMPG-SF hydrogels), blank (serum-free DMEM), negative (DMEM/10% FBS) and positive (DMEM + zinc acetate) controls. (Lower) Cell viability percentage after exposed to the extracted media. The dash line indicates 70% viability, the cut-point for determining cytotoxicity of the materials according to the ISO standard.

1.4.3. Viability and morphology of cells encapsulated in DMPG-SF hydrogels

The viability of L929 encapsulated in 10 mM DMPG-3% SF hydrogels was visualized at day 1, 3, 7, 14 and 21 using live/dead staining (**Figure 38A-E**). It can be noticed that the living cells were distributed in the hydrogel matrices, and able to survive and proliferate over 2 to 3 weeks. This could indicate the applicability of such DMPG-SF hydrogels in the encapsulation process. Additionally, the morphology of encapsulated cells at day 21 were round. The result was corroborated with the previous study comparing the cell encapsulation in PEG and RGD-modified polyethylene glycol (PEG) hydrogels [169]. The cells with rounded morphology were observed in non-modified PEG group, due to the low concentration of cell adhesion motifs presented in the PEG. Because the lack of cell adhesive sequences presented

in SF extracted from *Bombyx mori* silk cocoons [52], this could result in a low attachment of cultured cells.

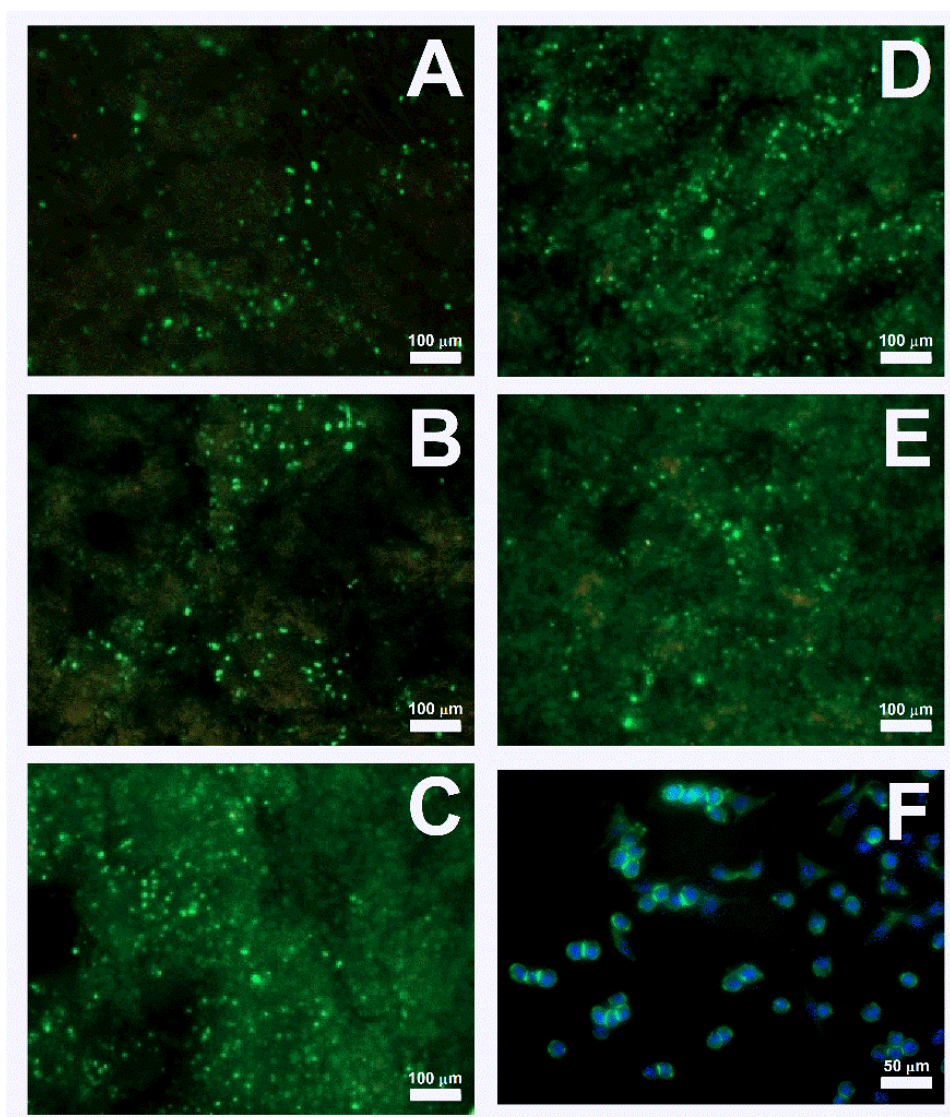


Figure 38 Live/dead staining of encapsulated L929 cells in 10 mM DMPG-3% SF hydrogels at day 1 (A), 3 (B), 7 (C), 14 (D) and 21 (E). Green and red dots indicate live and dead cells, respectively. Scale bar = 100 μm . (F) Morphology of encapsulated L929 at day 21. Blue and green stains represent nucleus and cytoskeleton, respectively. Scale bar = 50 μm .

1.4.4. Proliferation of encapsulated cells

The proliferation of cells encapsulated in the 5, 10, and 15 mM DMPG-3% SF hydrogels were evaluated by cell metabolic activity MTT assay. The absorbance values were converted to the number of cells using the standard curve. It is worth noting that MTT assay is an indirect method for determining the cell number, since the mechanisms of the assay relates to the reduce activity of NADH-dependent oxidoreductase enzymes. The activities of the

enzymes relate to the number of viable cells in certain conditions. The different culture conditions, such as exhausted medium, cell over-confluency, and different treatments, can affect the correlation between the MTT results and the number of cells [170, 171].

Encapsulated L929 (**Figure 39A**) and NIH/3T3 (**Figure 39B**) showed an exponential growth phase from 3 to 14 days. The lag phase was longer than those exhibited in the 2D cultures (**Figure 36A&B**). The population doubling time of L929 and NIH/3T3 cultured in the hydrogels were significantly higher than the culture on TCP (**Table 8**). The previous study indicated that the cell population in G0/G1 phase was higher while culture in 3D environment, leading to the higher cells in the quiescence state with slower proliferation rate but remaining viable [172]. Contact inhibition from the confinement in 3D microenvironment could be an important factor limiting cell activities [173].

Encapsulated SaOS-2 showed no proliferation until the end of 21-day period (**Figure 39C**). Therefore, it was impossible to calculate the PDT. Presumably, the stiffness of the matrices as well as the cell morphology can affect the behaviors of osteoblast-like cells. Several reports stated that the cell spreading and morphology influenced by the surrounding microarchitectures led to a distinct proliferation and differentiation of bone cells [174]. Hence, the rounded shape of SaOS-2 while encapsulated might not favor to the proliferation.

Interestingly, the growth of encapsulated CaSki presented an exponential phase from 7 to 21 days (**Figure 39D**). The number of cells at day 21 as well as the PDT of cells cultured in the SF hydrogels with different DMPG concentrations were significantly different. An increase of DMPG content led to a lower cell number and an extended growth rate.

It is well known that the presence of cell binding motifs in the hydrogel materials supports greater cell activities in proliferation and differentiation. It is possible that the extended lag phase and delayed growth rate of cells encapsulated in DMPG-SF hydrogels could result from the absence of cell adhesion motifs of SF biomaterials. **Table 9** shows the proliferation of various cells in the unmodified SF hydrogels. The delayed lag phase and slow proliferation or no growth can be noticed, which is in accordance with this study. The bioinert properties of SF can be improved using the strategies applied to other inert materials, such as alginate and polyethylene glycol, by conjugation with cell binding motifs or blending with other polymers [175, 176]. For example, SF was crosslinked with laminin-derived peptides, IKVAV, for the preparation of neural stem cell encapsulation using sonication [76]. A greater cell viability and higher differentiation potential were noticed comparing to those in the unmodified SF hydrogels.

Apart from inherent characteristics of hydrogels, the mechanical properties can play an important role on the bioactivities of the encapsulated cells. Cells in the hydrogels prepared from RGD-containing materials, namely collagen [177], gelatin [178], and RGD-conjugated polyethylene glycol [176], displayed different cell viability and cell number depending on the stiffness.

Hydrogels with higher elastic modulus can deteriorate the activities of encapsulated cells. This is a reason why the awareness of tuning the mechanical properties of the materials matching the matrix elasticity of target tissues has been raised. To exemplify, the elastic modulus of sonicated SF hydrogels for injecting to the brain cavity was within a range of 0.1-1 kPa, which is an elastic modulus of brains [77]. Encapsulated cells were able to proliferate in all hydrogels, but the shorter lag phase and higher cell number were observed in the softest hydrogel. These phenomena were widely discussed that several factors contributed to the 3D microenvironment could influence the encapsulated cells. Several studies argued that 3D cell culture in the softer hydrogels showed a better cell viability [176-178]. Since the soft materials are resulted from a lower solid content or crosslinking degree, the mesh size and the degradation should be different. Larger mesh size can enhance the diffusivity of hydrogels for the exchange of gas, nutrients, and waste, and the appropriate degradation rate could allow an optimum matrix remodeling processes of cells. These are the reasons why the hydrogel properties should be finely tuned to achieve a suitable activity of encapsulated cells.

Cell encapsulation technology provided abundant applications including cell supporting abilities, maintaining cell viability, enhancing cell growth, and promoting cell differentiation [179]. Cell-encapsulated hydrogels were useful for cell therapy; 3D cell culture model for pathophysiological studies or drug screening; 3D cell or tissue printing; and a large-scale cell-related bioprocessing. Recently, encapsulation matrix for hibernating cells was increasingly needed form the clinical advancement in collecting stem cells at youth and supposing to use as needed or at senescence [180]. The main aims of this encapsulation strategy were to maintain the inherent properties of cells and prevent them from external stresses, such as temperature fluctuation. The promotion of the growth of encapsulated cells was not needed but their viability and activities must be preserved. For example, mesenchymal stem cells were encapsulated in the hydrogels made of bioinert materials, namely, alginate [181], methacrylated polyethylene glycol, and hyaluronic acid [182]. Their viability and the differentiation potential were confirmed even after a long time preservation and several freeze-thawed cycles. Therefore, encapsulation in SF hydrogels, as shown in this study, could be a potential strategy due to the bioinertness of SF as well as the results of this study showed that the encapsulated cells were still viable in the hydrogels. Further study is required to explore the suitability of DMPG-SF hydrogels for cell preservation by mimicking the cell storage conditions, such as keeping in different temperature, and evaluating the cell activities afterwards.

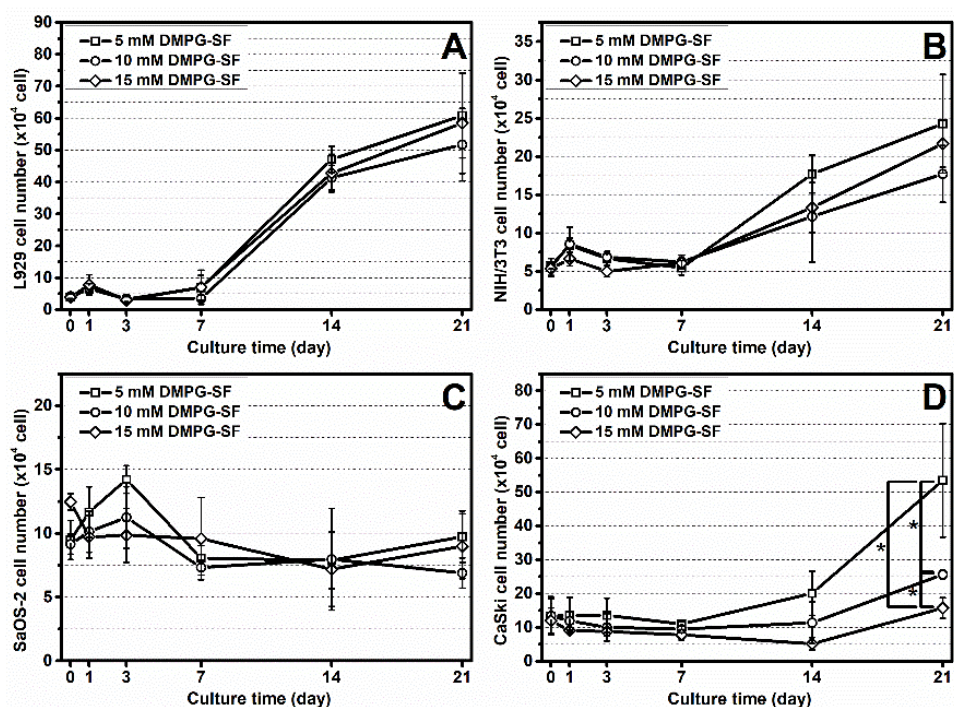


Figure 39 Proliferation profile of encapsulated (A) L929, (B) NIH/3T3, (C) SaOS-2 and (D) CaSki in the 5, 10, and 15 mM DMPG-3% SF hydrogels. The asterisk (*) represents the statistical difference at p -value ≤ 0.05 .

Table 8 Population doubling time (day) of encapsulated cells in DMPG-SF hydrogels, compared to 2D culture on tissue culture plate (TCP).

Cells	5 mM DMPG-SF	10 mM DMPG-SF	15 mM DMPG-SF	TCP
L929	2.82	2.88	2.85	0.68
NIH/3T3	8.12	10.01	8.11	0.93
SaOS-2	N/A	N/A	N/A	1.32
CaSki	6.12	9.73	13.80	1.01

Table 9 Proliferation of the encapsulated cells in SF hydrogels induced by various methods and with different SF concentration

Cell type	Cell density (cells/ml of hydrogel)	SF concentration (%w/v)	Gelation method	Culture time (day)	Lag time (day)	Cell proliferation	Ref.
hMSC	0.5×10^6	4, 8, 12	Sonication	21	No growth	No growth	[35]
hNSC	4×10^6	1	Sonication	7	No growth	No growth	[76]
mMSC	4×10^6	2, 3, 4	Sonication	15	5-10	Early growth phase and high cell number in SF hydrogel with low solid content (2%)	[77]
hMSC	$0.5-1 \times 10^6$	3	HRP	29	10	Growth phase in 10-21 days	[106]
HeLa	1×10^6	1	HRP	14	7-10	Growth phase in day 10 before stationary phase	[37]

Abbreviations: hMSC = human mesenchymal stem cells, hNSC = human neural stem cells, mMSC = mouse mesenchymal stem cells, HRP = horseradish peroxidase enzyme

In summary, the rapid gelation of regenerated SF solution can be achieved using DMPG phospholipid as an inducer. The gelation kinetics depended on the DMPG concentration, the lipid charge, and the presence of cations. The structural transition from random coil to beta sheet was in accordance with the SF gelation, indicating that DMPG induced the self-assembly of SF. Electrostatic forces between negative-charged DMPG and SF molecules together with hydrophobic interaction were proposed as the main driving forces. The biological experiment confirmed the feasibility of the obtained hydrogels in the application as a 3D cell culture matrix.



2. Liposome-induced silk fibroin hydrogels for drug delivery system

From the previous section, the rapid gelation of SF can be induced by the phospholipid DMPG. Hence, the DMPG-based liposomes were prepared and used as the dual-functional liposomes for accelerating the SF gelation and drug delivery system. Curcumin was selected as an entrapped herbal drug in the liposomes and delivered from the hydrogels. The properties of the liposomes and liposome-SF hydrogels were determined as well as the biological properties against normal and cancer cell lines.

2.1. Characterizations of curcumin-loaded DMPG-based liposomes

2.1.1. Yield, size, and curcumin content analysis

Table 10 presented the yield of preparation, the analysis of curcumin content, and the size and size distribution of the liposomes. Approximately 80-90% yield was obtained after the preparation process of the liposomes. Regarding an entrapment of curcumin in liposomes, 50-100% EE and 1-5% LD were achieved, and the amount of entrapped curcumin related to the cholesterol content and the ratio of DMPG:DMPC. An increase of cholesterol presence in the liposome formation led to a lower %EE. It was possible that cholesterol and cur, which were lipophilic molecules, localized in the same hydrophobic region of lipid bilayers [154, 183]. The competitive localization could occur and result in a low entrapment of cur. Furthermore, with a presence of 8.7% w/w cholesterol (A1-D1) and 16.0% w/w cholesterol (A2-D2), a lower DMPG:DMPC ratio from 10:0 to 3:7 related to an increase of %EE and %LD.

An average size of the liposomes was in the range of 100 to 300 nm, except A0 and B0, which their size was large, and the distribution was highly scattered. The liposomes with lower DMPG ratio, such as C0 and D0, presented a narrow size distribution. Furthermore, an addition of cholesterol resulted in a more controllable size.

Table 10 Yield, encapsulation efficiency (EE) and loading capacity (LD) percentage of curcumin in the liposomes, and size and polydispersity index (PDI) of the liposomes

Liposomes	Yield (%)	EE (%)	LD (%)	Size (nm)	PDI
A0	94.60 ± 8.34	69.82 ± 19.09	3.33 ± 0.91	1054.74 ± 2085.78	0.3609 ± 0.1472
B0	81.27 ± 10.60	105.14 ± 11.74	5.01 ± 0.56	298.89 ± 574.85	0.2154 ± 0.2403
C0	81.90 ± 16.67	97.68 ± 14.31	4.65 ± 0.68	104.61 ± 8.28	0.2392 ± 0.0519
D0	78.10 ± 19.85	102.67 ± 9.34	4.88 ± 0.44	135.07 ± 10.24	0.2282 ± 0.0397
A1	88.84 ± 14.81	52.01 ± 11.50	2.26 ± 0.50	160.18 ± 73.14	0.1981 ± 0.0516
B1	85.22 ± 18.21	62.77 ± 17.76	2.73 ± 0.77	160.79 ± 50.91	0.2037 ± 0.0650
C1	89.57 ± 13.17	65.49 ± 23.46	2.85 ± 1.02	111.83 ± 19.36	0.2122 ± 0.0346

D1	84.64 ± 13.06	94.06 ± 17.99	4.09 ± 0.78	167.50 ± 23.41	0.2258 ± 0.0307
A2	84.80 ± 11.95	39.65 ± 7.72	1.59 ± 0.31	134.50 ± 32.75	0.2161 ± 0.0726
B2	79.73 ± 8.97	51.92 ± 15.27	2.08 ± 0.61	181.84 ± 26.60	0.2244 ± 0.0175
C2	75.47 ± 15.34	52.37 ± 9.81	2.10 ± 0.39	152.91 ± 29.94	0.2306 ± 0.0303
D2	83.20 ± 10.07	66.36 ± 22.66	2.65 ± 0.91	274.54 ± 50.49	0.2201 ± 0.0304

The stability of the liposomes after storage at 4°C was evaluated from the size changes. No significant difference in the size of after-prepared and 2-week old liposomes was noticed except the noticeable broad size distribution of A0 and B0 (**Figure 40**).

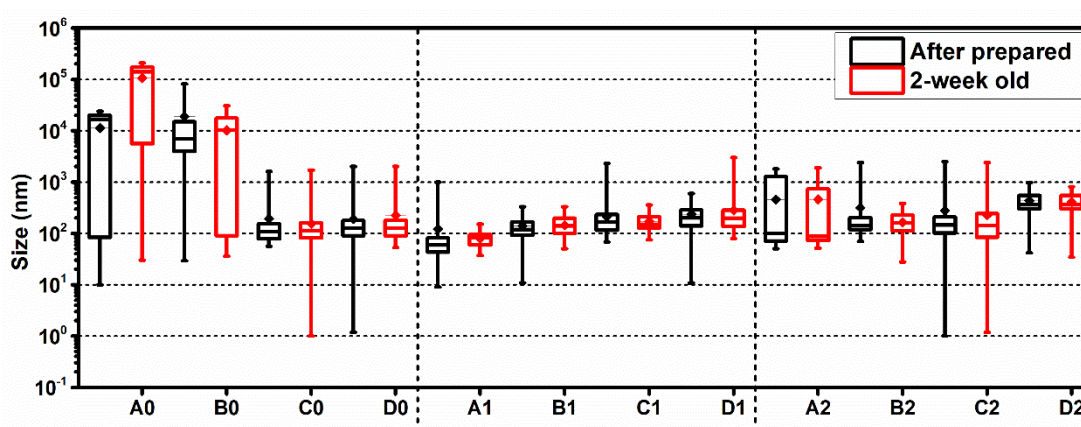


Figure 40 Box plot of the size and size distribution of the liposomes comparing between after-prepared liposomes (black box) and the liposomes stored at 4°C for 2 weeks (red box)

2.1.2. TEM images of the liposomes

Nanostructures of the liposomes A1, B1, C1 and D1 were visualized by TEM and the images were shown in **Figure 41**. The round morphology and the unilamellar vesicular structures were noticed. Shape irregularity and aggregation were observed in A1 and B1. Possibly, a high DMPG ratio in the liposome formulation related to a broad size variation and aggregation. Generally, an addition of DMPG in a small amount in liposome formulation is known to prevent aggregation, reduce physical degradation of the liposomal structures [183], and exert the negative charges for the electrostatic interactions [184]. However, the preparation of DMPG-based liposomes was not reported much in the literatures. Some study reported the application of DMPG-based liposomes as a dry powder for aerosol administration [185]. So, the liposomes with a high DMPG content might not be practical and result in the shape irregularity, broad size distribution and vesicle aggregation.

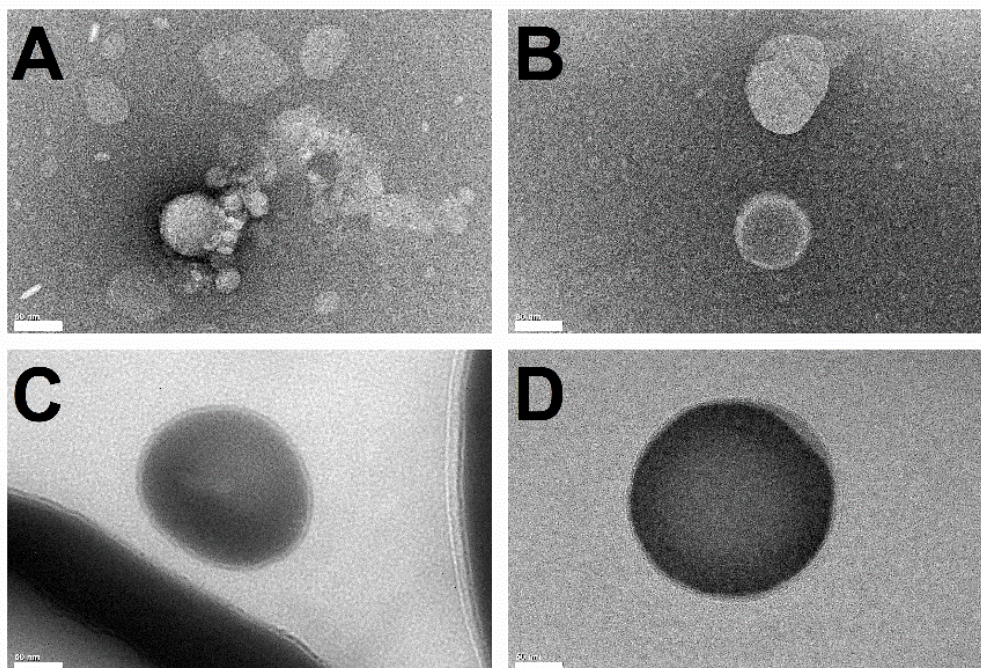


Figure 41 TEM images of the liposome (A) A1, (B) B1, (C) C1 and (D) D1 (scale bar = 50 nm)

2.1.3. Content and stability of active curcuminoids

Due to the lack of one and two methoxy groups attached to the phenolic rings of DMC and BDM, respectively, the hydrophobicity of the substances is lesser. Hence, the retention time of the less hydrophobic molecules from the reverse phase hydrophobic column is faster. Cur, DMC and BDM was eluted from the column at about 6.2, 6.5 and 6.9 min (**Figure 42A**), respectively, which can be defined from their correspondence mass of 307.02, 337.09 and 367.08 (**Figure 42B**).

The amount of active curcuminoids, summed of the amount of cur, DMC and BDM, was analyzed from the area under the PDA curve and normalized by the curcumin amount determined by the colorimetric assay. The comparison between the results obtained from the after-prepared and 2-week old liposomes was presented in **Figure 42C&D**. Approximately 0.2-0.7 mg of active curcuminoids per ml of liposomes were retained, corresponding to 30-50% when normalized by the amount of curcumin assessed by the colorimetric assay. The curcuminoid amounts were lower with a higher cholesterol ratio. Furthermore, the stability of entrapped curcuminoids showed no or slight difference between after-prepared and 2-week old liposomes.

The aqueous solubility of curcumin was enhanced significantly while entrapped in the liposomes. Comparing to directly dissolve curcumin powder in water, only 541.8 ng/ml curcuminoids was detected in the 0.2 mg/ml curcumin solution. After 2 weeks of storage, only 51.2 ng/ml curcuminoids were presented, indicating about 90% degradation in aqueous medium. The

rapid degradation of curcumin in water and buffers was reported and the major degradation products were biologically inactive [186]. The results confirmed that the encapsulation of curcumin in the liposome formulations can enhance the aqueous solubility and prevent the chemical degradations, such as photo-degradation or hydrolysis [154].

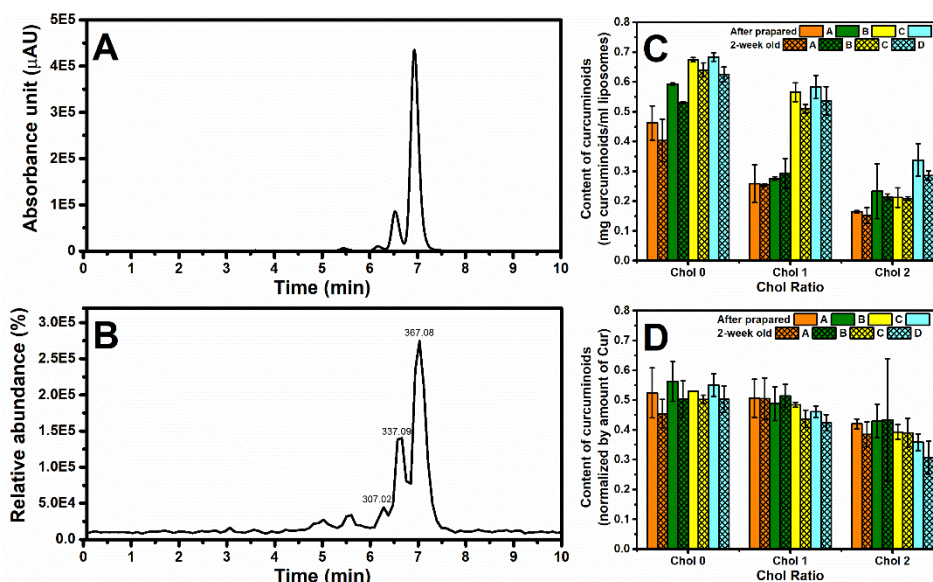


Figure 42 (A) PDA and (B) MS spectra of standard cur. Curcuminoid contents of freshly prepared (clear column) and 2-week old (patterned column) liposomes presenting as (C) actual content and (D) the amount normalized by curcumin amount determined by colorimetric assay.

2.2. Gelation time of liposome-SF mixtures

The reported sol-to-gel transition time of regenerated SF solution was about 5 days to more than 2 weeks, depending on the concentration of the solution and incubation temperature [12]. From the previous section, DMPG can induce the gelation of SF solution and accelerate the gelation time to 10 to 40 min. In this part, DMPG-based liposomes, with an amount equivalent to 15 mM phospholipids, were mixed with 3% SF solution, and the gelation time ranged from less than 5 min to more than 2 h (**Table 11**). For D0-SF and D1-SF mixtures, the gelation did not occur within 6 h but the gels were formed after incubating overnight. No gelation was observed for the D2-SF mixture.

Faster gelation than those in previous part was noticed because of an absence of buffer, in which ionic salts presented, can interfere the interactions between DMPG and SF. Noticeably, the gelation time of SF depended on the DMPG:DMPC ratio and the amount of cholesterol. A lower ratio of DMPG:DMPC from 10:0 to 3:7 as well as an increase of cholesterol obviously delayed the SF gelation. Presumably, an incorporation of cholesterol could enhance the integrity of lipid bilayers, leading to a more difficulty of SF chain in inserting to the lipid membranes. This could result in less hydrophobic

interactions between hydrophobic regions of SF and the alkyl chains of phospholipids.

Table 11 Gelation time (average \pm s.d.) of the 10 mg/ml liposomes and 3% SF mixtures. Asterisk (*) indicates no gelation within 6 h.

Liposomes	Gelation time (min)		
	Chol 0	Chol 1	Chol 2
A	3.4 \pm 0.7	7.3 \pm 2.0	18.9 \pm 6.5
B	14.2 \pm 4.0	22.0 \pm 8.3	167.8 \pm 34.0
C	79.6 \pm 32.7	145.4 \pm 49.8	-*
D	-*	-*	-*

* Chol = Cholesterol

2.3. Physical properties of liposome-loaded SF hydrogels

2.3.1. Microstructures and element compositions of freeze-dried hydrogels

Micromorphological structures of the freeze-dried liposome-SF hydrogels were determined using SEM as well as the elemental components using EDX. Sonicated SF and Curcumin-SF hydrogels were used as controls. The porous structures with leaf-like wall morphology can be visualized in all samples. The elemental analysis revealed a presence of Na and P, the characteristic elements presenting in DMPG, in the liposome-SF hydrogels. Interestingly, small particles, which can be the precipitates of cur, were noticed, while such characters were invisible in SF or liposome-SF hydrogels. This could result from the low aqueous solubility of curcumin directly loaded in the SF solution before forming the hydrogels.

Figure 44 shows the images of liposome-SF hydrogels visualized by TEM. Regarding to the A1-SF hydrogels, smaller vesicles than those observed in the neat liposomes (**Figure 41A**) were noticed. The results could confirm the proposed mechanisms of DMPG-induced SF gelation that SF chains insert through the lipid bilayers and interact with the hydrophobic regions of the liposomes. This phenomenon could lead to a vesicular breakage of the liposomes.

For other liposome-SF hydrogels, most of the liposomes retained their size and shape similar to their neat liposomes. It was possible that the higher DMPC ratio in the liposome formulation and an incorporation of cholesterol might increase the integrity of lipid bilayers. However, it was worth noting that the staining time, which was 2 min, was less than the gelation time. Hence, the gelation of SF induced by the liposomes B1, C1 and D1 was not complete. Moreover, the nanofibrous structures of SF chains can be observed in all samples.

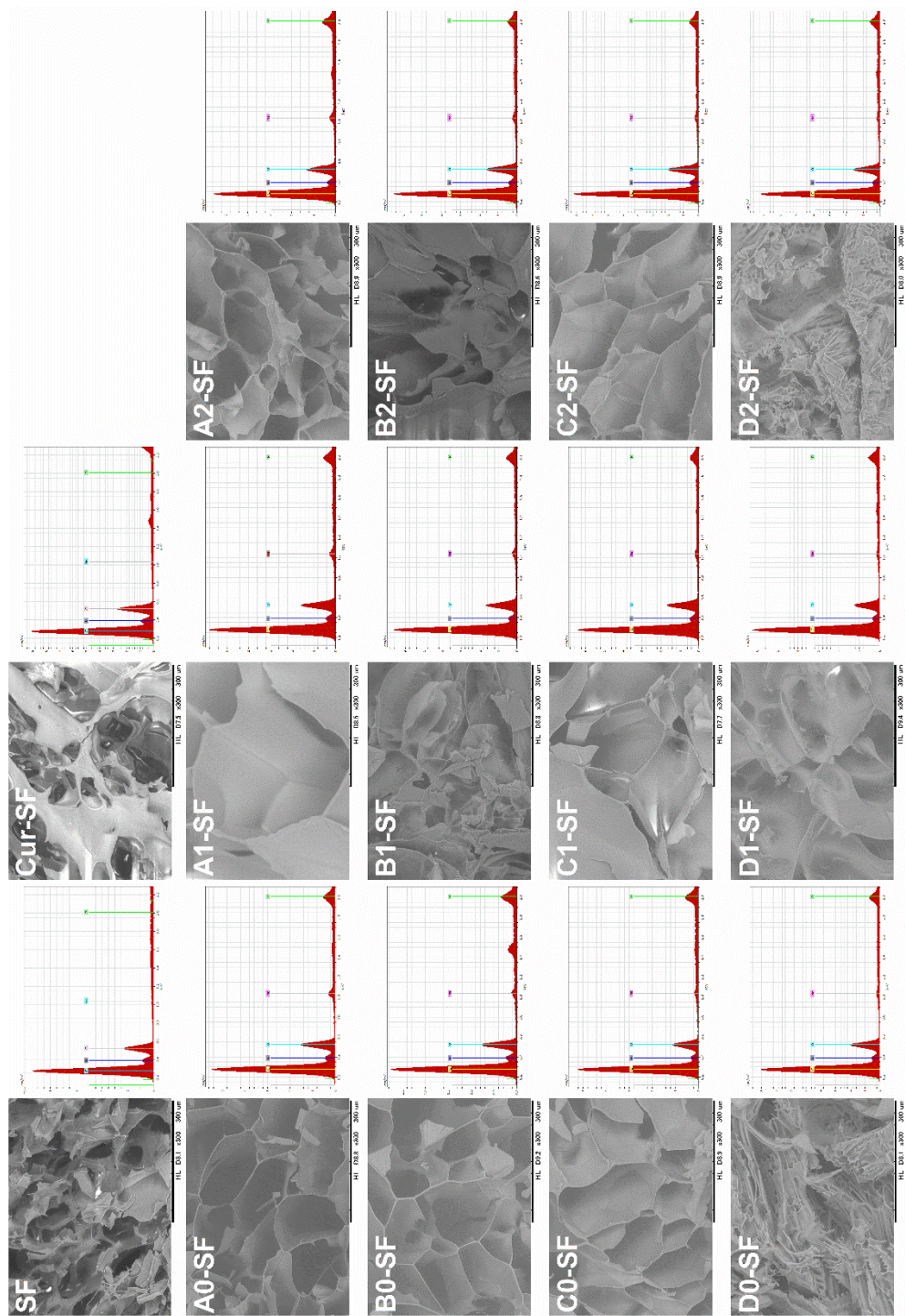


Figure 43 SEM images and elemental analysis of sonicated SF hydrogel and Curcumin-SF hydrogel, and liposome-SF hydrogels (scale bar = 300 μm)

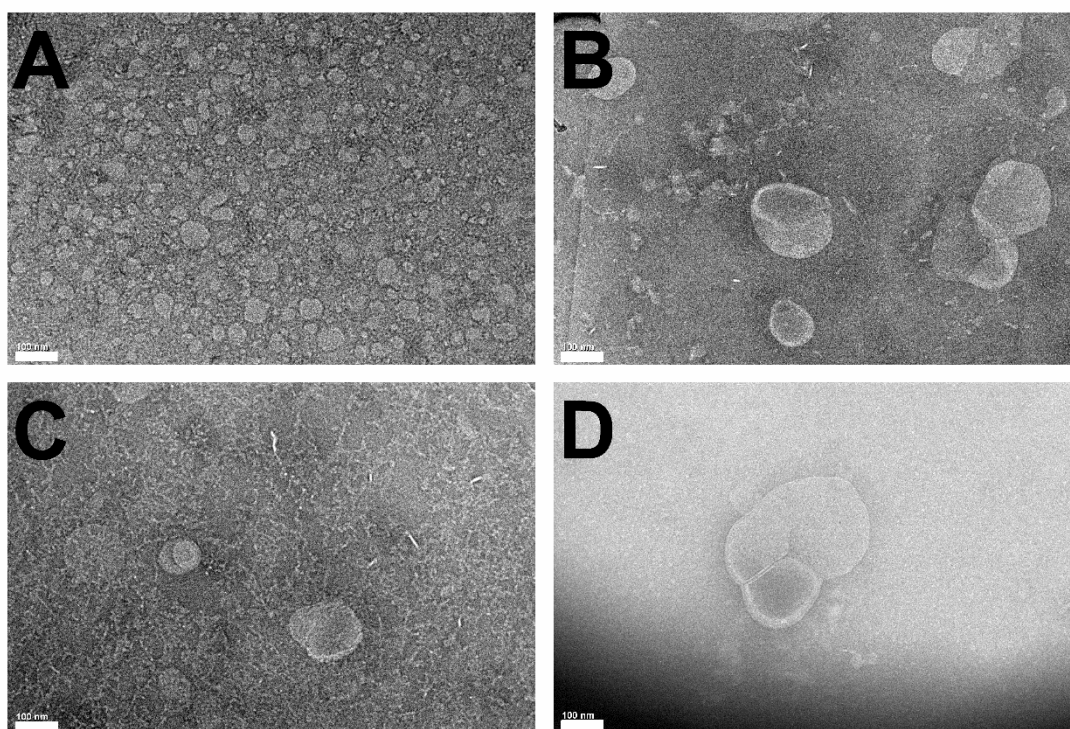


Figure 44 TEM images of liposome-3% SF hydrogels; (A) A1-SF, (B) B1-SF, (C) C1-SF and (D) D1-SF (scale bar = 100 μm)

2.3.2. Curcumin release from the hydrogels

The release of curcumin from the hydrogels was conducted in PBS supplemented with FBS. The conditions were set to mimic the ionic conditions as well as the proteins presented in cell culture medium or physiological milieu. **Figure 45A** and **Figure 45B** present the cumulative dose release of curcumin and cumulative percentage release of curcumin over 7 days, respectively. The burst release in the first 24 h before gradual release can be noticed for all samples. Approximately 20-35% of entrapped curcumin was released from the hydrogels within 7 days. Comparing within the liposome-SF hydrogels, the cumulative dose was in an order of D1>C1>B1>A1, which was in a similar trend of %EE. The release of curcumin from Curcumin-SF hydrogels was comparable to those of D1-SF hydrogels. The slow release of curcumin from directly entrapped curcumin in the SF scaffolds was reported as a result of the binding between lipophilic curcumin and the hydrophobic regions of the SF chains [187]. Furthermore, the precipitation of curcumin within the Curcumin-SF hydrogels (**Figure 43**) could act as a reservoir for the slow release of curcumin from the hydrogels.

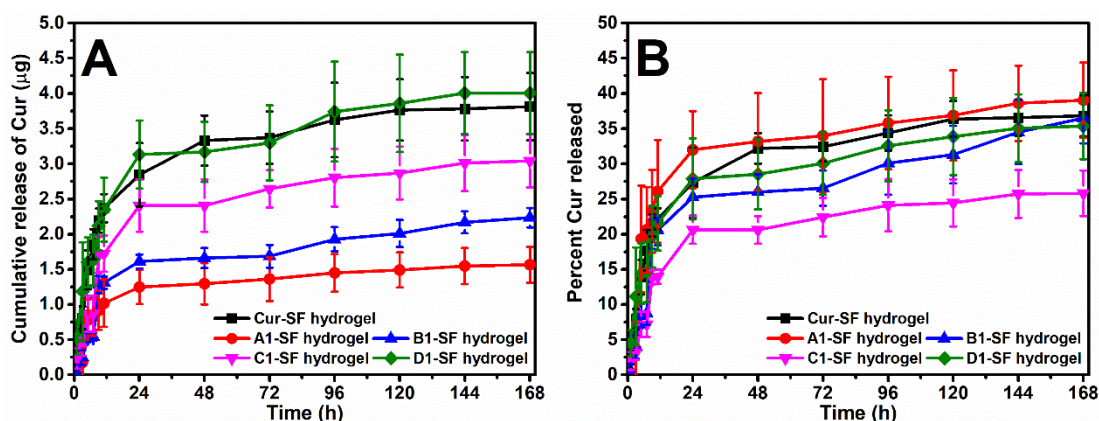


Figure 45 Release of curcumin from sonicated Curcumin-SF hydrogels and liposome-induced SF hydrogels presented as (A) cumulative release amount of curcumin and (B) cumulative percentage release of cur

2.3.3. Compressive mechanical properties of liposome-SF hydrogels

The mechanical properties of the hydrogels were assessed using the unconfined compression test in the fully hydrate state. The stress-strain curves of the tested samples were presented in **Figure 46**. The SF hydrogels induced by the liposomes with high DMPG content, namely A1-SF and B1-SF, showed the characteristic of brittleness. While other hydrogels possessed the ductile properties. According to the analysis of elastic modulus, yield stress and strain (**Figure 47**), the elastic modulus of all samples were almost comparable, while the yield stress and strain of A1-SF and B1-SF were distinct. The obviously higher stress and strain at the yield point of the test materials were noticed. Presumably, the higher DMPG ratio related to a higher amount of SF chains inserting to the lipid bilayers. The higher interactions between SF and phospholipids could result in the distinct mechanical properties.

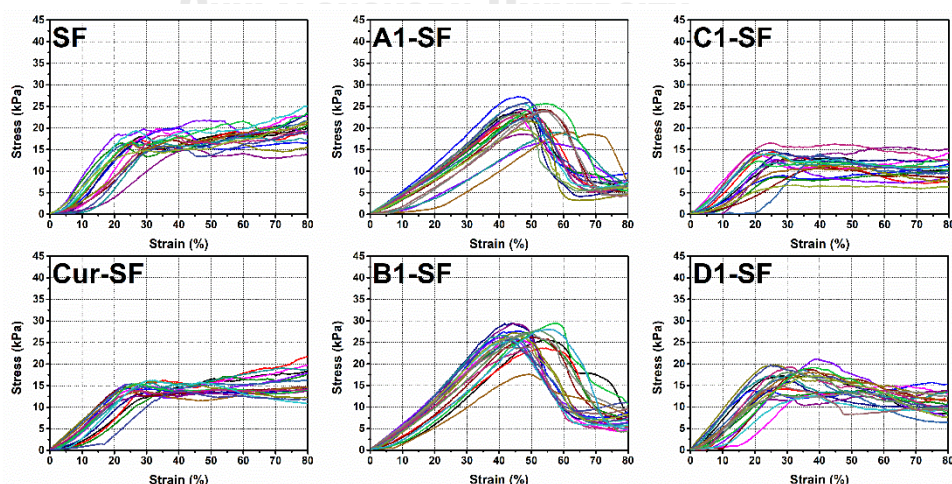


Figure 46 Stress-strain plots of the sonicated 3% SF and cur-3% SF hydrogels, and liposome-3% SF hydrogels. The hydrated samples were tested by the unconfined compression at room temperature.

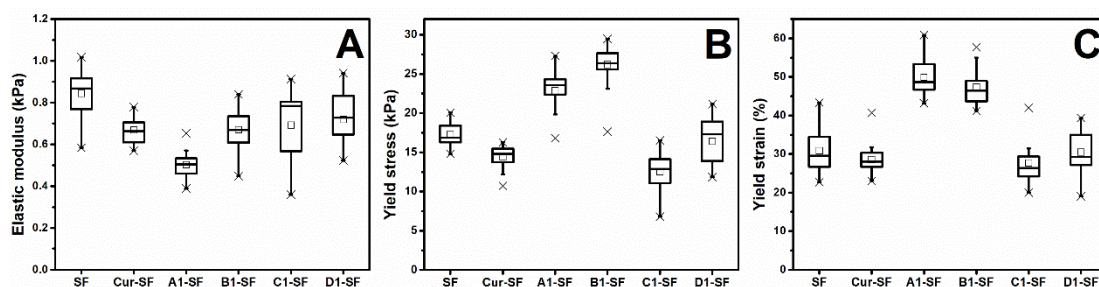


Figure 47 Compressive mechanical properties of the sonicated SF and Curcumin-SF hydrogels, and liposome-SF hydrogels; (A) elastic modulus, (B) yield stress and (C) yield strain

2.4. Biological properties of curcumin-loaded liposome-SF hydrogels

2.4.1. Viability and proliferation of L929 and MDA-MB-231

The indirect contact experiment was set up to assess the responses of L929 and MDA-MB-231 after exposed to curcumin released from the hydrogels. The metabolic activities of both cells are demonstrated in **Figure 48**. For L929, the metabolic activities of cells at day 7 was comparable in all groups. However, the significantly low cell metabolism was noticed at day 3 in the cur-entrapped hydrogels, including Curcumin-SF and liposome-SF hydrogels. On the contrary, the metabolic activities of MDA-MB-231 were significantly low in the cur-loaded SF hydrogel groups, comparing to blank (TCP) and negative control (SF hydrogels). However, the metabolism of MDA-MB-231 after exposed to the A1-SF and B1-SF hydrogels for 7 days were not significantly different from the SF hydrogels. The order of the viability of cancer cells was in the same trend as the curcumin content analysis shown in **Table 10**.

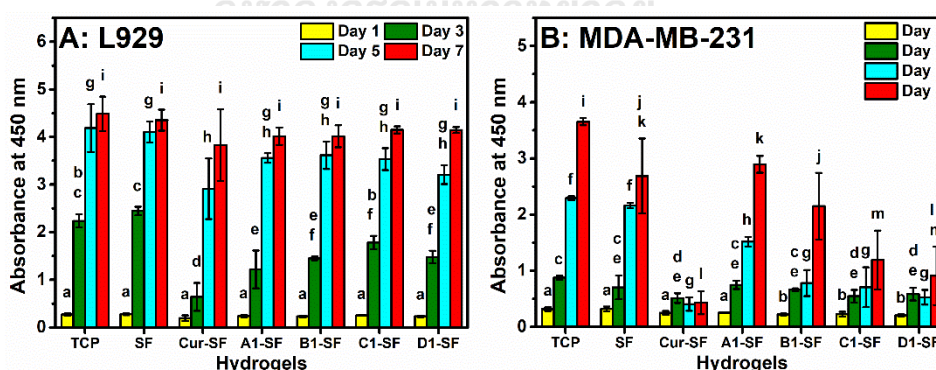


Figure 48 The metabolic activity of (A) L929 and (B) MDA-MB-231 assessed by WST-1 assay in the indirect contact experiment. Cells were plated on the TCP and exposed to the release curcumin from the hydrogels. The alphabets indicate the statistic difference at p -value ≤ 0.05 comparing within the same time-point.

The viability and proliferation of cells directly cultured on the hydrogels were also evaluated using WST-1 assay (**Figure 49A&B**) and DNA

quantification (Figure 49C&D). The significant low cell metabolism and the number of cells were noticed in all cur-loaded samples, comparing to blank and negative control. Interestingly, the cells cultured on the SF hydrogel showed low metabolic activity as well as the low cell number. Presumably, a lack of cell adhesion motifs in SF led to a low cell attachment and delayed cell proliferation [68, 69], but the cells were able to proliferate. Furthermore, the cells cultured on SF hydrogels showed low metabolic activity per cell especially of MDA-MB-231 (Figure 49F). Antiproliferative properties of the cur-loaded hydrogels were observed not only in MDA-MB-231 but also the L929 cell line. The cytotoxicity of curcumin to L929 was reported in a dose-dependent manner [188], due to a generation of reactive oxygen species and an activation of cellular apoptosis. The low attachment and the low number of cells on the SF hydrogels could synergize with the antiproliferation of cur, leading to the low viable cells.

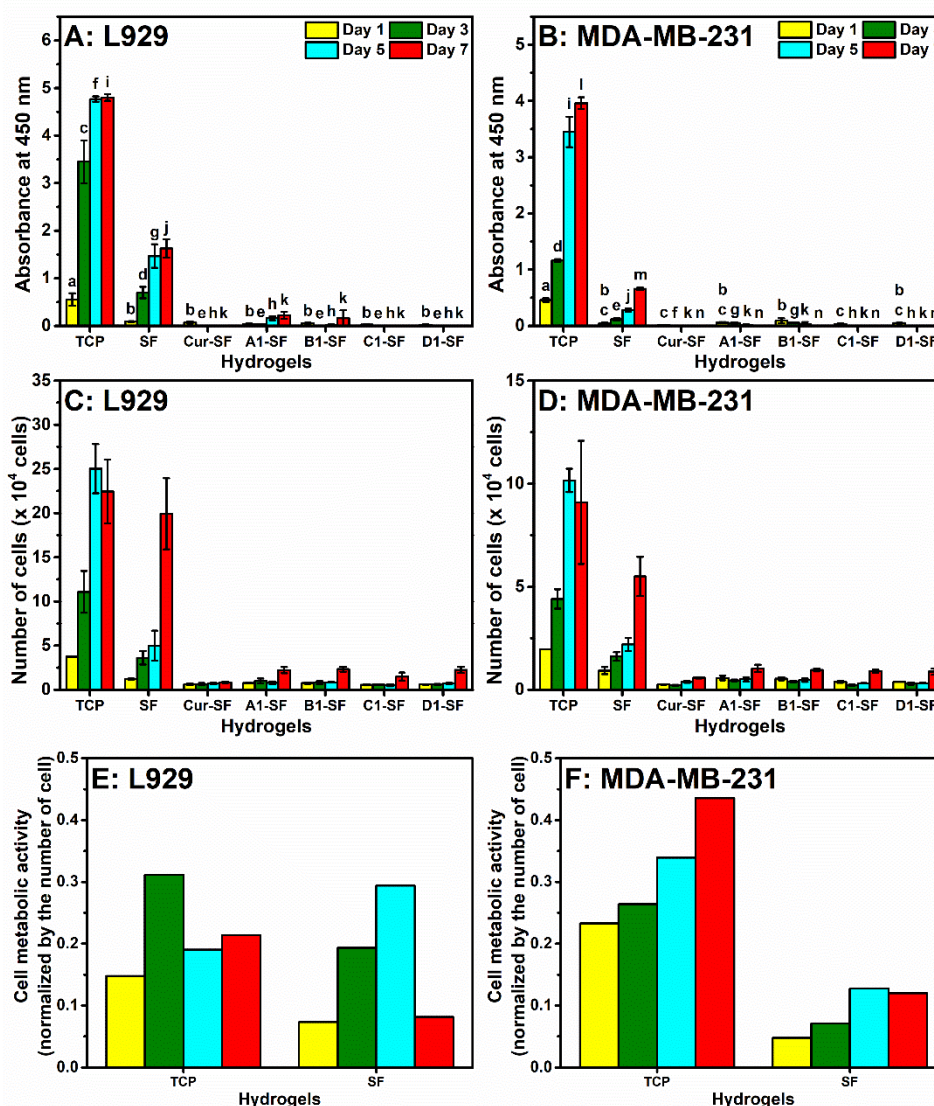


Figure 49 Cell metabolic activity of (A) L929 and (B) MDA-MB-231 cultured on the hydrogels assessed by WST-1 assay. The number of cells evaluated by DNA

quantification of (C) L929 and (D) MDA-MB-231, and (E&F) the metabolic activity normalized by the number of cells, reported only the results of cells cultured on TCP and SF hydrogels.

2.4.2. Cell apoptosis staining and cell imaging

Due to the autofluorescence of cur, the cells cultured on the cur-loaded hydrogels cannot be visualized by the fluorescence imaging. However, the cells on the SF hydrogels were stained by annexin V and 7-AAD, and no staining was observed for both cells cultured for 1 and 3 days (**Figure 50**). The cells can survive and proliferate, as noticed from **Figure 49**, confirming the cytocompatibility of SF.

From the indirect contact assessment, the stained L929 showed no green and red fluorescence in both TCP and SF hydrogel groups, while the dual staining was noticed in some cells in the cur-loaded hydrogel groups, indicating cell death or cells populated in the late apoptosis (**Figure 51A**). Similarly, no stained MDA-MB-231 was observed in the TCP and SF hydrogel groups (**Figure 51B**). Cells exposed to curcumin released from A1-SF, B1-SF and C1-SF hydrogels were stained by both dyes. Interestingly, many cells in Curcumin-SF and D1-SF hydrogel groups were stained only by annexin V, indicating the early apoptosis. Curcumin has been known for its anti-cancer properties by inhibition of cell overgrowth and initiation of cellular apoptosis through a suppression of NF- κ B and tumor necrosis factors, a down-regulation of cyclin D, and an activation of caspase families [154, 189]. The results confirmed the bioactivities of entrapped curcumin in the hydrogels for its anti-proliferation of cancer cells.

Figure 52 and **Figure 53** show the morphology of cells cultured on TCP and the hydrogels. The amount of visible cells was related to the results assessed by the cell metabolic activity assay and DNA quantification (**Figure 49**). Generally, the cells plated on the cell-supporting surfaces, such as TCP, were spread and conquered the culture area within 1 day, but the cells on SF hydrogels presented the rounded morphology. These phenomena could be interpreted that the SF was not favorable for cell attachment. However, L929 and MDA-MB-231 were spread after cultured for 5 and 7 days, respectively, which might result from the matrix remodeling or the deposition of cell adhesive proteins on the SF surfaces.

Taken together, the low attachment of the cells on the SF hydrogels as well as the cytotoxicity of curcumin resulted in a very low number of cells survived on the cur-loaded hydrogel samples. This could lead to an application of the developed hydrogels which required a filler property of the hydrogel together with the cell cytotoxicity of cur, such as a sealant used after tumor resection. The liposome-loaded SF hydrogels might be used as an injectable hydrogel to fill the space after an operation and the entrapped curcumin was used to eradicate the residual tumor cells.

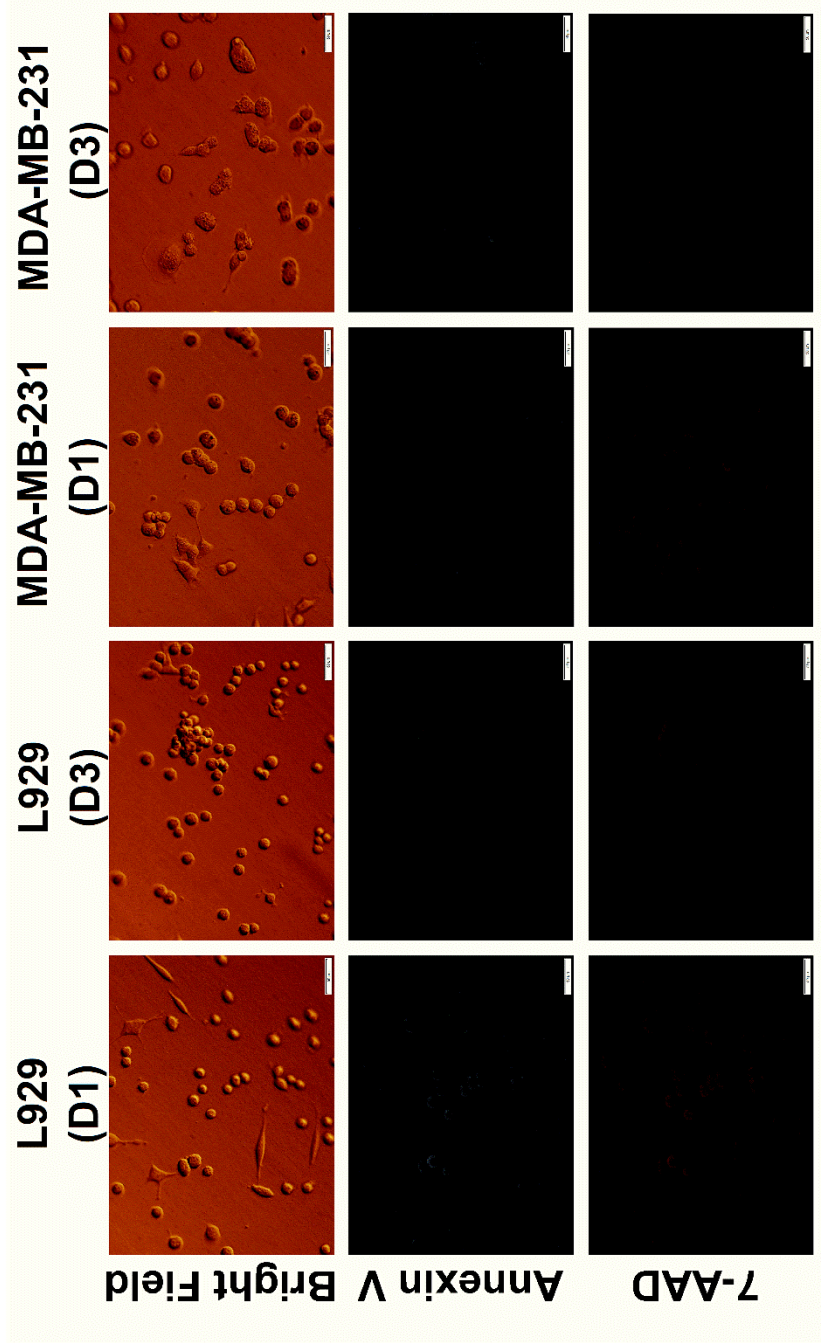


Figure 50 Bright field and fluorescence images of stained L929 and MDA-MB-231 cultured on SF hydrogel for 1 and 3 days. Annexin V and 7-AAD staining is presented by green and red fluorescence, respectively. Scale bar = 50 μ m

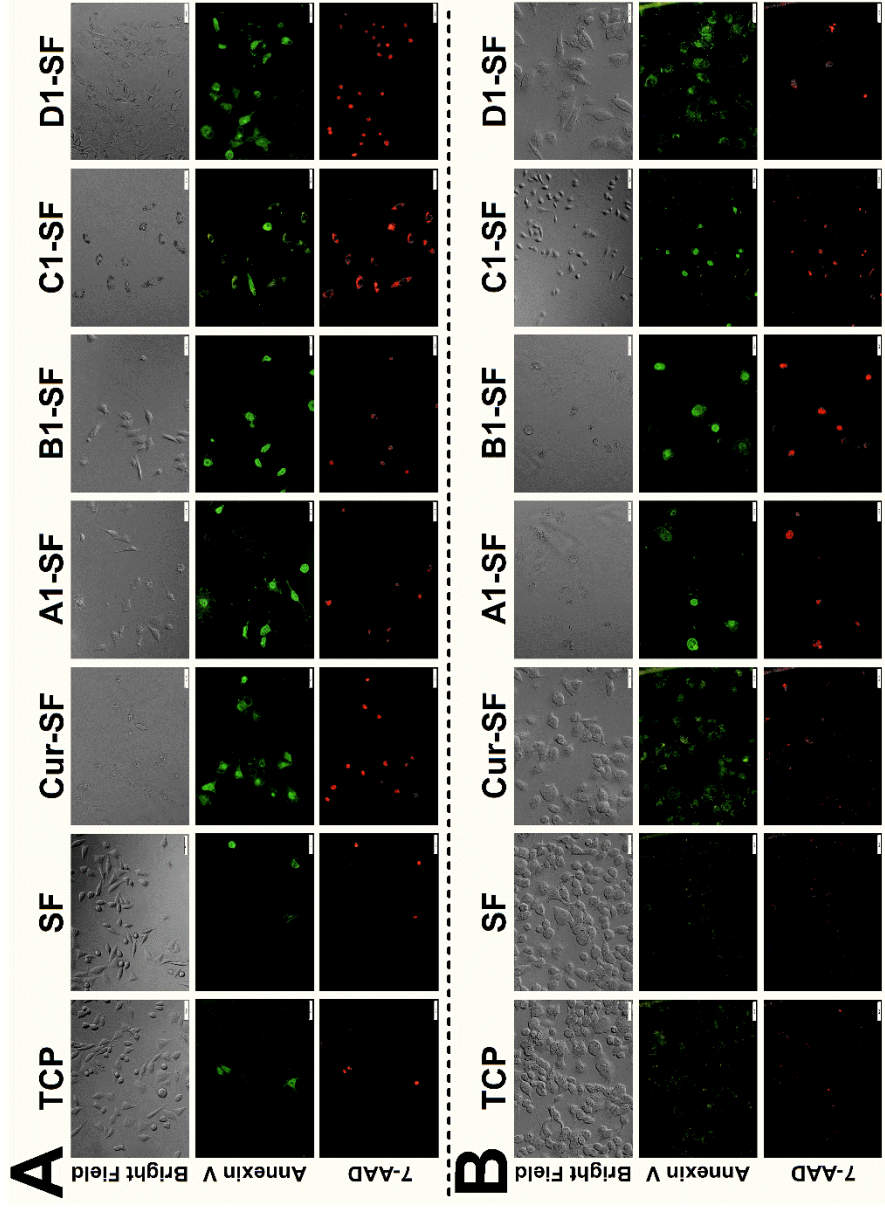


Figure 5I Bright field and fluorescence images of (A) L929 and (B) MDA-MB-231 of the indirect contact experiment after exposing for 1 day. The staining by annexin V (green) and 7-AAD (red) was performed (scale bar = 50 μ m). Single staining by annexin V indicates the early apoptosis, while dual staining indicates the late apoptosis or cell necrosis.

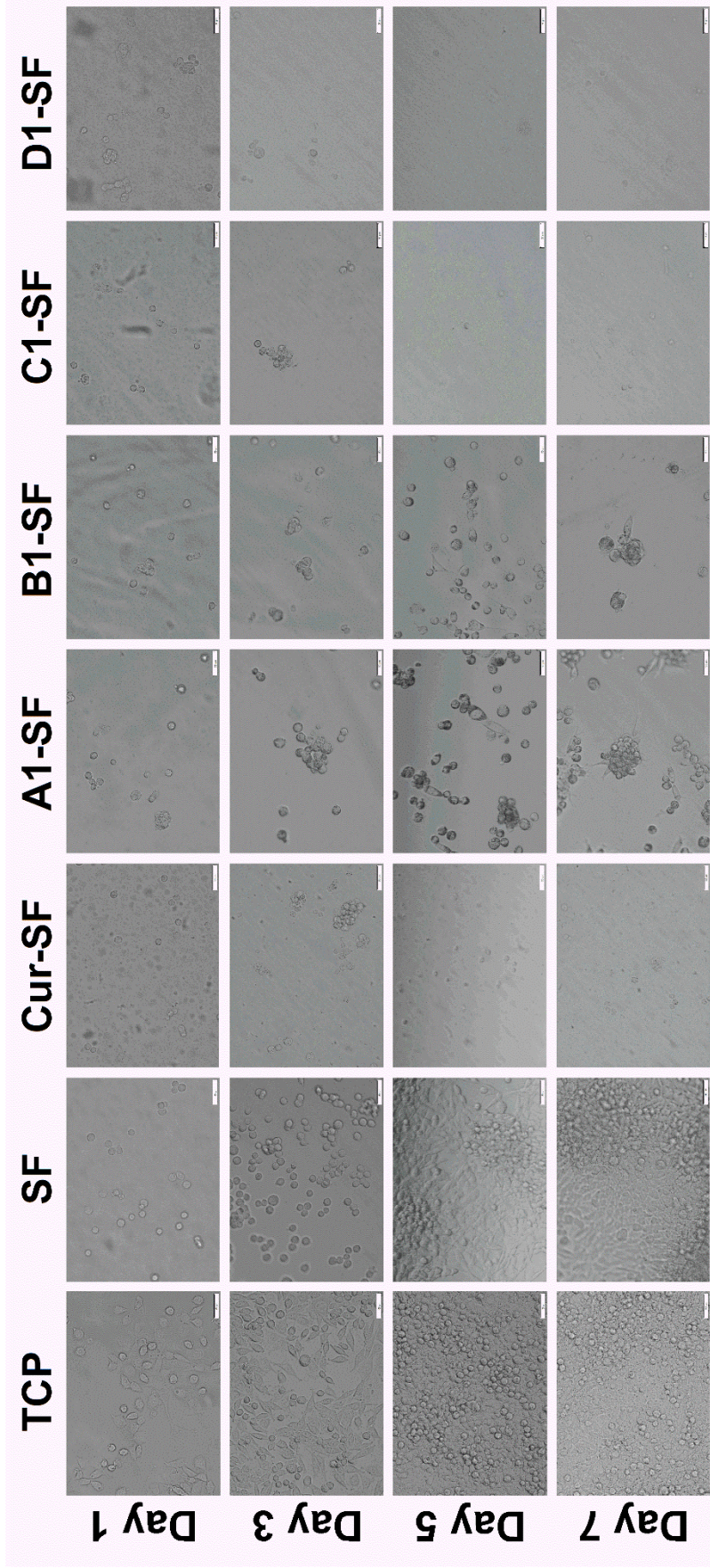


Figure 52 Morphology of L929 cultured on tissue culture plate (TCP) and the hydrogels for 1, 3, 5 and 7 days (scale bar = 50 μm)

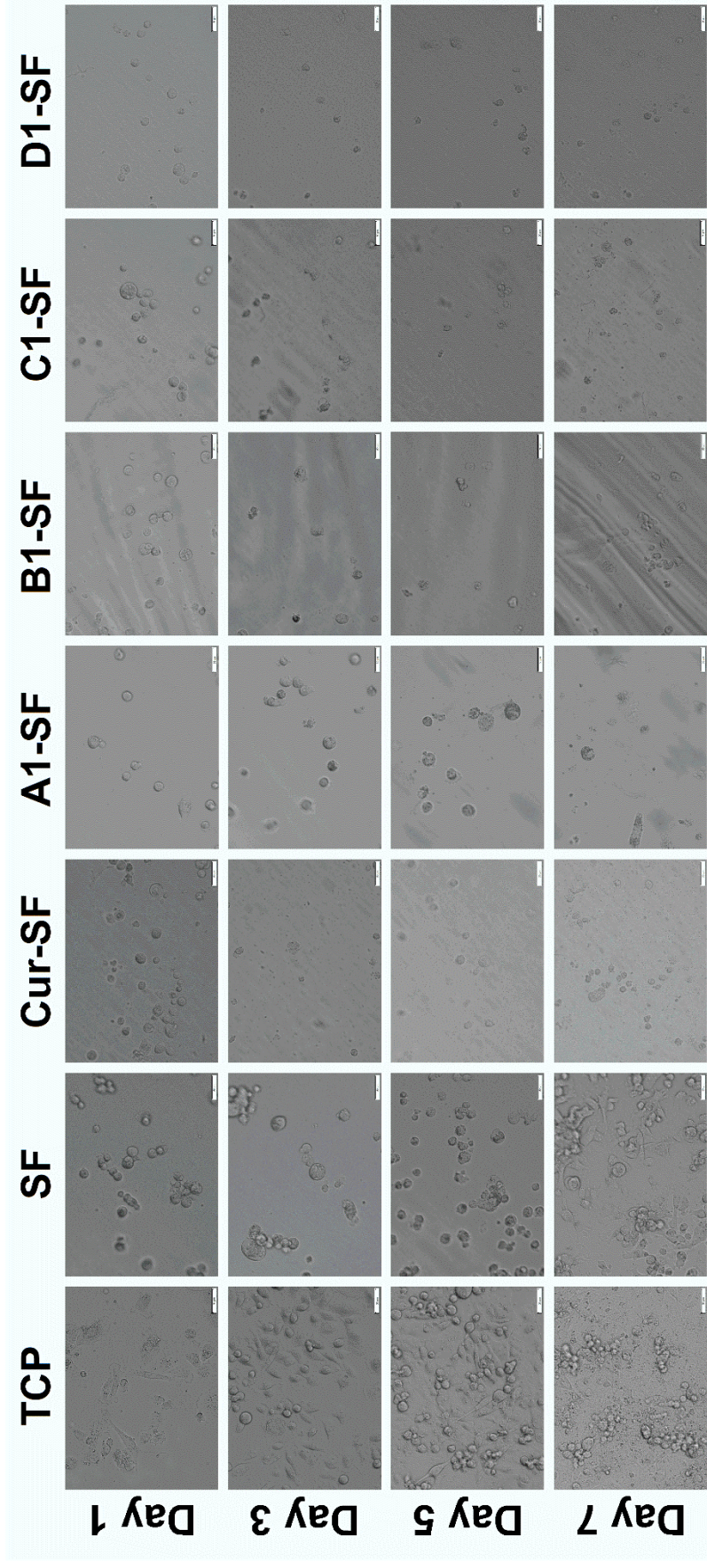


Figure 53 Morphology of MDA-MB-231 cultured on TCP and the hydrogels for 1, 3, 5 and 7 days (scale bar = 50 μ m)

3. Gold-induced silk fibroin hydrogels and the cytocompatibility of hydrogels

The roles of Au^{3+} salt in the acceleration of SF gelation were investigated, comparing to the thiol functionalized SF. The mechanisms of the SF and tSF gelation mediated by Au^{3+} were profoundly evaluated. Finally, the cytocompatibility of the hydrogels was determined using the fibroblast and the cancer cell line, to assess the potential of the hydrogels as the biomaterials as well as other biological activities, such as anti-proliferation of cancer cells.

3.1. Amount of sulfhydryl group of thiolated SF

The mechanisms of thiol functionalization of proteins, such as SF, using 2-IT were that the electrophilic 2-IT rings were attacked by the nucleophilic primary amines presented in the proteins. Then, the 2-IT rings were opened and the thioamidine groups were attached to the amine. This thiolation can be processed as the one-pot reaction in mild conditions and without using organic solvents. Hence, thiolation using 2-IT has been an approach for various amine-containing macromolecules served as biomaterials [190].

There is a very low amount of sulfur-containing amino acid residues, such as cysteine, presented in the SF molecules [52, 58]. Three cysteines were presented at the C-terminal and linked with the light chain by a disulfide bond. Therefore, thiol-functionalization of SF was conducted to increase the amount of sulfhydryl groups, which are highly reactive groups and able to undergo click chemistry or Michael addition reaction [190]. From **Figure 54**, it was noticed an increment of available sulfhydryl groups relating to an increase of the concentration of the 2-IT reactant. The tSF solution prepared by using 50 mM 2-IT was used in further experiments. The higher 2-IT concentration than 50 mM cannot be conducted due to the solubility issue. The precipitates formed immediately after mixing 2-IT and DMAP with SF solution when the concentration of those reactants was higher than 50 mM.

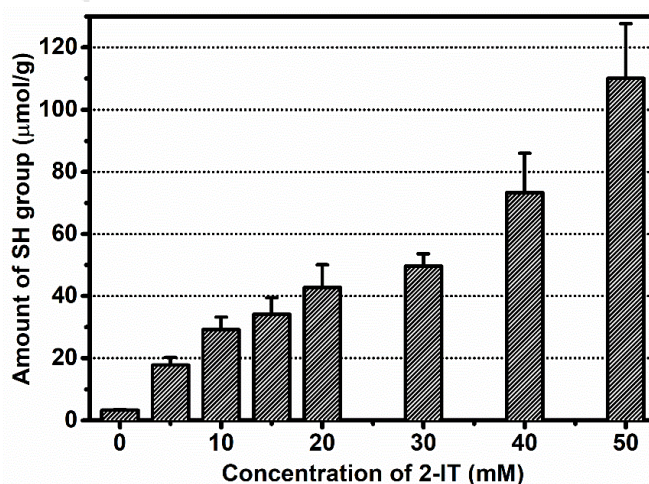


Figure 54 The amount of available sulfhydryl group assessed by Ellman reagent assay of regenerated SF and tSF solution after reacting with different 2-IT concentrations

3.2. Gelation and kinetic structural transition of Au-SF and Au-tSF

3.2.1. Gelation of Au-SF and Au-tSF

Regenerated SF and tSF solutions with and without a presence of Au^{3+} were incubated at 37°C for 14 days and the changes were periodically observed (**Figure 55**). Both 3% SF and tSF solutions without Au^{3+} turned gels after 3 days. The gelation of SF and tSF solution was accelerated by an addition of Au^{3+} in a dose-dependent manner. The SF and tSF solution formed the hydrogels within 3 days and 1 day when 0.5 and 1 mM Au^{3+} was added, respectively. The immediate gelation occurred in the 5 mM Au-SF and Au-tSF mixtures. Interestingly, the hydrogels with distinct appearances were noticed, clearly seen from 1 mM Au-SF and Au-tSF hydrogels. The Au-SF gel gradually turned from its initial yellow to a red-to-purple color, while Au-tSF hydrogels maintained the yellow color until the end of the observation. This red-to-purple color could indicate the formation of Au nanoparticles (AuNPs), because of the characteristic optical properties of the AuNPs [191]. The different color can also be observed in the 5 mM Au-SF hydrogel, but a local phase separation occurred due to the rapid hydrogel formation, leading to non-homogeneous mixtures.

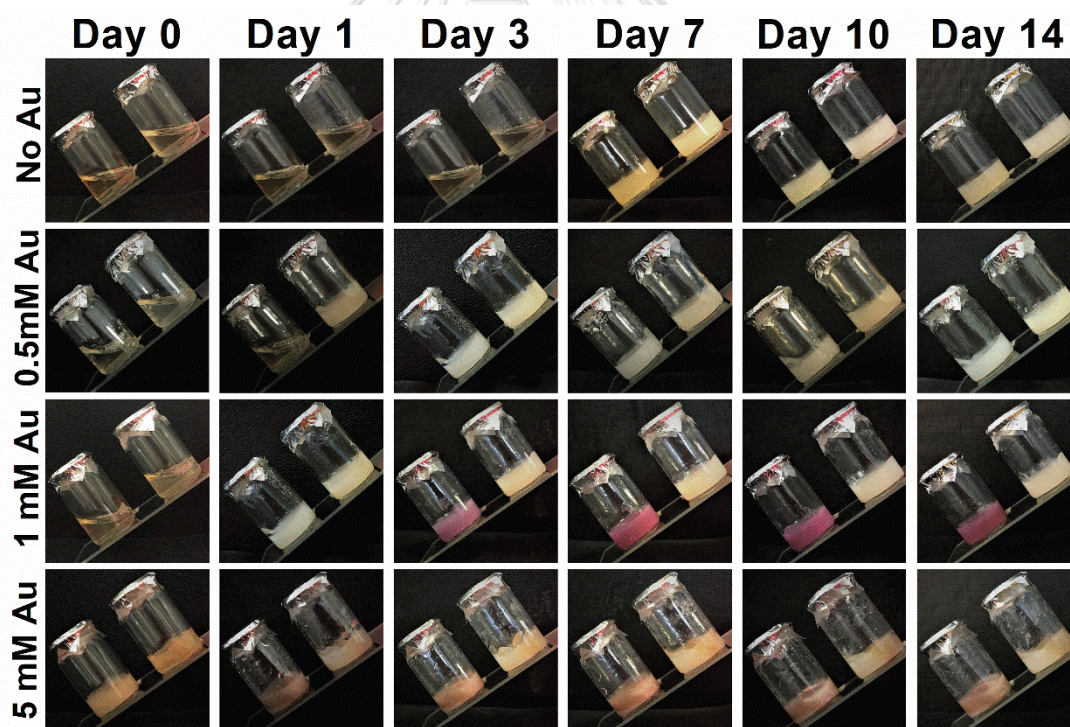


Figure 55 Appearances of regenerated 3% SF (left vial) and 3% tSF (right vial) solution (no Au^{3+}), and Au-SF and Au-tSF mixtures with different Au^{3+} concentrations

3.2.2. Conformational changes of SF and tSF mediated by Au^{3+}

The chemical properties of the freeze-dried hydrogels obtained from the designated time-points were performed using FTIR and the secondary

structures were quantified by FSD and curve-fitting techniques. The beta sheet content was analyzed because this secondary structure related to the self-assembly of SF to form the hydrogels [12]. For regenerated SF and tSF, a gradual increase of beta sheet was noticed in the first 7 days, before reaching the plateau afterwards (**Figure 56**). The beta sheet content was related to the sol-to-gel transition as shown in **Figure 55**. However, the gelation of Au-SF and Au-tSF showed no correlation with the transition of beta sheet. For example, at day 1, the 0.5 mM Au-SF mixture did not turn to gel, while the gelation of 0.5 mM Au-tSF was completed. But their beta sheet content was almost comparable ($28.7 \pm 3.8\%$ vs $30.4 \pm 1.5\%$ for Au-SF and Au-tSF, respectively). Furthermore, 5 mM Au-SF and Au-tSF mixtures formed gels immediately after mixing, but the beta sheet content was not significantly different from those of the regenerated SF and tSF solutions. The results could imply that the structural transition of SF was not the major mechanism of the SF gelation induced by Au^{3+} . However, an increase of beta sheet as well as a decrease of other conformations were faster in all Au^{3+} -mediated SF and tSF solution, comparing to regenerated SF and tSF solutions (**Figure 57**).

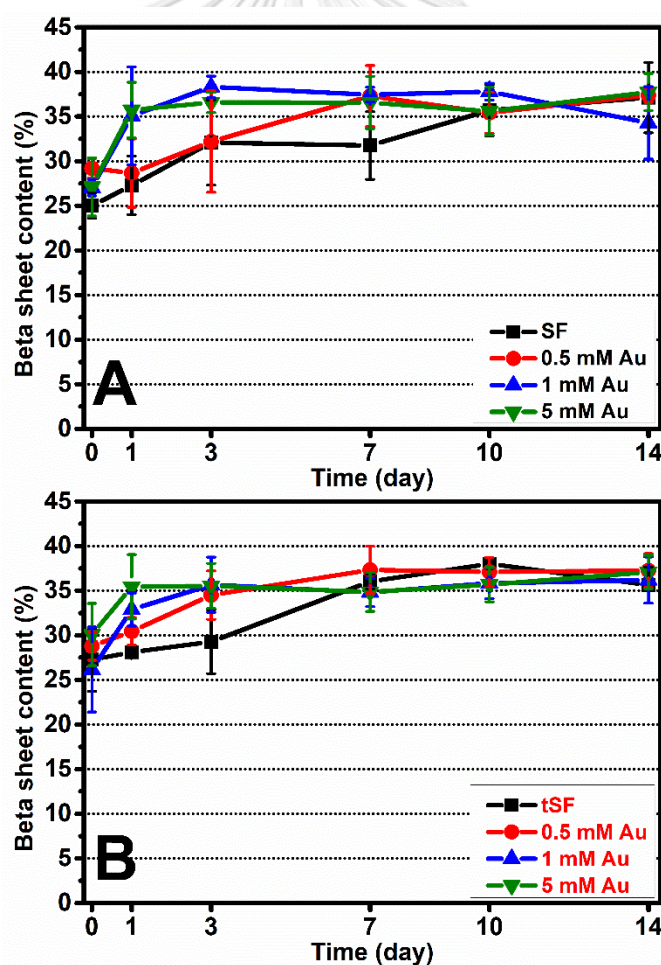


Figure 56 Beta sheet content of freeze-dried (A) SF and (B) tSF hydrogels with different Au^{3+} concentrations determined from FTIR spectra in amide I region using FSD and curve-fitting techniques

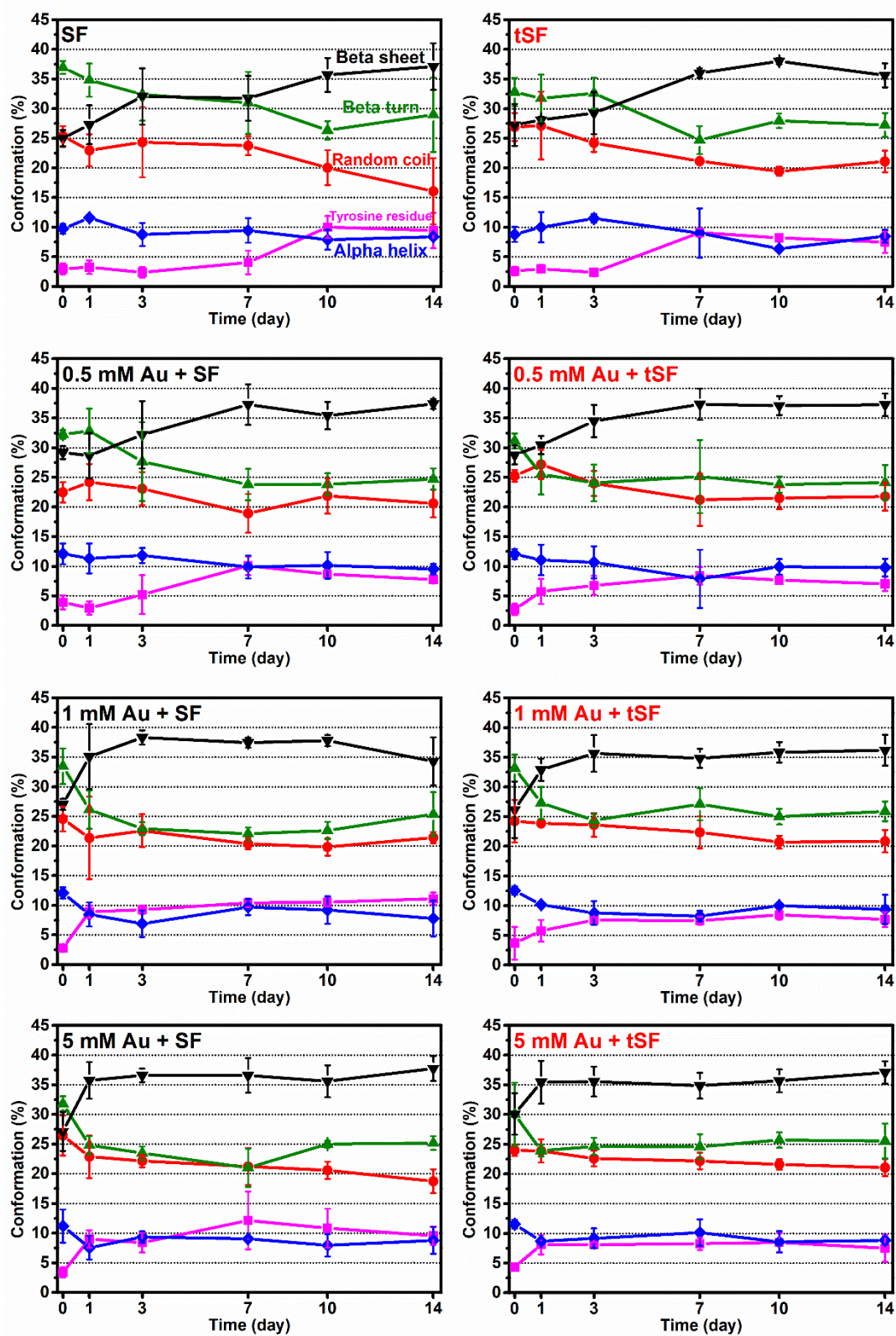


Figure 57 Analysis of secondary structures of the freeze-dried hydrogels, including regenerated 3% SF and tSF hydrogels, and 0.5, 1, and 5 mM Au-SF and Au-tSF hydrogels using FSD and curve-fitting techniques of FTIR spectra in amide I region

3.3. Gelation mechanisms of Au-mediated SF and tSF hydrogels

3.3.1. Dityrosine and Au-S bond formation and a presence of AuNPs

As previously discussed, the FTIR results showed that the acceleration of SF self-assembly through the beta sheet formation could not be a major mechanism of the formation of SF and tSF gels mediated by Au^{3+} . Furthermore, the noticeable color changes of Au-SF mixtures upon the gelation possibly related to the transition of Au chemical state. The reduction of Au salts, which its most stable state is Au^{3+} , to Au^+ by amino ($-\text{NH}_2$) or thiol ($-\text{SH}$) groups presenting in proteins is reported [24]. The Au^+ can then either accept the electron from the cresol part of tyrosine, resulting in the formation of dityrosine and the reduction to Au^0 , or form the strong bond between Au^+ and sulfur [25, 192, 193]. These properties of Au salts are advantageous for the AuNPs preparation using biomolecules from plant extracts or natural proteins [24, 145], or the *in situ* crosslinking of thiolated polymers [25, 26].

The formation of dityrosine was fluorospectroscopically determined and the results were shown in **Figure 58A**. An increase of the fluorescence intensity was related to the amount of added Au^{3+} . A higher fluorescence signals of SF group than those of tSF were obtained at a lower Au^{3+} concentrations.

A free SH group presented in tSF after adding the various amount of Au^{3+} was assessed by the Ellman reagent assay (**Figure 58B**). A decrease of free SH group was noticed with an increase amount of Au^{3+} up to 1 mM. The results could correlate with the formation of dityrosine in tSF because the fluorescence signal steeply rose after the addition of 1 mM Au^{3+} . It could be described that an excess amount of Au^{3+} after being reduced and bound to sulfur was able to accept the electron donation from the tyrosine, resulting in the dityrosine formation.

The formation of AuNPs was determined from the visible light absorbance band locating between 525 and 535 nm, corresponding to the surface plasmon resonance of AuNPs [160]. For SF samples, the band was clearly noticed with an addition of 1 mM Au^{3+} (**Figure 58C**), while the band of tSF samples can be seen at the higher Au^{3+} concentrations (**Figure 58B**). This could confirm the reduction of Au^{3+} to Au^0 , which was able to form AuNPs, by amino group and the tyrosine in the SF. A higher Au^{3+} was needed for tSF since the sulfhydryl groups can prevent the further reduction from Au^+ to Au^0 [25, 193].

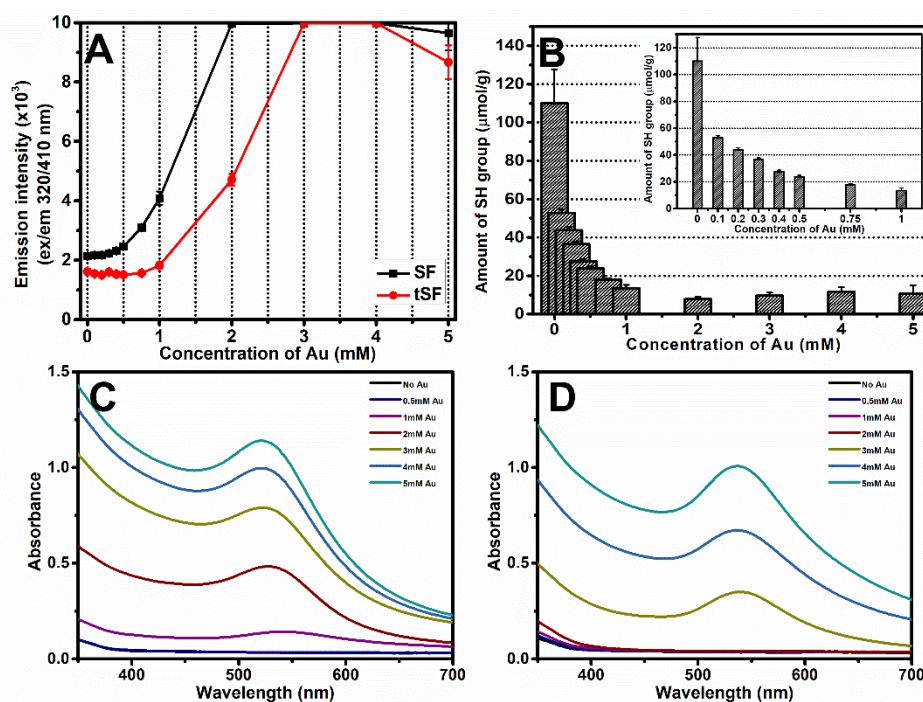


Figure 58 (A) Fluorescence measurement (ex 320 nm/em 410 nm) of SF and tSF with different Au³⁺ concentrations, indicating the formation of dityrosine (B) Amount of the available SH group of tSF mixed with various Au³⁺ concentrations. UV-vis absorbance spectra of (C) Au-SF and (D) Au-tSF mixtures, presenting the surface plasmon resonance band of AuNPs.

3.3.2. XPS analysis for the chemical states of Au and S

XPS analysis was conducted to determine the chemical state of Au and S presenting in the freeze-dried 1 mM Au-3% SF and 1 mM Au-3% tSF hydrogels. The XPS spectra in Au4f region were fitted with three peaks locating between the binding energy (BE) of 83.0-86.5 eV (**Figure 59A&B**). The peaks located near 84.0 and 85.5 eV correspond to the metallic Au⁰ and Au³⁺, respectively. The middle peak, which shifts from the Au⁰ peak around 0.5-0.6 eV, represents the Au⁺ state [161]. For the analysis of the chemical state of S in tSF, the S2p spectrum was analyzed and two components were assigned based on the spin-orbit splitting doublet, including S2p_{3/2} (162.2 and 164.2 eV) and S2p_{1/2} (163.2 and 165.4 eV). The chemical states of S were identified from the S2p_{3/2} region. The first component at 162.2 eV was regarded as bound or chemisorbed sulfur, while the peak at 164.2 eV corresponded to free or physisorbed sulfur [162]. Quantification of the chemical state of Au and S was conducted by the curve-fitting techniques and presented in **Table 12**.

For 1 mM Au-SF hydrogels, the majority state of Au was Au⁰, confirming the reduction of Au salts and the formation of AuNPs. While both Au⁰ and Au⁺ were noticed in the Au-tSF hydrogels. Moreover, the bound S was noticed in the Au-tSF hydrogels which confirmed the formation of the strong bonds, such as Au-S or S-S bonds.

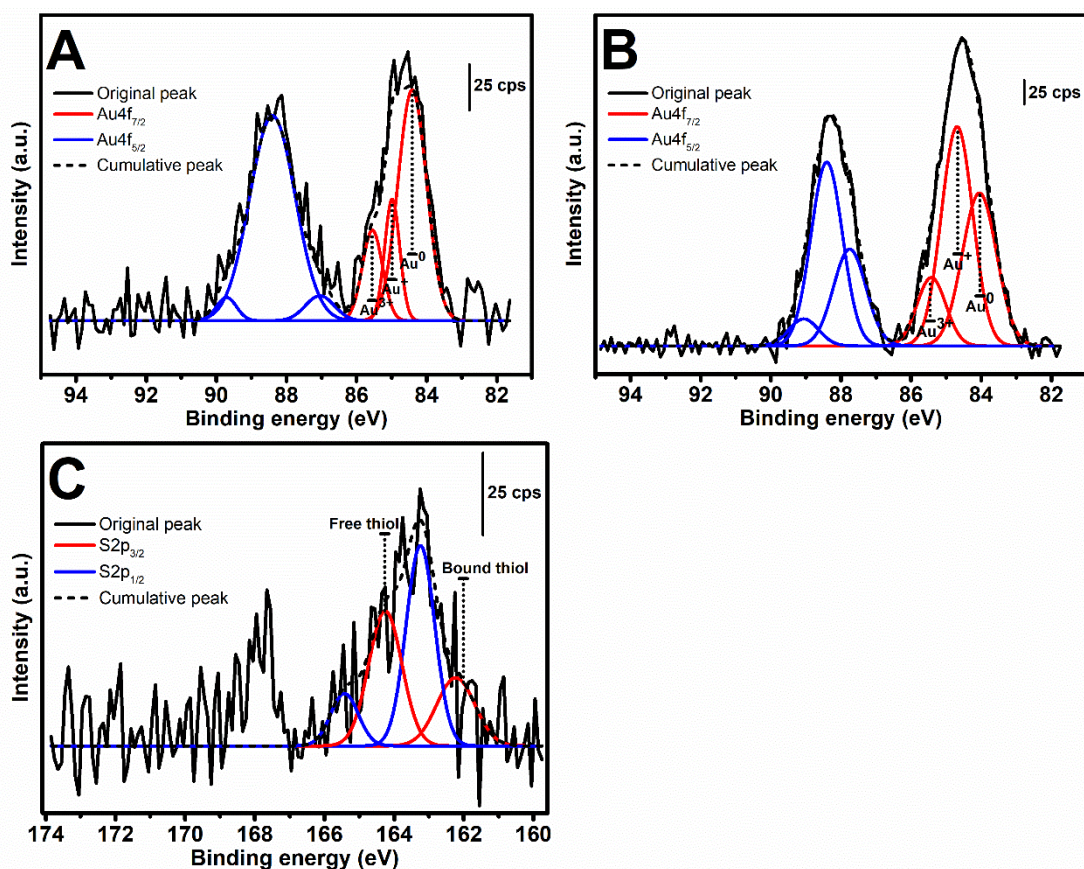


Figure 59 XPS spectra in Au4f region of (A) 1 mM Au-3% SF and (B) 1 mM Au-3% tSF, and (C) in S2p region of Au-tSF

Table 12 The relative amount percentage of different chemical state analyzed from XPS spectra in Au4f_{7/2} and S2p_{3/2} regions of the freeze-fried 1 mM Au-3% SF and 1 mM Au-3% tSF hydrogels

XPS region	Chemical state	1 mM Au-3% SF		1 mM Au-3% tSF	
		BE (eV)	Relative amount (%)	BE (eV)	Relative amount (%)
Au4f _{7/2}	Au ⁰	84.4	31.7	84.0	21.9
	Au ⁺	84.9	8.9	84.6	28.9
	Au ³⁺	85.5	8.8	85.4	8.3
S2p _{3/2}	Bound S	N/A		162.2	18.2
	Free S	N/A		164.2	31.4

The obvious color changes of 1 mM Au-SF mixtures (**Figure 55**) as well as the noticeable surface plasmon resonance band at 525 nm indicated the generation of AuNPs (**Figure 58C**). The XPS results also confirmed the presence of Au⁰ (**Table 12**), which was the chemical state of Au generally

presented in AuNPs. The reduction of Au^{3+} to Au^+ by the amino ($-\text{NH}_2$) groups in SF can be proposed. Subsequently, the cresol part of tyrosine side chains, which possessed the strong electron donation property, transfer an electron to the Au^+ . The Au^+ was then converted to Au^0 and formed the AuNPs, while the two tyrosyl radicals formed a covalent dityrosine [192, 194].

Contrariwise, the Au-tSF hydrogels showed no color changes (**Figure 55**), and the XPS results indicated the high ratio of Au^+ (**Table 12**). An addition of Au^{3+} led to a decrease of available SH group (**Figure 58B**), and the bound S can be noticed from the XPS analysis. It was possible that the Au^{3+} was firstly reduced to Au^+ by the amino ($-\text{NH}_2$) or thiol ($-\text{SH}$) groups in tSF, but the free SH groups prevented the further reduction to Au^0 by forming the Au-S bond [193].

Even the secondary structural transition did not directly relate to the gelation kinetics of Au-SF and Au-tSF, an increase of beta sheet was more rapid with the presence of Au^{3+} . Presumably, the reduction of Au^{3+} and the dityrosine formation in Au-SF as well as the oxidation of the sulfhydryl groups to form S-S or Au-S bonds resulted in the generation of protons. A higher concentration of protons, therefore, led to a decrease of local pH. The pH of Au-SF and Au-tSF could shift towards the isoelectric point (pI of SF = 4.59-5.06 [12]), resulting in the chain aggregation and the gel formation as previously reported by Matsumoto *et al* [12]. The proposed mechanisms of Au^{3+} -mediated SF and tSF gelation were illustrated in **Figure 60**.

At 5 mM Au^{3+} , an immediate gelation of SF occurred, resulting in a non-homogeneous and partial gel formation. Noticeably, the color change to the red-to-purple hydrogel cannot be clearly visualized, possibly relating to a low or incomplete generation of AuNPs. It can be proposed that the high concentration protons from HAuCl_4 decreased the pH of the mixtures. The reported pKa of tyrosine is about 10. The proton-coupled electron transfer reaction could occur with the more difficulty when the phenolic group of tyrosine was protonated [192].

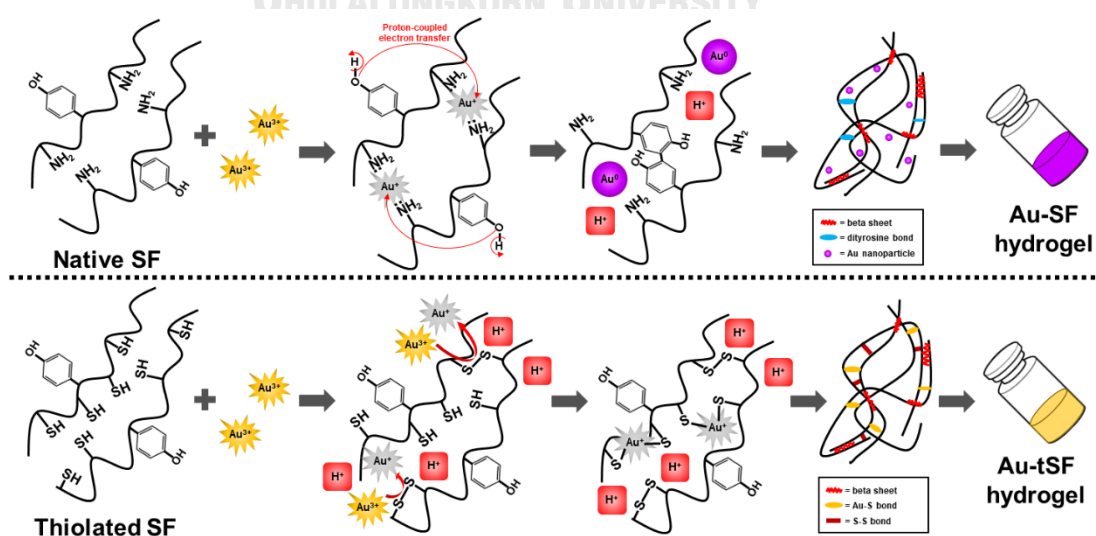


Figure 60 The proposed mechanisms of Au^{3+} -mediated SF and tSF hydrogels. For Au-SF (upper), Au^{3+} was reduced to Au^+ by the amine groups. The proton-coupled transfer reaction was then occurred by an electron donation of tyrosine residues, resulting in a generation of protons and the formation of dityrosine. Au^+ was reduced to Au^0 and formed the AuNPs. An increase of protons led to a lower local pH, enhancing the SF chain aggregation and hydrogel formation. For tSF (lower), the reduction of Au^{3+} to Au^+ occurred. The Au^+ formed Au-S bonds without further reduction. The generation of protons from S-S and Au-S bond formation resulted in a beta sheet formation of tSF.

3.4. Physical properties of Au-SF and Au-tSF hydrogels

3.4.1. Microstructural features of freeze-dried Au-SF and Au-tSF hydrogels

The microstructures of the freeze-dried 1 mM Au-3% SF and 1 mM Au-3% tSF were examined by SEM (**Figure 61**). The leaf-like structures and interconnected pores with the size larger than $50\ \mu\text{m}$ were noticed in the Au-SF hydrogels (**Figure 61A**), while the Au-tSF hydrogels showed a micro- or nano-fibrous structures (**Figure 61C**). At a high magnification, distributed particulate structures with the diameter of about 20 nm can be visualized in the Au-SF gel matrices (**Figure 61B**), while these features cannot be seen in the Au-tSF samples (**Figure 61D**). The presence of the particles in Au-SF hydrogels could confirm the generation of AuNPs as discussed previously.

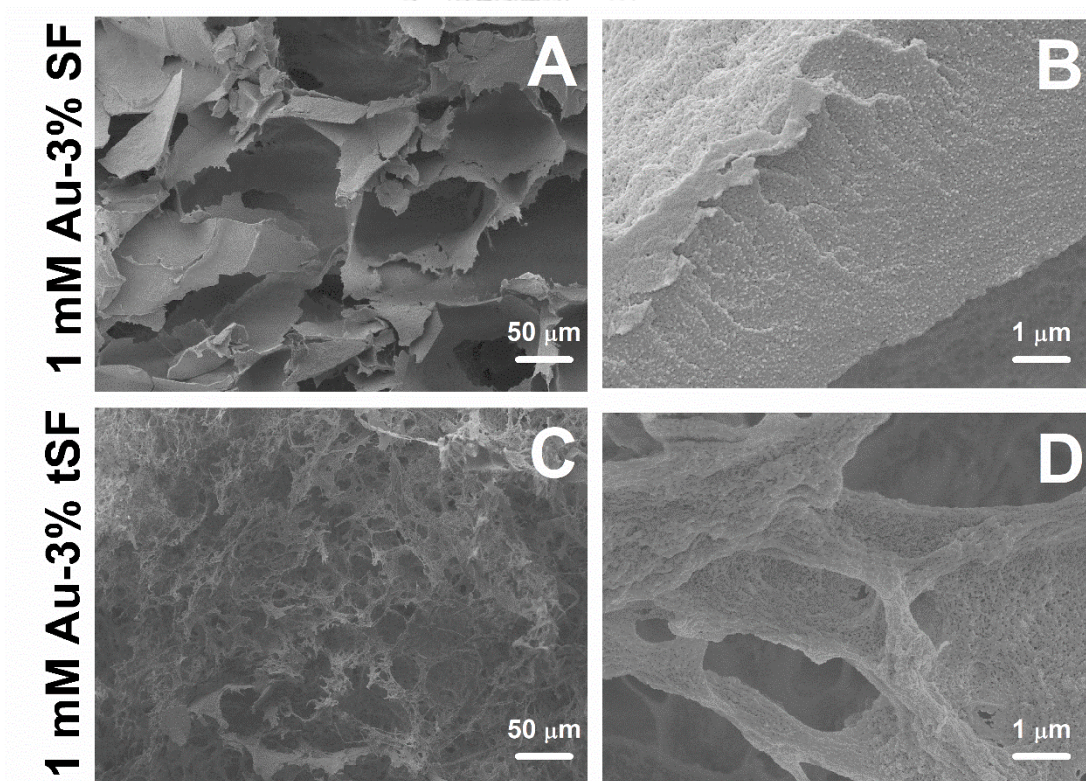


Figure 61 SEM images of the freeze-dried (A&B) 1 mM Au-3% SF and (C&D) 1 mM Au-3% tSF hydrogels

3.4.2. Viscoelastic properties of Au-SF and Au-tSF

The complex modulus (G^*), G' and G'' of the regenerated SF and tSF and their mixtures with different Au^{3+} concentrations were collected and presented in **Figure 62**. In all samples, the constant moduli were noticed within 0.01-10 Hz before steep increase afterwards. The regenerated solutions showed the low G^* as well as the almost equal G' and G'' , corresponding to the solution state. The addition of 0.5 mM Au^{3+} led to slightly increase of the moduli in the range of 1-20 Pa for Au-SF, but the higher moduli, approximately 15-50 Pa, were obtained in Au-tSF samples. This could indicate the rapid formation of Au-S or S-S bonds in the Au-tSF due to the click chemistry [25], while the dityrosine bonding in Au-SF required a longer formation time. Moreover, an increasing of Au^{3+} concentrations resulted in the higher moduli with the maximum G^* or G' of approximately 50 Pa.

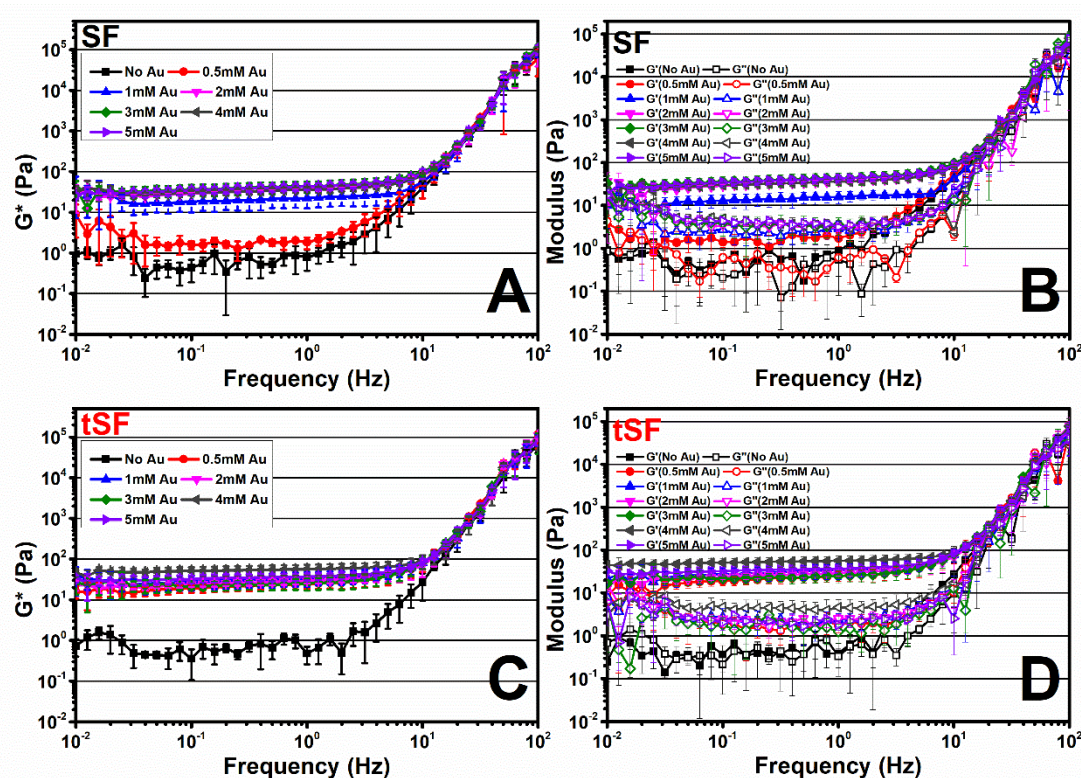


Figure 62 The complex (G^*), elastic (G') and viscous (G'') moduli of the regenerated and the mixtures with different concentrations of Au^{3+} , (A&B) SF and (C&D) tSF, collected over a range of frequency between 0.01-100 Hz with a fixed 0.1% strain

3.5. Cytocompatibility and bioactivities of Au-SF and Au-tSF hydrogels

3.5.1. Viability and proliferation of L929 and MCF-7 cultured on Au-SF and Au-tSF hydrogels

The viability and proliferation of L929 and MCF-7 cultured on regenerated SF and tSF hydrogels as well as Au-SF and Au-tSF hydrogels were evaluated at different time-point using the cell metabolic activity MTS assay (**Figure 63**). Cells cultured on TCP were regarded as controls. The lower metabolic activity comparing to those of TCP can be noticed in all groups. Comparing between the cells on regenerated SF and tSF hydrogels, the SF groups showed lower cell metabolic activity than the tSF samples. As previously discussed, SF was lack of the cell adhesion motifs, resulting in the low cell attachment and proliferation [68, 69]. The thiolation of SF might increase the cell affinity to the materials. As the biocompatibility of SF was well reported [6], the results also confirmed the cytocompatibility of tSF, indicating its potential as a biomaterial.

The presence of Au^{3+} increased the metabolism of both cells on SF hydrogels, which can be noticed from the cell metabolic activity on day 7. However, this phenomenon was not shown in the tSF groups. Furthermore, the lower cell metabolism upon an increase of Au^{3+} was presented in the MCF-7. Even the cytotoxicity of HAuCl_4 was reported as low as 0.077 mM [195], the developed hydrogels containing the higher Au^{3+} concentrations did not show the toxicity to the cultured cells. Possibly, the reduction and stabilization of Au^{3+} by the functional groups presenting in SF and tSF might possess a preventive effect against the cytotoxicity of Au salts.

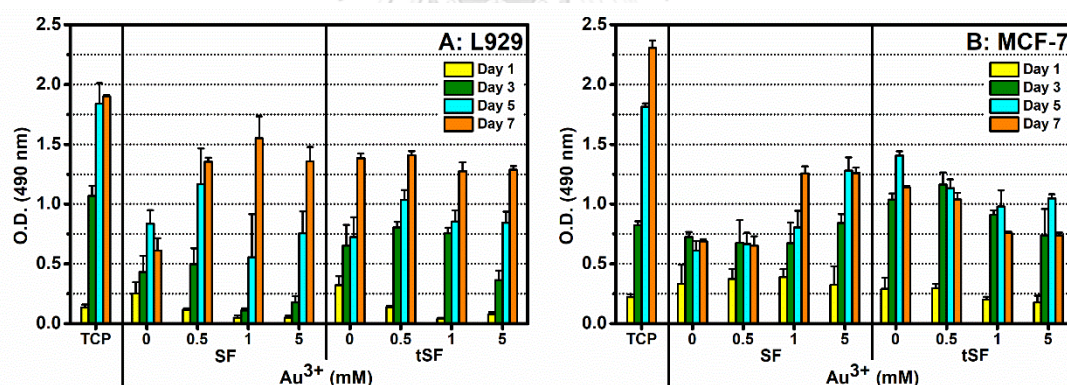


Figure 63 Metabolic activities of (A) L929 and (B) MCF-7 cultured on SF and tSF hydrogels with different Au^{3+} concentration. The cells cultured on TCP were regarded as controls.

3.5.2. Cellular apoptosis by an activation of caspase-3

The apoptotic event of MCF-7 was determined from the activation of caspase-3, a cell apoptosis marker (**Figure 64**). The enzyme activation can be noticed from the cells cultured on 1 mM Au-3% SF hydrogels. However, the normal cell growth was noticed, indicating the ineffectiveness against the cancer cell overgrowth. Presumably, the concentration of AuNPs presenting in the Au-SF hydrogels was less than the effective dose against the growth of cancer cells. Also, the slow degradation of SF hydrogels can be proposed, resulting in a low release of AuNPs to the milieu.

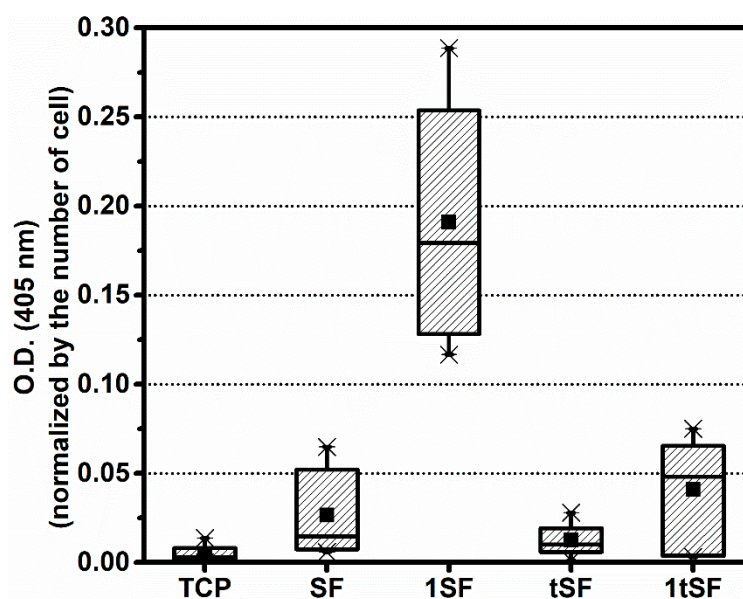


Figure 64 The activation of caspase-3, a cell apoptosis marker, of MCF-7 cultured for 72 h on the samples (TCP, regenerated SF and tSF hydrogels, and 1 mM Au-3% SF (1SF) and 1 mM Au-3% tSF (1tSF))

In conclusion, Au^{3+} can crosslink the regenerated SF and tSF solution, leading to a rapid gelation. Different appearances of Au-SF and Au-tSF were noticed, indicating the different gelation mechanisms. The formation of dityrosine as well as the generation of AuNPs, relating to the reduction of Au^{3+} to Au^0 , were evidenced for the Au-SF hydrogel. While the thiol groups presenting in the tSF transferred electron to Au^+ , resulting in the formation of Au-S bonds and the prevention of the further reduction to Au^0 . The cytocompatibility of the developed hydrogels was proven by cell culture experiments.

Chapter 5

Conclusion

Hydrogels are one of the biomaterial formats widely used in tissue engineering and drug delivery, due to their high water content as well as the microstructures and the physicochemical properties resembling the extracellular matrix of native tissues. Forming the hydrogels upon usage, so-called *in situ* gelation, allow the broad applications of hydrogels, such as cell carrier or 3D printing. Different biopolymers have been used for the *in situ* hydrogel fabrication. Among those, SF have been chosen as the based biomaterial for the *in situ* gelation, due to its excellent mechanical properties, tunable degradation rate, and biocompatibility.

Commonly, the sol-gel transition of the regenerated SF solution is quite long (~7 days), being impractical for any *in situ* applications. Physical and chemical-induced self-assembly, enzymatic and photo-crosslinking, and the modification of SF structure have been utilized to accelerate the SF gelation. Herein, two chemical additives were introduced, including DMPG phospholipid and Au³⁺ salt. The gelation kinetics and the mechanisms of gelation were investigated, as well as the physical and biological properties of the obtained hydrogels.

An anionic phospholipid, DMPG, can accelerate the gelation of regenerated SF solution. The hydrogels were obtained within 10-40 min depending on the concentration of DMPG. Furthermore, the lipid charge and the presence of cations interfered the gelation kinetics. Noticeably, the structural transition from the predominated random coil in the sol state to the beta sheet in the gel state was noticed. The interactions between SF proteins and lipids were evidenced from the fluorescence quenching, indicating the hydrophobic interaction. The gelation mechanisms were proposed as following. The negative charges of DMPG induced the SF chain extension due to the repulsion force, allowing the hydrophobic interactions between the hydrophobic regions of SF chains or between the alkyl chains of DMPG and SF. The chain association led to the formation of stable beta sheet structures, which linked to the hydrogel network formation.

The DMPG-SF hydrogels were proven non-cytotoxic according to ISO 10993-1. The hydrogels were used to perform 3D cell encapsulation using four cell lines. Viability and proliferation tests of the encapsulated cells showed the different growth behavior depending on the cell types. For example, the fibroblast cells exhibited the normal growth with delayed lag time, while the epithelial-type cells (SaOS-2 and CaSki) showed low proliferation rate while entrapped. However, the overall results confirmed that the DMPG-SF hydrogels were a good candidate as the substrates for 3D cell carrier.

As the DMPG phospholipid can be a component in liposome formulations, the DMPG-based liposomes were prepared to utilize as the drug delivery carrier of curcumin with an ability in inducing the rapid gelation of SF. The

formulations were varied by the ratio between DMPG and DMPC and the amount of added cholesterol. The size of the liposomes was more controllable with a decrease DMPG-to-DMPC ratio and an increase of cholesterol, along with the lower aggregation. Curcumin was entrapped in the liposomes with 50-100% efficiency, which the entrapped amount was lower with the higher cholesterol. Loading curcumin in the liposomes can increase the amount in aqueous medium and prevent the degradation of such bioactive compounds by hydrolysis or photo-lysis. By mixing the developed liposomes with the regenerated SF solution, the rapid gelation occurred, and the gelation time was tunable by the liposome formulations. The release of curcumin from the liposome-SF hydrogel was controlled by the diffusion mechanism.

The activities of curcumin released from the hydrogels were tested against mouse fibroblasts and human cancer cells. The delayed growth of fibroblasts was noticed in the initial period, before returning to normal afterward, while a low cell number was observed for cancer cells. Apoptosis and necrosis cells were observed after exposed to the curcumin. By culturing the cells on the hydrogel surface, both cells exhibited very low viability, which resulted from the low affinity to the SF and the cytotoxicity of curcumin. The developed liposome-SF hydrogels showed a potential to be used as delivery systems administered into a space after surgical resection of solid tumors.

The second system implemented for accelerating the SF gelation is Au^{3+} -mediated gelation. The gelation of regenerated SF with Au^{3+} was compared with the thiol-functionalized SF or tSF. The gelation occurred immediately or within 1 day depending on the added amount of Au^{3+} . The appearances of Au-SF and Au-tSF were different, which the Au-SF gel turned to purple-red color and the Au-tSF hydrogel maintained its initial color. The different gelation mechanisms were proposed. In SF, the amino groups presenting in SF firstly transferred the electron pair to Au^{3+} , yielding Au^+ . Subsequently, the phenol groups of tyrosine residues transfer an electron coupling with a proton to Au^+ and reduced to Au^0 , which further form AuNPs. The tyrosine became reactive, which can readily form a bond with an available tyrosine, leading a dityrosine linkage. While the thiol groups presenting in the tSF prevented the reduction of Au^+ to Au by forming Au-S bonds. The AuNPs in the Au-SF hydrogels possessed characteristic optical properties. Therefore, the appearances of the hydrogels gradually changed due to the surface plasmon absorption of AuNPs.

The obtained Au-SF and Au-tSF hydrogels were tested for their cytocompatibility. The results showed that there was no residual toxic from the thiol functionalization of SF by a chemical reaction. Cultured cells can survive and proliferate on the hydrogels.

In summary, both developed SF hydrogels; the phospholipid-induced and Au^{3+} -mediated hydrogels, showed potential as biomaterials used for biomedical applications, as they exhibited *in vitro* cytocompatibility. The gelation kinetics as well as the gelation mechanisms were evaluated, demonstrating a tunable gelation time based on specific purposes. The mechanical properties and the degradability of the hydrogels can be further evaluated by tuning the concentration of SF to achieve different features. The

developed hydrogel systems can be used for the substrate for the cell culture *in vitro*. Furthermore, *in vivo* experiments can be conducted for further applications in clinical settings.



REFERENCES

1. Langer, R. and J.P. Vacanti, *Tissue engineering*. Science, 1993. **260**(5110): p. 920.
2. Murphy, C.M., et al., *Cell-scaffold interactions in the bone tissue engineering triad*. Eur Cell Mater, 2013. **26**: p. 120-32.
3. Drury, J.L. and D.J. Mooney, *Hydrogels for tissue engineering: scaffold design variables and applications*. Biomaterials, 2003. **24**(24): p. 4337-4351.
4. Peppas, N.A., et al., *Hydrogels in Biology and Medicine: From Molecular Principles to Bionanotechnology*. Advanced Materials, 2006. **18**(11): p. 1345-1360.
5. Nicodemus, G.D. and S.J. Bryant, *Cell encapsulation in biodegradable hydrogels for tissue engineering applications*. Tissue engineering. Part B, Reviews, 2008. **14**(2): p. 149-165.
6. Altman, G.H., et al., *Silk-based biomaterials*. Biomaterials, 2003. **24**(3): p. 401-416.
7. Kundu, B., et al., *Silk fibroin biomaterials for tissue regenerations*. Advanced Drug Delivery Reviews, 2013. **65**(4): p. 457-470.
8. Mano, J.F., et al., *Natural origin biodegradable systems in tissue engineering and regenerative medicine: present status and some moving trends*. Journal of The Royal Society Interface, 2007. **4**(17): p. 999-1030.
9. Gasperini, L., J.F. Mano, and R.L. Reis, *Natural polymers for the microencapsulation of cells*. Journal of The Royal Society, Interface, 2014. **11**(100): p. 20140817-20140817.
10. Naskar, D., et al., *1 - Introduction to silk biomaterials*, in *Silk Biomaterials for Tissue Engineering and Regenerative Medicine*, S.C. Kundu, Editor. 2014, Woodhead Publishing. p. 3-40.
11. Murphy, A.R. and I.S. Romero, *8 - Biochemical and biophysical properties of native Bombyx mori silk for tissue engineering applications*, in *Silk Biomaterials for Tissue Engineering and Regenerative Medicine*, S.C. Kundu, Editor. 2014, Woodhead Publishing. p. 219-238.
12. Matsumoto, A., et al., *Mechanisms of Silk Fibroin Sol–Gel Transitions*. The Journal of Physical Chemistry B, 2006. **110**(43): p. 21630-21638.
13. Kim, U.-J., et al., *Three-dimensional aqueous-derived biomaterial scaffolds from silk fibroin*. Biomaterials, 2005. **26**(15): p. 2775-2785.
14. Ajisawa, A., *Dissolution of silk fibroin with calciumchloride/ethanol aqueous solution*. The Journal of Sericultural Science of Japan, 1998. **67**(2): p. 91-94.
15. Yamada, H., et al., *Preparation of undegraded native molecular fibroin solution from silkworm cocoons*. Materials Science and Engineering: C, 2001. **14**(1): p. 41-46.
16. Kim, U.-J., et al., *Structure and Properties of Silk Hydrogels*. Biomacromolecules, 2004. **5**(3): p. 786-792.
17. Ayub, Z.H., M. Arai, and K. Hirabayashi, *Mechanism of the Gelation of Fibroin Solution*. Bioscience, Biotechnology, and Biochemistry, 1993. **57**(11): p. 1910-1912.
18. Li, J., et al., *A review on phospholipids and their main applications in drug delivery systems*. Asian Journal of Pharmaceutical Sciences, 2015. **10**(2): p. 81-

- 98.
19. Monteiro, N., et al., *Liposomes in tissue engineering and regenerative medicine*. Journal of The Royal Society Interface, 2014. **11**(101): p. 20140459.
 20. Buckland, A.G. and D.C. Wilton, *Anionic phospholipids, interfacial binding and the regulation of cell functions*. Biochimica et Biophysica Acta (BBA) - Molecular and Cell Biology of Lipids, 2000. **1483**(2): p. 199-216.
 21. Zhang, X. and T.A. Keiderling, *Lipid-Induced Conformational Transitions of β -Lactoglobulin*. Biochemistry, 2006. **45**(27): p. 8444-8452.
 22. Bañuelos, S. and A. Muga, *Structural Requirements for the Association of Native and Partially Folded Conformations of α -Lactalbumin with Model Membranes*. Biochemistry, 1996. **35**(13): p. 3892-3898.
 23. Choi, J., et al., *Silk Hydrogels Crosslinked by the Fenton Reaction*. Advanced Healthcare Materials, 2019. **8**(17): p. 1900644.
 24. Elahi, N., M. Kamali, and M.H. Baghersad, *Recent biomedical applications of gold nanoparticles: A review*. Talanta, 2018. **184**: p. 537-556.
 25. Casuso, P., et al., *Injectable and Self-Healing Dynamic Hydrogels Based on Metal(I)-Thiolate/Disulfide Exchange as Biomaterials with Tunable Mechanical Properties*. Biomacromolecules, 2015. **16**(11): p. 3552-3561.
 26. Casuso, P., et al., *Auophilically cross-linked "dynamic" hydrogels mimicking healthy synovial fluid properties*. Chemical Communications, 2014. **50**(96): p. 15199-15201.
 27. Langer, R., *Biomaterials in Drug Delivery and Tissue Engineering: One Laboratory's Experience*. Accounts of Chemical Research, 2000. **33**(2): p. 94-101.
 28. Kowalski, P.S., et al., *Smart Biomaterials: Recent Advances and Future Directions*. ACS Biomaterials Science & Engineering, 2018. **4**(11): p. 3809-3817.
 29. Van Vlierberghe, S., P. Dubruel, and E. Schacht, *Biopolymer-Based Hydrogels As Scaffolds for Tissue Engineering Applications: A Review*. Biomacromolecules, 2011. **12**(5): p. 1387-1408.
 30. Malafaya, P.B., G.A. Silva, and R.L. Reis, *Natural-origin polymers as carriers and scaffolds for biomolecules and cell delivery in tissue engineering applications*. Advanced Drug Delivery Reviews, 2007. **59**(4): p. 207-233.
 31. Hayashi, T., *Biodegradable polymers for biomedical uses*. Progress in Polymer Science, 1994. **19**(4): p. 663-702.
 32. Nair, L.S. and C.T. Laurencin, *Biodegradable polymers as biomaterials*. Progress in Polymer Science, 2007. **32**(8): p. 762-798.
 33. Wang, Y., et al., *Stem cell-based tissue engineering with silk biomaterials*. Biomaterials, 2006. **27**(36): p. 6064-6082.
 34. Hoffman, A.S., *Hydrogels for biomedical applications*. Advanced Drug Delivery Reviews, 2012. **64**: p. 18-23.
 35. Wang, X., et al., *Sonication-induced gelation of silk fibroin for cell encapsulation*. Biomaterials, 2008. **29**(8): p. 1054-1064.
 36. Yucel, T., P. Cebe, and D.L. Kaplan, *Vortex-induced injectable silk fibroin hydrogels*. Biophysical journal, 2009. **97**(7): p. 2044-2050.
 37. Yan, L.-P., et al., *Tumor Growth Suppression Induced by Biomimetic Silk Fibroin Hydrogels*. Scientific Reports, 2016. **6**: p. 31037.

38. Dubey, P., et al., *Sophorolipid assisted tunable and rapid gelation of silk fibroin to form porous biomedical scaffolds*. RSC Advances, 2015. **5**(43): p. 33955-33962.
39. Das, S., et al., *Bioprintable, cell-laden silk fibroin–gelatin hydrogel supporting multilineage differentiation of stem cells for fabrication of three-dimensional tissue constructs*. Acta Biomaterialia, 2015. **11**: p. 233-246.
40. Zhang, Y.S. and A. Khademhosseini, *Advances in engineering hydrogels*. Science, 2017. **356**(6337): p. eaaf3627.
41. Lim, K.S., P. Martens, and L. Poole-Warren, *Biosynthetic Hydrogels for Cell Encapsulation*, in *Functional Hydrogels as Biomaterials*, J. Li, Y. Osada, and J. Cooper-White, Editors. 2018, Springer Berlin Heidelberg: Berlin, Heidelberg. p. 1-29.
42. Kretlow, J.D., L. Klouda, and A.G. Mikos, *Injectable matrices and scaffolds for drug delivery in tissue engineering*. Advanced Drug Delivery Reviews, 2007. **59**(4): p. 263-273.
43. Van Tomme, S.R., G. Storm, and W.E. Hennink, *In situ gelling hydrogels for pharmaceutical and biomedical applications*. International Journal of Pharmaceutics, 2008. **355**(1): p. 1-18.
44. Ko, D.Y., et al., *Recent progress of in situ formed gels for biomedical applications*. Progress in Polymer Science, 2013. **38**(3): p. 672-701.
45. Bae, J.W., et al., *Horseradish peroxidase-catalysed in situ-forming hydrogels for tissue-engineering applications*. Journal of Tissue Engineering and Regenerative Medicine, 2015. **9**(11): p. 1225-1232.
46. Kaplan, D., et al., *Silk: Biology, Structure, Properties, and Genetics*, in *Silk Polymers*. 1993, American Chemical Society. p. 2-16.
47. Ma, M., et al., *Characterization of the pigment in naturally yellow-colored domestic silk*. Dyes and Pigments, 2016. **124**: p. 6-11.
48. Kaplan, D.L., et al., *Silks*, in *Biomaterials: Novel Materials from Biological Sources*, D. Byrom, Editor. 1991, Palgrave Macmillan: UK.
49. Römer, L. and T. Scheibel, *The elaborate structure of spider silk: structure and function of a natural high performance fiber*. Prion, 2008. **2**(4): p. 154-161.
50. Tokareva, O., et al., *Recombinant DNA production of spider silk proteins*. Microbial biotechnology, 2013. **6**(6): p. 651-663.
51. DeFrancesco, L., *Hanging on a thread*. Nature Biotechnology, 2017. **35**(6): p. 496-499.
52. Zhou, C.-Z., et al., *Silk fibroin: Structural implications of a remarkable amino acid sequence*. Proteins: Structure, Function, and Bioinformatics, 2001. **44**(2): p. 119-122.
53. Malay, A.D., et al., *Relationships between physical properties and sequence in silkworm silks*. Scientific Reports, 2016. **6**(1): p. 27573.
54. Silva, S.S., et al., *Chinese Oak Tasar Silkworm Antheraea pernyi Silk Proteins: Current Strategies and Future Perspectives for Biomedical Applications*. Macromolecular Bioscience, 2019. **19**(3): p. 1800252.
55. Lucas, F., J.T.B. Shaw, and S.G. Smith, *Comparative studies of fibroins: I. The amino acid composition of various fibroins and its significance in relation to their crystal structure and taxonomy*. Journal of Molecular Biology, 1960. **2**(6): p. 339-349.

56. Lombardi, S.J. and D.L. Kaplan, *The Amino Acid Composition of Major Ampullate Gland Silk (Dragline) of Nephila Clavipes (Araneae, Tetragnathidae)*. The Journal of Arachnology, 1990. **18**(3): p. 297-306.
57. Work, R.W. and C.T. Young, *The Amino Acid Compositions of Major and Minor Ampullate Silks of Certain Orb-Web-Building Spiders (Araneae, Araneidae)*. The Journal of Arachnology, 1987. **15**(1): p. 65-80.
58. Kaewprasit, K., et al., *Physico-chemical properties and in vitro response of silk fibroin from various domestic races*. Journal of Biomedical Materials Research Part B: Applied Biomaterials, 2014. **102**(8): p. 1639-1647.
59. Koh, L.-D., et al., *Structures, mechanical properties and applications of silk fibroin materials*. Progress in Polymer Science, 2015. **46**: p. 86-110.
60. Cunniff, P.M., et al., *Mechanical and thermal properties of dragline silk from the spider Nephila clavipes*. Polymers for Advanced Technologies, 1994. **5**(8): p. 401-410.
61. Ittah, S., et al., *An Essential Role for the C-Terminal Domain of A Dragline Spider Silk Protein in Directing Fiber Formation*. Biomacromolecules, 2006. **7**(6): p. 1790-1795.
62. Li, M. and J. Li, *12 - Biodegradation behavior of silk biomaterials*, in *Silk Biomaterials for Tissue Engineering and Regenerative Medicine*, S.C. Kundu, Editor. 2014, Woodhead Publishing. p. 330-348.
63. Li, M., M. Ogiso, and N. Minoura, *Enzymatic degradation behavior of porous silk fibroin sheets*. Biomaterials, 2003. **24**(2): p. 357-365.
64. Meinel, L., et al., *The inflammatory responses to silk films in vitro and in vivo*. Biomaterials, 2005. **26**(2): p. 147-155.
65. Panilaitis, B., et al., *Macrophage responses to silk*. Biomaterials, 2003. **24**(18): p. 3079-3085.
66. Tungtasana, H., et al., *Tissue response and biodegradation of composite scaffolds prepared from Thai silk fibroin, gelatin and hydroxyapatite*. Journal of Materials Science: Materials in Medicine, 2010. **21**(12): p. 3151-3162.
67. Amornsudthiwat, P., et al., *Improvement of early cell adhesion on Thai silk fibroin surface by low energy plasma*. Colloids and Surfaces B: Biointerfaces, 2013. **111**: p. 579-586.
68. Acharya, C., S.K. Ghosh, and S.C. Kundu, *Silk fibroin protein from mulberry and non-mulberry silkworms: cytotoxicity, biocompatibility and kinetics of L929 murine fibroblast adhesion*. Journal of Materials Science: Materials in Medicine, 2008. **19**(8): p. 2827-2836.
69. Madden, P.W., et al., *Human corneal endothelial cell growth on a silk fibroin membrane*. Biomaterials, 2011. **32**(17): p. 4076-4084.
70. Mehrotra, S., S.K. Nandi, and B.B. Mandal, *Stacked silk-cell monolayers as a biomimetic three dimensional construct for cardiac tissue reconstruction*. Journal of Materials Chemistry B, 2017. **5**(31): p. 6325-6338.
71. Zhou, J., et al., *In vitro and in vivo degradation behavior of aqueous-derived electrospun silk fibroin scaffolds*. Polymer Degradation and Stability, 2010. **95**(9): p. 1679-1685.
72. Sang, Y., et al., *Biomimetic Silk Scaffolds with an Amorphous Structure for Soft Tissue Engineering*. ACS Applied Materials & Interfaces, 2018. **10**(11): p. 9290-9300.

73. Leng, X., et al., *In situ ultrasound imaging of silk hydrogel degradation and neovascularization*. Journal of Tissue Engineering and Regenerative Medicine, 2017. **11**(3): p. 822-830.
74. Chiarini, A., et al., *Biocompatible Silk Noil-Based Three-Dimensional Carded-Needled Nonwoven Scaffolds Guide the Engineering of Novel Skin Connective Tissue*. Tissue Engineering Part A, 2016. **22**(15-16): p. 1047-1060.
75. Nagarkar, S., et al., *Structure and gelation mechanism of silk hydrogels*. Physical Chemistry Chemical Physics, 2010. **12**(15): p. 3834-3844.
76. Sun, W., et al., *Viability and neuronal differentiation of neural stem cells encapsulated in silk fibroin hydrogel functionalized with an IKVAV peptide*. Journal of Tissue Engineering and Regenerative Medicine, 2017. **11**(5): p. 1532-1541.
77. Osama, I., et al., *In vitro studies on space-conforming self-assembling silk hydrogels as a mesenchymal stem cell-support matrix suitable for minimally invasive brain application*. Scientific Reports, 2018. **8**(1): p. 13655.
78. Zhang, W., et al., *The use of injectable sonication-induced silk hydrogel for VEGF(165) and BMP-2 delivery for elevation of the maxillary sinus floor*. Biomaterials, 2011. **32**(35): p. 9415-9424.
79. Calabrese, R., et al., *Silk-ionomer and silk-tropoelastin hydrogels as charged three-dimensional culture platforms for the regulation of hMSC response*. Journal of Tissue Engineering and Regenerative Medicine, 2017. **11**(9): p. 2549-2564.
80. Calabrese, R. and D.L. Kaplan, *Silk ionomers for encapsulation and differentiation of human MSCs*. Biomaterials, 2012. **33**(30): p. 7375-7385.
81. Hamilton, D.C., et al., *A silk-based encapsulation platform for pancreatic islet transplantation improves islet function in vivo*. Journal of Tissue Engineering and Regenerative Medicine, 2017. **11**(3): p. 887-895.
82. Leisk, G.G., et al., *Electrogelation for Protein Adhesives*. Advanced Materials, 2010. **22**(6): p. 711-715.
83. Elia, R., et al., *Silk electrogel coatings for titanium dental implants*. Journal of Biomaterials Applications, 2014. **29**(9): p. 1247-1255.
84. Qu, Y., et al., *Evaluation of silk fibroin electrogel coating for zirconia material surface*. Dental Materials Journal, 2019. **38**(5): p. 813-820.
85. Yin, Z., et al., *A silk fibroin hydrogel with reversible sol-gel transition*. RSC Advances, 2017. **7**(39): p. 24085-24096.
86. Yin, Z., et al., *Self-Assembling Silk-Based Nanofibers with Hierarchical Structures*. ACS Biomaterials Science & Engineering, 2017. **3**(10): p. 2617-2627.
87. Gou, S., et al., *Injectable, Thixotropic, and Multiresponsive Silk Fibroin Hydrogel for Localized and Synergistic Tumor Therapy*. ACS Biomaterials Science & Engineering, 2020. **6**(2): p. 1052-1063.
88. Li, X., et al., *Soft freezing-induced self-assembly of silk fibroin for tunable gelation*. International Journal of Biological Macromolecules, 2018. **117**: p. 691-695.
89. Motta, A., et al., *Fibroin hydrogels for biomedical applications: preparation, characterization and in vitro cell culture studies*. Journal of Biomaterials Science, Polymer Edition, 2004. **15**(7): p. 851-864.

90. Liu, Y., et al., *Thixotropic silk nanofibril-based hydrogel with extracellular matrix-like structure*. *Biomaterials Science*, 2014. **2**(10): p. 1338-1342.
91. Numata, K., T. Katashima, and T. Sakai, *State of Water, Molecular Structure, and Cytotoxicity of Silk Hydrogels*. *Biomacromolecules*, 2011. **12**(6): p. 2137-2144.
92. Kaewprasit, K., T. Kobayashi, and S. Damrongsakkul, *Thai silk fibroin gelation process enhancing by monohydric and polyhydric alcohols*. *International Journal of Biological Macromolecules*, 2018. **118**: p. 1726-1735.
93. Kaewprasit, K., T. Kobayashi, and S. Damrongsakkul, *Alcohol-triggered silk fibroin hydrogels having random coil and β -turn structures enhanced for cytocompatible cell response*. *Journal of Applied Polymer Science*, 2020. **137**(21): p. 48731.
94. Wu, X., et al., *Sodium dodecyl sulfate-induced rapid gelation of silk fibroin*. *Acta Biomaterialia*, 2012. **8**(6): p. 2185-2192.
95. Hirlekar, S., et al., *Silk Fibroin–Sodium Dodecyl Sulfate Gelation: Molecular, Structural, and Rheological Insights*. *Langmuir*, 2019. **35**(46): p. 14870-14878.
96. Lu, Y., et al., *Silk/agarose scaffolds with tunable properties via SDS assisted rapid gelation*. *RSC Advances*, 2017. **7**(35): p. 21740-21748.
97. Chantong, N., S. Damrongsakkul, and J. Ratanavaraporn, *Gelation Process and Physicochemical Properties of Thai Silk Fibroin Hydrogels Induced by Various Anionic Surfactants for Controlled Release of Curcumin*. *Journal of Surfactants and Detergents*, 2019. **22**(6): p. 1395-1407.
98. Zhang, F., et al., *Potential of biocompatible regenerated silk fibroin/sodium *N*-lauroyl sarcosinate hydrogels*. *Journal of Biomaterials Science, Polymer Edition*, 2015. **26**(12): p. 780-795.
99. Yang, Y., et al., *Sodium oleate induced rapid gelation of silk fibroin*. *Journal of Biomaterials Science, Polymer Edition*, 2018. **29**(10): p. 1219-1231.
100. Park, J.H., et al., *Effect of surfactants on sol–gel transition of silk fibroin*. *Journal of Sol-Gel Science and Technology*, 2014. **71**(2): p. 364-371.
101. Lu, S., et al., *Cationic Surfactant-Induced Instantaneous Gelation of Silk Fibroin Solution*. *Asian Journal of Chemistry*, 2014. **26**: p. 5667-5672.
102. Dubey, P., et al., *Silk Fibroin-Sophorolipid Gelation: Deciphering the Underlying Mechanism*. *Biomacromolecules*, 2016. **17**(10): p. 3318-3327.
103. Dubey, P., et al., *pH dependent sophorolipid assemblies and their influence on gelation of silk fibroin protein*. *Materials Chemistry and Physics*, 2018. **203**: p. 9-16.
104. Im, S.D., et al., *Gelation Behaviors and Mechanism of Silk Fibroin According to the Addition of Nitrate Salts*. *International Journal of Molecular Sciences*, 2016. **17**(10).
105. Jing, J., et al., *Fabrication of Hybrid Hydrogels from Silk Fibroin and Tannic Acid with Enhanced Gelation and Antibacterial Activities*. *ACS Biomaterials Science & Engineering*, 2019. **5**(9): p. 4601-4611.
106. Partlow, B.P., et al., *Highly tunable elastomeric silk biomaterials*. *Advanced functional materials*, 2014. **24**(29): p. 4615-4624.
107. Niu, C., et al., *Design and performance of a poly(vinyl alcohol)/silk fibroin enzymatically crosslinked semi-interpenetrating hydrogel for a potential hydrophobic drug delivery*. *RSC Advances*, 2019. **9**(70): p. 41074-41082.

108. Hasturk, O., et al., *Enzymatically crosslinked silk and silk-gelatin hydrogels with tunable gelation kinetics, mechanical properties and bioactivity for cell culture and encapsulation*. *Biomaterials*, 2020. **232**: p. 119720.
109. Kuang, D., et al., *Highly elastomeric photocurable silk hydrogels*. *International Journal of Biological Macromolecules*, 2019. **134**: p. 838-845.
110. Kang, G.-D., et al., *Effects of poloxamer on the gelation of silk fibroin*. *Macromolecular Rapid Communications*, 2000. **21**(11): p. 788-791.
111. Wang, X., et al., *Injectable silk-polyethylene glycol hydrogels*. *Acta biomaterialia*, 2015. **12**: p. 51-61.
112. Wei, W., et al., *Gellable silk fibroin-polyethylene sponge for hemostasis*. *Artificial Cells, Nanomedicine, and Biotechnology*, 2020. **48**(1): p. 28-36.
113. Liu, H., et al., *A dopamine-functionalized aqueous-based silk protein hydrogel bioadhesive for biomedical wound closure*. *New Journal of Chemistry*, 2020. **44**(3): p. 884-891.
114. Gong, Z., et al., *Injectable thixotropic hydrogel comprising regenerated silk fibroin and hydroxypropylcellulose*. *Soft Matter*, 2012. **8**(10): p. 2875-2883.
115. Cao, H., et al., *Dual-loaded, long-term sustained drug releasing and thixotropic hydrogel for localized chemotherapy of cancer*. *Biomaterials Science*, 2019. **7**(7): p. 2975-2985.
116. Luo, K., Y. Yang, and Z. Shao, *Physically Crosslinked Biocompatible Silk-Fibroin-Based Hydrogels with High Mechanical Performance*. *Advanced Functional Materials*, 2016. **26**(6): p. 872-880.
117. Cheng, B., et al., *Cooperative Assembly of a Peptide Gelator and Silk Fibroin Afford an Injectable Hydrogel for Tissue Engineering*. *ACS Applied Materials & Interfaces*, 2018. **10**(15): p. 12474-12484.
118. Yan, Y., et al., *Enhanced Osteogenesis of Bone Marrow-Derived Mesenchymal Stem Cells by a Functionalized Silk Fibroin Hydrogel for Bone Defect Repair*. *Advanced Healthcare Materials*, 2019. **8**(3): p. 1801043.
119. Li, X., et al., *Tuning the structure and performance of silk biomaterials by combining mulberry and non-mulberry silk fibroin*. *Polymer Degradation and Stability*, 2018. **147**: p. 57-63.
120. Chouhan, D., et al., *In Situ Forming Injectable Silk Fibroin Hydrogel Promotes Skin Regeneration in Full Thickness Burn Wounds*. *Advanced Healthcare Materials*, 2018. **7**(24): p. 1801092.
121. Bhunia, B.K. and B.B. Mandal, *Exploring Gelation and Physicochemical Behavior of in Situ Bioresponsive Silk Hydrogels for Disc Degeneration Therapy*. *ACS Biomaterials Science & Engineering*, 2019. **5**(2): p. 870-886.
122. Kumar, M., et al., *Immunomodulatory injectable silk hydrogels maintaining functional islets and promoting anti-inflammatory M2 macrophage polarization*. *Biomaterials*, 2018. **187**: p. 1-17.
123. Whittaker, J.L., et al., *Facile and rapid ruthenium mediated photo-crosslinking of Bombyx mori silk fibroin*. *Journal of materials chemistry. B*, 2014. **2**(37): p. 6259-6270.
124. Cui, X., et al., *Rapid Photocrosslinking of Silk Hydrogels with High Cell Density and Enhanced Shape Fidelity*. *Advanced Healthcare Materials*, 2020. **9**(4): p. 1901667.
125. Kim, H.H., et al., *Characterization of silk hydrogel formed with hydrolyzed silk*

- fibroin-methacrylate via photopolymerization*. Polymer, 2018. **153**: p. 232-240.
126. Kim, S.H., et al., *Precisely printable and biocompatible silk fibroin bioink for digital light processing 3D printing*. Nature Communications, 2018. **9**(1): p. 1620.
 127. Hong, H., et al., *Digital light processing 3D printed silk fibroin hydrogel for cartilage tissue engineering*. Biomaterials, 2020. **232**: p. 119679.
 128. Liang, J., et al., *Thiol–Ene Click Reaction Initiated Rapid Gelation of PEGDA/Silk Fibroin Hydrogels*. Polymers, 2019. **11**(12).
 129. Shi, L., et al., *Self-Healing Silk Fibroin-Based Hydrogel for Bone Regeneration: Dynamic Metal-Ligand Self-Assembly Approach*. Advanced Functional Materials, 2017. **27**(37): p. 1700591.
 130. Lu, Q., et al., *Silk fibroin electrogelation mechanisms*. Acta Biomaterialia, 2011. **7**(6): p. 2394-2400.
 131. Zhang, Q., et al., *Facile Preparation of Mechanical Reinforced and Biocompatible Silk Gels*. Fibers and Polymers, 2019. **20**(4): p. 675-682.
 132. Li, X., et al., *Water-stable silk fibroin nerve conduits with tunable degradation prepared by a mild freezing-induced assembly*. Polymer Degradation and Stability, 2019. **164**: p. 61-68.
 133. Otzen, D., *Protein–surfactant interactions: A tale of many states*. Biochimica et Biophysica Acta (BBA) - Proteins and Proteomics, 2011. **1814**(5): p. 562-591.
 134. Ribeiro, V.P., et al., *Enzymatically Cross-Linked Silk Fibroin-Based Hierarchical Scaffolds for Osteochondral Regeneration*. ACS Applied Materials & Interfaces, 2019. **11**(4): p. 3781-3799.
 135. Kang, G.D., et al., *Crosslinking reaction of phenolic side chains in silk fibroin by tyrosinase*. Fibers and Polymers, 2004. **5**(3): p. 234.
 136. Zhong, N., et al., *A novel 3D-printed silk fibroin-based scaffold facilitates tracheal epithelium proliferation in vitro*. Journal of Biomaterials Applications, 2019. **34**(1): p. 3-11.
 137. Dong, T., et al., *The regenerated silk fibroin hydrogel with designed architecture bioprinted by its microhydrogel*. Journal of Materials Chemistry B, 2019. **7**(27): p. 4328-4337.
 138. Bergers, J.J., et al., *The role of protein charge in protein-lipid interactions. pH-Dependent changes of the electrophoretic mobility of liposomes through adsorption of water-soluble, globular proteins*. Biochemistry, 1993. **32**(17): p. 4641-4649.
 139. Snel, M.M.E., A.I.P.M. de Kroon, and D. Marsh, *Mitochondrial Presequence Inserts Differently into Membranes Containing Cardiolipin and Phosphatidylglycerol*. Biochemistry, 1995. **34**(11): p. 3605-3613.
 140. Leenhouts, J.M., et al., *Anionic phospholipids can mediate membrane insertion of the anionic part of a bound peptide*. FEBS Letters, 1995. **370**(3): p. 189-192.
 141. Akbarzadeh, A., et al., *Liposome: classification, preparation, and applications*. Nanoscale Research Letters, 2013. **8**(1): p. 102.
 142. Monteiro, N., et al., *On the use of dexamethasone-loaded liposomes to induce the osteogenic differentiation of human mesenchymal stem cells*. Journal of Tissue Engineering and Regenerative Medicine, 2015. **9**(9): p. 1056-1066.
 143. Shaw, C.F., *Gold-Based Therapeutic Agents*. Chemical Reviews, 1999. **99**(9): p. 2589-2600.

144. Basu, N., R. Bhattacharya, and P. Mukherjee, *Protein-mediated autoreduction of gold salts to gold nanoparticles*. Biomedical Materials, 2008. **3**(3): p. 034105.
145. Lakshmeesha Rao, B., et al., *Rapid synthesis of gold nanoparticles using silk fibroin: characterization, antibacterial activity, and anticancer properties*. Gold Bulletin, 2017. **50**(4): p. 289-297.
146. Jain, P.K., et al., *Noble Metals on the Nanoscale: Optical and Photothermal Properties and Some Applications in Imaging, Sensing, Biology, and Medicine*. Accounts of Chemical Research, 2008. **41**(12): p. 1578-1586.
147. Yadid, M., R. Feiner, and T. Dvir, *Gold Nanoparticle-Integrated Scaffolds for Tissue Engineering and Regenerative Medicine*. Nano Letters, 2019. **19**(4): p. 2198-2206.
148. Hu, X., D. Kaplan, and P. Cebe, *Determining Beta-Sheet Crystallinity in Fibrous Proteins by Thermal Analysis and Infrared Spectroscopy*. Macromolecules, 2006. **39**(18): p. 6161-6170.
149. Lakowicz, J.R., *Principles of fluorescence spectroscopy*. 1999: Second edition. New York : Kluwer Academic/Plenum, [1999] ©1999.
150. Yan, C. and D.J. Pochan, *Rheological properties of peptide-based hydrogels for biomedical and other applications*. Chemical Society Reviews, 2010. **39**(9): p. 3528-3540.
151. ISO, *Part 1: Evaluation and testing within a risk management process*, in *ISO 10993-1:2018 Biological evaluation of medical devices*. 2018.
152. ISO, *Part 5: Tests for in vitro cytotoxicity*, in *ISO 10993-5:2009 Biological evaluation of medical devices*. 2009.
153. Carvalho, A.F., et al., *Control of osmotic pressure to improve cell viability in cell-laden tissue engineering constructs*. Journal of Tissue Engineering and Regenerative Medicine, 2018. **12**(2): p. e1063-e1067.
154. Mehanny, M., et al., *Exploring the use of nanocarrier systems to deliver the magical molecule; Curcumin and its derivatives*. Journal of Controlled Release, 2016. **225**: p. 1-30.
155. Ramalingam, P. and Y.T. Ko, *A validated LC-MS/MS method for quantitative analysis of curcumin in mouse plasma and brain tissue and its application in pharmacokinetic and brain distribution studies*. Journal of Chromatography B, 2014. **969**: p. 101-108.
156. Paul, J.H. and B. Myers, *Fluorometric determination of DNA in aquatic microorganisms by use of hoechst 33258*. Applied and environmental microbiology, 1982. **43**(6): p. 1393-1399.
157. Monteiro, N., et al., *Immobilization of bioactive factor-loaded liposomes on the surface of electrospun nanofibers targeting tissue engineering*. Biomaterials Science, 2014. **2**(9): p. 1195-1209.
158. Ellman, G.L., *Tissue sulfhydryl groups*. Archives of Biochemistry and Biophysics, 1959. **82**(1): p. 70-77.
159. Malencik, D.A. and S.R. Anderson, *Dityrosine as a product of oxidative stress and fluorescent probe*. Amino Acids, 2003. **25**(3): p. 233-247.
160. Mulvaney, P., *Surface Plasmon Spectroscopy of Nanosized Metal Particles*. Langmuir, 1996. **12**(3): p. 788-800.
161. Karpenko, A., et al., *The role of cationic Au³⁺ and nonionic Au⁰ species in the low-temperature water-gas shift reaction on Au/CeO₂ catalysts*. Journal of

- Catalysis, 2007. **252**(2): p. 231-242.
162. Castner, D.G., K. Hinds, and D.W. Grainger, *X-ray Photoelectron Spectroscopy Sulfur 2p Study of Organic Thiol and Disulfide Binding Interactions with Gold Surfaces*. Langmuir, 1996. **12**(21): p. 5083-5086.
163. Pedersen, U.R., et al., *The effect of calcium on the properties of charged phospholipid bilayers*. Biochimica et Biophysica Acta (BBA) - Biomembranes, 2006. **1758**(5): p. 573-582.
164. Garidel, P., A. Blume, and W. Hübner, *A Fourier transform infrared spectroscopic study of the interaction of alkaline earth cations with the negatively charged phospholipid 1,2-dimyristoyl-sn-glycero-3-phosphoglycerol*. Biochimica et Biophysica Acta (BBA) - Biomembranes, 2000. **1466**(1): p. 245-259.
165. Reddy, S.B., W.A. Linden, and K. Lübbers, *A comparative study of four sublines of mouse fibroblast cells*. Acta Histochemica, 1976. **56**(1): p. 115-119.
166. DSMZ, L.I. NIH-3T3. [cited 2020 25 Mar 2020]; Available from: <https://www.dsmz.de/collection/catalogue/details/culture/ACC-59>.
167. DSMZ, L.I. SaOS-2. [cited 2020 25 Mar 2020]; Available from: <https://www.dsmz.de/collection/catalogue/details/culture/ACC-243>.
168. Pradier, O., et al., *Effects of docetaxel in combination with radiation on human head and neck cancer cells (ZMK-1) and cervical squamous cell carcinoma cells (CaSki)*. International Journal of Cancer, 2001. **91**(6): p. 840-845.
169. Jongpaiboonkit, L., W.J. King, and W.L. Murphy, *Screening for 3D environments that support human mesenchymal stem cell viability using hydrogel arrays*. Tissue engineering. Part A, 2009. **15**(2): p. 343-353.
170. Kupcsik, L., *Estimation of Cell Number Based on Metabolic Activity: The MTT Reduction Assay*, in *Mammalian Cell Viability: Methods and Protocols*, M.J. Stoddart, Editor. 2011, Humana Press: Totowa, NJ. p. 13-19.
171. Quent, V.M.C., et al., *Discrepancies between metabolic activity and DNA content as tool to assess cell proliferation in cancer research*. Journal of Cellular and Molecular Medicine, 2010. **14**(4): p. 1003-1013.
172. Ravi, M., et al., *3D Cell Culture Systems: Advantages and Applications*. Journal of Cellular Physiology, 2015. **230**(1): p. 16-26.
173. Streichan, S.J., et al., *Spatial constraints control cell proliferation in tissues*. Proceedings of the National Academy of Sciences of the United States of America, 2014. **111**(15): p. 5586-5591.
174. Boyan, B.D., et al., *Role of material surfaces in regulating bone and cartilage cell response*. Biomaterials, 1996. **17**(2): p. 137-146.
175. Andersen, T., P. Auk-Emblem, and M. Dornish, *3D Cell Culture in Alginate Hydrogels*. Microarrays (Basel, Switzerland), 2015. **4**(2): p. 133-161.
176. Pradhan, S. and J.H. Slater, *Tunable hydrogels for controlling phenotypic cancer cell states to model breast cancer dormancy and reactivation*. Biomaterials, 2019. **215**: p. 119177.
177. Leipzig, N.D. and M.S. Shoichet, *The effect of substrate stiffness on adult neural stem cell behavior*. Biomaterials, 2009. **30**(36): p. 6867-6878.
178. Žigon-Branc, S., et al., *Impact of Hydrogel Stiffness on Differentiation of Human Adipose-Derived Stem Cell Microspheroids*. Tissue Engineering Part A, 2019. **25**(19-20): p. 1369-1380.

179. Kim, H., et al., *Mesenchymal stem cell 3D encapsulation technologies for biomimetic microenvironment in tissue regeneration*. Stem cell research & therapy, 2019. **10**(1): p. 51-51.
180. Swioklo, S. and C.J. Connon, *Keeping cells in their place: the future of stem cell encapsulation*. Expert Opinion on Biological Therapy, 2016. **16**(10): p. 1181-1183.
181. Swioklo, S., A. Constantinescu, and C.J. Connon, *Alginate-Encapsulation for the Improved Hypothermic Preservation of Human Adipose-Derived Stem Cells*. STEM CELLS Translational Medicine, 2016. **5**(3): p. 339-349.
182. Khetan, S. and O. Corey, *Maintenance of stem cell viability and differentiation potential following cryopreservation within 3-dimensional hyaluronic acid hydrogels*. Cryobiology, 2019. **90**: p. 83-88.
183. New, R.R.C., *Liposomes : a practical approach*. The Practical approach series. 1990, New York: Oxford University Press.
184. Were, L.M., et al., *Size, Stability, and Entrapment Efficiency of Phospholipid Nanocapsules Containing Polypeptide Antimicrobials*. Journal of Agricultural and Food Chemistry, 2003. **51**(27): p. 8073-8079.
185. Desai, T.R., R.E.W. Hancock, and W.H. Finlay, *A facile method of delivery of liposomes by nebulization*. Journal of Controlled Release, 2002. **84**(1): p. 69-78.
186. Wang, Y.-J., et al., *Stability of curcumin in buffer solutions and characterization of its degradation products*. Journal of Pharmaceutical and Biomedical Analysis, 1997. **15**(12): p. 1867-1876.
187. Kasoju, N. and U. Bora, *Fabrication and characterization of curcumin-releasing silk fibroin scaffold*. Journal of Biomedical Materials Research Part B: Applied Biomaterials, 2012. **100B**(7): p. 1854-1866.
188. Thayyullathil, F., et al., *Rapid reactive oxygen species (ROS) generation induced by curcumin leads to caspase-dependent and -independent apoptosis in L929 cells*. Free Radical Biology and Medicine, 2008. **45**(10): p. 1403-1412.
189. Shishodia, S., M.M. Chaturvedi, and B.B. Aggarwal, *Role of Curcumin in Cancer Therapy*. Current Problems in Cancer, 2007. **31**(4): p. 243-305.
190. Gajendiran, M., J.-S. Rhee, and K. Kim, *Recent Developments in Thiolated Polymeric Hydrogels for Tissue Engineering Applications*. Tissue Engineering Part B: Reviews, 2017. **24**(1): p. 66-74.
191. Huang, X. and M.A. El-Sayed, *Gold nanoparticles: Optical properties and implementations in cancer diagnosis and photothermal therapy*. Journal of Advanced Research, 2010. **1**(1): p. 13-28.
192. Si, S., et al., *A Mechanistic and Kinetic Study of the Formation of Metal Nanoparticles by Using Synthetic Tyrosine-Based Oligopeptides*. Chemistry – A European Journal, 2006. **12**(4): p. 1256-1265.
193. Jung, Y.L., et al., *Label-free colorimetric detection of biological thiols based on target-triggered inhibition of photoinduced formation of AuNPs*. Nanotechnology, 2015. **27**(5): p. 055501.
194. Xu, Y., et al., *The role of protein characteristics in the formation and fluorescence of Au nanoclusters*. Nanoscale, 2014. **6**(3): p. 1515-1524.
195. Schedle, A., et al., *Response of L-929 Fibroblasts, Human Gingival Fibroblasts, and Human Tissue Mast Cells to Various Metal Cations*. Journal of Dental Research, 1995. **74**(8): p. 1513-1520.



จุฬาลงกรณ์มหาวิทยาลัย
CHULALONGKORN UNIVERSITY



จุฬาลงกรณ์มหาวิทยาลัย
CHULALONGKORN UNIVERSITY

VITA

NAME	Chavee Laomeephol
DATE OF BIRTH	25 May 1988
PLACE OF BIRTH	Bangkok
INSTITUTIONS ATTENDED	Bachelor of Science in Pharmacy, Faculty of Pharmaceutical Sciences, Chulalongkorn University, Thailand
HOME ADDRESS	145/6 Payapilom building, Taksin 22, Bukkaloo, Thonburi, Bangkok 10600, Thailand
PUBLICATION	<ol style="list-style-type: none"> 1. Laomeephol, C.; Guedes, M.; Ferreira, H.; Reis, R.L.; Kanokpanont, S.; Damrongsakkul, S.; Neves, N.M. Phospholipid-induced silk fibroin hydrogels and their potential as cell carriers for tissue regeneration. <i>J Tissue Eng Regen Med.</i> 2020; 14: 160– 172. 2. Laomeephol, C.; Ferreira, H.; Yodmuang, S.; Reis, R.L.; Damrongsakkul, S.; Neves, N.M. Exploring the Gelation Mechanisms and Cytocompatibility of Gold (III)-Mediated Regenerated and Thiolated Silk Fibroin Hydrogels. <i>Biomolecules.</i> 2020; 10: 466. 3. Laomeephol, C.; Ferreira, H.; Kanokpanont, S.; Damrongsakkul, S.; Neves, N.M. Process to accelerate gelation of silk fibroin solution using phospholipid (กรรมวิธี การเร่งกระบวนการเกิดเจลของสารละลายโปรตีนไฟโบรอินในน้ำโดยฟอสโฟลิปิด). Thai patent-pending no.1801004182 (2018).
AWARD RECEIVED	<ol style="list-style-type: none"> 1. The 100th Anniversary Chulalongkorn University Fund for Doctoral Scholarship and the 90th Anniversary Chulalongkorn University Fund (Ratchadaphiseksomphot Endowment Fund) 2. REMIX project – HORIZON 2020 Marie Skłodowska-Curie actions G.A. 778078 3. Erasmus+ program – International credit mobility 4. International Cooperative Graduate School (ICGS) fellowship under the Chulalongkorn University NIMS cooperative graduate school program